BULLETIN OF RUSSIAN STATE MEDICAL UNIVERSITY

BIOMEDICAL JOURNAL OF PIROGOV RUSSIAN NATIONAL RESEARCH MEDICAL UNIVERSITY

SUBMISSION http://vestnikrgmu.ru/login?lang=en
CORRESPONDENCE editor@vestnikrgmu.ru
COLLABORATION manager@vestnikrgmu.ru
ADDRESS ul. Ostrovityanova, d. 1, Moscow, Russia, 117997

Indexed in Scopus. CiteScore 2020: 0.4

Indexed in WoS. JCR 2020: 0.4

Five-year h-index is 6

Indexed in RSCI. IF 2018: 0,5

Listed in HAC 31.01.2020 (№ 507)

Open access to archive

Issue DOI: 10.24075/brsmu.2021-06
The mass media registration certificate № 012769 issued on July 29, 1994
Founder and publisher is Pirogov Russian National Research Medical University (Moscow, Russia)

Approved for print 31.12.2021
Circulation: 100 copies. Printed by Print.Formula
www.print-formula.ru

ВЕСТНИК РОССИЙСКОГО ГОСУДАРСТВЕННОГО МЕДИЦИНСКОГО УНИВЕРСИТЕТА

НАУЧНЫЙ МЕДИЦИНСКИЙ ЖУРНАЛ РНИМУ ИМ. Н. И. ПИРОГОВА

ПОДАЧА РУКОПИСЕЙ http://vestnikrgmu.ru/login
ПЕРЕПИСКА С РЕДАКЦИЕЙ editor@vestnikrgmu.ru
СОТРУДНИЧЕСТВО manager@vestnikrgmu.ru
АДРЕС РЕДАКЦИИ ул. Островитянова, д. 1, г. Москва, 117997

Журнал включен в Scopus. CiteScore 2020: 0,4

Журнал включен в WoS. JCR 2020: 0,4

Индекс Хирша (h^5) журнала по оценке Google Scholar: 6

Журнал включен в РИНЦ. IF 2018: 0,5

Журнал включен в Перечень 31.01.2020 (№ 507)

Здесь находится открытый архив журнала

DOI выпуска: 10.24075/vrgmu.2021-06
Свидетельство о регистрации средства массовой информации № 012769 от 29 июля 1994 г.
Учредитель и издатель — Российский национальный исследовательский медицинский университет имени Н. И. Пирогова (Москва, Россия)

Подписано в печать 31.12.2021
Тираж 100 экз. Отпечатано в типографии Print.Formula
www.print-formula.ru

BULLETIN OF RSMU **6, 2021**
ВЕСТНИК РГМУ

Contents
Содержание

NEW NON-INVASIVE APPROACHES TO THE DIAGNOSIS OF LYMPH NODE METASTASES FROM BREAST CANCER BY MASS SPECTROMETRY

Tokareva AO[1,2], Chagovets VV[1], Rodionov VV[1], Kometova VV[1], Rodionova MV[1], Starodubtseva NL[1,2], Frankevich VE[1] ✉

[1] Kulakov National Medical Research Center for Obstetrics, Gynecology and Perinatology, Moscow, Russia

[2] V. L. Talrose Institute for Energy Problems of Chemical Physics, Moscow, Russia

Early diagnosis of metastasis makes it possible to select the optimal treatment protocol and improve patient survival. Noninvasive and minimally invasive diagnostic techniques help to make a diagnosis with minimal damage to the body. The study was aimed to find biomarkers, being the hallmarks of the metastatic process initiation, and to develop a diagnostic model based on the plasma lipid profile using liquid chromatography-mass spectrometry. We studied blood plasma of 55 patients, 28 of them were diagnosed with the regional lymph node metastasis; the control group comprised 27 patients. The levels of lipids, belonging to the groups, such as oxidized lipids and sphingomyelins, in patients with metastases were significantly higher and significantly lower, respectively. The lipid panels were created by multivariate analysis, and the models based on these panels showed sensitivity and specificity of 79 and 74% (positive ion mode), and of 50 and 85% (negative ion mode) in leave-one-out cross-validation.

Keywords: lipids, regional metastasis, breast cancer, blood plasma, molecular markers

Funding: the study was funded by RFBR and National Natural Science Foundation of China within the framework of the scientific project № 19-515-55021

Compliance with ethical standards: the study was approved by the Ethics Committee of Kulakov National Medical Research Center for Obstetrics, Gynecology and Perinatology (protocol № 9 dated November 22, 2018); the study was carried out in accordance with the requirements of the Declaration of Helsinki, International Council for Harmonisation (ICF), Good Clinical Practice (GCP) guidelines, Federal Law 323-FZ dated November 21, 2011 "On the Basics of Protecting the Health of Citizens in the Russian Federation"; the informed consent was submitted by all patients.

✉ **Correspondence should be addressed:** Vladimir E. Frankevich
Oparina, 4, Moscow, 117997, Russia; vfrankevich@gmail.com

Received: 26.10.2021 **Accepted:** 08.11.2021 **Published online:** 10.11.2021

DOI: 10.24075/brsmu.2021.053

НОВЫЕ НЕИНВАЗИВНЫЕ ПОДХОДЫ К ДИАГНОСТИКЕ МЕТАСТАТИЧЕСКОГО ПОРАЖЕНИЯ ЛИМФОУЗЛОВ ПРИ РАКЕ МОЛОЧНОЙ ЖЕЛЕЗЫ МЕТОДОМ МАСС-СПЕКТРОМЕТРИИ

А. О. Токарева[1,2], В. В. Чаговец[1], В. В. Родионов[1], В. В. Кометова[1], М. В. Родионова[1], Н. Л. Стародубцева[1,2], В. Е. Франкевич[1] ✉

[1] Национальный медицинский исследовательский центр акушерства, гинекологии и перинатологии имени В. И. Кулакова, Москва, Россия

[2] Институт энергетических проблем химической физики имени В. Л. Тальрозе, Москва, Россия

Ранняя диагностика процесса метастазирования позволяет выбрать оптимальный протокол лечения и повысить выживаемость пациенток. Неинвазивные и малоинвазивные методы диагностики помогают ставить диагноз с минимальным ущербом для организма. Целью исследования было найти биомаркеры, характеризующие начало метастатического процесса и создать диагностическую модель по липидному профилю плазмы крови с использованием жидкостной хромато-масс-спектрометрии. Исследовали плазму крови 55 пациенток, у 28 из которых было диагностировано метастазирование в региональные лимфоузлы, 27 пациенток составили контрольную группу. Липиды, относящиеся к окисленным липидам и сфингомиелинам имели при метастазировании статистически значимо более высокий и более низкий уровни соответственно. С использованием методов многомерного анализа были составлены панели липидов, и модели на их основе в ходе кросс-валидации по отдельному объекту имели чувствительность и специфичность 79 и 74% (режим положительных ионов) и 50 и 85% (режим отрицательных ионов).

Ключевые слова: липиды, регионарное метастазирование, рак молочной железы, плазма крови, молекулярные маркеры

Финансирование: работа выполнена при финансовой поддержке РФФИ и ГФЕН в рамках научного проекта № 19-515-55021

Соблюдение этических стандартов: исследование одобрено этическим комитетом НМИЦ АГП им. В. И. Кулакова (протокол № 9 от 22 ноября 2018 г.), проведено в соответствии с требованиями Хельсинкской декларации, Международной конференции по гармонизации (ICF), Стандартов надлежащей клинической практики (GCP), ФЗ № 323-ФЗ от 21 ноября 2011 г. «Об основах охраны здоровья граждан в Российской Федерации»; все пациентки подписали добровольное информированное согласие на участие в исследовании.

✉ **Для корреспонденции:** Владимир Евгеньевич Франкевич
ул. Опарина, д. 4, г. Москва, 117997, Россия; vfrankevich@gmail.com

Статья получена: 26.10.2021 **Статья принята к печати:** 08.11.2021 **Опубликована онлайн:** 10.11.2021

DOI: 10.24075/vrgmu.2021.053

The spread of cancer cells throughout the body from the primary tumor occurs through the biofluids, such as blood and lymph [1]. Axillary lymph node dissection and sentinel lymph node biopsy make it possible to define the onset of the regional lymph nodes metastasis with 100% accuracy. However, the risk of complications associated with the build-up of lymph in the tissues is high due to high invasiveness of the procedures [2, 3]. The noninvasive techniques for diagnosis of regional metastasis are as follows: ultrasound imaging, magnetic resonance imaging and positron emission tomography (MRI and PET). Ultrasound imaging is a standard technique used to search for the regional lymph node metastases, however, the method sensitivity and specificity depend on the equipment quality and the operator's experience [4]. The use of MRI is limited by contraindications in people with kidney failure, allergy, and artificial cardiac pacemakers. PET has low sensitivity in assessment of axillary lymph node status [5].

Analysis of blood plasma is a minimally invasive method. The method may be used for diagnosis of Alzheimer's disease [6], cervical cancer [7], lung cancer [8], and cystic fibrosis affecting liver and the lungs [9] based on the plasma molecular profile. Furthermore, the protein markers of metastasis in colorectal cancer [10] and oral cancer [11] have been found in blood plasma, along with the markers of regional metastasis,

Table 1. Relative intensities (arbitrary units) of lipids, showing significant differences in plasma in the presence or absence of metastases, in the positive ion mode

Lipids	Metastasis	No metastasis	*p*
OxTG 16:0_16:0_18:3(OO)	6.86×10^5 (4.46×10^5; 8.94×10^5)	5.00×10^5 (2.43×10^5; 6.39×10^6)	0.04
OxTG 16:0_18:0_18:3(OH)	1.96×10^6 (4.77×10^5; 2.42×10^6)	4.63×10^5 (3.27×10^5; 9.94×10^5)	0.003
OxTG 18:1_18:1_18:2(OOH)	2.72×10^6 (1.70×10^6; 3.72×10^6)	1.86×10^6 (1.27×10^6; 2.50×10^6)	0.03
TG 14:0_16:0_18:1	2.43×10^6 (2.05×10^6; 2.84×10^6)	1.85×10^6 (1.45×10^6; 2.57×10^6)	0.04

Table 2. Relative intensities (conventional units) of lipids, showing significant differences in plasma in the presence or absence of metastases, in the negative ion mode

Lipids	Metastasis	No metastasis	*p*
OxPC 16:0_18:2(2O)	4.66×10^5 (3.35×10^5; 8.20×10^5)	2.58×10^5 (1.42×10^5; 5.22×10^5)	0.02
OxPC 16:0_22:5(OH)	1.15×10^5 (8.32×10^4; 1.39×10^5)	7.93×10^4 (5.10×10^4; 1.10×10^5)	0.04
OxPC 18:0_18:2(OOH)	1.99×10^5 (1.41×10^5; 3.81×10^5)	1.08×10^5 (6.15×10^4; 2.02×10^5)	0.008
OxPC 18:0_20:4(2O)	1.31×10^5 (8.47×10^4; 2.14×10^5)	7.08×10^4 (5.21×10^4; 1.66×10^5)	0.04
SM d22:0/20:3	5.71×10^6 (5.17×10^6; 6.49×10^6)	6.94×10^6 (5.28×10^6; 7.38×10^6)	0.01
SM d22:0/20:4	4.21×10^5 (3.56×10^5; 4.90×10^5)	4.76×10^5 (4.08×10^5; 5.45×10^5)	0.02

however, the biomarker panel has been specific for the cancer type (lobular or ductal) [12]. Lipids, being a part of the molecular profile, are involved in important metabolic pathways [13]. The plasma lipid profile, obtained by high performance liquid chromatography-mass spectrometry, has made it possible to build an effective classification model for breast cancer and benign breast lesions based on the selected markers [14], which, combined with the listed above examples, allows one to assume the presence of metastasis markers in blood plasma.

The study was aimed to search for lipid markers of regional metastasis in blood plasma of patients with confirmed breast cancer by liquid chromatography-mass spectrometry, and to assess the possibility of creating the diagnostic panel.

METHODS

A total of 55 women diagnosed with breast cancer, who were treated in the Kulakov National Medical Research Center for Obstetrics, Gynecology and Perinatology (Russia), were enrolled. Inclusion criteria: submitted informed consent to surgery and enrollment in the study, age 18–80 years; diagnosis of breast cancer confirmed by cytological or histological findings. Exclusion criteria: neoadjuvant therapy and the presence of malignant neoplasms of other localization before the breast cancer diagnosis. The regional lymph node metastases were revealed in 28 women, and the control group comprised 27 women. Lipids were extracted from 40 μL of plasma by the Folch method [15]: 480 μL of $CHCl_3$ / MeOH (1 / 1) were added to 40 μL of plasma and 5 μL of the internal standard, and soaked in the ultrasonic bath for 10 min. Then the mixture was stirred for 10 s and centrifuged for 5 min at 15,000 G. The organic phase containing lipids was collected in the separate vial. The water phase was mixed with 250 μL of $CHCl_3$ / MeOH (1 / 1) and centrifuged for 5 min at 15,000 G. The lower organic phase was collected again and mixed with the previously collected sample. The lipid solution was dried in a stream of nitrogen and redissolved in 200 μL of IPA / ACN (1 / 1) for further analysis.

The extracted lipids were analyzed using the Dionex UltiMate 3000 liquid chromatography system (Thermo Scientific; Germany), coupled with the Maxis Impact qTOF mass spectrometer, equipped with the ESI ion source (Bruker Daltonics; Germany). The samples were separated by reversed phase chromatography using the Zorbax C18 column (150 × 2.1 mm, 5 μm; Agilent, USA) with linear gradient from 30 to 90% of eluent B (solution of acetonitrile / isopropanol / water in a ratio of 90 / 8 / 2 by volume with the addition of 0.1% formic acid and 10 mmol/L ammonium formate) for 20 min. The solution of acetonitrile / water in a ratio of 60 / 40 by volume with the addition of 0.1% formic acid and 10 mmol/L ammonium formate was used as eluent A. The eluent flow rate was 40 μL/min, and the sample injection volume was 3 μL. Mass spectra were acquired in the positive and negative ion mode in the m / z range of 100–1700 using the following settings: capillary voltage 4.1 kV and 3.0 kV for the positive and negative ion mode; nebulizer gas pressure 0.7 bar; drying gas flow rate 6 L/min, drying gas temperature 200 oC.

Lipids were identified using the Lipid Match R script [16] based on the exact mass and the characteristic tandem mass spectra (MS / MS).

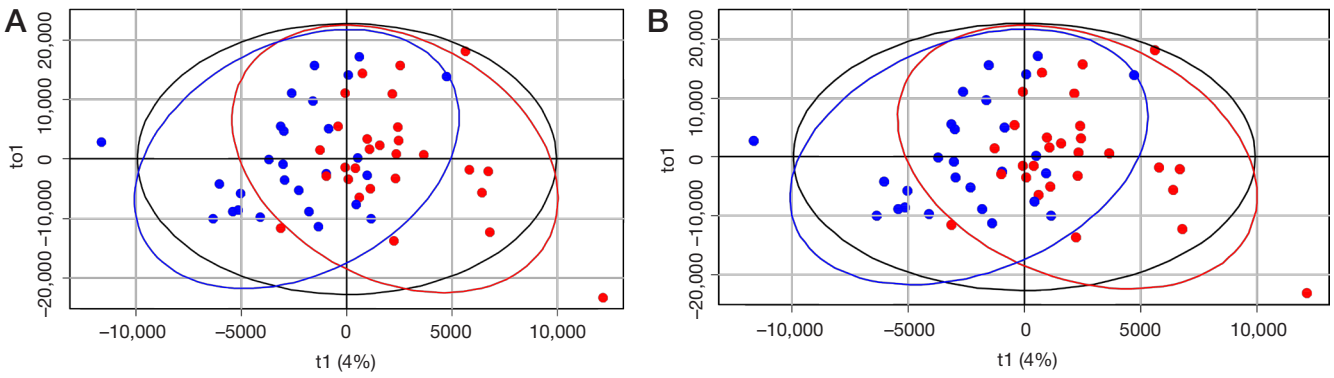

Fig. 1. Graphs of counts made for orthogonal projections to latent structures in the positive ion mode (**A**) and in the negative ion mode (**B**). The samples obtained from patients with regional metastases are marked with *red dots*, and the samples obtained from patients with no metastasis are marked with *blue dots*

Table 3. Compounds used to build the logistic regression model, β coefficients (conventional units), confidence interval (CI) for β coefficients (conventional units), Wald test, likelihood that coefficient *p* differs from zero in the positive ion mode

Lipids	β	CI β	Wald test	*p*
Intercept term	–3.98	–15.96–6.27	–0.74	0.46
CE 20:4	3.44×10^{-7}	1.30×10^{-7}–6.54×10^{-7}	2.64	0.008
LPC 18:2	2.37×10^{-7}	7.21×10^{-8}–4.72×10^{-7}	2.44	0.01
OxTG 16:0_18:0_18:3(OH)	1.56×10^{-6}	6.37×10^{-7}–2.89×10^{-6}	2.83	0.005
PC 16:0_22:5	2.66×10^{-7}	1.09×10^{-7}–5.17×10^{-7}	2.55	0.01
SM d18:2/24:1	-4.72×10^{-7}	-9.01×10^{-7}–-1.70×10^{-7}	–2.60	0.009
SM d18:1/24:0	-3.92×10^{-7}	-8.47×10^{-7}–-1.25×10^{-7}	–2.26	0.02
SM d18:1/22:0	3.85×10^{-7}	6.70×10^{-8}–8.51×10^{-7}	2.01	0.04

Table 4. Compounds used to build the logistic regression model, β coefficients (conventional units), confidence interval (CI) for β coefficients (conventional units), Wald test, likelihood that coefficient *p* differs from zero in the negative ion mode

Lipids	β	CI β	Wald test	*p*
Intercept term	3.71	–1.28–9.09	1.43	0.15
PC 16:0_22:5	$4.89*10^{-7}$	$1.37*10^{-7}$–$9.45*10^{-7}$	2.40	0.02
SM d22:0/20:3	$-1.05*10^{-6}$	$-1.98*10^{-6}$–$-2.52*10^{-7}$	–2.42	0.02

Statistical processing of the results was performed using R scripts [17] in the Rstudio environment [18].

The search for compounds, showing significant differences in plasma levels in patients with metastases and patients with no metastases, was performed using the Mann–Whitney U-test for pairwise comparison of groups. Median (Me) and quartiles Q_1 and Q_3 were used to describe the quantitative data. The significance threshold was set at $p = 0.05$.

The diagnostic model based on logistic regression was built by calculating the projection of the variable using the orthogonal projection to latent structures solution [19] and selecting the compounds with the variable projection value exceeding 1. The variables were selected from the selected variables using the step-by-step approach based on the Akaike information criterion (AIC) [20] until this led to the decrease in AIC. To build the final model, the variables, the coefficients of which were not significantly different from 0 ($p > 0.05$), were removed from the regression in a step-by-step manner. The quality of the resulting diagnostic model was tested by leave-one-out cross-validation. Area under the ROC curve, sensitivity and specificity were used for assessment.

RESULTS

During the study, we identified 183 lipid compounds in the positive ion mode and 161 compounds in the negative ion mode. Of those, four compounds showed significant differences in their levels in the positive ion mode (Table 1), and six compounds showed significant differences in the negative ion mode (Table 2). The levels of oxylipins (oxo-triglycerides in the positive ion mode and oxo-phosphotidylcholines in the negative ion mode) increased in case of metastasis. The levels of sphingomyelins, on the contrary, decreased in the presence of metastases.

Based on the constructed orthogonal projections to latent structures (Fig. 1), we selected 36 lipids in the positive ion mode and 29 lipids in the negative ion mode with the variable projection (VP) value exceeding 1.

We used seven compounds in the positive ion mode, which allowed us to build a model with the area under the ROC curve of 0.84 (Table 3; Fig. 2A), and two compounds in the negative ion mode, allowing us to build a model with the area under the ROC curve of 0.71 (Table 4; Fig. 2B). Sensitivity and specificity

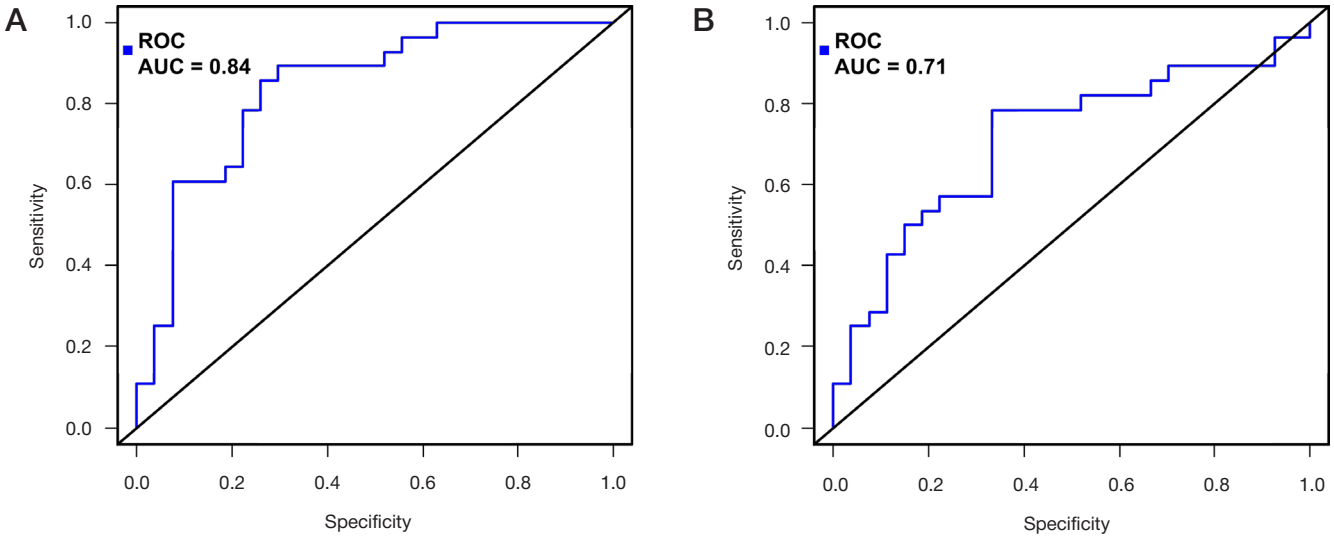

Fig. 2. ROC curve plotted during cross-validation of the diagnostic model in the positive ion mode (**A**) and negative ion mode (**B**)

of the model in the positive ion mode were 79 and 74%, respectively, and these indicators of the model in the negative ion mode were 50 and 85%, respectively.

DISCUSSION

Most of the lipids, the levels of significantly increase in case of metastasis, are the oxidized lipids. The oxidized lipids are formed primarily in the apoptotic cells. Furthermore, the oxidized lipids are involved in inflammation [21]. These have been also isolated as the predictors of coronary heart disease in blood plasma [22]. The panels created comprise mostly sphingomyelins together with lyso- and phosphotidylcholines, containing long acyl chains. The association of fatty acid synthases and omega-6 polyunsaturated fatty acids with metastasis is known today [23, 24], and elevated levels of sphingomyelins and lysophosphotidylcholines in relation to phosphotidylcholines have been registered in mice's plasma with advanced metastatic breast cancer [25]. However, in this study, the significantly decreased levels of sphingomyelins upon the onset of metastasis were observed in plasma. The varying changes in the sphingomyelin levels upon the onset of metastasis were revealed during the analysis of malignant tissue (decreased levels) and the nearby normal breast tissue (increased levels) [26]. Of the lipids, grouped together into the diagnostic panel, only two compounds show significant differences in their levels in the presence or absence of metastases. This is because the diagnostic panel has been created using multivariate analysis taking into account the associations between lipids. The use of this method for marker selection is justifiable in terms of applying the model to a multi-component space with non-orthogonal components, such as blood lipid profile. The use of univariate analysis methods makes it possible to assess the lipid profile changes with respect to the further investigation of metastatic process pathophysiology.

CONCLUSIONS

This study analyzed the lipid profile of patients with breast cancer using high-performance liquid chromatography-mass spectrometry. The lipids, showing significant differences in their levels, were the oxidized lipids and sphingomyelins. The lipids, included in the diagnostic panels, belonged mostly to the classes of sphingomyelins and phosphotidylcholines, and were characterized by increased unsaturation of acyl chains and the length of 20–24 carbon atoms. The diagnostic model obtained may be used for further research focused on developing the method for minimally invasive diagnosis of metastasis.

References

1. Fidler IJ. The pathogenesis of cancer metastasis: the 'seed and soil' hypothesis revisited. Nat Rev Cancer. 2003; 3 (6): 453–8.
2. Silberman AW, McVay C, Cohen JS, Altura JF, Brackert S, Sarna GP, et al. Comparative Morbidity of Axillary Lymph Node Dissection and the Sentinel Lymph Node Technique. Ann Surg. 2004; 240 (1): 1–6.
3. Schrenk P, Rieger R, Shamiyeh A, Wayand W. Morbidity following sentinel lymph node biopsy versus axillary lymph node dissection for patients with breast carcinoma. Cancer. 2000; 88 (3): 608–14.
4. Sukhikh GT, Sencha AN. Multiparametric ultrasound diagnosis of breast diseases. Cham: Springer, 2018.
5. Zhou M, Lu B, Lv G, Tang Q, Zhu J, Li J, et al. Differential diagnosis between metastatic and non-metastatic lymph nodes using DW-MRI: a meta-analysis of diagnostic accuracy studies. J Cancer Res Clin Oncol. 2015; 141 (6): 1119–30.
6. Wang T, Xiao S, Liu Y, Lin Z, Su N, Li X, et al. The efficacy of plasma biomarkers in early diagnosis of Alzheimer's disease. Int J Geriatr Psychiatry. 2014; 29 (7): 713–9.
7. Lin YW, Lai HC, Lin CY, Chiou JY, Shui HA, Chang CC, et al. Plasma proteomic profiling for detecting and differentiating in situ and invasive carcinomas of the uterine cervix. Int J Gynecol Cancer. 2006; 16 (3): 1216–24.
8. Zhong L, Coe SP, Stromberg AJ, Khattar NH, Jett JR, Hirschowitz EA. Profiling tumor-associated antibodies for early detection of non-small cell lung cancer. J Thorac Oncol. 2006; 1 (6): 513–9.
9. Schwarz KB, Rosensweig J, Sharma S, Jones L, Durant M, Potter C, et al. Plasma markers of platelet activation in cystic fibrosis liver and lung disease. J Pediatr Gastroenterol Nutr. 2003; 37 (2): 187–91.
10. Langenskiöld M, Holmdahl L, Falk P, Ivarsson ML. Increased plasma MMP-2 protein expression in lymph node-positive patients with colorectal cancer. Int J Colorectal Dis. 2005; 20 (3): 245–52.
11. Chai YD, Zhang L, Yang Y, Su T. Discovery of potential serum protein biomarkers for lymph-node metastasis in oral cancer. Head Neck. 2015; 38 (1): 118–25.
12. Yigitbasi T, Calibasi-Kocal G, Buyukuslu N, Kemal Atahan M, Kupeli H, Yigit S, et al. SELDI-TOF-MS Profiling of Metastatic Phenotype in Histopathological Subtypes of Breast Cancer. Curr Proteomics. 2018; 15 (3): 214–20.
13. Bandu R, Mok HJ, Kim KP. Phospholipids as cancer biomarkers: mass spectrometry-based analysis. Mass Spectrom Rev. 2016; 47 (3): 1–32.
14. Chen X, Chen H, Dai M, Ai J, Li Y, Mahon B, et al. Plasma lipidomics profiling identified lipid biomarkers in distinguishing early-stage breast cancer from benign lesions. Oncotarget. 2016; 7 (24): 36622–31.
15. Folch J, Lees M, Sloane Stanley GH. A simple method for the isolation and purification of total lipides from animal tissues. J Biol Chem. 1957; 226 (1): 497–509.
16. Koelmel JP, Kroeger NM, Ulmer CZ, Bowden JA, Patterson RE, Cochran JA, et al. LipidMatch: An automated workflow for rule-based lipid identification using untargeted high-resolution tandem mass spectrometry data. BMC Bioinformatics. 2017; 18 (1): 1–11.
17. R Development Core Team. A Language and Environment for Statistical Computing. R Found Stat Comput. 2019.
18. R team. R Studio: Integrated Development for R. 2016.
19. Galindo-Prieto B, Eriksson L, Trygg J. Variable influence on projection (VIP) for OPLS models and its applicability in multivariate time series analysis. Chemom Intell Lab Syst. 2015; 146: 297–304.
20. Akaike H. A New Look at the Statistical Model Identification. IEEE Trans Automat Contr. 1974; 19 (6): 716–23.
21. Miller YI, Shyy JYJ. Context-Dependent Role of Oxidized Lipids and Lipoproteins in Inflammation. Trends Endocrinol Metab. 2017; 28 (2): 143–52.
22. Paynter NP, Balasubramanian R, Giulianini F, Wang DD, Tinker LF, Gopal S etc. Metabolic predictors of incident coronary heart disease in women. Circulation. 2018; 137 (8): 841–53.
23. Ferreri C, Sansone A, Ferreri R, Amézaga J, Tueros I. Fatty acids and membrane lipidomics in oncology: A cross-road of nutritional, signaling and metabolic pathways. Metabolites. 2020; 10 (9): 1–26.
24. Maan M, Peters JM, Dutta M, Patterson AD. Lipid metabolism and lipophagy in cancer. Biochem Biophys Res Commun. 2018; 504 (3): 582–9.
25. Kus K, Kij A, Zakrzewska A, Jasztal A, Stojak M, Walczak M, et al. Alterations in arginine and energy metabolism, structural and signalling lipids in metastatic breast cancer in mice detected in plasma by targeted metabolomics and lipidomics. Breast Cancer

Res. 2018; 20 (1): 1–13.
26. Tokareva AO, Chagovets VV, Rodionov VV, Kometova VV, Rodionova MV, Starodubtseva NL, i dr. Lipidnye markery metastaticheskogo porazhenija regionarnyh limfouzlov u bol'nyh rakom molochnoj zhelezy. Akusherstvo i ginekologija. 2020; 8: 133–40. Russia.

Литература

1. Fidler IJ. The pathogenesis of cancer metastasis: the 'seed and soil' hypothesis revisited. Nat Rev Cancer. 2003; 3 (6): 453–8.
2. Silberman AW, McVay C, Cohen JS, Altura JF, Brackert S, Sarna GP, et al. Comparative Morbidity of Axillary Lymph Node Dissection and the Sentinel Lymph Node Technique. Ann Surg. 2004; 240 (1): 1–6.
3. Schrenk P, Rieger R, Shamiyeh A, Wayand W. Morbidity following sentinel lymph node biopsy versus axillary lymph node dissection for patients with breast carcinoma. Cancer. 2000; 88 (3): 608–14.
4. Sukhikh GT, Sencha AN. Multiparametric ultrasound diagnosis of breast diseases. Cham: Springer, 2018.
5. Zhou M, Lu B, Lv G, Tang Q, Zhu J, Li J, et al. Differential diagnosis between metastatic and non-metastatic lymph nodes using DW-MRI: a meta-analysis of diagnostic accuracy studies. J Cancer Res Clin Oncol. 2015; 141 (6): 1119–30.
6. Wang T, Xiao S, Liu Y, Lin Z, Su N, Li X, et al. The efficacy of plasma biomarkers in early diagnosis of Alzheimer's disease. Int J Geriatr Psychiatry. 2014; 29 (7): 713–9.
7. Lin YW, Lai HC, Lin CY, Chiou JY, Shui HA, Chang CC, et al. Plasma proteomic profiling for detecting and differentiating in situ and invasive carcinomas of the uterine cervix. Int J Gynecol Cancer. 2006; 16 (3): 1216–24.
8. Zhong L, Coe SP, Stromberg AJ, Khattar NH, Jett JR, Hirschowitz EA. Profiling tumor-associated antibodies for early detection of non-small cell lung cancer. J Thorac Oncol. 2006; 1 (6): 513–9.
9. Schwarz KB, Rosensweig J, Sharma S, Jones L, Durant M, Potter C, et al. Plasma markers of platelet activation in cystic fibrosis liver and lung disease. J Pediatr Gastroenterol Nutr. 2003; 37 (2): 187–91.
10. Langenskiöld M, Holmdahl L, Falk P, Ivarsson ML. Increased plasma MMP-2 protein expression in lymph node-positive patients with colorectal cancer. Int J Colorectal Dis. 2005; 20 (3): 245–52.
11. Chai YD, Zhang L, Yang Y, Su T. Discovery of potential serum protein biomarkers for lymph-node metastasis in oral cancer. Head Neck. 2015; 38 (1): 118–25.
12. Yigitbasi T, Calibasi-Kocal G, Buyukuslu N, Kemal Atahan M, Kupeli H, Yigit S, et al. SELDI-TOF-MS Profiling of Metastatic Phenotype in Histopathological Subtypes of Breast Cancer. Curr Proteomics. 2018; 15 (3): 214–20.
13. Bandu R, Mok HJ, Kim KP. Phospholipids as cancer biomarkers: mass spectrometry-based analysis. Mass Spectrom Rev. 2016; 47 (3): 1–32.
14. Chen X, Chen H, Dai M, Ai J, Li Y, Mahon B, et al. Plasma lipidomics profiling identified lipid biomarkers in distinguishing early-stage breast cancer from benign lesions. Oncotarget. 2016; 7 (24): 36622–31.
15. Folch J, Lees M, Sloane Stanley GH. A simple method for the isolation and purification of total lipides from animal tissues. J Biol Chem. 1957; 226 (1): 497–509.
16. Koelmel JP, Kroeger NM, Ulmer CZ, Bowden JA, Patterson RE, Cochran JA, et al. LipidMatch: An automated workflow for rule-based lipid identification using untargeted high-resolution tandem mass spectrometry data. BMC Bioinformatics. 2017; 18 (1): 1–11.
17. R Development Core Team. A Language and Environment for Statistical Computing. R Found Stat Comput. 2019.
18. R team. R Studio: Integrated Development for R. 2016.
19. Galindo-Prieto B, Eriksson L, Trygg J. Variable influence on projection (VIP) for OPLS models and its applicability in multivariate time series analysis. Chemom Intell Lab Syst. 2015; 146: 297–304.
20. Akaike H. A New Look at the Statistical Model Identification. IEEE Trans Automat Contr. 1974; 19 (6): 716–23.
21. Miller YI, Shyy JYJ. Context-Dependent Role of Oxidized Lipids and Lipoproteins in Inflammation. Trends Endocrinol Metab. 2017; 28 (2): 143–52.
22. Paynter NP, Balasubramanian R, Giulianini F, Wang DD, Tinker LF, Gopal S etc. Metabolic predictors of incident coronary heart disease in women. Circulation. 2018; 137 (8): 841–53.
23. Ferreri C, Sansone A, Ferreri R, Amézaga J, Tueros I. Fatty acids and membrane lipidomics in oncology: A cross-road of nutritional, signaling and metabolic pathways. Metabolites. 2020; 10 (9): 1–26.
24. Maan M, Peters JM, Dutta M, Patterson AD. Lipid metabolism and lipophagy in cancer. Biochem Biophys Res Commun. 2018; 504 (3): 582–9.
25. Kus K, Kij A, Zakrzewska A, Jasztal A, Stojak M, Walczak M, et al. Alterations in arginine and energy metabolism, structural and signalling lipids in metastatic breast cancer in mice detected in plasma by targeted metabolomics and lipidomics. Breast Cancer Res. 2018; 20 (1): 1–13.
26. Токарева А. О., Чаговец В. В., Родионов В. В., Кометова В. В., Родионова М. В., Стародубцева Н. Л. и др. Липидные маркеры метастатического поражения регионарных лимфоузлов у больных раком молочной железы. Акушерство и гинекология. 2020; 8: 133–40.

METABOLIC "FOOTPRINTS" OF THE CIRCULATING CANCER MUCINS: CA125 IN THE HIGH-GRADE OVARIAN CANCER

Chagovets VV[1] ✉, Vasil'ev VG[2], Iurova MV[1,3], Khabas GN[1], Pavlovich SV[1,3], Starodubtseva NL[1], Mayboroda OA[4,5]

[1] Kulakov National Medical Research Center for Obstetrics, Gynecology and Perinatology, Moscow, Russia

[2] Peoples' Friendship University of Russia, Moscow, Russia

[3] Sechenov First Moscow State Medical University, Moscow, Russia

[4] Leiden University Medical Center, Leiden, The Netherlands

[5] Tomsk State University, Tomsk, Russia

Mucins are large glycoproteins characterized by the abundant O-linked oligosaccharides (O-glycans) clustered on a protein backbone. Most of the circulating mucins are rapidly cleared by glycan-recognizing hepatic clearance receptors in the liver. Those mucins that remain in the bloodstream are most commonly used as markers in clinical diagnostics. One of such circulating mucins is MUC16; a peptide epitope of which is known as CA125 antigen — a marker for ovarian cancer. Here, using a targeted 1H-NMR profiling of plasma we are exploring a link between the measured CA125 values and the systemic metabolism of the patients within a group with confirmed high-grade ovarian cancer. The study allowed identifying statistically significant associations between the measured values of CA125 epitope and the plasma concentrations of glucose, glutamine, alanine, betaine and serine. The significance of the identified associations for the listed compounds is below 0.01. This, in turn, enables us to hypothesize about a possibility of including the metabolic measures into a composite score of the ovarian cancer based on the CA125 epitope of MUC16.

Keywords: metabolomics, NMR, circulating mucins, CA125, ovarian cancer

Funding: the study was supported by a grant from the Russian Science Foundation (project #20-65-46014).

Author contribution: Chagovets VV — study planning, sample preparation, discussion of NMR data processing, manuscript authoring and editing; Vasil'ev VG — sample preparation, NMR analysis; Iurova MV, Khabas GN — collection and characterization of clinical samples, discussion of the results; Pavlovich SV — study research, discussion of the results; Starodubtseva NL — study planning, clinical data processing; Mayboroda OA — study planning and management, manuscript authoring, NMR data processing.

Compliance with ethical standards: the study was approved by the Ethics Committee of the V.I. Kulakov National Medical Research Center for Obstetrics, Gynecology and Perinatology (Minutes #10 of December 05, 2019), conducted in accordance with federal laws of the Russian Federation (#152, 323 etc.) and the Declaration of Helsinki of 1964 with all subsequent extensions and amendments regulating scientific research involving biomaterials obtained from human beings.

✉ **Correspondence should be addressed:** Vitaly V. Chagovets
Akademika Oparina, 4, Moscow, 117997, Russia; vvchagovets@gmail.com

Received: 01.12.2021 **Accepted:** 16.12.2021 **Published online:** 29.12.2021

DOI: 10.24075/brsmu.2021.065

МЕТАБОЛОМНАЯ ПОДПИСЬ СВОБОДНЫХ МУЦИНОВ ПРИ ОНКОЛОГИЧЕСКИХ ЗАБОЛЕВАНИЯХ: CA125 И РАК ЯИЧНИКОВ ВЫСОКОЙ СТЕПЕНИ ЗЛОКАЧЕСТВЕННОСТИ

В. В. Чаговец[1] ✉, В. Г. Васильев[2], М. В. Юрова[1,3], Г. Н. Хабас[1], С. В. Павлович[1,3], Н. Л. Стародубцева[1], О. А. Майборода[4,5]

[1] Национальный медицинский исследовательский центр акушерства, гинекологии и перинатологии имени В. И. Кулакова, Москва, Россия

[2] Российский университет дружбы народов, Москва, Россия

[3] Первый Московский государственный медицинский университет имени И. М. Сеченова, Москва, Россия

[4] Медицинский центр Лейденского университета, Лейден, Нидерланды

[5] Томский государственный университет, Томск, Россия

Муцины — это высокомолекулярные гликопротеины, характерной чертой которых является большое количество О-связанных олигосахаридов (О-гликанов), присоединенных к белковому остову. Основная часть циркулирующих муцинов быстро выводится с помощью рецепторов печени, распознающих гликаны. Муцины, которые не выводятся из организма и остаются в кровотоке, наиболее часто используют в качестве клинических диагностических маркеров. Пептидный эпитоп одного из таких циркулирующих муцинов, называемого MUC16, известен как антиген CA125, маркер рака яичников. Целью работы было провести профилирование метаболитов плазмы с помощью 1H-ЯМР анализа и изучить связь между измеренными значениями CA125 и системным метаболизмом пациентов в группе с подтвержденным раком яичников высокой степени злокачественности. В результате исследования были обнаружены статистически значимые ассоциации между измеренными значениями эпитопа CA125 и концентрациями глюкозы, глутамина, аланина, бетаина и серина в плазме. Значимость выявленных ассоциаций для перечисленных соединений меньше 0,01. Это позволяет выдвинуть гипотезу о возможности включения метаболических показателей в диагностику рака яичников.

Ключевые слова: метаболомика, ЯМР, циркулирующие муцины, CA125, рак яичников

Финансирование: исследование выполнено за счет гранта Российского научного фонда (проект № 20-65-46014).

Вклад авторов: В. В. Чаговец — планирование исследования, подготовка образцов, обсуждение обработки данных ЯМР, написание и редактирование рукописи; В. Г. Васильев — пробоподготовка, ЯМР-анализ; М. В. Юрова, Г. Н. Хабас — сбор и характеристика клинических образцов, обсуждение результатов; С. В. Павлович — планирование исследования, обсуждение результатов; Н. Л. Стародубцева — планирование исследования, обработка клинических данных; О. А. Майборода — планирование исследования и руководство им, написание рукописи, обработка данных ЯМР.

Соблюдение этических стандартов: исследование одобрено этическим комитетом Национального медицинского исследовательского центра акушерства, гинекологии и перинатологии имени В. И. Кулакова (протокол № 10 от 05 декабря 2019 г.), проведено в соответствии с федеральными законами Российской Федерации (№№ 152, 323 и др.) и Хельсинкской декларацией 1964 г. со всеми последующими дополнениями и изменениями, регламентирующими научные исследования на биоматериалах, полученных от людей.

✉ **Для корреспонденции:** Виталий Викторович Чаговец
ул. Академика Опарина, д. 4, г. Москва, 117997, Россия; vvchagovets@gmail.com

Статья получена: 01.12.2021 **Статья принята к печати:** 16.12.2021 **Опубликована онлайн:** 29.12.2021

DOI: 10.24075/vrgmu.2021.065

Mucins are large glycoproteins characterized by the abundant O-linked oligosaccharides (O-glycans) clustered on a protein backbone. They are usually localized on the surface of the epithelium, but potential sites of proteolytic cleavage are found in most mucin genes, which explains their appearance in the systemic circulation [1]. Most of the circulating mucins are rapidly cleared by glycan-recognizing hepatic clearance receptors in the liver. Those which evade the clearance and remain in the circulation are the most frequently used as the clinical diagnostic markers. One of such circulating mucins is MUC16; its peptide epitope is known as the CA125 antigen, a marker of ovarian cancer [2].

CA125 has been known for over three decades [3]. A number of large-scale clinical studies have evaluated the potential use of serum CA125 as a marker of ovarian cancer (OC). While the structural identity of the epitope remains elusive and its practical value is being challenged from time to time [4], CA125 remains the only clinically reliable diagnostic marker of ovarian cancer [5]. Here, however, we are not going to question the diagnostic value of the CA125 epitope. We address a different question, namely to which extend the CA125 values can be associated with a metabolic status of the patients. Ever since Otto Warburg discovery of the tumor cells altered metabolism a view of the cancer as a metabolic disease is steadily gaining acceptance [6]. Indeed, there is strong evidence that increased glucose consumption and increased lactate secretion in tumors promote their growth [7]. As the tumor grows, so does its need for bioenergetic resources and structural blocks. This growing need changes the systemic metabolism, which can be seen in the patient's blood. Thus, we hypothesize that the measured values of the CA125, as a tumor marker, will have their correlates or “footprint” in the metabolic profile of plasma. To test this hypothesis, we applied targeted 1H-NMR profiling within a homogeneous selection of the patients with confirmed high-grade ovarian cancer. To find these correlates or associations, we applied an approach based on the multiple linear models adjusted for confounding variables (age and body mass index of a patient in our case).

METHODS

The study included 67 patients with histologically verified high-grade (HG) serous OC. They donated venous blood plasma samples immediately before the operation, before administration of antibacterial, analgesic and other drugs.

The inclusions criteria were: age over 18 years; histological verification of the diagnosis (HG serous OC, stage I–IV as per the FIGO (International Federation of Gynecology and Obstetrics) scale).

The non-inclusion criteria were: age below 18 years; 6 or more months of intake of hormonal drugs (combined oral contraceptives, hormone replacement therapy or menopausal therapy); US-confirmed pathology of pelvic organs and/or manifestations of the already diagnosed reproductive diseases; proliferative processes; active cancer at the time of the study or in history (any nosology other than the one studied); pelvic organ surgery; various histotype neoplasms in one patient; pregnancy.

The exclusion criteria were: histotype of the malignant ovarian tumor different from HG OC or concomitant thereto, as established through repeated examination of histological micropreparations; primary multiple neoplastic diseases not identified at the time the patient applied to the Center seeking assistance about ovarian oncoma (data on the presence thereof were obtained during the post-surgery observation).

The quantity of CA125 tumor marker in blood samples was established through the enzyme immunoassay analysis.

Preparation of samples for NMR analysis

All chemicals used in the buffers were purchased from Sigma-Aldrich (USA), with the exception of D_2O heavy water (Cortecnet; France) and 3-(trimethylsilyl) propionic-2,2,3,3-d4 acid sodium salt (TSP) (Cambridge Isotope Laboratories Inc., UK). We made two buffer solutions. Buffer A was a sodium phosphate buffer in H_2O/D_2O (80/20) with pH 7.4, containing 6.15 mmol/L NaN3 and 4.64 mmol/L TSP. Buffer B was a sodium phosphate buffer in D_2O (pH 7.4), containing 1.5 mol/L K_2HPO_4, 2 mmol/L NaN3, and 4 mmol/L TSP. Ritter Deepwell 96-well plates were purchased from Novaveth BV (Netherlands), NMR tubes from Bruker Biospin Ltd (Germany). The plasma samples were thawed at 4 °C and mixed through 10 rotations of the tubes. After that, samples (120 µl) were mixed with 120 µl of buffer solution. For each sample, 190 µl of buffer and plasma mixture were transferred to 5 mm tubes with the help of a modified Gilson 215 tube filling station, and then kept at 6 °C in the sample changer.

NMR analysis and spectral data processing

1H NMR data were collected using a Bruker 700 MHz AVANCE NEO spectrometer equipped with a 5 mm Prodigy cryogenic probe head. A Bruker sample changer (Bruker; Germany) was used to feed and retrieve samples (according to the two NMR protocols: one for plasma samples and one for all other samples).

All experiments were recorded at 310 K. A fresh sample of 99.8% methanol-d4 enabled temperature calibration. Axial shimming was automatically optimized before each measurement. Duration of 90° pulses was automatically calibrated for each individual sample using a homonuclear-gated mutation experiment on the locked and shimmed samples after automatic tuning and matching of the probe head. For each plasma sample a Purcell–Meiboom–Gill (CPMG) experiment was recorded. A standard 1D CPMG pulse sequence with presaturation was used to for the acquisition of T2-filtered spectra. A pulse train of 128 refocusing pulses with individual spin echo delays of 0.6 ms was applied resulting in a total T2 filtering delay of 78 ms. After applying 4 dummy scans, a total of 73,728 data points covering a spectral width of 12,019 Hz were collected.

Identification and quantification of metabolites

Metabolites were identified by searching the full 1D and 2D JRES data using the proprietary Bbiorefcode (Bruker Biospin Ltd; Germany).

Table 1. Age and BMI of the patients with I–II and III–IV stages of HG OC (no statistically significant differences found; the method used is the Mann–Whitney U-test)

HGOC stage	Age, years		*p*	BMI, kg/m^2		*p*
	Me	Q_1–Q_3		Me	Q_1–Q_3	
I–II	53	46–59	0.51	24	21–27	0.65
III–IV	54	49–61		25	23–28	

The quantification of metabolites in blood samples was semi-automatic and relied on the Chenomx NMR Suite 9.0 software (Chenomx Inc; Canada). The results of this semi-automatic quantification were processed manually. The concentrations were calculated based on the known TSP concentration (0.4 mmol/L).

Data analysis

All data were analyzed in the R software environment (http://www.r-project.org/, versions R 4.1.1, 4.1.2). The initial processing of the data tables relied on the tidyverse (version 1.3.1) and readxl (1.3.1) packages. Ggplot2 (version 3.3.5) and ggforestplot (version 0.1.0) enabled visualization of the results.

RESULTS

The sample included 67 patients, of which 11 patients had stage I or II UG OC and 56 patients — stage III or IV HG OC. The patients were comparable by age and body mass index (BMI; Table 1). The median age of patients was 53 (46; 59) years and 54 (49; 61) years, which is comparable with the data of population studies [8]. The median BMIs of the patients were 24 (21; 27) kg/m^2 and 25 (23; 28) kg/m^2.

Figure 1 shows a histogram of CA125 levels in the studied sample in the original (A) and logarithmic scales (B). The distribution based on raw values is strongly shifted to the right (median 200 U/ml, mean 742.2 U/ml). Thus, to remain within the basic assumptions of the linear models, we further used the log-transformed values of the CA125.

To get an overview of the plasma metabolites, we used a targeted 1H-NMR profiling and quantified 33 metabolites. Table 2 summarizes their medians and interquartile range values. To expand the set of parameters related to the metabolic status of patients, a set of physiologically meaningful ratios was added to the data set. Those ratios could be useful for getting insight into the amino acids metabolism and enzymatic interconversions (e.g., alanine/glutamine), gluconeogenesis (e.g., alanine/citrate), and ketogenesis (e.g., acetate/acetoacetate).

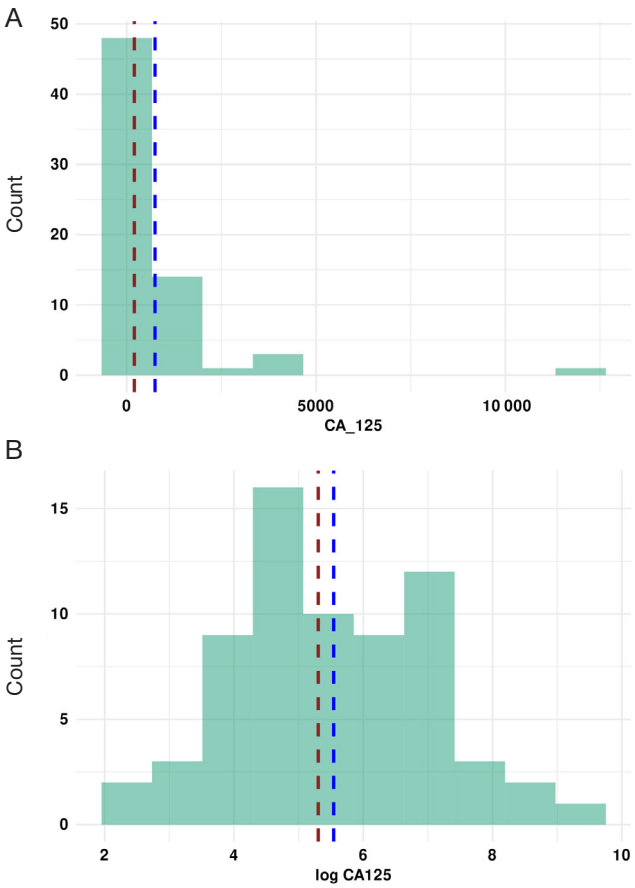

Fig. 1. CA125 levels histogram. **A**. baseline and logarithmic levels. **B**. The dark red line indicates the median and the blue line indicates the mean of the distribution

All the calculated ratios, their medians and interquartile rangeare summarized in the Table 3.

We used the linear regression models to study the relationships between metabolites and their correlations: the metabolites were used as the dependent variable and CA125

Table 2. List of quantified metabolites in plasma of patients with HG OC. The values are given as median/interquartile range and rounded to the nearest whole number

Metabolite	Concentrations (μM) Median (IQR)	Metabolite	Concentrations (μM) Median (IQR)
2-Aminobutyrate	41 (27.55)	Glutamine	310 (241.407)
2-Hydroxybutyrate	104 (81.127)	Glycine	149 (106.229)
2-Oxoglutarate	30 (18.48)	Isoleucine	45 (31.64)
3-Hydroxybutyrate	206 (122.460)	Isopropanol	10 (7.18)
Acetate	21 (15.28)	Lactate	1191 (817.2000)
Acetoacetate	107 (55.199)	Leucine	125 (84.150)
Acetone	103 (58.177)	Lysine	91 (62.115)
Alanine	185 (114.251)	Methanol	50 (35.63)
Arginine	89 (65.130)	Pyruvate	41 (30.57)
Betaine	71 (50.97)	Serine	119 (89.155)
Citrate	38 (29.59)	Succinate	24 (6.53)
Creatine	33 (20.46)	Threonine	141 (112.190)
Creatinine	40 (29.48)	TMAO	45 (30.57)
Ethanol	35 (30.49)	Tyrosine	42 (28.57)
Formate	27 (20.35)	Valine	168 (108.201)
Glucose	3052 (2080.4199)	Myolnositol	60 (45.82)
Glutamate	111 (81.156)		

Note: IQR — Interquartile Range.

Table 3. Summary of the calculated metabolite relationships. The values are given as median/interquartile range

Ratio	Median (IQR)	Ratio	Median (IQR)
Ala/Gln	0.58 (0.45, 0.67)	Glc/Cit	80 (42, 128)
Ala/Leu	1.54 (1.19, 1.94)	Gln/Cit	9.7 (4.5, 13.8)
Ala/Ile	3.98 (2.99, 5.08)	Glc/Pyr	65 (49, 125)
Ala/Tyr	4.23 (3.51, 5.03)	Gln/Glc	0.102 (0.090, 0.120)
Ala/Val	1.11 (0.90, 1.39)	Gln/Pyr	7 (5, 12)
Gln/Leu	2.77 (2.24, 3.24)	Lac/Ala	6.53 (5.27, 9.01)
Gln/Ile	7.10 (5.58, 8.47)	Lac/Cit	32 (16, 55)
Gln/Tyr	7.51 (6.34, 9.85)	Lac/Glc	0.38 (0.31, 0.53)
Gln/Val	2.06 (1.68, 2.38)	Lac/Gln	3.92 (3.02, 5.27)
Ile/Leu	0.38 (0.32, 0.46)	Lac/Pyr	27 (18, 46)
Ile/Tyr	1.08 (0.87, 1.40)	Pyr/Cit	0.90 (0.58, 1.36)
Ile/Val	0.29 (0.25, 0.35)	AcO/AcAcO	0.23 (0.12, 0.32)
Leu/Tyr	2.71 (2.25, 3.21)	n3_HBut/AcAcO	2.43 (1.84, 2.97)
Leu/Val	0.74 (0.69, 0.84)	n3_HBut/AcO	11 (6, 19)
Tyr/Val	0.27 (0.23, 0.33)	Ile/Glc	0.014 (0.012, 0.017)
Ala/Cit	4.61 (2.27, 7.95)	Leu/Glc	0.036 (0.032, 0.045)
Ala/Pyr	3.9 (2.6, 7.5)	Val/Glc	0.048 (0.043, 0.057)
Ala/Glc	0.057 (0.049, 0.070)	Gln/Glu	2.93 (2.41, 3.46)

Note: Ala/Gln — alanine/glutamine, Ala/Leu — alanine/leucine, Ala/Ile — alanine/isoleucine, Ala/Tyr — alanine/tyrosine, Ala/Val — alanine/valine, Gln/Leu —glutamine/leucine — glutamine/leucine/tyrosine, Gln/Val — glutamine/valine, Ile/Leu — isoleucine/leucine, Ile/Tyr — isoleucine/tyrosine, Ile/Val — isoleucine/valine, Leu/Tyr — leucine/tyrosine, Leu/Val — leucine/valine, Tyr/Val — tyrosine/valine, Ala/Pyr — alanine/pyruvate, Ala/Glc — alanine/glucose, Glc/Cit — glucose/citrate, Gln/Cit — glutamine/citrate, Glc/Pyr — glucose/pyruvate, Gln/Glc — glutamine/glucose, Gln/Pyr — glutamine/ pyruvate, Lac/Ala — lactate/alanine, Lac/Cit — lactate/citrate, Lac/Glc — lactate/glucose, Lac/Gln — lactate/glutamine, Lac/Pyr — lactate/pyruvate, Pyr/Cit — pyruvate/citrate, AcO/AcAcO — acetate/acetoacetic acid, n3_Hbut/AcAcO — n3_Hydroxybutyrate/acetoacetic acid, n3_Hbut/AcO — n3_Hydroxyglucine/acetate, Ile/Glc — isoleucine/glucose, Leu/Glc — leucine/glucose, Val/Glc — valine/glucose, Gln/Glu — glutamine/glutamate.

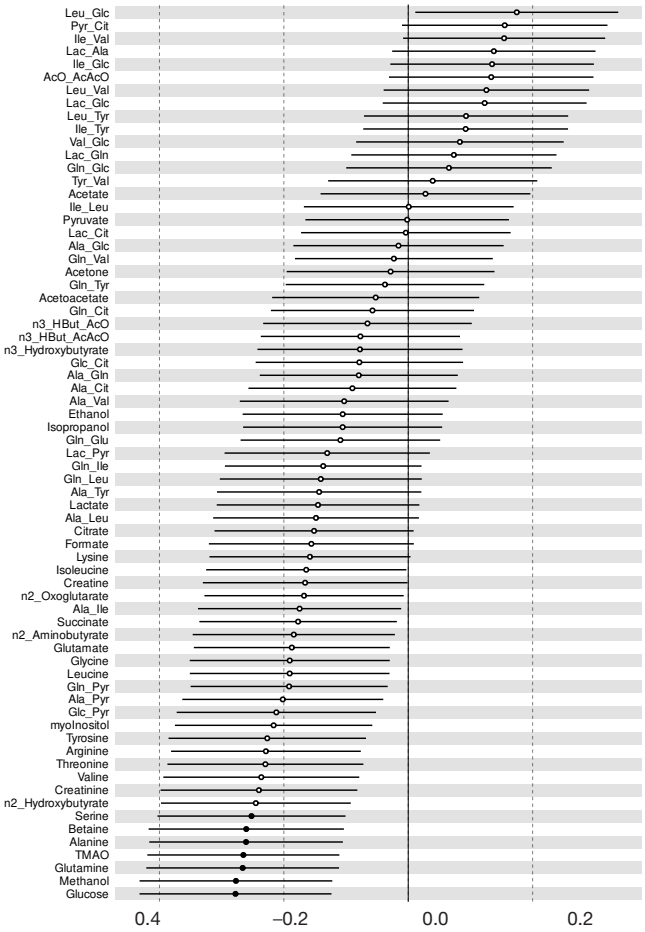

Fig. 2. Forest diagram summarizing all calculated regression models. The models are sorted by their standardized ratios (*x*-axis). Statistically significant (after adjustment for multiple testing) models are highlighted (*filled dots*)

Table 4. Summary of the regression models shown in Figure 3

Outcome	St. β (SE)	F-statistic	Adjusted R2	Pr (> Chi)
Glucose	–0.277 (0.078)	4.483	0.137	0.0008
Methanol	–0.277 (0.079)	4.267	0.129	0.0008
Glutamine	–0.266 (0.079)	4.261	0.129	0.001
TMAO	–0.265 (0.078)	4.456	0.136	0.001
Alanine	–0.261 (0.079)	4.036	0.121	0.002
Betaine	–0.260 (0.080)	3.606	0.106	0.002
Serine	–0.252 (0.077)	5.548	0.171	0.002

Note: St. β St. — standardized β.

as a predictor. To correct for the known confounding factors, we added age and BMI as the model terms. All the values were scaled to enable a direct comparison of the magnitude of associations between all metabolites and their relationships. Figure 2 shows a summary of all the models. The data sorting criterium is the standardized coefficient values (descending). Filled dots correspond to the statistically significant models (correction for multiple hypothesis testing was factored in for the statistical significance *p*). The model characteristics for each significant association are given in Table 4 and Fig. 3.

DISCUSSION

The main goal of this study is to explore the associations between the measured values of CA125 and concentrations of plasma metabolites within a homogeneous group of the patients with clinically confirmed high grade ovarian cancer. The results indicate that CA125 levels are inversely associated with several plasma metabolites (see Fig. 2). Of all the associations, only the presence of methanol could raise questions. Nevertheless, methanol is a normal component of human plasma [9]. Its origin is mostly dietary (consumption of fresh fruits and fermented drinks); intestinal microflora also contributes to its generation. Under normal conditions, such low or "physiological" methanol concentrations are metabolized in the liver [10]. The negative association between methanol and CA125 appears to be contra intuitive, but changes in the patients' dietary habits and decreased microbiota activity at the late stages of cancer may explain this observation. The significant negative relationship between CA125 and trimethylamine oxide, which is often interpreted as a microbiota-specific metabolite [11], serves as an additional argument in favor of the microbiotic origin of methanol. All other significant associations (glucose, glutamine, alanine, betaine, and serine) are in agreement with the changes in the systemic metabolism at the advanced stages of malignancy. While the phenomenon of glucose and amino acids (especially glutamine and alanine) depletion in the body fluids of the cancer patients

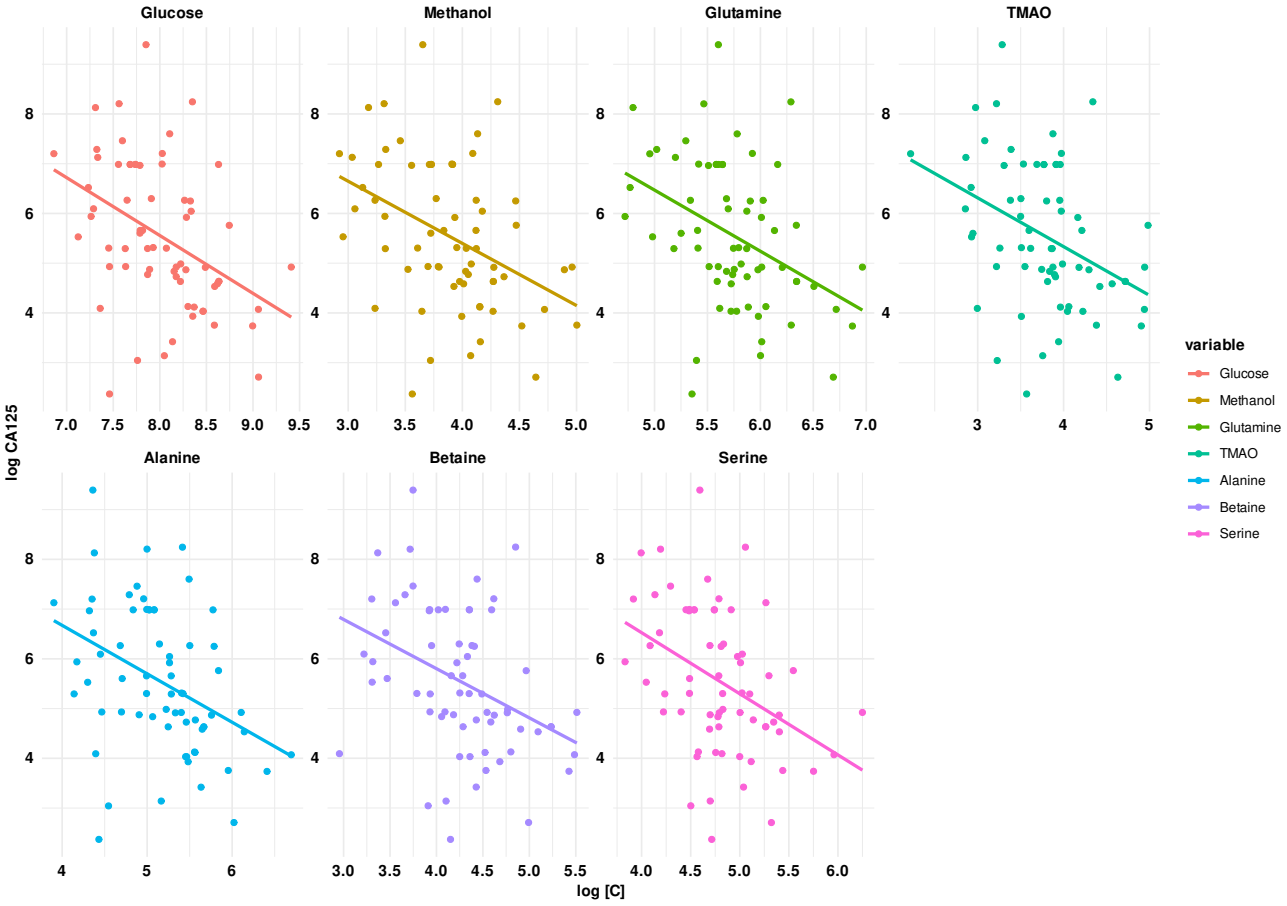

Fig. 3. Scatter plots with regression lines illustrating statistically significant dependences of CA125 on metabolite concentrations

has been reported many times, the detailed physiological mechanism of the effect remain unexplored. The decrease of alanine with a progression of malignancy cloud be explained by its increased utilization as a major gluconeogenic precursor, to meet the high glucose consumption by the tumor cells [12]. A decrease in the level of glutamine may be associated with more active glutaminolysis, which is required to provide precursors for the synthesis of nucleic acids [12,13]. There is no simple mechanistic explanation for the role of betaine in the physiology of malignant neoplasms. However, a recent meta-analysis has shown that betaine levels reduce the risk of cancer [14]. Indeed, as the main donor of the methyl group in the conversion of homocysteine to methionine, betaine plays a significant role in pathologies associated with altered systemic metabolism of homocysteine, folic acid, and B vitamins. Cancer, or more specifically ovarian cancer is just one of them.

Yet, looking into the model metrics for the each association (Table 4, Fig. 3) we cannot ignore the fact that despite being significant the models cover only between 10 and 15% of the variance in the data (adjusted R2). Such “noisy” models are revealing the main weakness of our study, namely a rather limited pool of the patients. Another possible source of the noise is unaccounted confounding factors. In fact, while for all patients included in the current report the samples were collected before initiation of the treatment, there is no realistic way to control their dietary history and the history of medicament use before the admission.

CONCLUSIONS

The study allowed identifying statistically significant associations between the measured (log) values of CA125 epitope and the plasma concentrations of a number of metabolites. Showing a link between the CA125 plasma values and metabolic composition of the plasma we for the first time describe a metabolic “footprint” of the circulated mucins. This, in its turn, allows suggesting inclusion of metabolic indicators into the CA125-based OC progress assessment.

Since CA125 discovery our understanding of ovarian cancer biology has changed to the point that these tumors are classified not only by histological attributes, but also (and mainly) on the basis their molecular phenotype. Thus, the gradual integration of metabolic parameters into the list of diagnostic methods used for stage I–IV OC is only logical.

References

1. Hollingsworth MA, Swanson BJ. Mucins in cancer: protection and control of the cell surface. Nat Rev Cancer. 2004; 4 (1): 45–60. DOI: 10.1038/NRC1251.
2. Yin BWT, Dnistrian A, Lloyd KO. Ovarian cancer antigen CA125 is encoded by the MUC16 mucin gene. Int J cancer. 2002; 98 (5): 737–40. DOI: 10.1002/IJC.10250.
3. Devine PL, McGuckin MA, Ward BG. Circulating mucins as tumor markers in ovarian cancer (review). Anticancer Res. 1992; 12 (3): 709–17. Accessed November 27, 2021. Available from: https://www.researchgate.net/publication/21533861_Circulating_mucins_as_tumor_markers_in_ovarian_cancer_Review.
4. Pavlovich SV, Yurova MV, Melkumyan AG, Frankevich VE, Chagovets VV, Khabas GN. Biomarkers in ovarian neoplasms: opportunities, limitations, and prospects for using in reproductive-aged women. Akush Ginekol (Sofiia). 2019; 11 (2019): 65–73. DOI: 10.18565/aig.2019.11.65–73.
5. Felder M, Kapur A, Gonzalez-Bosquet J, et al. MUC16 (CA125): tumor biomarker to cancer therapy, a work in progress. Mol Cancer. 2014; 13 (1): 1–15. DOI: 10.1186/1476-4598-13-129.
6. Seyfried TN, Flores RE, Poff AM, D’Agostino DP. Cancer as a metabolic disease: implications for novel therapeutics. Carcinogenesis. 2014; 35 (3): 515. DOI:10.1093/CARCIN/BGT480.
7. Coller HA. Is Cancer a Metabolic Disease? Am J Pathol. 2014; 184 (1): 4. DOI:10.1016/J.AJPATH.2013.07.035.
8. Kaprin AD, Starinskij VV, Shahzadova AO, redaktory. Sostojanie onkologicheskoj pomoshhi naseleniju Rossii v 2019 godu. M.: MNIOI im. P. A. Gercena — filial FGBU «NMIC radiologii», 2020; 239 s. Russian.
9. Psychogios N, Hau DD, Peng J, et al. The Human Serum Metabolome. PLoS One. 2011; 6 (2): e16957. DOI: 10.1371/JOURNAL.PONE.0016957.
10. Dorokhov YL, Shindyapina AV, Sheshukova EV, Komarova TV. Metabolic methanol: molecular pathways and physiological roles. Physiol Rev. 2015; 95 (2): 603–44. DOI: 10.1152/PHYSREV.00034.2014.
11. Tang WHW, Wang Z, Kennedy DJ, et al. Gut microbiota-dependent trimethylamine N-oxide (TMAO) pathway contributes to both development of renal insufficiency and mortality risk in chronic kidney disease. Circ Res. 2015; 116 (3): 448–55. DOI: 10.1161/CIRCRESAHA.116.305360.
12. Lai HS, Lee JC, Lee PH, Wang ST, Chen WJ. Plasma free amino acid profile in cancer patients. Semin Cancer Biol. 2005; 15 (4): 267–76. DOI: 10.1016/J.SEMCANCER.2005.04.003.
13. Altman BJ, Stine ZE, Dang CV. From Krebs to clinic: glutamine metabolism to cancer therapy. Nat Rev Cancer. 2016; 16 (10): 619–34. DOI: 10.1038/NRC.2016.71.
14. Youn J, Cho E, Lee JE. Association of choline and betaine levels with cancer incidence and survival: A meta-analysis. Clin Nutr. 2019; 38 (1): 100–09. DOI: 10.1016/J.CLNU.2018.01.042.

Литература

1. Hollingsworth MA, Swanson BJ. Mucins in cancer: protection and control of the cell surface. Nat Rev Cancer. 2004; 4 (1): 45–60. DOI: 10.1038/NRC1251.
2. Yin BWT, Dnistrian A, Lloyd KO. Ovarian cancer antigen CA125 is encoded by the MUC16 mucin gene. Int J cancer. 2002; 98 (5): 737–40. DOI: 10.1002/IJC.10250.
3. Devine PL, McGuckin MA, Ward BG. Circulating mucins as tumor markers in ovarian cancer (review). Anticancer Res. 1992; 12 (3): 709–17. Accessed November 27, 2021. Available from: https://www.researchgate.net/publication/21533861_Circulating_mucins_as_tumor_markers_in_ovarian_cancer_Review.
4. Pavlovich SV, Yurova MV, Melkumyan AG, Frankevich VE, Chagovets VV, Khabas GN. Biomarkers in ovarian neoplasms: opportunities, limitations, and prospects for using in reproductive-aged women. Akush Ginekol (Sofiia). 2019; 11 (2019): 65–73. DOI: 10.18565/aig.2019.11.65–73.
5. Felder M, Kapur A, Gonzalez-Bosquet J, et al. MUC16 (CA125): tumor biomarker to cancer therapy, a work in progress. Mol Cancer. 2014; 13 (1): 1–15. DOI: 10.1186/1476-4598-13-129.
6. Seyfried TN, Flores RE, Poff AM, D’Agostino DP. Cancer as a metabolic disease: implications for novel therapeutics. Carcinogenesis. 2014; 35 (3): 515. DOI:10.1093/CARCIN/BGT480.
7. Coller HA. Is Cancer a Metabolic Disease? Am J Pathol. 2014; 184 (1): 4. DOI:10.1016/J.AJPATH.2013.07.035.
8. Каприн А. Д., Старинский В. В., Шахзадова А. О., редакторы. Состояние онкологической помощи населению России в 2019 году. М.: МНИОИ им. П. А. Герцена — филиал ФГБУ «НМИЦ радиологии», 2020; 239 с.

9. Psychogios N, Hau DD, Peng J, et al. The Human Serum Metabolome. PLoS One. 2011; 6 (2): e16957. DOI: 10.1371/JOURNAL.PONE.0016957.
10. Dorokhov YL, Shindyapina AV, Sheshukova EV, Komarova TV. Metabolic methanol: molecular pathways and physiological roles. Physiol Rev. 2015; 95 (2): 603–44. DOI: 10.1152/PHYSREV.00034.2014.
11. Tang WHW, Wang Z, Kennedy DJ, et al. Gut microbiota-dependent trimethylamine N-oxide (TMAO) pathway contributes to both development of renal insufficiency and mortality risk in chronic kidney disease. Circ Res. 2015; 116 (3): 448–55. DOI: 10.1161/CIRCRESAHA.116.305360.
12. Lai HS, Lee JC, Lee PH, Wang ST, Chen WJ. Plasma free amino acid profile in cancer patients. Semin Cancer Biol. 2005; 15 (4): 267–76. DOI: 10.1016/J.SEMCANCER.2005.04.003.
13. Altman BJ, Stine ZE, Dang CV. From Krebs to clinic: glutamine metabolism to cancer therapy. Nat Rev Cancer. 2016; 16 (10): 619–34. DOI: 10.1038/NRC.2016.71.
14. Youn J, Cho E, Lee JE. Association of choline and betaine levels with cancer incidence and survival: A meta-analysis. Clin Nutr. 2019; 38 (1): 100–09. DOI: 10.1016/J.CLNU.2018.01.042.

SIGNIFICANCE OF ANALYSIS OF LIPID EXTRACTS IN CERVICAL CANAL SECRETION FOR DIAGNOSING OF PLACENTA-ASSOCIATED COMPLICATIONS OF PREGNANCY

Lomova NA ✉, Chagovets VV, Tokareva AO, Dolgopolova EL, Karapetyan TE, Magomedova AP, Shmakov RG

Kulakov National Medical Research Center for Obstetrics, Gynecology and Perinatology, Moscow, Russia

Omics technologies hold great potential as the basis for development of the new diagnostic approaches in obstetrics. Cervicovaginal fluid (CVF) as part of the mother-placenta-fetus system can be used to diagnose obstetric complications. This study aimed to identify the features of lipid composition of the cervical canal secretion peculiar to Intrauterine Growth Restriction (IUGR) and preeclampsia (PE). We took CVF samples from 57 pregnant women and subjected them to an in-depth clinical-anamnestic and mass-spectrometric analysis. Lipid extracts of CVF were analyzed with a liquid chromatography system coupled with a mass analyzer. As a result, we identified 239 lipid compounds. In case of 17 lipids, mathematical analysis revealed significant differences between samples from women with normal pregnancy indicator values (normal group) and patients from the IUGR group ($p < 0.05$). As for the normal group and PE group patients, there were significant differences identified for 3 lipids ($p < 0.05$). Comparison of samples from the PE and IUGR groups yielded statistically significant differences in levels of two lipids ($p < 0.05$). Mainly, the lipids were oxylipins, sphingomyelins, triglycerides, and cardiolipins. The developed diagnostic model had the sensitivity of 0.81 and specificity of 0.91 (cut-off level — 0.50; AUC — 0.85). The data obtained are valuable in the context of development of the new methods of diagnosing placenta-associated complications of pregnancy and for understanding new mechanisms of pathogenesis of these complications.

Keywords: prodnostic value, non-invasive diagnostics, preeclampsia, intrauterine growth restriction, lipidomics

Funding: the study was supported through the state assignment of the Ministry of Health of the Russian Federation [State registration number AAAA-A18-118053190026-6].

Acknowledgements: the authors are grateful to Dr. V. E. Frankevich, Head of the Department of Systems Biology in Reproduction of the V. I. Kulakov National Medical Research Center for Obstetrics, Gynecology and Perinatology, for his help in organization of the study, systematic analysis and manuscript editing.

Author contribution: Lomova NA — analysis of clinical data, systematic analysis, manuscript authoring; Chagovets VV — metabolic analysis (mass spectrometry), statistical analysis of the data obtained, manuscript editing; Tokareva AO — metabolic analysis (mass spectrometry), mass spectrometry data processing; Dolgopolova EL — collection and preparation of biological fluids, statistical analysis of the results; Karapetyan TE — analysis of clinical data, statistical analysis of the results; Magomedova AP — collection and preparation of biological fluids; Shmakov RG — analysis of clinical data, systematic analysis, manuscript editing.

Compliance with ethical standards: the study was approved by the ethical committee of Kulakov National Medical Research Center for Obstetrics, Gynecology and Perinatology (Minutes #11 of November 11, 2021), conducted in accordance with the requirements of the Declaration of Helsinki, International Conference on Harmonization (ICH), Standards of Good Clinical Practice (GCP), Federal Law "On the Basics of Health Protection of Citizens in the Russian Federation"; all patients signed a voluntary informed consent to participate in the study.

✉ **Correspondence should be addressed:** Natalya A. Lomova
Akademika Oparina, 4, Moscow, 117997, Russia; natasha-lomova@yandex.ru

Received: 23.11.2021 **Accepted:** 20.12.2021 **Published online:** 29.12.2021

DOI: 10.24075/brsmu.2021.066

ЗНАЧИМОСТЬ АНАЛИЗА ЛИПИДНЫХ ЭКСТРАКТОВ ИЗ ОТДЕЛЯЕМОГО ЦЕРВИКАЛЬНОГО КАНАЛА ДЛЯ ДИАГНОСТИКИ ПЛАЦЕНТА-АССОЦИИРОВАННЫХ ОСЛОЖНЕНИЙ БЕРЕМЕННОСТИ

Н. А. Ломова ✉, В. В. Чаговец, А. О. Токарева, Е. Л. Долгополова, Т. Э. Карапетян, А. П. Магомедова, Р. Г. Шмаков

Национальный медицинский исследовательский центр акушерства, гинекологии и перинатологии имени В. И. Кулакова, Москва, Россия

Использование омиксных технологий имеет на сегодняшний день большой потенциал для разработки новых диагностических подходов в акушерстве. Цервико-вагинальная жидкость (ЦВЖ) как часть системы «мать–плацента–плод» может быть использована для диагностики акушерских осложнений. Целью исследования было выявить особенности липидного состава отделяемого цервикального канала у беременных с задержкой роста плода и преэклампсией. Выполнен углубленный клинико-анамнестический и масс-спектрометрический анализ ЦВЖ, полученный от 57 беременных женщин. Липидные экстракты ЦВЖ анализировали на жидкостном хроматографе, соединенном с масс-анализатором. В результате исследования идентифицировано 239 соединений липидов. Математический анализ выявил значимые различия между пациентками группы нормы и с задержкой развития плода (ЗРП) для 17 липидов ($p < 0,05$). Между пациентками группы нормы и преэклампсии (ПЭ) значимые различия были обнаружены для трех липидов ($p < 0,05$). Между пациентками с ПЭ и пациентками с ЗРП статистически значимая разница в уровнях была выявлена для двух липидов ($p < 0,05$). Показано, что липиды относились преимущественно к классам оксилипидов, сфингомиелинов, триглицеридов и кардиолипинов. При построении диагностической модели достигнута чувствительность 0,81 и специфичность 0,91 (порог отсечки — 0,50; AUC — 0,85). Полученные данные перспективны для разработки методов диагностики плацента-ассоциированных осложнений беременности и понимания новых механизмов патогенеза данных осложнений.

Ключевые слова: прогностическая значимость, неинвазивная диагностика, преэклампсия, задержка роста плода, липидомика

Финансирование: исследование выполнено при поддержке государственного задания Министерства здравоохранения Российской Федерации [Государственный регистрационный номер. АААА-А18-118053190026-6].

Благодарности: авторы выражают особую благодарность д.ф.-м.н., руководителю отдела системной биологии в репродукции Национального медицинского исследовательского центра акушерства, гинекологии и перинатологии имени В. И. Кулакова В. Е. Франкевичу за помощь в подготовке исследования, систематическом анализе и редактировании рукописи.

Вклад авторов: Н. А. Ломова — анализ клинических данных, систематический анализ, написание рукописи; В. В. Чаговец — проведение метаболомного анализа методом масс-спектрометрии, статистический анализ полученных данных, редактирование рукописи; А. О. Токарева — проведение метаболомного анализа методом масс-спектрометрии, обработка масс-спектрометрических данных; Е. Л. Долгополова — сбор и подготовка биологических сред, статистический анализ результатов; Т. Э. Карапетян — анализ клинических данных, статистический анализ результатов; А. П. Магомедова — сбор и подготовка биологических сред; Р. Г. Шмаков — анализ клинических данных, систематический анализ, редактирование рукописи.

Соблюдение этических стандартов: исследование одобрено этическим комитетом НЦАГиП им. В. И. Кулакова (протокол № 11 от 11 ноября 2021 г.), проведено в соответствии с требованиями Хельсинкской декларации, Международной конференции по гармонизации (ICF), Стандартами надлежащей клинической практики (GCP), ФЗ «Об основах охраны здоровья граждан в Российской Федерации»; все пациентки подписали добровольное информированное согласие на участие в исследовании.

✉ **Для корреспонденции:** Наталья Анатольевна Ломова
ул. Академика Опарина, д. 4, г. Москва, 117997; natasha-lomova@yandex.ru

Статья получена: 23.11.2021 **Статья принята к печати:** 20.12.2021 **Опубликована онлайн:** 29.12.2021

DOI: 10.24075/vrgmu.2021.066

It has earlier been established that such common complications of pregnancy as Intrauterine Growth Restriction (IUGR) and preeclampsia (PE) are associated with placental dysfunction. With these pathologies, metabolic and circulatory systems fail to adapt to changes caused by pregnancy, which leads to hypertension and impaired placental blood flow. This not only causes undesirable consequences for the health of the mother and child during gestation, but can also affect their future health. In recent years, 10 to 20% of pregnancies in the economically developed countries have been complicated by some form of hypertension [1]. Preeclampsia is a pregnancy complication that occurs in the placenta and negatively affects both the mother and the fetus. PE is diagnosed in 5–7% of pregnant women worldwide [2]. This condition can develop after 20th week of pregnancy; its manifestations are hypertension, proteinuria and edema. Subsequently, it causes fetal distress and diminishes the chances of positive pregnancy outcome. IUGR prevents the fetus from realizing its growth potential in full: the weight and the body mass index (BMI) of the newborn are abnormal for the respective number of gestational weeks. About 4–8% of newborns are diagnosed with IUGR in industrialized countries, and in the developing countries this figure ranges from 6 to 30% [3, 4]. The causes of IUGR are distinguished into internal, peculiar to the fetus or placenta, and external, the mother-side factors affecting mainly the placenta and the fetus. There are also combinations of internal and external IUGR causes.

To date, there have not been developed adequate methods of prediction of these pregnancy complications, which obviously necessitates development of non-invasive and objective methods of prenatal diagnostics and monitoring.

Today, post-genomic omics technologies, including metabolomics and lipidomics, are growing rapidly and become more and more common in the routine clinical practice. With regard to the pathologies considered in this work, significant changes in the levels of metabolites were found even before preeclampsia manifested clinically, and these changes increase with the progression of the disorder [5–7]. Metabolomics can help detect the specific features of these conditions at the molecular level and aid in identification of the biological mechanisms underlying them, as well as in discovery of the new biomarkers. Metabolomics also offers a unique set of tools enabling identification of various endotypes of pathological conditions [7, 8] and diagnosing of different complications of pregnancy. Similar observations have been made for IUGR [9]. In the aforementioned works, researchers analyzed blood metabolome. Blood sampling is an invasive method of obtaining biological material. This study discusses the possibility of using cervical canal secretion to make PE or IUGR development prediction non-invasive.

Currently, the search for non-invasive and minimally invasive diagnostic markers in obstetrics is a promising area of scientific research. Cervical canal is one of the potential loci for minimally invasive sampling of biological material. There have been described potential biomarkers of spontaneous preterm labor that were identified through targeted proteomic analysis of cervicovaginal fluid samples from asymptomatic high-risk women. The proteins in cervicovaginal fluid of patients that experienced spontaneous preterm labor are extracellular matrix proteins that can also regulate the physiology of cell membranes [10]. In 2020, a statistically significant difference in the level of cytokines from cervicovaginal fluid samples, especially IL6 and IL17α, was found in the group of women with preterm labor and premature rupture of the membranes in the history. These indicators may be more accurate prognostic markers of preterm labor than fetal fibronectin that is the standard indicator relied on in clinical practice today [11]. During pregnancy, dysbiosis of the vaginal microbiota directly affects metabolic profiles, which can trigger premature birth. In 2020, researchers used nuclear magnetic resonance spectroscopy to analyze metabolic profile of cervicovaginal fluid and identified metabolic markers that can help predict preterm labor. The assessment of the ROC curve showed that acetone, ethylene glycol, formate, glycolate, isopropanol, methanol, and trimethylamine oxide were the best in the matter of predicting preterm labor. These metabolites can be useful markers clinically and for prognosis of preterm labor [12]. Thus, to date, it has been proven that the cervicovaginal fluid, which is part of the mother-placenta-fetus system, contains a number of biologically active components that can potentially be used for predicting and diagnosing obstetric pathology.

There is a wide range of methods applied to identify and validate biomarkers in metabolomic studies: ultraviolet and infrared spectroscopy, nuclear magnetic resonance spectroscopy, electrophoresis. However, the most common are metabolomic platforms based on liquid chromatography with mass spectrometric detection (LC-MS).

Metabolomics as part of studies of obstetric syndromes associated with placental insufficiency (PE and IUGR) can greatly facilitate understanding of the pathogenesis of these complications of pregnancy and development of new diagnostic and prognostic approaches.

The purpose of the study was to search for differences in the lipids of cervical canal secretion of patients with normal pregnancy and patients with fetal growth retardation and preeclampsia, as well as to develop mathematical models based on the differences found with the aim to create non-invasive methods for antenatal diagnosis of PE and IUGR .

METHODS

This was a case-control study conducted at the Kulakov National Medical Research Center for Obstetrics, Gynecology and Perinatology (Russia) from January to December 2020. The study involved 57 pregnant women, observed and helped to deliver within the study timeframe in the Center. The women were divided into three groups: Group I — 18 patients with preeclampsia, Group II — 19 patients with IUGR , Group III — 20 pregnant women without these complications, conditionally healthy (control group). Group I inclusion criteria: SBP ≥ 140 mmHg and/or DBP ≥ 90 mmHg after 20th week of pregnancy regardless of the history of blood pressure, in combination with proteinuria ≥ 0.3 g per day or ≥ 0.3 g/l in two portions of urine taken 6 hours apart. Group II inclusion criteria: IUGR diagnosed through a ultrasound study, if there was a slowdown in the rate of increase of the estimated fetal weight (EFW) and/or abdominal circumference (AC) < 10^{th} percentile, in combination with pathological blood flow as shown with Doppler ultrasonography or EFW and/or AC values < 3^{rd} percentile. Exclusion criteria: multiple pregnancy, cervical pathology, diabetes mellitus, impaired renal function, chronic arterial hypertension, oncological and infectious-inflammatory diseases during this pregnancy. This study did not include the cases of combined PE and IUGR. All patients delivered by caesarean section.

Collection and preparation of samples

On the day of admission to the Center, all pregnant women included in the study had their cervicovaginal secretion sampled before vaginal examination. To detect any infectious

Table 1. Clinical characteristics of the groups

Parameter	Descriptive parameter statistics			Statistical significance of differences in parameters in pairwise comparison of groups (*p*-value)		
	PE (*n* =18)	IUGR (*n* =19)	Normal (*n* = 20)	PE–Normal	IUGR–Normal	PE–UGR
Age, years	31 ± 5	34 ± 8	31 ± 5	0,769	0,21	0,331
BMI	28 ± 4	23 ± 4	27 ± 3	0,666	0,005	0,0045
Delivery time, weeks	36 ± 3	37 ± 3,1	40 ± 1	< 0,001	< 0,001	0,342
Birth height, cm	46,6 ± 4,5	45,2 ± 5,3	52,6 ± 2,4	0,001	< 0,001	0,452
Birth weight, g	2341 ± 633,6	2128,7 ± 602	3493,6 ± 303,6	< 0,001	< 0,001	0,383
Apgar score, first minute	8 (7;8)	8 (8;8)	8 (8;8)	0,04	0,135	0,845
Apgar score, fifth minute	9 (8;9)	9 (8;9)	9 (9;9)	0,131	0,05	0,859

and inflammatory diseases of the urogenital tract, a smear was taken to established cleanliness and microbiological composition of the vagina. On average, the samples were taken 10–14 days before delivery.

The cervicovaginal secretion samples were collected with a disposable vaginal elevator and sterile disposable cytobrushes. After introduction of the elevator and visual identification of the external canal of the cervix, a cytobrush was inserted into the cervical canal to a depth of 0.5 cm and, after a clockwise rotation, removed in such a way as to avoid contact with the walls of the vagina and external genital organs. After collection the samples were cooled in liquid nitrogen and stored at –80 °C.

Before analysis, the samples were subjected to liquid-liquid extraction to obtain the lipid fraction. For this purpose, 500 µL of an H_2O/methanol (1:1) solution were added to the test tube with the cytobrush, then mixed thoroughly for 5 minutes and sonicated for another 5 minutes. After that, the cytobrush was removed from the test tube, 1 ml of chloroform added thereto and the tube stirred for 10 minutes. Next, it was centrifuged for 5 minutes at 13000 G at ambient temperature, 925 µL of the lower layer taken, dried in a nitrogen flow and redissolved in 200 µL of isopropanol/acetonitrile (1:1) solution for further analysis.

Mass spectrometric analysis of lipid extracts

Lipid extracts were analyzed in a Dionex UltiMate 3000 liquid chromatography system (Thermo Scientific; Germany) connected to a MaXis Impact qTOF mass analyzer with an electrospray ionization source (Bruker Daltonics; Germany). Samples were separated by reversed-phase chromatography in a Zorbax C18 column (150 × 2.1 mm, 5 µm; Agilent, United States) with a linear gradient from 30 to 90% of eluent B in 20 minutes. Eluent A was a 60:40 acetonitrile/water solution with

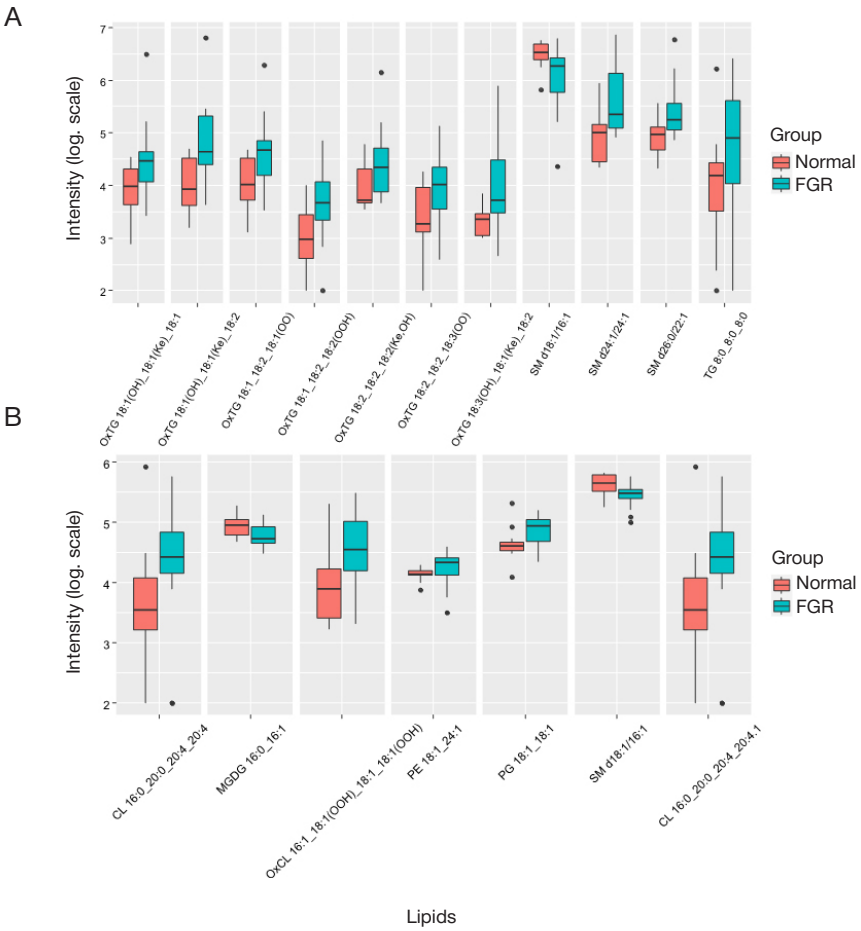

Fig. 1. Plotting of lipid levels. Significant differences between lipid levels, comparison of the normal and the IUGR groups, positive ion mode (**A**) and negative ion mode (**B**)

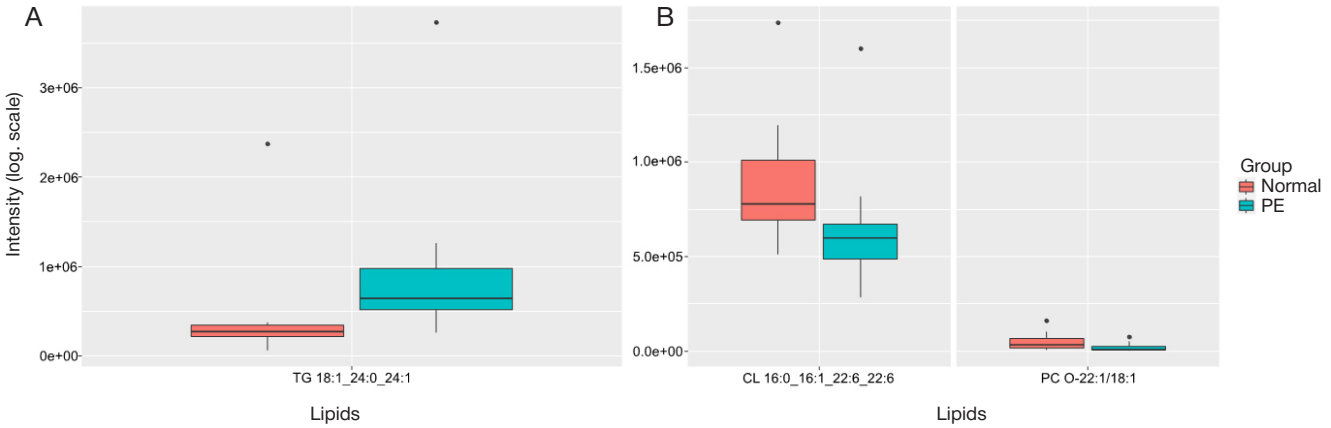

Fig. 2. Plotting of lipid levels. Significant differences between lipid levels, comparison of the normal and the PE groups, positive ion mode (**A**) and negative ion mode (**B**)

some 0.1% formic acid and 10 mmol/L ammonium formate; eluent B was a 90:8:2 isopropanol/acetonitrile/water solution with some 0.1% formic acid and 10 mmol/L ammonium formate. The elution flow rate was 40 μL/min, and the volume of the injected sample was 3 μL. The mass spectra were obtained in the positive and negative ions mode in the range of m/z 100–1700 Da, with the following settings: voltage across the capillary at 4.1 kV in the positive ion mode and –3.2 kV in the negative ion mode; pressure of the sputtering gas at 0.7 bar, drying gas flow rate 6 L/min, drying gas temperature 200 °C.

The initial mass spectrometric data were processed with the help of msConvert software from the Proteowizard 3.0.9987 package [13], MzMine [14]. Lipid identification was performed with LipidMatch scripts [15] using the exact mass and characteristic tandem mass spectra (MS/MS). The list of lipids is consistent with LipidMaps [16]

Statistical analysis

We used scripts written in the R language version 3.3.3 [17] and RStudio 1.383 [18] to process the results statistically.

The analyzed parameters were checked against the law of normal distribution with the help of Shapiro–Wilk test. When the distribution of the examined value was normal, we used the Student's t test for statistical analysis, and for the abnormal distribution cases we relied on the Mann-Whitney test for pairwise comparisons. To describe the quantitative data with normal distribution, we used arithmetic mean (M) and standard deviation (SD) in the M (SD) format. Features with distribution different from normal were described as a median (Me) and quartiles Q_1 and Q_3 in the Me format (Q_1; Q_3). The value of the threshold significance level p was taken at 0.05.

We developed the logistic regression models in order to assess the possibility of classifying patients into groups. Lipids showing statistically significant differences in levels between the groups were independent variables in the models. Akaike information criterion (AIC) enabled selection of the variables [19]. We continued selecting variables in stages while this action resulted in an increase in AIC. The quality of the resulting diagnostic model was tested by internal cross-validation with control for individual objects. The values of the area under the operating curve, sensitivity and specificity were used for assessment. The patient's group membership was the dependent variable. For each model, we determined the Wald test, 95% confidence interval (CI), odds ratio (OR) and its confidence interval. The quality of the developed models was determined by constructing the ROC curve, determining the area under the ROC curve, and calculating the sensitivity and specificity.

RESULTS

Table 1 gives the results of analysis of the clinical parameters of the groups.

It was found that the BMI of pregnant women from the IUGR group is significantly lower than that of women in the "normal" and "preeclampsia" groups (p = 0.005 and p = 0.0045, respectively).

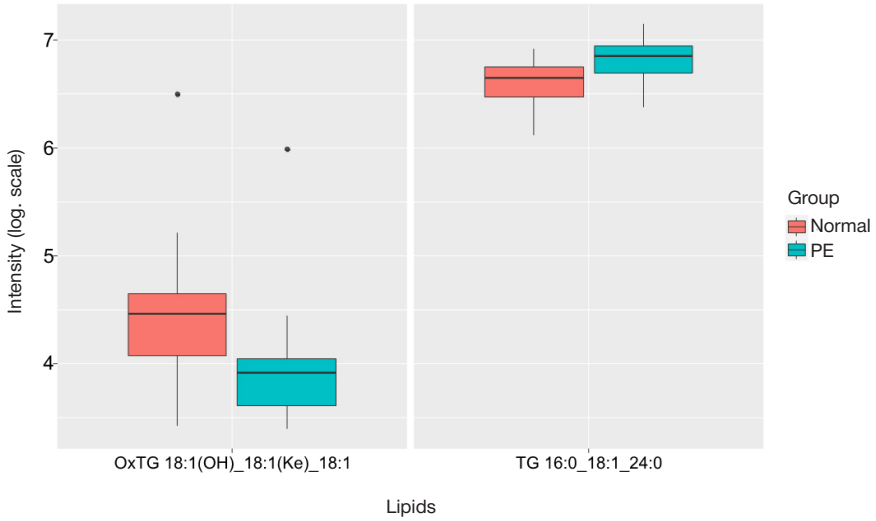

Fig. 3. Plotting of lipid levels. Significant differences between lipid levels, comparison of the PE and the IUGR groups, positive ion mode

Table 2. Characteristics of the components used to build logistic regression models enabling allocation of the patients to the IUGR , PE and Normal (control) groups by the lipid profile established for the cervical canal secretion: independent variable, its coefficient β, confidence interval (CI) of β, Wald test, probability of coefficient value differing from P zero

Lipids	β	ДИ β	Wald test	*p*
IUGR/Normal, positive ion mode				
Free term	–0,93	–2,63–0,43	–1,20	0,23
OxTG 18:3(OH)_18:1(Ke)_18:2	$3{,}01{\cdot}10^{-4}$	$5{,}99{\cdot}10^{-5}$–$8{,}16{\cdot}10^{-4}$	1,38	0,17
IUGR/Normal, negative ion mode				
Free term	–10,73	–31,29–1,54	–1,62	0,1
SM d22:3/22:4	$3{,}20{\cdot}10^{-3}$	$6{,}28{\cdot}10^{-4}$–$8{,}88{\cdot}10^{-3}$	1,65	0,1
PE 18:1_24:1	5,84e–04	$1{,}72{\cdot}10^{-4}$–$1{,}49{\cdot}10^{-3}$	1,96	0,05
MGDG 16:0_16:1	$-3{,}01{\cdot}10^{-5}$	$-8{,}54{\cdot}10^{-5}$–$4{,}33{\cdot}10^{-6}$	–1,45	0,15
PE/Normal, positive ion mode				
Free term	–0,75	–2,23–0,45	–1,14	0,25
TG 18:1_24:0_24:1	$1{,}06{\cdot}10^{-6}$	$-2{,}27{\cdot}10^{-7}$–$3{,}53{\cdot}10^{-6}$	1,19	0,24
PE/IUGR, positive ion mode				
Free term	2,71	0,71–5,45	2,31	0,02
TG 16:0_18:1_24:0	$-3{,}91{\cdot}10^{-7}$	$-8{,}39{\cdot}10^{-7}$–$7{,}62{\cdot}10^{-8}$	–2,07	0,04

All women delivered in the third trimester of pregnancy. The delivery time for the PE and IUGR groups significantly differed from that for the control group ($p < 0.001$), which is explained by the need for accelerated delivery based on obstetric indications. The share of preterm delivery in the PE group was 33.3% (six cases), in the IUGR group — 31.6% (six cases).

The average weight of newborns in the control group was 3493.6 g, compared to 2341 g and 2128.7 g in PE and IUGR groups, respectively ($p \leq 0.001$).

It should be noted that, compared to the control group, the Apgar score in the PE group was significantly lower at the first minute of life ($p = 0.04$) and in the IUGR group — at the fifth minute ($p = 0.05$). One of the possible reasons behind the observations is that a newborn that suffered chronic hypoxia and growth retardation for a long period has the reserves of his/her compensatory mechanisms depleted and experiences early neonatal adaptation in severe form. One child was diagnosed with moderate asphyxia at birth, which required additional respiratory support.

Analysis of lipid composition of the cervical canal secretion was enabled by LC-MS. LC-MS experiments were performed in both positive and negative ion modes, since this approach allows expanding the coverage of registered and identified lipids. LC-MS in positive ion mode allowed identifying 129 lipids, LC-MS in negative ion mode — 110 lipid compounds. Comparison of the relative lipid levels between the control group and the IUGR group revealed 10 lipids with levels differing significantly as registered in positive ion mode and 7 lipids with significantly different levels as registered in negative ion mode (Fig. 1). The results of the comparison of control and PE groups were 1 lipid with significant level difference found in positive ion mode analysis and 2 such lipids discovered negative ion mode (Fig. 2). As for the PE to IUGR groups comparison, there were two lipids the levels of which differed significantly (Fig. 3). Mainly, the lipids were oxylipins (oxytriglycerides and oxycardiolipins), sphingomyelins, triglycerides, and cardiolipins.

Relying on the data obtained, we built the logistic regression models seeking to identify patients who may develop IUGR or PE, such identification based on the levels of lipids in the cervical canal secretion (Table 2). A ROC analysis enabled assessment of quality of the built models; Table 3 and Figures 4 and 5 present the results of this analysis. The models enabling allocation to the control and the IUGR groups had the best parameters; they made use of data obtained with both positive ion mode and negative ion mode. The AUC was 0.70 and 0.85, respectively. The model that enabled allocation to the PE and control groups had a rather high specificity (0.91) but low sensitivity (0.30). Thus, of the obstetric pathologies considered in this work (IUGR and PE), the non-invasive approach to lipid profiling based on the cervical canal secretion seems most promising for detection of IUGR. As for PE diagnosing, applicability of the described approach requires additional research. The IUGR /Normal and IUGR /PE models built on the positive ion mode and negative ion mode data can be considered for further improvement and validation.

DISCUSSION

The study allowed identifying 129 lipids with positive ion mode and 110 lipid compounds with negative ion mode; they are simple lipids, glycerides and complex lipids, which in turn are divided into glycerophospholipids and sphingolipids. The natural organic compounds of this large group, including fats and fat-like substances, participate in construction of cell membranes and regulation of metabolism. The group is undoubtedly interesting as a research subject in the context

Table 3. Characteristics of the logistic regression models enabling allocation of the patients to the IUGR, PE and Normal (control) groups by the lipid profile established for the cervical canal secretion. PPV — positive predictive value, NPV — negative predictive value

Patient groups	MS technique (positive ion/ negative ion)	Sensitivity	Specificity	Threshold	AUC	PPV	NPV
IUGR/Normal	positive	0,63	0,91	0,2	0,7	0,6	0,89
IUGR/Normal	positive	0,81	0,91	0,5	0,85	0,79	0,9
PE/Normal	positive	0,3	0,91	0,1	0,67	0,27	0,88
IUGR/PE	positive	0,67	0,6	0,5	0,66	0,6	0,58

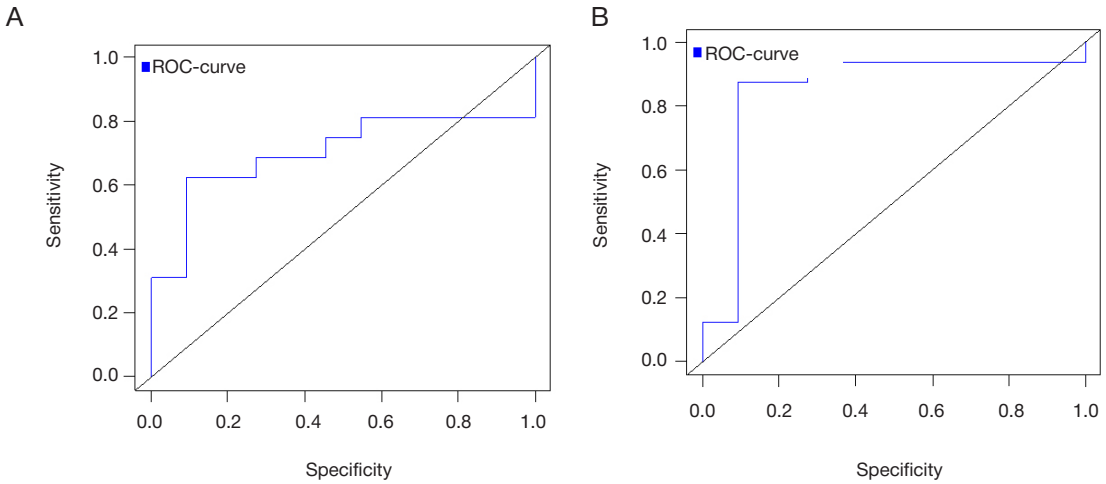

Fig. 4. Operational curve plotted for the IUGR/Normal model based on the positive ion mode (**A**) and negative ion mode (**B**) data

of obstetric pathologies. In particular, there may be value in investigation of changes in the group associated with the said pathologies and, specifically, tracking the fluctuations at the interface of the mother-placenta-fetus system. Fatty acids and lipids play a primary role in growth and development during the embryonic period. Unbalanced intake of fatty acids during the perinatal period alters the composition of fatty acids in the membrane phospholipids of the fetus, which can cause structural and functional problems in its cells. In addition, the metabolic and neuroendocrine environment of the fetus and the newborn plays a key role in the energy balance regulation. Lack of proper balance between fatty acids and lipids during pregnancy can lead to irreversible changes in the control of neuroendocrine function and energy metabolism in the fetus, leading to metabolic programming. Thus, control of the lipid levels enables detection of abnormalities in the mother-placenta-fetus system even at the preclinical stage [20]. It has been shown (in both animal and human experiments) that the metabolic pathway of sphingolipids plays a critical role in fetal and maternal tolerance, regulating innate immunity at the mother-fetus interface. These findings may help develop new therapeutic strategies for obstetric complications [21].

During pregnancy, metabolic changes occur in all systems and processes of the woman's body, including lipid metabolism. Cholesterol and free fatty acids are essential for cellular synthesis of embryonic membranes. The fetus synthesizes lipids and makes extensive use of maternal lipids, although free transplacental transport of maternal lipoproteins is limited by the "placental barrier" [22]. Phospholipids and triacylglycerols (TAGs) from the mother's body do not penetrate directly to the fetus. There is a number of mechanisms enabling transportation of fatty acids to the fetus; these mechanisms imply binding fatty acids [23] and transporting them intensively across the placenta. Circulating lipids have a variety of effects on the endothelial cell function. Dyslipidemia is often associated with dysfunction of these cells [24]. Several studies have shown a concentration-dependent relationship between elevated TAG levels and the risk of PE. There are many mechanisms that may be used as explanation of the correlation between dyslipidemia and PE. For example, increased levels of lipid fractions (such as TAG) trigger their accumulation in endothelial cells and subdue production of prostacyclin, which subsequently leads to endothelial dysfunction [25]. In our study, the level of TG 18: 1_24: 0_24: 1, CL 16: 0_16: 1_22: 6_22: 6, PC O-22: 1/18: 1 had significant differences in the PE-Normal groups comparison (p = 0.008, p = 0.02, p = 0.04, respectively). The specificity achieved for the PE/Normal diagnostic model is 0.91 (cut-off threshold — 0.10; AUC — 0.67).

In case of IUGR, placenta does not function properly and has its structure compromised, and the manifestations of the problem are detectable with the fetus but not with the mother's body. Several researchers [26, 27] have found that during pregnancy complicated by IUGR, there is a decrease in the level of lipids in the umbilical cord blood and the mother's blood, and the number of their receptors goes down, too. Low levels of lipids and their receptors in the feto-placental complex will probably have very serious consequences for the normal growth and development of the fetus, since they

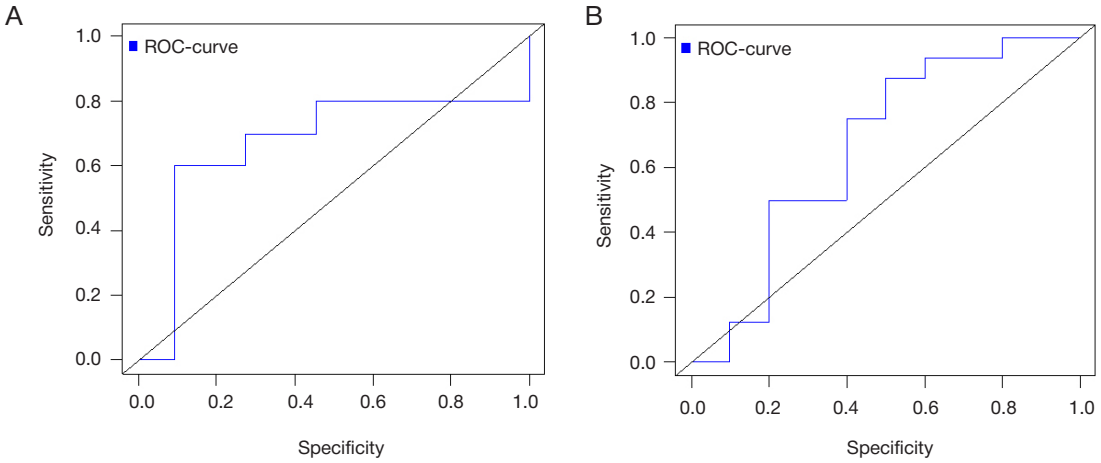

Fig. 5. Operational curve plotted for the PE/Normal model (**A**), IUGR/PE model based on the positive ion mode data (**B**)

will only insufficiently enable transport of cholesterol, normal functioning of the placenta and harmonious growth of the fetus. As we have registered in our study, the levels of 17 lipids (Table 2) were significantly different in the IUGR and the Normal groups ($p < 0.05$). The specificity achieved for the PE/Normal diagnostic model is 0.91, sensitivity is 0.81 (cut-off threshold –0.50; AUC — 0.85).

The significant difference in the results of examination of cervicovaginal secretion samples taken in the IUGR and PE groups ($p = 0.04$) is of particular interest. This difference clearly demonstrates that these pregnancy complications, initially considered to stem from the common placental dysfunction, are not the same on the pathogenetic level.

CONCLUSIONS

Our study clearly demonstrates the possibility of using cervicovaginal fluid in complex diagnostic monitoring of pregnant women with placenta-associated obstetric complications. We performed an in-depth clinical-anamnestic and mass-spectrometric analysis of samples taken from 57 pregnant women. Analysis of the cervical canal secretion of pregnant women with IUGR and PE revealed 129 lipid compounds when using LC-MS in positive ion mode and 110 lipid compounds with LC-MS in negative ion mode. The level of a number of lipids differed significantly between the PE and Normal groups and the IUGR and Normal groups. This observation may indicate the existing differences in the chain of biological processes of the pathogenesis of these pregnancy complications that are commonly believed to stem from placental dysfunction. Further research in this direction may help identify new approaches to the development of targeted therapy for the "major obstetric syndromes." The lipids were mainly oxylipins (oxytriglycerides and oxycardiolipins), sphingomyelins, triglycerides, and cardiolipins, which means this method may be used as part of a complex of predictive measures. Based on the differences identified, we built logistic regression models that can contribute to the development of methods of non-invasive diagnostics of these diseases. The result of our effort is the clear demonstration of the possibility to determine the level of lipids in the cervicovaginal fluid non-invasively in the context of complex diagnostic monitoring of pregnant women with placenta-associated obstetric complications.

References

1. Sutton ALM, Harper LM, Tita ATN. Hypertensive Disorders in Pregnancy. Obstet Gynecol Clin North Am. 2018; 45 (2): 333–47.
2. Gestational Hypertension and Preeclampsia. Obstet Gynecol. 2020; 135 (6): 1492–5.
3. Nardozza LMM, Caetano ACR, Zamarian ACP, Mazzola JB, Silva CP, Marçal VMG, et al. Fetal growth restriction: current knowledge. Arch Gynecol Obstet. 2017; 295 (5): 1061–77.
4. Gaccioli F, Lager S. Placental Nutrient Transport and Intrauterine Growth Restriction. Front Physiol. 2016; 7. DOI: 10.3389/fphys.2016.00040.
5. Benton SJ, Ly C, Vukovic S, Bainbridge SA. Andrée Gruslin award lecture: Metabolomics as an important modality to better understand preeclampsia. Placenta. 2017; 60: S32–S40.
6. Kenny LC, Broadhurst D, Brown M, Dunn WB, Redman CWG, Kell DB, et al. Detection and identification of novel metabolomic biomarkers in preeclampsia. Reprod Sci. 2008; 15 (6): 591–7.
7. Anderson, Deborah K., Liang JW and CL. Applications of Metabolomics in the Study and Management of Preeclampsia; A Review of the Literature Rachel. Metabolomics. 2017; 13 (7): 86.
8. Comhair SAA, McDunn J, Bennett C, Fettig J, Erzurum SC, Kalhan SC. Metabolomic Endotype of Asthma. J Immunol. 2015; 195 (2): 643–50.
9. Moros G, Boutsikou T, Fotakis C, Iliodromiti Z, Sokou R, Katsila T, et al. Insights into intrauterine growth restriction based on maternal and umbilical cord blood metabolomics. Sci Rep. 2021; 11 (1): 1–10.
10. Parry S, Leite R, Esplin MS, Bukowski R, Zhang H, Varner M, Andrews WW, Saade GR, Ilekis J, Reddy UM, Huang H, Sadovsky Y, Blair IA, Biggio J; Cervicovaginal fluid proteomic analysis to identify potential biomarkers for preterm birth. Am J Obstet Gynecol. 2020; 222 (5): 493.e1–493.e13. DOI: 10.1016/j.ajog.2019.11.1252. Epub 2019 Nov 20.
11. Park S, You YA, Yun H, Choi SJ, Hwang HS, Choi SK, Lee SM, Kim YJ. Cervicovaginal fluid cytokines as predictive markers of preterm birth in symptomatic women. Obstet Gynecol Sci. 2020; 63 (4): 455–63. DOI: 10.5468/ogs.19131. Epub 2020 Jun 19.
12. AbuZar Ansari, Heeyeon Lee, Young-Ah You, Youngae Jung, Sunwha Park, Soo Min Kim, Geum-Sook Hwang, Young Ju Kim. Identification of Potential Biomarkers in the Cervicovaginal Fluid by Metabolic Profiling for Preterm Birth Metabolites. 2020; 10 (9): 349. DOI: 10.3390/metabo10090349.
13. Chambers MC, MacLean B, Burke R, Amodei D, Ruderman DL, Neumann S, et al. A cross-platform toolkit for mass spectrometry and proteomics. Nature Biotechnology. 2012; 30 (10): 918–20.
14. Pluskal T, Castillo S, Villar-Briones A, Orešič M. MZmine 2: Modular framework for processing, visualizing, and analyzing mass spectrometry-based molecular profile data. BMC Bioinformatics. 2010; 11. DOI: 10.1186/1471-2105-11-395.
15. Koelmel JP, Kroeger NM, Ulmer CZ, Bowden JA, Patterson RE, Cochran JA, et al. LipidMatch: An automated workflow for rule-based lipid identification using untargeted high-resolution tandem mass spectrometry data. BMC Bioinformatics. 2017; 18 (1): 1–11.
16. Liebisch G, Vizcaíno JA, Köfeler H, Trötzmüller M, Griffiths WJ, Schmitz G, et al. Shorthand notation for lipid structures derived from mass spectrometry. J Lipid Res. 2013; 54 (6): 1523–30.
17. R : A Language and Environment for Statistical Computing. 2018. Vienna, Austria. R Foundation for Statistical Computing.
18. R team. R Studio: Integrated Development for R. 2016.
19. Bozdogan H. Model selection and Akaike's Information Criterion (AIC): The general theory and its analytical extensions. Psychometrika. 1987; 52 (3): 345–70.
20. Kabaran S, Besler HT. Do fatty acids affect fetal programming? J Health Popul Nutr. 2015; 33: 14. DOI: 10.1186/s41043-015-0018-9.PMID: 26825664.
21. Mizugishi K, Inoue T, Hatayama H, Bielawski J, Pierce JS, Sato Y, Takaori-Kondo A, Konishi I, Yamashita K. Sphingolipid pathway regulates innate immune responses at the fetomaternal interface during pregnancy. J Biol Chem. 2015; 290 (4): 2053–68. DOI: 10.1074/jbc.M114.628867. Epub 2014 Dec 11.PMID: 25505239.
22. Herrera E. Maternal-fetal transfer of lipid metabolites. In: RA Polin, WW Fox, SH Abman, editors. Fetal and Neonatal Physiology. 2004; p. 375–388.
23. Pogorelova TN, Linde VA, Gunko VO, Krukier II, Seljutina SN. Metabolizm, transport i sostav lipidov v placente. Fundamental'nye issledovanija. 2015; 2 (26): 5832–6. Russian.
24. Stewart DJ, Monge JC. Hyperlipidemia and endothelial dysfunction. Curr Opin Lipidol. 1993; 4: 319–24.
25. Wiznitzer A, Mayer A, Novack V. Association of lipid levels during gestation with preeclampsia and gestational diabetes mellitus: a population-based study. American Journal of Obstetrics and Gynecology. 2009; 201 (5): 482.e1–482.
26. Jin W-Y, Lin S-L, Hou R-L, Xiao-Yang Chen, Ting Han, Yan Jin, et al. Associations between maternal lipid profile and pregnancy complications and perinatal outcomes: a population-based study from China. BMC Pregnancy and Childbirth. 2016; 16: 60.

Available from: https://doi.org/10.1186/s12884-016-0852-9.
27. Oluwole AA, Adegbesan-Omilabu MA, Okunade KS. Preterm delivery and low maternal serum cholesterol level: Any correlation? Nigerian Medical Journal: Journal of the Nigeria Medical Association. 2014; 55: 5: 406–10. Available from: https://doi.org/10.4103/0300-1652.140381.

Литература

1. Sutton ALM, Harper LM, Tita ATN. Hypertensive Disorders in Pregnancy. Obstet Gynecol Clin North Am. 2018; 45 (2): 333–47.
2. Gestational Hypertension and Preeclampsia. Obstet Gynecol. 2020; 135 (6): 1492–5.
3. Nardozza LMM, Caetano ACR, Zamarian ACP, Mazzola JB, Silva CP, Marçal VMG, et al. Fetal growth restriction: current knowledge. Arch Gynecol Obstet. 2017; 295 (5): 1061–77.
4. Gaccioli F, Lager S. Placental Nutrient Transport and Intrauterine Growth Restriction. Front Physiol. 2016; 7. DOI: 10.3389/fphys.2016.00040.
5. Benton SJ, Ly C, Vukovic S, Bainbridge SA. Andrée Gruslin award lecture: Metabolomics as an important modality to better understand preeclampsia. Placenta. 2017; 60: S32–S40.
6. Kenny LC, Broadhurst D, Brown M, Dunn WB, Redman CWG, Kell DB, et al. Detection and identification of novel metabolomic biomarkers in preeclampsia. Reprod Sci. 2008; 15 (6): 591–7.
7. Anderson, Deborah K., Liang JW and CL. Applications of Metabolomics in the Study and Management of Preeclampsia; A Review of the Literature Rachel. Metabolomics. 2017; 13 (7): 86.
8. Comhair SAA, McDunn J, Bennett C, Fettig J, Erzurum SC, Kalhan SC. Metabolomic Endotype of Asthma. J Immunol. 2015; 195 (2): 643–50.
9. Moros G, Boutsikou T, Fotakis C, Iliodromiti Z, Sokou R, Katsila T, et al. Insights into intrauterine growth restriction based on maternal and umbilical cord blood metabolomics. Sci Rep. 2021; 11 (1): 1–10.
10. Parry S, Leite R, Esplin MS, Bukowski R, Zhang H, Varner M, Andrews WW, Saade GR, Ilekis J, Reddy UM, Huang H, Sadovsky Y, Blair IA, Biggio J; Cervicovaginal fluid proteomic analysis to identify potential biomarkers for preterm birth. Am J Obstet Gynecol. 2020; 222 (5): 493.e1–493.e13. DOI: 10.1016/j.ajog.2019.11.1252. Epub 2019 Nov 20.
11. Park S, You YA, Yun H, Choi SJ, Hwang HS, Choi SK, Lee SM, Kim YJ. Cervicovaginal fluid cytokines as predictive markers of preterm birth in symptomatic women. Obstet Gynecol Sci. 2020; 63 (4): 455–63. DOI: 10.5468/ogs.19131. Epub 2020 Jun 19.
12. AbuZar Ansari, Heeyeon Lee, Young-Ah You, Youngae Jung, Sunwha Park, Soo Min Kim, Geum-Sook Hwang, Young Ju Kim. Identification of Potential Biomarkers in the Cervicovaginal Fluid by Metabolic Profiling for Preterm Birth Metabolites. 2020; 10 (9): 349. DOI: 10.3390/metabo10090349.
13. Chambers MC, MacLean B, Burke R, Amodei D, Ruderman DL, Neumann S, et al. A cross-platform toolkit for mass spectrometry and proteomics. Nature Biotechnology. 2012; 30 (10): 918–20.
14. Pluskal T, Castillo S, Villar-Briones A, Orešič M. MZmine 2: Modular framework for processing, visualizing, and analyzing mass spectrometry-based molecular profile data. BMC Bioinformatics. 2010; 11. DOI: 10.1186/1471-2105-11-395.
15. Koelmel JP, Kroeger NM, Ulmer CZ, Bowden JA, Patterson RE, Cochran JA, et al. LipidMatch: An automated workflow for rule-based lipid identification using untargeted high-resolution tandem mass spectrometry data. BMC Bioinformatics. 2017; 18 (1): 1–11.
16. Liebisch G, Vizcaíno JA, Köfeler H, Trötzmüller M, Griffiths WJ, Schmitz G, et al. Shorthand notation for lipid structures derived from mass spectrometry. J Lipid Res. 2013; 54 (6): 1523–30.
17. R : A Language and Environment for Statistical Computing. 2018. Vienna, Austria. R Foundation for Statistical Computing.
18. R team. R Studio: Integrated Development for R. 2016.
19. Bozdogan H. Model selection and Akaike's Information Criterion (AIC): The general theory and its analytical extensions. Psychometrika. 1987; 52 (3): 345–70.
20. Kabaran S, Besler HT. Do fatty acids affect fetal programming? J Health Popul Nutr. 2015; 33: 14. DOI: 10.1186/s41043-015-0018-9.PMID: 26825664.
21. Mizugishi K, Inoue T, Hatayama H, Bielawski J, Pierce JS, Sato Y, Takaori-Kondo A, Konishi I, Yamashita K. Sphingolipid pathway regulates innate immune responses at the fetomaternal interface during pregnancy. J Biol Chem. 2015; 290 (4): 2053–68. DOI: 10.1074/jbc.M114.628867. Epub 2014 Dec 11.PMID: 25505239.
22. Herrera E. Maternal-fetal transfer of lipid metabolites. In: RA Polin, WW Fox, SH Abman, editors. Fetal and Neonatal Physiology. 2004; p. 375–388.
23. Погорелова Т. Н. Линде В. А., Гунько В. О., Крукиер И. И., Селютина С. Н. Метаболизм, транспорт и состав липидов в плаценте. Фундаментальные исследования. 2015; 2 (26): 5832–6.
24. Stewart DJ, Monge JC. Hyperlipidemia and endothelial dysfunction. Curr Opin Lipidol. 1993; 4: 319–24.
25. Wiznitzer A, Mayer A, Novack V. Association of lipid levels during gestation with preeclampsia and gestational diabetes mellitus: a population-based study. American Journal of Obstetrics and Gynecology. 2009; 201 (5): 482.e1–482.
26. Jin W-Y, Lin S-L, Hou R-L, Xiao-Yang Chen, Ting Han, Yan Jin, et al. Associations between maternal lipid profile and pregnancy complications and perinatal outcomes: a population-based study from China. BMC Pregnancy and Childbirth. 2016; 16: 60. Available from: https://doi.org/10.1186/s12884-016-0852-9.
27. Oluwole AA, Adegbesan-Omilabu MA, Okunade KS. Preterm delivery and low maternal serum cholesterol level: Any correlation? Nigerian Medical Journal: Journal of the Nigeria Medical Association. 2014; 55: 5: 406–10. Available from: https://doi.org/10.4103/0300-1652.140381.

FEATURES OF THE DECIDUALIZED ENDOMETRIOSIS DIAGNOSIS AND COURSE DURING PREGNANCY

Gerasimova AA[1,2], Asyrafyan LA[3], Manuchin IB[4], Shamarakova MV[2], Miryasova MS[5], Klimenko PA[6] ✉

[1] Peoples' Friendship University of Russia, Moscow, Russia
[2] Family Planning and Reproduction Center, Moscow, Russia
[3] Kulakov National Medical Research Center for Obstetrics, Gynecology and Perinatology, Moscow, Russia
[4] Yevdokimov Moscow State University of Medicine and Dentistry, Moscow, Russia
[5] Sechenov First Moscow State Medical University, Moscow, Russia
[6] Pirogov Russian National Research Medical University, Moscow, Russia

Currently, surgical treatment aimed to exclude the malignant ovarian tumors is performed in almost 90% of patients with decidualized endometrial cysts (DEC). However, unnecessary surgical interventions increase the risk to maternal and fetal health. The study was aimed to perform a differential diagnosis of DEC in pregnant women in order to define the rational treatment. A total of 82 female patients were included in the study: 63 had endometrial cysts (EC), 16 had DEC, 3 had rare forms of endometriosis, and 10 had ovarian serous papillary borderline tumors. When performing the diagnostic ultrasound, our proposed model was used. The ultrasound imaging data obtained were juxtaposed with the concentration of the protein tumor markers (CA-125), the risk of malignancy index (RMI) was calculated, and the morphological assessment of the masses was performed. The ultrasound imaging parameters, being the most valuable for differential diagnosis of EC, DEC, and serous borderline tumors, were as follows: the altered mass wall thickness, the existence and shape of papillary masses, avascular echogenic inclusions with blurry contour, blood circulation and arrangement of blood vessels, ascites. The frequency analysis revealed the differences between groups based on the ultrasound imaging data (in 60–100% of observations). Histological examination revealed the differences between groups in 100% of observations. Our findings have made it impossible to prolong pregnancy in patients with DEC without performing surgery. The results of treatment provided to patients with DEC during pregnancy were worse compared to those in patients with no prominent decidualization in ovarian EC. Today, the diagnosis of DEC and the treatment of patients during pregnancy remain unsophisticated. Further clinical observation and the search for more reliable methods of the diagnosis and rational treatment of pregnant women with DEC are required.

Keywords: ultrasound examination, morphological analysis, ovarian tumors, pregnant women

Author contributions: the authors contributed to the study and preparation of the article equally, they read and approved the final version of the article prior to publication.

Compliance with ethical standards: the study was approved by the Ethics Committee of Pirogov Russian National Research Medical University (protocol № 176 dated June 25, 2018). The informed consent was submitted by all patients.

✉ **Correspondence should be addressed:** Pyotr A. Klimenko
Sevastolopsky prospect, 24a, Moscow, 117209, Russia; pa.klimenko@mail.ru

Received: 23.11.2021 **Accepted:** 06.12.2021 **Published online:** 12.12.2021

DOI: 10.24075/brsmu.2021.059

ОСОБЕННОСТИ ДИАГНОСТИКИ И ТЕЧЕНИЯ ЭНДОМЕТРИОЗА С ДЕЦИДУАЛЬНЫМ МЕТАМОРФОЗОМ ВО ВРЕМЯ БЕРЕМЕННОСТИ

А. А. Герасимова[1,2], Л. А. Ашрафян[3], И. Б. Манухин[4], М. В. Шамаракова[2], М. С. Мирясова[5], П. А. Клименко[6] ✉

[1] Российский университет дружбы народов, Москва, Россия
[2] Центр планирования семьи и репродукции, Москва, Россия
[3] Национальный медицинский исследовательский центр акушерства, гинекологии и перинатологии имени В. И. Кулакова, Москва, Россия
[4] Московский государственный медико-стоматологический университет имени А. И. Евдокимова, Москва, Россия
[5] Первый Московский государственный медицинский университет имени И. М. Сеченова, Москва
[6] Российский национальный исследовательский медицинский университет имени Н. И. Пирогова, Москва, Россия

В настоящее время при наличии децидуализированных эндометриоидных кист яичников (ДЭК) хирургическое лечение для исключения злокачественных опухолей яичников выполняют практически в 90% случаев. Неоправданные хирургические вмешательства при этом увеличивают риск для здоровья матери и плода. Целью исследования было провести дифференциальную диагностику ДЭК у беременных для определения рационального лечения. В исследование включены 82 пациентки: 63 из них были с эндометриоидными кистами (ЭК), 16 — с ДЭК, 3 — с редкими формами эндометриоза и 10 — с серозными папиллярными пограничными опухолями яичников. Для ультразвуковой (УЗ) диагностики использовали предложенную авторами модель. Полученные УЗ-данные сопоставляли с концентрацией белка-онкомаркера (CA-125), рассчитывали индекс RMI (risk of malignancy index), выполняли морфологическое исследование образований. Особо ценными УЗ-параметрами при дифференциальной диагностике ЭК, ДЭК и пограничных серозных опухолей были: измененная толщина стенки образования, наличие и форма папиллярных образований, аваскулярные эхогенные включения без четких контуров, кровоток и расположение сосудов, асцит. Результаты частотного анализа показали различия между группами по данным УЗИ (в 60–100% наблюдений). Гистологическое исследование выявило различие между группами в 100% наблюдений. Полученные результаты не позволили нам пролонгировать беременность при ДЭК без выполнения хирургического лечения. Результаты лечения пациенток с ДЭК во время беременности были хуже таковых без выраженной децидуальной трансформации ЭК яичников. В настоящее время диагностика ДЭК и лечение больных во время беременности остаются несовершенными. Необходимы дальнейшие клинические наблюдения и поиск более надежных способов диагностики и рационального лечения беременных с ДЭК.

Ключевые слова: ультразвуковое исследование, морфологическое исследование, опухоли яичников, беременность

Вклад авторов: авторы внесли равнозначный вклад в проведение исследования и подготовку статьи, прочли и одобрили ее финальную версию перед публикацией.

Соблюдение этических стандартов: исследование одобрено этическим комитетом РНИМУ им. Н. И. Пирогова (протокол № 176 от 25 июня 2018 г.). Все пациенты подписали информированное согласие на участие в исследовании.

✉ **Для корреспонденции:** Петр Афанасьевич Клименко
Севастопольский проспект, д. 24а, г. Москва, 117209, Россия; pa.klimenko@mail.ru

Статья получена: 23.11.2021 **Статья принята к печати:** 06.12.2021 **Опубликована онлайн:** 12.12.2021

DOI: 10.24075/vrgmu.2021.059

Ovarian endometriosis is a chronic tumor-like lesion observed in 1–2% of pregnant women [1]. In 12% of women, the foci of endometriosis may undergo decidualization, and emerge as early as at 9 weeks of gestation [2].

Decidualization is a benign transient lesion, observed during gestation. It is usually found during the caesarian section or surgical treatment of masses with high risk of malignization. The decidual regression occurs in 4–6 weeks after delivery [3]. According to some reports, lower levels of decidualization in the postpartum period [4] are associated with high progesterone levels, absence of menstrual periods, and increased apoptosis being the key factor of endometriosis regression.

Decidualized endometrial cysts (DEC) are almost always asymptomatic during pregnancy. When performing the ultrasound examination of DEC, the majority of authors distinguish the combination of the cystic cavity with a large amount of suspended debris, typical for EC, and papillary projections with increased vascularity. These echographic characteristics are similar to those of malignant ovarian tumors. Surgical interventions aimed to exclude the malignant ovarian tumors in patients with DEC are performed in almost 90% of observations [5, 6]. Unnecessary surgical interventions increase the risk to maternal and fetal health [7–11].

Thus, despite the fact that in pregnant women decidualization is characterized by benign course, it becomes the cause of numerous complications, and the presence of macroscopic features similar to those of malignant tumors may result in unnecessary therapeutic interventions.

The study was aimed to perform a differential diagnosis of DEC in pregnant women in order to define the rational treatment.

METHODS

A total of 82 female patients with endometriosis verified by histology were enrolled in the study, which was carried out in 2000–2021. The age of the patients examined varied between 19–41 years (the median age was 31 years). Inclusion criteria: consent to participate in the study; pregnancy; ultrasonography confirmed ovarian endometriosis in the pregravid period or during pregnancy; subsequent surgical treatment and morphological verification. Exclusion criteria: pregnant woman's refusal to participate in the study; threatened abortion; intrauterine infection; prenatal injury identified before the study.

In group 1 (control group), ultrasound examination performed during pregnancy revealed no signs of decidualization in 63 patients out of 82. These patients had a caesarean delivery due to combined indications: endometriosis and breech presentation in 9 patients, acute fetal hypoxia in 10 patients, unprepared birth canal and hypotonic labor in 11 patients, postterm pregnancy and threats to the fetus in 10 patients, severe preeclampsia in 4 patients, symphysitis in 5 patients, uterine scar in 6 patients, placenta praevia in 4 patients, primary infertility and *in vitro* fertilization (IVF) in 4 patients. After the delivery and histological examination of ovarian masses (OM), decidualization in the ovaries was the finding revealed in 43 of these patients.

Among 63 deliveries, 5 (7.9%) were preterm. Of those in 1 case severe preeclampsia developed at 29 weeks, and the treatment was ineffective; in 2 cases at 32 weeks there were placenta previa with hemorrhage (1 patient) and premature rupture of membranes (PROM) (1 patient); in 2 cases at 35–36 weeks there were placenta previa with hemorrhage (1 patient) and acute fetal hypoxia (1 patient).

In 16 patients of group 2, decidualization in the ovary was found at 16–28 weeks (the median value was 17) of pregnancy, having the signs resembling malignization, that is why laparoscopic adnexectomy (one case) with oophorectomy (four cases) was performed, as well as laparotomy with adnexectomy (four cases) and oophorectomy (seven cases). When performing laparotomy, the abdominal cavity revision was performed, together with tissue specimen collection and rapid morphological examination.

Three patients had the severe decidual reaction and rare complications of endometriosis. In one patient, who had the caesarian delivery, endometrial implants were found during the surgical procedure. The foci of deciduosis were located on the uterine surface, omentum, peritoneum, and were represented by numerous yellowish elastic nodules of various sizes, the largest of which were almost 4 cm in diameter. In two women, decidualization was diagnosed in the colon wall, resected on days 2 and 5 after delivery due to the symptoms of acute abdomen.

When performing a differential diagnosis of DEC, we used the earlier results (control group 2) [12] obtained for 10 patients with ovarian serous papillary borderline tumors.

Ultrasound examination was performed with the Voluson E8 ultrasound machine (General Electric; USA) with the use of

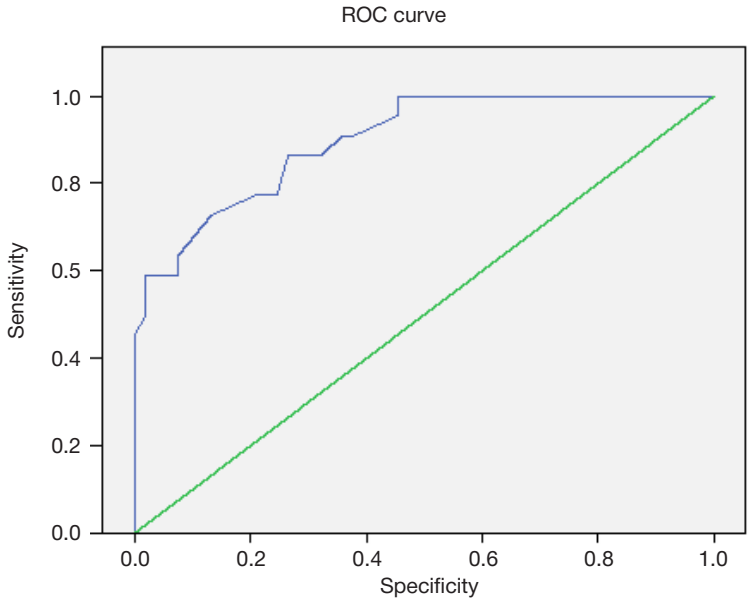

Fig. 1. ROC curve of the model for identification of endometrial cysts

transabdominal and transvaginal color Doppler imaging and pulsed wave Doppler velocimetry. Ultrasound characteristics of the tumors were assessed using the earlier proposed models [13]. The 2D and 3D comprehensive ultrasound examination was combined with color Doppler (CD) and power Doppler (PD), as well as with 3D angiography. Diagnostic ultrasound was performed with the use of our proposed model, allowing one to distinguish between benign, borderline and malignant tumors [13]. When assessing the model accuracy, sensitivity (Se) and specificity (Sp) were used along with the count of correct assignments.

The concentration of CA-125 was assessed by enzyme immunoassay using the test system (Siemens; Germany).

RMI was defined in accordance with the guidelines [14, 15] using the following formula:

$$RMI = M \times U \times CA\text{-}125,$$

where M — menopausal status in points, U — ultrasound results in points, C — serum CA-125 level (IU/mL).

RMI ≥ 200 was regarded as a sign of the high likelihood of epithelial ovarian cancer.

Tissue specimens stained with hematoxylin and eosin were assessed by different pathologists. Morphological diagnosis was established in accordance with the WHO classification of tumours of the female reproductive organs (2014). Paraffin-embedded tissue blocks were selected for immunohistochemistry: 15 blocks from patients with EC, and 10 blocks from patients with DEC. Morphological assessment was performed by standard methods. The diagnosis of deciduosis was confirmed by immunohistochemistry with the use of Vimentin (3B4, Ventana) and CD10 (56C6, Ventana) antibodies, being the markers of mesenchymal tissue and endometrial stroma, respectively. Intestinal tissue specimens were used as a positive control when assessing the expression of Vimentin, and the tonsillar tissue specimens were used when studying the CD10 immunoreactivity; when performing immunohistochemistry, the samples of the studied tissue not treated with primary antibodies were used as a negative control for both markers. Positive staining for both markers was subjectively classified as weak, moderate, or strong.

In addition, medical records together with the pregnancy and childbirth outcomes were studied in these 82 patients after treatment.

Statistical data processing was carried out using the SPSS 15.0 software package (IBM; USA). The data were subjected to frequency analysis by constructing the crosstabs. The differences were considered significant when $p < 0.05$.

RESULTS

Ultrasonography showed that in the majority of observations in group 1, EC (n = 63) were small, located inside the ovaries, with smooth outer and inner contours, the cyst content was of moderate or high echogenicity, blood vessels were visible in the walls. A total of 60 EC (95%) were unilateral: right-sided in 18 patients (30%), left-sided in 42 patients (70%). Bilateral cysts were found in three observations (5%).

The cyst size varied between 25 × 20 and 127 × 83 mm, the average size was 47.5 ± 4.8 × 31.8 ± 3.1 mm, (the median value was 41.5 × 28.5 mm). In 48 pregnant women (76%) of group 1, EC had the characteristic echographic features (lied in a fixed position close to the posterior uterine wall, had a thickened wall, creating the effect of double contour, non-movable finely dispersed suspended material (ground-glass opacity)), not differing substantially from the typical echographic features observed in the non-pregnant state. CD and PD

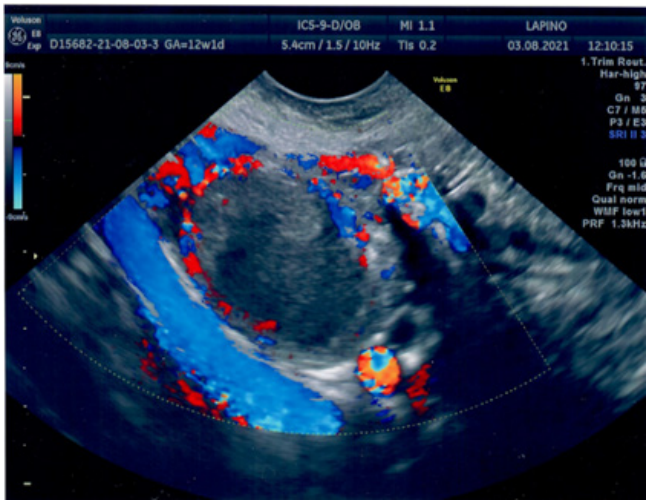

Fig. 2. Doppler ultrasonography of the endometrial cyst. Longitudinal transabdominal scan. Multiple coloured loci of blood flow and low resistive index values

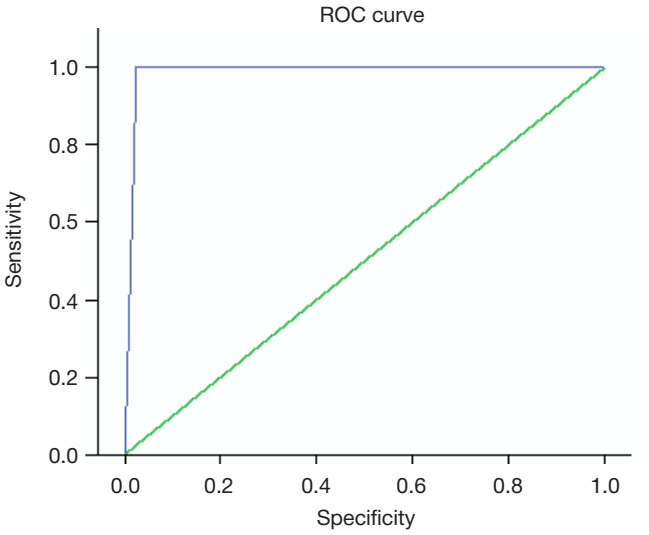

Fig. 3. ROC curve of the model for diagnosis of malignant and borderline tumors in pregnant women

revealed the sporadic coloured loci with high or medium resistance blood flow within a cyst wall. Bilateral cysts were found in three observations. In about 5% of 63 observations, EC had intracystic masses of moderate or high echogenicity in the form of blood clots and multiple sponge-like zones with undulating contour in the inner surface of the mass. In 12 observations (19%), EC visible on the image looked like serous cystadenomas, round shaped hypoechoic masses with small amount of suspended material, avascular on CD images.

When performing the differential diagnosis of EC with the use of our proposed method [13], the patient's age, blood vessel arrangement, and the resistive index (RI) were of the greatest informational value. The maximum EC score obtained using the decision procedure did not exceed 2 points.

Performance of the model for EC identification (Fig. 1) was 84%, however, the area under the ROC curve was very large, indicating the high quality of the model.

Preoperative evaluation of the patients in group 1 revealed no peculiarities in the ultrasound imaging parameters, CA-125, RMI in puerperant women with no deciduosis and those who had deciduosis, which was identified as a finding when performing the histological examination.

Blood levels of CA-125 in patients varied between 7.3 and 131.2 U/mL, the average level was 61.1 ± 8.5 U/mL

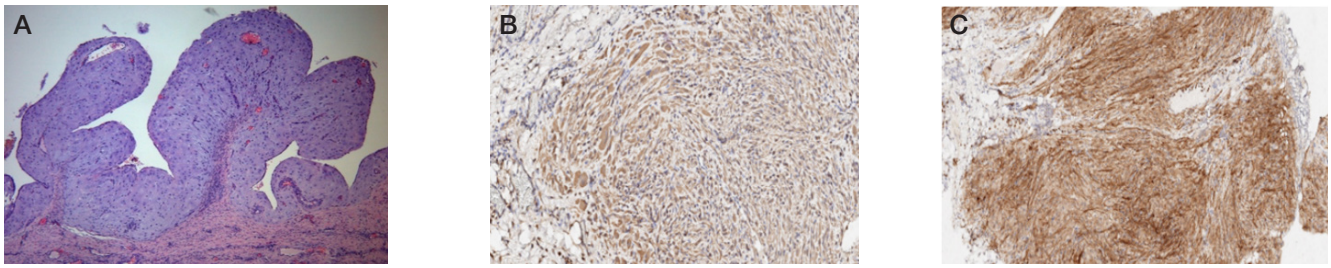

Fig. 4. Endometrial cyst with prominent decidualization and the formation of pseudopapillary structures. **A**. DEC (hematoxylin and eosin, ×50). **B**. CD10 — prominent diffuse membranous and cytoplasmic expression. **C**. Vimentin — prominent diffuse cytoplasmic expression

(the median value was 53 U/mL). Furthermore, in 19 patients (30%), this value was below the threshold (7.3–33.4 U/mL). In 31 patients (49%), this indicator showed the upward trend (44–94 U/mL), and in 13 patients (21%) the value exceeded 100 U/mL (100.2–131.2 U/mL). Our records show that CA-125 varies in the range of 8.5–280 U/mL during normal pregnancy (the median value is 95.6 U/mL).

RMI varied between 7.3 and 131.2, the average value was 65.4 ± 9 (the median value was 59). In the group of patients with EC, about 98% had RMI of less than 200. Moreover, in 19 patients (31%), RMI was below 25, in 28 patients (44%), it was 25–100, and only in 16 patients (25%), the observed RMI values exceeded 100, but never reached 200.

The planned caesarean section results in this group were as follows: all children were born in satisfactory condition. The Apgar score was 6–8 (the median value was 7.8) in premature babies and 8–9 (the median value was 8.9) in full-term babies. The birth weight was 1880–2840 g (the median value was 2640 g) in premature babies and 2660–4480 g (the median value was 3530 g) in full-term babies. Three premature babies needed the 2nd stage developmental care. In other babies, the early neonatal period went smoothly, the patients and their babies were discharged from the maternity hospital on day 5–7 after surgery. The morbidity rate was 3.2%.

Morphological examination of non-decidualized EC showed that the walls of ovarian cysts consisted of ovarian tissue with fibrotic changes, inner layer of cytogenic stroma with hemorrhages and hemosiderin deposition, and the lining epithelium was of endometrioid type. In DEC identified as findings, the fragments of the cystic ovarian endometrioma wall were defined with no lining epithelium, large areas of decidualization involving hypertrophy of endometrial stromal cells into polygonal cells with clear margins, abundant eosinophilic cytoplasm, round to oval nuclei with fine granular chromatin; no mitosis was detected.

When performing ultrasound examination in group 2 (n = 16), DEC were identified as the masses secured to the walls of the pelvis, located low relative to the gravid uterus. In 10 pregnant women (62.5%), DEC were unilateral, right-sided DEC were found in 7 patients (70%), and left-sided DEC were identified in three patients (30%). Bilateral ovarian lesions were reported in six observations (37.5%).

The cyst size varied between 20 × 30 and 108 × 161 mm, the average size was 73.7 ± 6.2 × 96.5 ± 7.5 mm (the median value was 76.5 × 108.5 mm) (significant differences with group 1, $p < 0.001$–0.05).

DEC were characterized by cystic and solid ovarian mass structure in all observations, multiloculated structure in four patients (25%), or incomplete septa in four observations (25%), irregular wall thickening with highly vascularized mural structures having multiple coloured loci of blood flow and low resistive index values in all masses.

Table. Comparative characteristics of EC, DEC and borderline tumors

Studied parameters	EC	DEC	Borderline tumors
Location of the mass	Posterior to the uterus, fixed low	Posterior to the uterus, fixed low	Beside the uterus, often at the level of the fundus
Structure: cystic, cystic and solid	Cystic	Cystic and solid	Cystic and solid
Type of suspended debris: coarse echogenic (ground-glass opacity), finely dispersed echogenic	Ground-glass opacity — coarse echogenic	Ground-glass opacity — coarse echogenic	Finely dispersed echogenic
Structure: unilocular, bilocular, trilocular	Unilocular	Unilocular, bilocular, trilocular	Unilocular, bilocular, trilocular
Wall of the mass: thickness, size of altered locus	Fragmented up to 2 mm	Total up to 3–6 mm	Fragmented up to 2 mm
Papillary growths: presence and shape	No	Regular round shape in 100%	Irregular shape in 100% (of cauliflower type)
Avascular echogenic inclusions with blurry contour	Extremely rare	Up to 97%	No
RI (resistive index)	0.54 (0.41–0.69)	0.44 (0.24–0.62)	0.42 (0.19–0.58)
PSV (peak systolic velocity)	9.6 (9.2–14.3)	13.2 (6.0–17.0)	14 (3.9–21.9)
PI (pulsatility index)	0.82 (0.51–1.22)	0.55 (0.25–0.87)	0.54 (0.27–0.88)
Blood circulation (arrangement of blood vessels)	No, single loci	Moderate to high circulation intensity	High circulation intensity in the wall, septa, and papillary growths
Ascites	no	no	present in 60%
CA-125 (U/mL)	61.1 ± 8.5 (median 53)	120 ± 31.6 (median 70.5)	135.4 ± 55.1 (median 80.5)
RMI	65.4 ± 9 (median 59)	348 ± 97 (median 212)	334.1 ± 147 (median 241.5)
Histological examination	Histological features of ovarian EC	Histological features of ovarian DEC	Histological features of ovarian serous papillary borderline tumors

When performing the differential diagnosis of DEC with the use of our proposed method [13], such factors as ovarian tissue, RI, PSV, and blood vessel arrangement were of great prognostic value. The maximum DEC score obtained using the decision procedure exceeded 4 points. Based on the ultrasound features, DEC (Fig. 2) could be identified as a malignant tumor.

The model obtained showed sensitivity of 100% and specificity of 92.3% in the test sample, with the overall accuracy of 92.8% (Fig. 3).

Blood levels of CA-125 in patients of group 2 varied between 17.6 and 361 U/mL, the average level was 120.1 ± 31.6 U/mL (the median value was 70.5 U/mL). Furthermore, in two pregnant women (12.5%), this value was below the threshold, in nine observations (56.25%), this indicator showed the upward trend (from 47.8 to 82.67 U/mL), and in five patients (31.25%), the value exceeded the threshold and reached 361 U/mL.

RMI varied between 69 and 1083, the average value was 348 ± 97 (the median value was 212, $p < 0.001$–0.05). In the group of patients with DEC, seven pregnant women (43.75%) had RMI values significantly higher than 200 (207–1083), five patients (31.25%) had RMI not exceeding 200, and only four patients (25%) had RMI values below 100.

In patients of group 2 with decidualization in the ovary, pregnancy evolved in different ways. In four patients out of 16 (25.0%), pregnancy was complicated by miscarriage after the surgical treatment due to suspected malignancy, performed at week 12–27 of pregnancy. Perinatal death at 23 weeks of gestation occurred in one patient, three patients gave birth prematurely, and 12 patients had a full term delivery. The Apgar scores of premature babies varied between 6–8 and 7–8 (the median value was 6–7). The birth weight of premature babies was 1880–2640 g, (the median value was 2010 g). In patients, who had a full term delivery, the Apgar scores of the newborns varied between 8–9 and 9–9 (the median value was 8–9), the Silverman Anderson score was 2–3, and the birth weight was 2810–3720 g (the median value was 3185 g). In one observation, the early neonatal period was spent in the intensive care unit, and in three observations, respiratory support and the treatment of respiratory distress syndrome were required. Subsequently, three newborns were transferred to the multidisciplinary children's hospital for the 2nd stage developmental care. Thus, perinatal mortality in group 2 was 62.5‰, and morbidity was 25.0%.

Fig. 4A demonstrates the wall of the cystic ovarian endometrioma with no lining epithelium, fibrotic changes of ovarian tissue, and prominent hypertrophy of endometrial stromal cells with the formation of the well vascularized papillary structures.

Immunohistochemistry performed in the group 2 on 10 selected paraffin-embedded tissue blocks confirmed decidualization in the cystic ovarian endometrioma walls in all observations. Morphological evaluation showed that the latter had a typical structure, were lined with epithelium of endometrioid type, with hemorrhagic foci and hemosiderin deposition within the wall. Immunohistochemistry revealed moderate positive cytoplasmic expression of CD10 in the stromal cells of the foci with decidualization (Fig. 4B) together with strong positive cytoplasmic immunoreactivity for Vimentin (Fig. 4C).

DISCUSSION

When reviewing the data obtained, it should be noted that EC with no prominent decidualization during pregnancy have a latent favorable course and do not result in pathological pregnancy and labor course, increased perinatal morbidity and mortality.

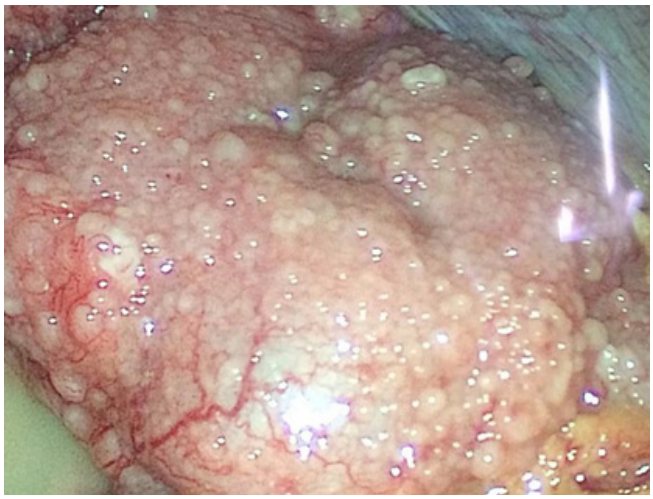

Fig. 5. Multiple regions of decidualization

According to literary sources, decidualized EC occurs in 12–20% of observations; the cyst size is reduced in 52% of observations, increased in 20% of observations, and unaffected in 28% of observations. Furthermore, the rate of DEC rupture is 3–4%, and the abscess formation is revealed in 4% of observations [16, 17].

Differential diagnosis of ovarian EC and DEC in pregnant women remains an obstetric challenge. Most authors distinguish the combination of the cystic cavity with a large amount of suspended debris, typical for EC, and papillary projections with increased vascularity among the echographic signs of DEC [7–11]. When there is a DEC, the sonographic features are similar to those observed in patients with malignant ovarian tumors based on the echographic characteristics. Our records (Table) show that today the use of generally accepted non-invasive preoperative diagnostic tests makes it possible to distinguish between EC, DEC, and borderline tumors with a high probability. The comparison of DEC with borderline tumors (with the control group 2) revealed significant fluctuations in the studied indicators, however, based on the ultrasound imaging data, these were distinguishable in the majority of observations. In modern medicine, the good test (marker) is the one that is not found in 70% of the comparison group when comparing two groups.

When performing the differential diagnosis of the studied groups (Table), the following ultrasound imaging parameters were the most valuable: the altered mass wall thickness, the existence and shape of papillary masses, avascular echogenic inclusions with blurry contour, blood circulation and arrangement of blood vessels, ascites. The frequency analysis showed that the DEC group differed from the groups with EC and borderline tumors in 60–100% of observations based on the sonographic markers. The results of histological examination made it possible to perform a differential diagnosis of EC, DEC, and borderline tumors in 100% of observations.

Given that the assessment of the studied sonographic markers is still subjective, and the findings have made it impossible to eliminate the high risk of the mass malignization in patients with DEC, these patients have undergone surgery in early pregnancy. Echographic image of DEC suspicious for malignization has made it impossible to prolong pregnancy for ethical reasons, even with the possibility of the increased rate of perinatal complications. The need for surgical treatment

aimed to exclude the malignant ovarian tumors in patients with decidualized EC (DEC) is in line with literature data [5, 6], this treatment method is applied in almost 90% of observations.

Adverse pregnancy outcomes in patients with endometriosis relate primarily to miscarriage, high risk of preterm labor and low birth weight babies [18–20].

Pregnancy and labor in patients with endometriosis are associated with high risk of complications, such as hemoperitoneum, bowel perforation, appendicitis, and EC rupture [19, 20].

Other complications of pregnancy are observed in patients with decidualization. Thus, in one of the trials, histological examination revealed decidual changes in all layers of appendix on day 5 after caesarian section and gangrenous appendicitis [21]. During our study, multiple yellowish elastic nodules of various size (up to 4 cm), located on the uterine surface, omentum, and peritoneum, were found during the surgical procedure in one patient, who had caesarian section for obstetric reasons (Fig. 5).

The fragments of omentum were resected for further histological examination, which revealed prominent decidual changes. In the other two patients, we had to perform re-surgery during the postoperative period (on days 2–5 after the caesarian section performed for obstetric reasons) due to acute abdomen. The macroscopically altered fragments of the colon with decidualization in the wall and multiple endometrioid heterotopias with decidual changes in all layers of the colon wall were resected.

There is evidence of similar immunohistochemistry features in the extrauterine mesenchymal cells that have undergone the decidual reaction, and decidualized endometrial stromal cells with positive expression of mesenchymal markers (Vimentin, Desmin), and progesterone receptors [22]. Reduced concentration of progesterone, resulting from pregnancy termination triggers the involution of foci with decidualization, which in some cases is followed by severe circulatory disorder and decidual tissue destruction, probably entailing the pain symptoms and hemorrhage [23, 24]. Intra-abdominal hemorrhage was revealed on day 7 after the caesarian section in the patient, having the focus with decidualization, located in the area of the uterine posterior wall on the left [25, 26].

Thus, decidualization in pregnant women is characterized by a benign course, however, it becomes the cause of numerous complications. The presence of macroscopic features similar to those of malignant tumors may result in unnecessary therapeutic interventions.

CONCLUSIONS

Currently, the diagnosis of DEC and the treatment of patients during pregnancy give rise to many questions. Further clinical observation and the search for more reliable methods of the DEC diagnosis and rational treatment in pregnant women are required.

References

1. Marino T, Craigo SD. Managing adnexal masses in pregnancy. Contemp Obstet Gynecol. 2000; 45: 130–43.
2. Kommos F, Pfisterer J, Peters F, et al. Ektope Dezidualreaktion — möglicher Anlass zur kolposkopischen, histologischen und intraoperativen Fehldiagnose. Geburtsh Frauenheilk. 1998; 58: 446–50.
3. Adhikari LJ, Rulong SR. Florid diffuse peritoneal deciduosis mimicking carcinomatosis in a primigravida patient: a case report and review of the literature. Int J Clin Exp Pathol. 2013; 6 (11): 2615–9.
4. Meresman GF, Auge L, Baranao RI, et al. Oral contraceptives suppress cell proliferation and enhance apoptosis of eutopic endometrial tissue from patients with endometriosis. Fertil Steril. 2002; 77: 1141–7.
5. Pateman K, Moro F, Mavrelos D, et al. Natural history of ovarian endometrioma in pregnancy. BMC Womens Health. 2014; 14: 128.
6. Leone Roberti Maggiore U, Ferrero S, Mangili G, et al. A systematic review on endometriosis during pregnancy: diagnosis, misdiagnosis, complications and outcomes. Hum Reprod Update. 2016; 22 (1): 70–103.
7. Groszmann Y, Howitt BE, Bromley B, Feltmate CM, Benacerraf BR. Decidualized endometrioma masquerading as ovarian cancer in pregnancy. J Ultrasound Med. 2014; 33 (11): 1909–15. DOI: 10.7863/ultra.33.11.1909.
8. Bailleux M, Bernard JP, Benachi A, Deffieux X. Ovarian endometriosis during pregnancy: a series of 53 endometriomas. Eur J Obstet Gynecol Reprod Biol. 2017; 209: 100–4. DOI: 10.1016/j.ejogrb.2015.09.037.
9. Mascilini F, Moruzzi C, Giansiracusa C, et al. Imaging in gynecological disease. 10: Clinical and ultrasound characteristics of decidualized endometriomas surgically removed during pregnancy. Ultrasound Obstet Gynecol. 2014; 3 (44): 354–60.
10. Barbieri M, Somigliana E, Oneda S, et al. Decidualized ovarian endometriosis in pregnancy: a challenging diagnostic entity. Hum Reprod. 2009; 8 (24): 1818–24.
11. Graupera B, Pascual M, Hereter L, et al. Dezidualization of endometrioma during pregnancy mimicking a malignant ovarian tumor. Ultrasound Obstet Gynecol. 2013; 42 (S1): 71.
12. Ashrafjan LA, Kurcer MA, Gerasimova AA, Klimenko PA. Pogranichnye i zlokachestvennye opuholi jaichnikov vo vremja beremennosti. Onkoginekologija. 2019; 3 (31): 68–77. Russian.
13. Gerasimova AA, Shvyrev SL, Solomatina AA, Gus AI, Klimenko PA. Sposob vyjavlenija haraktera jaichnikovyh obrazovanij. Onkologija. 2013; 1; 34–40. Russian.
14. Tingulstad S, Hagen B, Skjeldestad FE, et al. Evaluation of a risk of malignancy index based on serum CA125, ultrasound findings and menopausal status in the preoperative diagnosis of pelvic masses. Brit. J. Obstet. Gynaecol. 1996; 103 (8): 826–31.
15. Jacobs I, Oram D, Fairbanks J, et al. A risk of malignancy index incorporating CA125, ultrasound and menopausal status for the accurate pre-operative diagnosis of ovarian cancer. Brit J Obstet Gynaecol. 1990; 97; 922–9.
16. Bulanov MN, Gorta RN. Ul'trazvukovoe issledovanie jendometrioidnyh kist jaichnikov vo vremja beremennosti. Ul'trazvukovaja i funkcional'naja diagnostika. 2015; 1: 55–71. Russian.
17. Bromley B, Benacerraf B. Adnexal masses during pregnancy: accuracy of sonographic diagnosis and outcome. J Ultrasound Med. 1997; 7 (16); 447–52.
18. Ueda Y, Enomoto T, Miyatake T, et al. A retrospective analysis of ovarian endometriosis during pregnancy. Fertil Steril. 2010; 94 (1): 78–84.
19. Fruscella E, Testa AC, Ferrandina G, et al. Sonographic features of decidualized ovarian endometriosis suspicious for malignancy. Ultrasound Obstet Gynecol. 2004; 5 (24): 578–80.
20. Carvalho LFP, Rossener R, Azeem A, et al. From conception to birth — how endometriosis affects the development of each stage of reproductive life Minerva Ginecol. 2013; 65 (2): 181–98.
21. Vercellini P, Parazzini F, Pietropaolo G, et al. Pregnancy outcome in women with peritoneal, ovarian and rectovaginal endometriosis: a retrospective cohort study. BJOG. 2012; 119 (12): 1538–43. DOI: 10.1111/j.1471-0528.2012.03466.x.
22. Papp Z, Petri I, Villányi E, Tiszlavicz L, Ugocsai G. Deciduosis causing perforating appendicitis in the early postpartum period following caesarean section. Orv Hetil. 2008; 149 (7): 329–31. DOI: 10.1556/OH.2008.28227.
23. Heatley MK, Maxwell P, Toner PG. The immunophenotype

of human decidua and extrauterine decidual reactions. Histopathology. 1996; 29: 437–42.
24. Lockwood CJ, Kayisli UA, Stocco C, et al. Abruption-induced preterm delivery is associated with thrombin-mediated functional progesterone withdrawal in decidual cells. Am J Pathol. 2012; 181: 2138–48. DOI: 10.1016/j.ajpath.2012.08.036.
25. Lier MCI, Brosens IA, Mijatovic V, Habiba M, Benagiano G. Decidual bleeding as a cause of spontaneous hemoperitoneum in pregnancy and risk of preterm birth. Gynecol Obstet Invest. 2017; 82 (4): 313–21. DOI: 10.1159/000468933.
26. Lüdders DW, Henke RP, Saba M, et al. Severe maternal pre- and postpartum intra-abdominal bleeding due to deciduosis. Geburtshilfe Frauenheilkd. 2015; 75 (3): 259–62. DOI: 10.1055/s-0035-1545876.

Литература

1. Marino T, Craigo SD. Managing adnexal masses in pregnancy. Contemp Obstet Gynecol. 2000; 45: 130–43.
2. Kommos F, Pfisterer J, Peters F, et al. Ektope Dezidualreaktion — möglicher Anlass zur kolposkopischen, histologischen und intraoperativen Fehldiagnose. Geburtsh Frauenheilk. 1998; 58: 446–50.
3. Adhikari LJ, Rulong SR. Florid diffuse peritoneal deciduosis mimicking carcinomatosis in a primigravida patient: a case report and review of the literature. Int J Clin Exp Pathol. 2013; 6 (11): 2615–9.
4. Meresman GF, Auge L, Baranao RI, et al. Oral contraceptives suppress cell proliferation and enhance apoptosis of eutopic endometrial tissue from patients with endometriosis. Fertil Steril. 2002; 77: 1141–7.
5. Pateman K, Moro F, Mavrelos D, et al. Natural history of ovarian endometrioma in pregnancy. BMC Womens Health. 2014; 14: 128.
6. Leone Roberti Maggiore U, Ferrero S, Mangili G, et al. A systematic review on endometriosis during pregnancy: diagnosis, misdiagnosis, complications and outcomes. Hum Reprod Update. 2016; 22 (1): 70–103.
7. Groszmann Y, Howitt BE, Bromley B, Feltmate CM, Benacerraf BR. Decidualized endometrioma masquerading as ovarian cancer in pregnancy. J Ultrasound Med. 2014; 33 (11): 1909–15. DOI: 10.7863/ultra.33.11.1909.
8. Bailleux M, Bernard JP, Benachi A, Deffieux X. Ovarian endometriosis during pregnancy: a series of 53 endometriomas. Eur J Obstet Gynecol Reprod Biol. 2017; 209: 100–4. DOI: 10.1016/j.ejogrb.2015.09.037.
9. Mascilini F, Moruzzi C, Giansiracusa C, et al. Imaging in gynecological disease. 10: Clinical and ultrasound characteristics of decidualized endometriomas surgically removed during pregnancy. Ultrasound Obstet Gynecol. 2014; 3 (44): 354–60.
10. Barbieri M, Somigliana E, Oneda S, et al. Decidualized ovarian endometriosis in pregnancy: a challenging diagnostic entity. Hum Reprod. 2009; 8 (24): 1818–24.
11. Graupera B, Pascual M, Hereter L, et al. Dezidualization of endometrioma during pregnancy mimicking a malignant ovarian tumor. Ultrasound Obstet Gynecol. 2013; 42 (S1): 71.
12. Ашрафян Л. А., Курцер М. А., Герасимова А. А., Клименко П. А. Пограничные и злокачественные опухоли яичников во время беременности. Онкогинекология. 2019; 3 (31): 68–77.
13. Герасимова А. А., Швырев С. Л., Соломатина А. А., Гус А. И., Клименко П. А. Способ выявления характера яичниковых образований. Онкология. 2013; 1; 34–40.
14. Tingulstad S, Hagen B, Skjeldestad FE, et al. Evaluation of a risk of malignancy index based on serum CA125, ultrasound findings and menopausal status in the preoperative diagnosis of pelvic masses. Brit. J. Obstet. Gynaecol. 1996; 103 (8): 826–31.
15. Jacobs I, Oram D, Fairbanks J, et al. A risk of malignancy index incorporating CA125, ultrasound and menopausal status for the accurate pre-operative diagnosis of ovarian cancer. Brit J Obstet Gynaecol. 1990; 97; 922–9.
16. Буланов М. Н., Горта Р. Н. Ультразвуковое исследование эндометриоидных кист яичников во время беременности. Ультразвуковая и функциональная диагностика. 2015; 1: 55–71.
17. Bromley B, Benacerraf B. Adnexal masses during pregnancy: accuracy of sonographic diagnosis and outcome. J Ultrasound Med. 1997; 7 (16); 447–52.
18. Ueda Y, Enomoto T, Miyatake T, et al. A retrospective analysis of ovarian endometriosis during pregnancy. Fertil Steril. 2010; 94 (1): 78–84.
19. Fruscella E, Testa AC, Ferrandina G, et al. Sonographic features of decidualized ovarian endometriosis suspicious for malignancy. Ultrasound Obstet Gynecol. 2004; 5 (24): 578–80.
20. Carvalho LFP, Rossener R, Azeem A, et al. From conception to birth — how endometriosis affects the development of each stage of reproductive life Minerva Ginecol. 2013; 65 (2): 181–98.
21. Vercellini P, Parazzini F, Pietropaolo G, et al. Pregnancy outcome in women with peritoneal, ovarian and rectovaginal endometriosis: a retrospective cohort study. BJOG. 2012; 119 (12): 1538–43. DOI: 10.1111/j.1471-0528.2012.03466.x.
22. Papp Z, Petri I, Villányi E, Tiszlavicz L, Ugocsai G. Deciduosis causing perforating appendicitis in the early postpartum period following caesarean section. Orv Hetil. 2008; 149 (7): 329–31. DOI: 10.1556/OH.2008.28227.
23. Heatley MK, Maxwell P, Toner PG. The immunophenotype of human decidua and extrauterine decidual reactions. Histopathology. 1996; 29: 437–42.
24. Lockwood CJ, Kayisli UA, Stocco C, et al. Abruption-induced preterm delivery is associated with thrombin-mediated functional progesterone withdrawal in decidual cells. Am J Pathol. 2012; 181: 2138–48. DOI: 10.1016/j.ajpath.2012.08.036.
25. Lier MCI, Brosens IA, Mijatovic V, Habiba M, Benagiano G. Decidual bleeding as a cause of spontaneous hemoperitoneum in pregnancy and risk of preterm birth. Gynecol Obstet Invest. 2017; 82 (4): 313–21. DOI: 10.1159/000468933.
26. Lüdders DW, Henke RP, Saba M, et al. Severe maternal pre- and postpartum intra-abdominal bleeding due to deciduosis. Geburtshilfe Frauenheilkd. 2015; 75 (3): 259–62. DOI: 10.1055/s-0035-1545876.

RESISTIVE INDEX OF INTERNAL CAROTID ARTERY AND BRAIN NETWORKS IN PATIENTS WITH CHRONIC CEREBRAL ISCHEMIA

Fokin VF ✉, Ponomareva NV, Medvedev RB, Konovalov RN, Krotenkova MV, Lagoda OV, Tanashyan MM

Research Center of Neurology, Moscow, Russia

Quantitative assessment of cerebral hemodynamics is important for patients with chronic cerebral ischemia (CCI), as it helps to reveal the pathogenesis of the disease and set the course for effective prevention and treatment. The study was aimed to assess the correlation of the left carotid artery (ICA) resistive index (RI) with cognitive functions and brain network organization based on fMRI data in patients with CCI (51 males and 105 females). The listed above indicators were studied in patients with the left ICA RI values below and above the average (0.54 ± 0.013). The lower, normal physiological ICA resistance levels corresponded to the more successful realization of verbal cognitive functions. In the first group, RI was within normal range (RI = 0.42 ± 0.007), and in the second group RI exceeded normal levels (RI = 0.61 ± 0.01). Variation of the right ICA RI did not correlate with the characteristics of verbal cognitive functions. FMRI data analysis was used to assess the differences in connectivity between various brain regions in the groups with low and high RI. The normal physiological and elevated RI values of the left ICA correlated with differences in the organization of brain networks: normal physiological RI values corresponded to a better organization of hemispheric connections in the basal ganglia and brainstem, and high RI values corresponded to a better organization of connections between the frontal regions and the cerebellum as well as occipital areas of the cerebral cortex. The left ICA RI can be considered as a biomarker of cognitive decline and brain networks reorganization in patients with CCI.

Keywords: chronic cerebral ischemia, internal carotid artery, resistive index, cognitive functions, neural networks

Author contribution: Fokin VF — study concept, manuscript writing; Ponomareva NV — statistical analysis, manuscript writing; Medvedev RB — duplex ultrasonography, hemodynamic data analysis; Konovalov RN — fMRI data acquisition and analysis; Krotenkova MV — fMRI data analysis, study design; Lagoda OV — clinical data analysis; Tanashyan MM — clinical data analysis, study design.

Compliance with ethical standards: the study was approved by the Ethics Committee of the Research Center of Neurology (protocol № 11/14 dated November 19, 2014); the informed consent was submitted by all patients.

✉ **Correspondence should be addressed:** Vitaly F. Fokin
Volokolamskoye shosse, 80, Moscow, 125367; fvf@mail.ru

Received: 27.10.2021 **Accepted:** 15.11.2021 **Published online:** 27.11.2021

DOI: 10.24075/brsmu.2021.055

ИНДЕКС РЕЗИСТЕНТНОСТИ ВНУТРЕННИХ СОННЫХ АРТЕРИЙ И НЕЙРОСЕТИ МОЗГА ПРИ ХРОНИЧЕСКОЙ ЦЕРЕБРАЛЬНОЙ ИШЕМИИ

В. Ф. Фокин ✉, Н. В. Пономарева, Р. Б. Медведев, Р. Н. Коновалов, М. В. Кротенкова, О. В. Лагода, М. М. Танашян

Научный центр неврологии, Москва, Россия

Изучение количественных показателей церебральной гемодинамики актуально для больных хронической ишемией мозга (ХИМ), поскольку оно помогает раскрыть патогенез этого заболевания, а также определить направления его эффективной диагностики и лечения. Целью работы было оценить сопряженность индекса резистентности (RI) левой внутренней сонной артерии (ВСА) с когнитивными функциями и организацией церебральных нейросетей по данным фМРТ у больных ХИМ (51 мужчина и 105 женщин). Указанные показатели исследовали при значениях RI левой ВСА ниже и выше среднего уровня (0,54 ± 0,013). Более низкий, физиологически нормальный уровень резистентности левой ВСА соответствовал более успешному выполнению когнитивных вербальных функций. В первой группе RI находился в пределах физиологической нормы (RI = 0,42 ± 0,007), тогда как во второй RI был выше нормальных значений (RI = 0,61 ± 0,01). Вариация RI правой ВСА не была взаимосвязана с характеристиками вербальных функций. Посредством анализа фМРТ определяли разность показателей коннективности между различными областями мозга в группах с низким и высоким RI. Физиологически нормальный и повышенный RI левой ВСА сопряжены с различиями в организации нейросетей: при физиологически нормальном RI лучше выражены межполушарные коммуникации на уровне базальных ганглиев и ствола мозга, а при высоком — связи, соединяющие лобные области с мозжечком и затылочными областями коры. RI левой ВСА можно рассматривать как биомаркер когнитивного снижения и реорганизации нейронных сетей у больных ХИМ.

Ключевые слова: хроническая ишемия мозга, внутренняя сонная артерия, индекс резистентности, когнитивные функции, нейросети

Вклад авторов: В. Ф. Фокин — концепция исследования, написание статьи; Н. В. Пономарева — статистический анализ, написание статьи; Р. Б. Медведев — дуплексное сканирование; анализ гемодинамических данных; Р. Н. Коновалов — регистрация и анализ фМРТ; М. В. Кротенкова — анализ фМРТ, дизайн исследования; О. В. Лагода — клинический анализ; М. М. Танашян — клинический анализ, дизайн исследования.

Соблюдение этических стандартов: исследование одобрено этическим комитетом Научного центра неврологии (протокол № 11/14 от 19 ноября 2014 г.); все участники подписали информированное согласие на участие в исследовании.

✉ **Для корреспонденции:** Виталий Федорович Фокин
Волоколамское шоссе, д. 80, г. Москва, 125367; fvf@mail.ru

Статья получена: 27.10.2021 **Статья принята к печати:** 15.11.2021 **Опубликована онлайн:** 27.11.2021

DOI: 10.24075/vrgmu.2021.055

Chronic cerebral ischemia (CCI) is among prevalent socially significant vascular diseases [1]. Maintaining the normal levels of cerebral circulation is a major challenge for patients with CCI. In this regard, the internal carotid artery (ICA) blood flow plays a vital part in maintaining the normal function of the brain. There are numerous papers, which demonstrate that impaired cerebral circulation through ICA results in hypoxia, structural and functional changes in the basin of ICA, and cognitive impairment, especially in case of impaired left ICA blood flow, since the left hemisphere is involved in organization and regulation of many cognitive functions in right-handed individuals [2]. There is a number of cerebral blood flow indicators, commonly used to characterize circulation: linear blood flow velocity and volumetric blood flow rate, resistive index (RI), etc. RI has been used in our study, since this is a composite indicator being the difference between the systolic

and diastolic blood velocities divided by the systolic velocity. Along with the intima-media complex thickness, this indicator is used to describe cerebral arteriosclerosis. RI shows an upward trend with the progress of CCI and small vessel diseases [3].

Another aspect just as important in this problem pertains to the question of which neurophysiological mechanisms the increased ICA RI values are related to. Currently, the concept of "brain networks" is widely used, significantly owing its development to the success of functional MRI (fMRI). The concept of connectivity, i.e. the synchronized changes of blood oxygen level-dependent (BOLD) signal, which, according to many researchers, indicate the involvement of these regions in the joint functional system, is the key concept in brain network research. The BOLD signal changes reflect the transition of hemoglobin, contained in red blood cells, from oxidized to reduced form in various brain structures. Temporal correlations of low-frequency BOLD signal fluctuations in various brain regions reveal the organized functional brain networks. Connectivity, derived from resting state fMRI data, provides the means to describe and investigate intercentral relationships, it is considered a potential biomarker of neurological and mental disorders [4, 5].

Depicturing of neural networks made it possible to better understand the dynamics of nerve centers in cerebrovascular disorders leading to neuron dysfunction and their death.

With the development of chronic disorders of cerebral circulation, the cortical nerve centers and other structures of the brain are disproportionately affected, which leads to the emergence of a new neural organization. Thus, according to the authors of [6], the volume of the hippocampus, thalamus, putamen, angular gyrus and other structures depends on the level of oxygen saturation in the blood, but the structures listed above differ in their sensitivity to hypoxia. In addition, the density of neurons varies in different areas of the brain, and the density of capillaries is much more uniform [7]. Therefore, it can be assumed that increased arterial stiffness due to atherosclerosis, reflected in an increase in RI and accompanied by hemodynamic disorders, will affect the reorganization of the brain network due to hypoxia occurring in the most vulnerable areas of the brain [8]. This determines the relevance of studying RI in order to solve a whole range of problems related to the CCI. Two of these problems are the most significant: the correlation of the above indicator with cognitive functions and the relationship between RI and brain networks.

The study was aimed to assess the correlation of ICA RI with cognitive decline and the indicators of the resting-state networks in patients with CCI.

METHODS

The study was carried out in 2019–2021 at the Research Center of Neurology. A total of 156 patients with CCI (51 males and 105 females) aged 51–85 (the average age was 67.0 ± 0.69 years, SD 8.74) were enrolled. Cognitive impairment is observed in patients with CCI, the patients differ mainly in quantitative characteristics of memory impairment, performance, irritability, brainstem symptoms, etc. The main etiological causes of CCI in the patients examined were as follows: atherosclerosis, arterial hypertension (including the hypertension disease), venous insufficiency, etc. Arterial hypertension (stage 1 and stage 2 hypertension) was found in all patients. Patients with atherosclerotic plaque buildup in the ICA and ICA stenosis up to 60% were selected for the study.

Inclusion criteria: compliance with stage I or II dyscirculatory encephalopathy; patients, who did not need constant care in their daily life. The patients with stage I or II dyscirculatory encephalopathy differed mainly in quantitative characteristics of cognitive functions and had no history of acute cerebrovascular accidents. Exclusion criteria: dementia rated 1 or higher on the Clinical Dementia Rating Scale [9], the history of acute cerebrovascular accidents (all patients underwent MRI of the brain, in particular to exclude "silent" brain matter lesions, the diffusion-weighted imaging mode was used with a diffusion-weighting factor b = 1000), traumatic brain injuries, severe cardiac or metabolic (type 2 diabetes mellitus) decompensation, stages 3–5 of chronic kidney disease, uncompensated thyroid disease (hypothyroidism). All the subjects were right-handed. Contemporary ideas about the approaches to studying CCI, as well as about dyscirculatory encephalopathy, are described in detail in a number of papers [10–12].

The psychometric assessment included Luria's verbal memory test [13], adapted for patients with this type of vascular disorder. We estimated the total number of words memorized by the patients after five repetitions of 10 words. After the test, we performed a sequential countdown (subtraction from 100 to 7) and evaluated the number of words memorized. The fluency test took into account the number of memorized words beginning with the letters S-, K- and A-. Patients tried to name the maximum number of words (regular and proper nouns) beginning with the letters listed above, within one minute per letter. We estimated the overall (mean) scores on word recall and fluency stability based on the difference between the number of words memorized in the first and last letters. Patients also performed a letter recognition task based on the Kirschner n-back test (the subject found two identical letters next to each other in the free text without spaces), describing the ability to recognize letters non-verbally. pattern and concentration of attention [14].

Patients of both genders (20 males and 35 females) were subjected to T2*-weighted resting-state fMRI in order to detect the BOLD signal using the MAGNETOM Verio 3T MRI system (Siemens; Germany). The subjects were offered the following instruction: to relax as much as possible, to lie still with their eyes closed in order to avoid stimulation of the visual sensory system, and not to think of anything special. Preprocessing of MRI data was performed using SPM12 software (Functional Imaging Laboratory at University College London; UK) in the MATLAB environment (MathWorks; USA). Connectivity was assessed using the CONN-18b application (McGovern Institute for Brain Research, Massachusetts Institute of Technology; USA) of the SPM-12 software toolbox [15].

Table 1. Correlation between right and left ICA RI values and cognitive functions

	Right ICA RI	Left ICA RI
Recognition of nonverbal letter patterns	–0.24; n = 84; p = 0.026	
Stability of verbal fluency		–0.22; n = 82; p = 0.049
Immediate recall		–0.26; n = 67; p = 0.035
Delayed recall		–0.23; n = 77; p = 0.044

Note: n — number of examined patients; p — significance level, females; blank cells correspond to no significant correlation.

Duplex ultrasonography was performed in all patients. Linear and volumetric systolic and diastolic blood flow velocities were assessed in the right and left ICA. Color-flow duplex ultrasonography was carried out using the Toshiba Viamo system (Toshiba; Japan). The nature and the values of linear and volumetric systolic blood flow velocities and RI of the arteries were studied using a generally accepted method with the linear probe 5.0-12.0 MHz. RI was calculated as the difference between the systolic and diastolic blood flow velocities divided by the systolic blood flow velocity.

FMRI was used to assess brain network connectivity in 55 patients, being in a quiet waking state. Connectivity was compared between two groups of patients, which differed in RI. Connectivity between two brain structures is equal to the regression coefficient of BOLD signals in these structures. The differences in connectivity between groups with low and high RI were assessed based on the standardized regression coefficients adjusted for multiple comparisons (false discovery rate, FDR) [15]. The average RI values for both groups are provided in the Results section. This sample of patients (n = 55) was similar ($p > 0.05$) to the sample used for RI assessment (n = 156) based on RI values and psychological test scores.

Connectivity was assessed using the Statistica-12 software package (StatSoft; USA) for analysis of variance and other methods of studying variation, together with SPM-12 and CONN-18b applications in the MATLAB environment. Connectivity and the differences in connectivity between groups were assessed using multiple testing corrections taking into account FDR. The differences were considered significant when $p < 0.05$.

RESULTS

The right and left ICA RI values were not significantly different, these were 0.564 ± 0.011 and 0.548 ± 0.013 respectively. There were no significant differences in RI between the right and the left ICA in males and females (significance level for males p = 0.96, significance level for females p = 0.21). The right and left ICA RI values correlate with each other, and the correlation coefficient is significant with a very high significance level (r = 0.69; n = 154; $p < 0.000001$), that is why bilateral differences depend little on RI values, which may vary in different disease stages.

Studying the correlation of the right and the left ICA RI values with cognitive functions has shown that the main correlation is observed with the characteristics of blood flow through the left ICA (Table 1).

All the correlation coefficients were negative, which meant that the smaller the RI, the better the cognitive indicators (see Table 1). In men, there was a significant correlation between the left ICA RI and the delayed recall score (–0.37; n = 48; p = 0.009).

Characteristics of the right ICA RI correlated with recognition of nonverbal letter patterns, and the left ICA RI correlated with the characteristics of verbal fluency, immediate recall, and delayed recall.

Fig. 1 demonstrates the correlation of the left ICA RI with some cognitive indicators (verbal fluency and delayed recall) in the mixed-gender group. In both cases, lower RI values, which were closer to the normal physiological values, corresponded to better preserved cognitive functions.

The average verbal fluency in all examined patients was 12.9 ± 0.31 words (see Fig. 1A). The average value of this indicator in patients with low verbal fluency (less than 13 words (–1)) was 10.0 ± 0.23 words (SD = 2.03, n = 76). In the group with verbal fluency exceeding 13 words (1), the average value of the indicator was 16.2 ± 0.34 words (SD = 2.69, n = 62).

In a similar fashion, the low and high delayed recall scores were less or more than five words, i.e. the half of the maximum recall score of 10 (see Fig. 1B). In the group with low delayed recall score (–1), the average value was 3.0 ± 0.19 words (SD = 1.18, n = 40). In the group with high delayed recall score (1), the average value was 7.3 ± 0.44 words (SD = 1.19, n = 77).

Thus, the relatively preserved cognitive functions were associated with lower left ICA RI values with a rather high significance level ($p < 0.001$) (Fig. 1B).

RI values for delayed recall are of prime interest, since in this case it may be said that brain plasticity impairment, associated with poor vocabulary recall scores, starts when RI exceeds 0.55, i.e. when low delayed recall values are observed. RI values under 0.54 correspond to relatively normal delayed recall scores. Thus, a boundary between relatively normal and altered RI values is in the range of 0.54–0.55. It is interesting, because this is consistent with the average RI value of 0.54 ± 0.013.

The varying degrees of success in realization of cognitive functions depending on the left ICA RI raise the issue of the brain network state under these conditions. All subjects were divided into two groups with RI values above or below the average (the average values in these groups were 0.42 ± 0.007 and 0.61 ± 0.010, respectively). Fig. 2A demonstrates that higher indicators of interhemispheric connections in the basal ganglia, insular cortex, and cerebellum constitute the

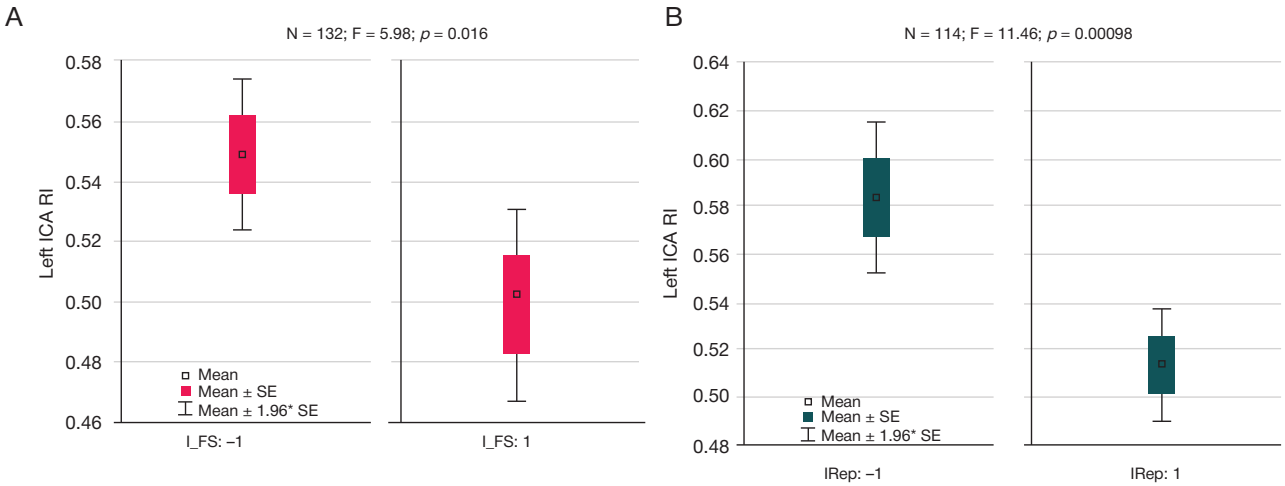

Fig. 1. Left ICA RI in patients with low and high cognitive test scores. **A**. Left ICA RI in patients with low (–1) and high (1) verbal fluency. **B**. Left ICA RI in patients with low (–1) and high (1) delayed recall score. I_FS — verbal fluency; IRep — delayed recall; N — number of examined patients; F — F-test; p — significance level; SE — standard error

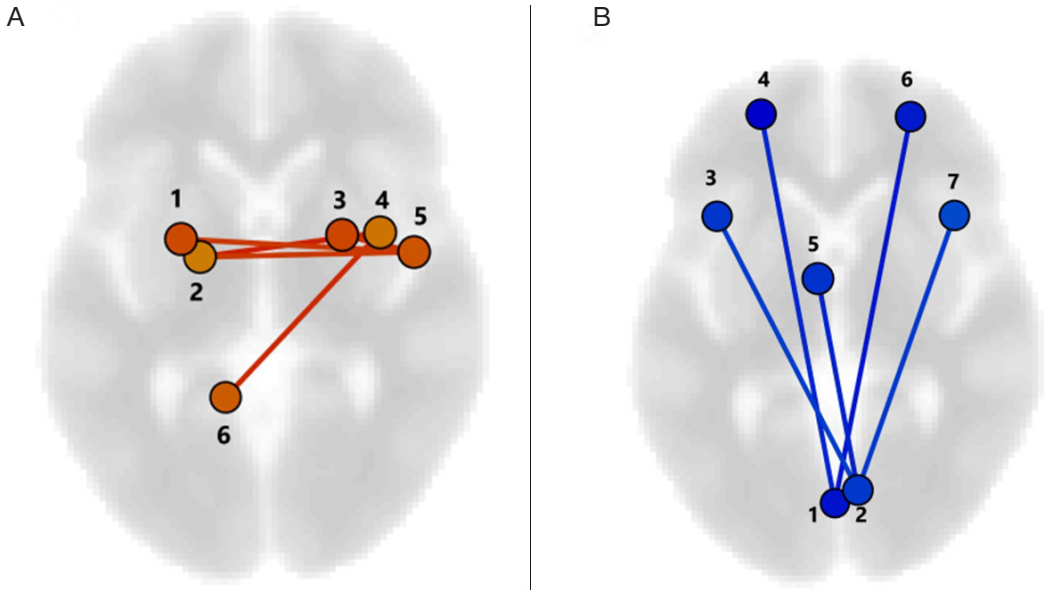

Fig. 2. Differences in connectivity between patients with low (**A**) and high (**B**) left ICA RI. **A**. Connectivity significantly prevailing in patients with low left ICA RI values compared to patients with high RI (r, l – right and left; 1, 3 – Putamen l, r; 2. – Pallidum; 4 – Insular Cortex (IC); 5 – Planum Polare (PP); 6 – Cerebellum). **B**. Connectivity significantly prevailing in patients with high left ICA RI values compared to patients with low RI (1 – NetWorks Cerebellar PosteRIor (NW Cereb Post); 2 – SupracalcaRIne Cortex (SCC); 4, 6 – Frontal Pole (FP) l, r; 3, 7 – Frontal Operculum (FO); 5 – Supplementary Motor Cortex (SMC))

main difference between brain networks in patients with normal physiological RI compared to blood flow in patients with more stiff vascular walls (high RI). The relatively higher connectivity of neuronal networks of the cerebellum and a part of sphenoidal cortex with the frontal regions, comprising frontal pole and motor regions, were observed in patients with higher RI. The reported effect did not correlate with age, since the group with lower RI was older (68.8 ± 1.5 years), and the group with higher RI was younger (62.9 ± 2.1 years).

The differences were statistically significant at $p = 0.025$. However, in the older group, higher indicators of cognitive functions were observed, especially indicators of delayed recall. This could be due to the peculiarities of the sample of a random variable, as well as to the different degree of malignancy of the disease in patients of different age groups, as in other diseases (Alzheimer's disease, etc.).

Statistical parameters of the discussed connections are presented in Table 2.

The data obtained demonstrate that strong interhemispheric connections in the basal ganglia and cerebral cortex are probably the factor associated with preserved cognitive functioning.

DISCUSSION

The average RI values in patients with CCI, registered during our study, were close to the index values, registered in older people of appropriate age. Some authors point out that RI of 0.7 is the upper boundary of the normal range in people of elderly and senile age [16]. Our records show that in patients with CCI this boundary for the left ICA passes through 0.55. Regardless of the system of the circle of Willis, blood flow through the left and right ICA has more to do with blood supply of ipsilateral hemisphere than with blood supply of contralateral hemisphere. Therefore, the decreased (primarily due to atherosclerosis) left or right carotid artery blood flow affects various cognitive functions or, according to some authors, verbal and nonverbal intelligence [2]. According to our information, cognitive processes, associated with verbal functions, correlate with the left ICA RI, and those, associated with nonverbal functions, correlate with the right ICA RI.

Mild cognitive impairment is often observed in patients with unilateral stenosis and high ICA RI. However, the functional and structural integrity of brain networks has been reported. Alternatively, the developing cognitive decline is almost always

Table 2. Significant differences in connectivity between patients with low and high left ICA RI values. **A**. Positive differences. **B**. Negative differences

Connectivity A	T values	*p* (unadjusted)	*p* (FDR)
PP r-Putamen r	T(49) = 3.39	0.0007	0.0487
PP r-Putamen l	T(49) = 3.34	0.0008	0.0487
PP r-Pallidum l	T(49) = 3.30	0.0009	0.0487
IC r-Pallidum l	T(49) = 3.65	0.0003	0.0388
IC r-Cerebellum9 l	T(49) = 3.52	0.0005	0.0388
Connectivity B			
SCC r-SMC l	T(49) = –3.70	0.0003	0.0420
SCC r-FO r	T(49) = –3.39	0.0007	0.0420
SCC r-FO l	T(49) = –3.35	0.0008	0.0420
NW Cereb Post-FP r	T(49) = –3.86	0.0002	0.0266
NW Cereb Post-FP l	T(49) = –3.64	0.0003	0.0266

Note: T — Student's *t*-test; *p* (unadjusted) — significance level unadjusted for multiple comparisons; *p* (FDR) — significance level adjusted for multiple comparisons; FDR — false discovery rate; other keys are provided in the notes to Fig. 2

accompanied by brain network alterations. Thus, cognitive deficit is an important indicator of the neuronal network rearrangement [4]. The fact, that blood flow through the left and right carotid arteries is strongly associated with blood supply of ipsilateral hemisphere, is important. This means that the decreased blood flow through the left ICA is followed by impaired cognitive, mainly verbal, functions, and the decreased blood flow through the right ICA is often asymptomatic and is seldom related to verbal functions. It is our assessment that structural impairments in neuronal networks, and cognitive decline in the context of abnormal hemodynamics and increased RI result from the functional decline in various brain structures due to unequal sensitivity of those to oxygen deficiency. This occurs for two reasons: because of different sensitivity of the cortex and subcortical structures to oxygen deficiency, and because of focal and diffuse lesion in brain structures, common to CCI. No MRI-visible foci were found in the studied sample.

However, brain self-regulation, being the principle of brain functioning, is preserved, but the functional system is formed by different neurons. Reorganization of the resting-state brain networks is observed in patients with stenosis in either one or both ICA. This is probably due to subtle white matter integrity disruptions. In general, hemodynamic disorders in one hemisphere, followed by cognitive impairment, often lead to changes in brain natworks, affecting both hemispheres [2, 4]. That is perfectly understandable, since both hemispheres are involved in realization of any cognitive function, however, parts, played by the right and the left hemisphere, may vary considerably. That is why interhemispheric communication assumes particular importance, which has been confirmed by our findings. This fact has been noted in some other papers. In particular, it has been shown, that reduced default mode network and frontoparietal networks connectivity correlates with lower verbal fluency and delayed recall scores [17].

The sample of patients with CCI, assessed using fMRI, was smaller compared to the sample of patients, assessed using duplex ultrasonography and psychological testing only. Nevertheless, this does not impose any serious restrictions on the interpretation of the results. The sample of subjects assessed using fMRI (55 patients with CCI) is to be considered representative: the patients were randomly selected; they did not differ in average RI values and psychological test scores. There is no reason to believe that two discussed above samples could reflect different patterns.

In general, juxtaposing the hemodynamic parameters of the major arteries of the head and the characteristics of fMRI BOLD signals is promising in terms of studying the pathogenesis of vascular diseases.

CONCLUSIONS

The left ICA resistive index (RI) correlates with preserved cognitive functions in patients with CCI. The left ICA RI below 0.55–0.54 corresponds to a more successful realization of verbal cognitive functions. Variation of the right ICA RI does not correlate with the characteristics of verbal cognitive functions. The left ICA RI correlates with differences in the organization of the brain networks: low, normal physiological RI values correspond to the better presented interhemispheric connections in the cerebral cortex, basal ganglia, and brainstem. High RI values correspond to higher connectivity between frontal and occipital cortical regions, as well as with cerebellum. In patients with CCI, the left ICA RI can be considered as a biomarker of cognitive decline and brain networks reorganization.

References

1. Suslina ZA, Illarioshkin SN, Piradov MA. Nevrologija i nejronauki — prognoz razvitija. Annaly klinicheskoj i jeksperimental'noj nevrologii. 2007; 1 (1): 5–9. Russian.
2. Hideyuki I, Fumiaki O, Satoshi S, et. al. Cognitive outcome differences on the side of carotid artery stenting. J Vasc Surg. 2013; 57 (1): 125–30. DOI: https://doi.org/10.1016/j.jvs.2012.07.043.
3. Rinjani A, Mesiano T, Andini PW, et al. Resistive index of internal carotid artery and common carotid artery in patients with cerebral small vascular disease. J Hypertens. 2021: 39: 16-e17. DOI: 10.1097/01.hjh.0000752596.61984.bf.
4. Avirame K, Lesemann A, List J, Witte AV, Schreiber SJ, Flöel A. Cerebral autoregulation and brain networks in occlusive processes of the internal carotid artery. J Cereb Blood Flow Metab. 2015; 35 (2): 240–7. DOI:10.1038/jcbfm.2014.190.
5. Greicius M. Resting-state functional connectivity in neuropsychiatric disorders. Curr Opin Neurol. 2008; 21: 424–30.
6. Marchi NA, Ramponi C, Hirotsu C, et al. Mean oxygen saturation during sleep is related to specific brain atrophy pattern. Ann Neurol. 2020 Jun; 87 (6): 921–30. DOI: 10.1002/ana.25728. Epub 2020 Apr 20. PMID: 32220084.
7. Ventura-Antunes L, Herculano-Houzel S. Energy supply per neuron is constrained by capillary density in the mouse brain. BioRxiv 2020.02.03.932434. DOI: https://doi.org/10.1101/2020.02.03.932434.
8. Marshall RS, Krakauer JW, Matejovsky T, et al. Hemodynamic impairment as a stimulus for functional brain reorganization. J Cereb Blood Flow Metab. 2006; 26 (10): 1256–62. DOI:10.1038/sj.jcbfm.9600274.
9. Morris JC. Clinical dementia rating: a reliable and valid diagnostic and staging measure for dementia of the Alzheimer type. Int Psychogeriatric. 1997; 9 Suppl 1: 173–6; discussion 177–8. DOI: 10.1017/s1041610297004870. PMID: 9447441.
10. Tanashjan MM, Maksimova MJu, Domashenko MA. Discirkuljatornaja jencefalopatija. Putevoditel' vrachebnyh naznachenij. Terapevticheskij spravochnik. 2015; 2: 1–25. Russian.
11. Batasheva TT, Artemova IJu, Vdovichenko TV. Hronicheskaja ishemija mozga: mehanizmy razvitija i sovremennoe kompleksnoe lechenie. Consilium medicum. 2004; 3 (4). Available from: http://old.consilium-medicum.com/media/refer/04_04/51.shtml. Russian.
12. Zaharov VV, Lokshina AB. Kognitivnye narushenija pri discirkuljatornoj jencefalopatii. RMZh. 2009; №20: 1325–31. Russian.
13. Lurija AR. Lekcii po obshhej psihologii. SPb.: Piter, 2006; 320 s. Russian.
14. Fokin VF, Shabalina AA, Ponomareva NV, Medvedev RB, Lagoda OV, Tanashjan MM. Soprjazhennost' pokazatelej jenergeticheskogo obmena i urovnja gormona stressa kortizola s kognitivnymi harakteristikami bol'nyh discirkuljatornoj jencefalopatiej. Annaly klinicheskoj i jeksperimental'noj nevrologii. 2018; 4 (12): 47–51. Russian.
15. Whitfield-Gabrieli S, Nieto-Castanon A. Conn: a functional connectivity toolbox for correlated and anticorrelated brain networks. Brain Connect. 2012; 2 (3): 125–41. DOI: 10.1089/brain.2012.0073.
16. Staub D, Meyerhans A, Bundi B, Schmid HP, Frauchiger B. Prediction of cardiovascular morbidity and mortality: comparison of the internal carotid artery resistive index with the common carotid artery intima-media thickness. Stroke. 2006 Mar; 37 (3):

800–5. DOI: 10.1161/01.STR.0000202589.47401.c6. Epub 2006 Jan 26. PMID: 16439703.
17. Wang Y, Risacher SL, West JD, McDonald BC, Magee TR, Farlow MR. Altered default mode network connectivity in older adults with cognitive complaints and amnestic mild cognitive impairment. J Alzheimers Dis. 2013; 35: 751–60.

Литература

1. Суслина З. А., Иллариошкин С. Н., Пирадов М. А. Неврология и нейронауки — прогноз развития. Анналы клинической и экспериментальной неврологии. 2007; 1 (1): 5–9.
2. Hideyuki I, Fumiaki O, Satoshi S, et. al. Cognitive outcome differences on the side of carotid artery stenting. J Vasc Surg. 2013; 57 (1): 125–30. DOI: https://doi.org/10.1016/j.jvs.2012.07.043.
3. Rinjani A, Mesiano T, Andini PW, et al. Resistive index of internal carotid artery and common carotid artery in patients with cerebral small vascular disease. J Hypertens. 2021: 39: 16-e17. DOI: 10.1097/01.hjh.0000752596.61984.bf.
4. Avirame K, Lesemann A, List J, Witte AV, Schreiber SJ, Flöel A. Cerebral autoregulation and brain networks in occlusive processes of the internal carotid artery. J Cereb Blood Flow Metab. 2015; 35 (2): 240–7. DOI:10.1038/jcbfm.2014.190.
5. Greicius M. Resting-state functional connectivity in neuropsychiatric disorders. Curr Opin Neurol. 2008; 21: 424–30.
6. Marchi NA, Ramponi C, Hirotsu C, et al. Mean oxygen saturation during sleep is related to specific brain atrophy pattern. Ann Neurol. 2020 Jun; 87 (6): 921–30. DOI: 10.1002/ana.25728. Epub 2020 Apr 20. PMID: 32220084.
7. Ventura-Antunes L, Herculano-Houzel S. Energy supply per neuron is constrained by capillary density in the mouse brain. BioRxiv 2020.02.03.932434. DOI: https://doi.org/10.1101/2020.02.03.932434.
8. Marshall RS, Krakauer JW, Matejovsky T, et al. Hemodynamic impairment as a stimulus for functional brain reorganization. J Cereb Blood Flow Metab. 2006; 26 (10): 1256–62. DOI:10.1038/sj.jcbfm.9600274.
9. Morris JC. Clinical dementia rating: a reliable and valid diagnostic and staging measure for dementia of the Alzheimer type. Int Psychogeriatric. 1997; 9 Suppl 1: 173–6; discussion 177–8. DOI: 10.1017/s1041610297004870. PMID: 9447441.
10. Танашян М. М., Максимова М. Ю., Домашенко М. А. Дисциркуляторная энцефалопатия. Путеводитель врачебных назначений. Терапевтический справочник. 2015; 2: 1–25.
11. Баташева Т. Т., Артемова И. Ю., Вдовиченко Т. В. Хроническая ишемия мозга: механизмы развития и современное комплексное лечение. Consilium medicum. 2004; 3 (4). Available from: http://old.consilium-medicum.com/media/refer/04_04/51.shtml.
12. Захаров В. В., Локшина А. Б. Когнитивные нарушения при дисциркуляторной энцефалопатии. РМЖ. 2009; №20: 1325–31.
13. Лурия А. Р. Лекции по общей психологии. СПб.: Питер, 2006; 320 с.
14. Фокин В. Ф., Шабалина А. А., Пономарева Н. В., Медведев Р. Б., Лагода О. В., Танашян М. М. Сопряженность показателей энергетического обмена и уровня гормона стресса кортизола с когнитивными характеристиками больных дисциркуляторной энцефалопатией. Анналы клинической и экспериментальной неврологии. 2018; 4 (12): 47–51.
15. Whitfield-Gabrieli S, Nieto-Castanon A. Conn: a functional connectivity toolbox for correlated and anticorrelated brain networks. Brain Connect. 2012; 2 (3): 125–41. DOI: 10.1089/brain.2012.0073.
16. Staub D, Meyerhans A, Bundi B, Schmid HP, Frauchiger B. Prediction of cardiovascular morbidity and mortality: comparison of the internal carotid artery resistive index with the common carotid artery intima-media thickness. Stroke. 2006 Mar; 37 (3): 800–5. DOI: 10.1161/01.STR.0000202589.47401.c6. Epub 2006 Jan 26. PMID: 16439703.
17. Wang Y, Risacher SL, West JD, McDonald BC, Magee TR, Farlow MR. Altered default mode network connectivity in older adults with cognitive complaints and amnestic mild cognitive impairment. J Alzheimers Dis. 2013; 35: 751–60.

PLASMA LOW MOLECULAR WEIGHT AMINOTHIOLS IN ISCHEMIC STROKE PATIENTS WITH TYPE 2 DIABETES MELLITUS

Maksimova MYu[1] ✉, Ivanov AV[2], Nikiforova KA[2], Virus ED[2], Suanova ET[3], Ochtova FR[3], Piradov MA[1], Kubatiev AA[2]

[1] Research Center of Neurology, Moscow, Russia

[2] Research Institute of General Pathology and Pathophysiology, Moscow, Russia

[3] Evdokimov Moscow State University of Medicine and Dentistry, Moscow, Russia

It was found that ischemic stroke (IS) results in decreased levels of a number of reduced forms of low molecular weight aminothiols (LMWTs). The study was aimed to assess the impact of type 2 diabetes mellitus (T2D) on the total content, reduced forms and redox status of LMWTs in patients with IS. A total of 175 patients with IS in the internal carotid artery basin (the average age was 62 (55–69)) years) were assessed, who were admitted to the Center within the first 10–24 h since the onset of neurological disorder. The index group included 68 patients with IS and T2D (males made up 41.2%). The comparison group consisted of 107 patients with IS and stress hyperglycemia (males made up 57%), and the control group included 31 non-diabetic patients with chronic cerebrovascular disease (CCVD) (males made up 54.8%). The admission plasma levels of LMWTs were assessed by liquid chromatography in all patients. It was found, that IS in patients with T2D was associated with the rapid decrease in total cysteine (tCys), total glutathione (tGSH), total homocysteine (tHcy), reduced glutathione (rGSH), and glutathione redox status (GSH RS), along with the increase in cysteine redox status (Cys RS) and homocysteine redox status (Hcy RS). In contrast to patients with stress hyperglycemia developing during the acute period of IS, patients with T2D had lower tCys, tGSH, and tHcy levels. Thus, GSH RS of 4.06% or lower in the first 24 hours after the IS in patients with T2D was a predictor of poor functional outcome (mRS score was 3 or more 3 weeks after IS).

Keywords: ischemic stroke, type 2 diabetes mellitus, low molecular weight aminothiols

Author contribution: Maksimova MYu — concept formulation, data synthesis, manuscript writing; Ivanov AV — concept formulation, literature analysis, assessment of low molecular weight aminothiols; Nikiforova KA — primary laboratory data acquisition; Virus ED — laboratory data synthesis; Suanova ET — statistical data processing; Ochtova FR — clinical assessment of patients; Piradov MA — study management; Kubatiev AA — study management.

Compliance with ethical standards: the study was approved by the Ethics Committee of the Research Center of Neurology (protocol № 3-1/16 dated March 16, 2016), it was carried out in accordance with the basic principles outlined in the Declaration of Helsinki.

✉ **Correspondence should be addressed:** Marina Yu. Maksimova
Volokolamskoe shosse, 80, Moscow, 125367, Russia; ncnmaximova@mail.ru

Received: 25.10.2021 **Accepted:** 13.11.2021 **Published online:** 08.12.2021

DOI: 10.24075/brsmu.2021.057

НИЗКОМОЛЕКУЛЯРНЫЕ АМИНОТИОЛЫ В ПЛАЗМЕ КРОВИ ПРИ ИШЕМИЧЕСКОМ ИНСУЛЬТЕ В СОЧЕТАНИИ С САХАРНЫМ ДИАБЕТОМ 2-ГО ТИПА

М. Ю. Максимова[1] ✉, А. В. Иванов[2], К. А. Никифорова[2], Э. Д. Вирюс[2], Е. Т. Суанова[3], Ф. Р. Охтова[3], М. А. Пирадов[1], А. А. Кубатиев[2]

[1] Научный центр неврологии, Москва, Россия

[2] Научно-исследовательский институт общей патологии и патофизиологии, Москва, Россия

[3] Московский государственный медико-стоматологический университет имени А. И. Евдокимова, Москва, Россия

Установлено, что ишемический инсульт (ИИ) приводит к снижению ряда восстановленных форм низкомолекулярных аминотиолов (НМАТ). Целью исследования было оценить влияние сахарного диабета 2-го типа (Т2СД) на общее содержание, восстановленные формы и редокс статус НМАТ у пациентов с ИИ. Обследованы 175 пациентов с ИИ в бассейне внутренних сонных артерий (средний возраст 62 (55–69)) года, поступившие в центр в первые 10–24 ч с момента возникновения неврологических нарушений. В основную группу вошли 68 пациентов (41,2% мужчин) с ИИ и Т2СД. Группу сравнения составили 107 пациентов (57% мужчин) с ИИ и стрессовой гипергликемией, контрольную группу — 31 пациент (54,8% мужчин) с хронической цереброваскулярной патологией (ЦВП) без СД. Во всех случаях пациентам при поступлении проводили исследование НМАТ в плазме крови методом жидкостной хроматографии. Установлено, что ИИ у пациентов с Т2СД ассоциируется с резким снижением уровней общего цистеина (оЦис), общего глутатиона (оГлн), общего гомоцистеина (оГцис), восстановленного глутатиона (вГлн), редокс-статуса глутатиона (РС Глн), а также повышением редокс-статуса цистеина (РС Цис) и редокс-статуса гомоцистеина (РС Нсу Гцис). У пациентов с Т2СД, в отличие от пациентов с развитием стрессовой гипергликемии в остром периоде ИИ, отмечены более низкие показатели оЦис, оГлн и оГцис. Таким образом, уровень РС Глн, составляющий 4,06% и менее в первые сутки ИИ у пациентов с Т2СД, является предиктором неблагоприятного функционального прогноза (оценка по шкале mRS составляет 3 балла и более спустя 3 недели после ИИ).

Ключевые слова: ишемический инсульт, сахарный диабет 2-го типа, низкомолекулярные аминотиолы

Вклад авторов: М. Ю. Максимова — разработка концепции, обобщающий анализ полученных данных, написание статьи; А. В. Иванов — разработка концепции, анализ литературы, исследование низкомолекулярных аминотиолов; К. А. Никифорова — сбор и первичный анализ лабораторных показателей; Э. Д. Вирюс — обобщающий анализ полученных лабораторных данных; Е. Т. Суанова — статистическая обработка полученных данных; Ф. Р. Охтова — проведение клинического обследования пациентов; М. А. Пирадов — организация исследования; А. А. Кубатиев — организация исследования

Соблюдение этических стандартов: исследование одобрено этическим комитетом ФГБНУ НЦН (протокол № 3-1/16 от 16 марта 2016 г.), проведено в соответствии с основными принципами Хельсинкской декларации.

✉ **Для корреспонденции:** Марина Юрьевна Максимова
Волоколамское шоссе, д. 80, г. Москва, 125367, Россия; ncnmaximova@mail.ru

Статья получена: 25.10.2021 **Статья принята к печати:** 13.11.2021 **Опубликована онлайн:** 08.12.2021

DOI: 10.24075/vrgmu.2021.057

Stroke is a major cause of morbidity, disability and mortality in the populations of many countries. Type 2 diabetes mellitus (T2D) increases the risk of ischemic stroke (IS) by 2–2.5 times, and the risk of death from stroke by 3 times [1, 2]. Hyperglycemia during the first hours of stroke could be the body's stress response to brain ischemia [3]. Severity of neurohormonal and metabolic disorder reflects the IS severity and contributes to the outcome of the disease [4].

High prevalence of the internal carotid artery (ICA) atherosclerosis in patients with T2D compared to non-diabetic patients has been reported. That is why atherothrombotic stroke is the most common IS pathogenetic subtype in individuals with T2D [5].

Oxidative stress is one of the key factors involved in the pathogenesis of IS. Accumulation of free radical oxidation products results in the enzyme SH group blockage and inactivation, DNA hydroxylation, DNA fragmentation, and the resulting destabilization of cell membranes [6, 7].

Low molecular weight aminothiols (LMWTs) are highly sensitive to oxidative stress. Oxidized forms of LMWTs predominate in blood plasma; redox status (RS) is the ratio between the reduced forms and the total content of each thiol. Experimental studies and clinical trials report the decrease in the levels of reduced forms during the acute period of IS, which could indicate activation of oxidative processes in case of insufficient antioxidant defence [8, 9].

Both the increase in total homocysteine content (tHcy) and the decrease in the total glutathione content (tGSH) in females were revealed in patients with T2D [10]. Other papers report the decreased glutathione redox status (GSH RS) in blood plasma [11] and whole blood [12] of patients with T2D. Negative correlation between hyperglycemia and plasma tGSH levels was observed in individuals with coronary artery disease (CAD) (r = –0.328; p = 0.011), furthermore, it was shown that T2D was a factor, having an additional negative effect on the tGSH levels [13]. Perhaps low plasma tGSH levels are associated with the increased activity of γ-glutamylcysteine transferase in hyperglycemia [10]. The decreased GSH synthesis along with the possible increase in GSH consumption in red blood cells of patients with T2D were also reported [14].

The study was aimed to assess the impact of T2D on the total content (t), reduced forms (r) and RS of plasma LMWTs in patients with IS.

METHODS

The study included 175 patients with IS in the ICA basin (89 males and 86 females aged 46–84 (the average age was 62 (55–69) years)), admitted to the Research Center of Neurology (Moscow; Russia) within the first 10–24 h since the onset of the neurological disorder. The index group consisted of 68 patients with IS and T2D (males made up 41.2%). The comparison group included 107 patients with IS and stress hyperglycemia (males made up 57%), and the control group consisted of 31 non-diabetic patients with chronic cerebrovascular disease (CCVD) (males made up 54.8%, the average age was 69 (60–75) years).

Inclusion criteria: age 45–85 years; the first IS; admission within the first 6–24 h since the onset of neurological symptoms; cerebral infarction in the ICA basin confirmed by neuroimaging data; T2D or stress hyperglycemia on admission; submitted informed consent to participation in the research study.

Exclusion criteria: T1D; acute myocardial infarction; decompensated kidney disease, liver failure or respiratory failure; class III–IV heart failure.

General medical examination and neurological examination were performed in all patients.

The neurological impairment severity was assessed on admission and in the end of the IS acute period using the National Institutes of Health Stroke Scale (NIHSS) [15]. Neurological impairment was considered mild when NIHSS < 7, moderate when 7 ≤ NIHSS < 14, and severe stroke when 14 ≤ NIHSS. The activities in daily living and the ability to function independently were evaluated on admission and on day 21 of IS using the Bartel Index (BI) [16], and the functional status was assessed with the use of the modified Rankin scale (mRs). The ability to perform all the routine tasks and to be engaged in daily activities corresponded to the mRs score of 0–2 by day 21, and poor functional outcome corresponded to the score of ≥ 3 [17].

IS was diagnosed based on the clinical features and magnetic resonance imaging data (Magneton Symphony and Magneton Avanto, 1.5 T) acquired using standard sequences (T2, T1, T2-FLAIR, T2*). Cerebral arteries were examined by 3D TOF MR angiography. Duplex ultasonography of the cerebral arteries was performed using the Philips iU22 ultrasound system (Philips; Netherlands).

Pathogenetic subtype of IS was defined in accordance with the internationally accepted TOAST (Trial of ORG 10172 in Acute Stroke Treatment) criteria [18].

Fibrinogen assay was carried out with the ACL 9000 coagulation analyzer (Instrumentation Laboratory; USA).

Glucose (hexokinase method), glycated hemoglobin (HbA1c) (immunoturbidimetric assay), total cholesterol, low-density lipoprotein, urea, and creatinine levels were assessed with the Konelab 30i clinical chemistry analyzer (Thermo Fisher Scientific; Finland) using the reagent kits (Randox; UK).

All patients with IS underwent blood glucose monitoring on admission. The HbA1c test was performed in patients with admission blood glucose levels of 6.1 mmol/L or more. The HbA1c levels reflect the blood glucose levels over the last 3 months. The diagnosis of T2D was established based on the American Diabetes Association criteria [19].

All patients with IS received backbone therapy, which included hypotensive, antithrombotic and lipid-lowering agents. Glucose-lowering therapy was used along with the blood glucose monitoring.

The content of LMWTs was defined as described previously [8]. Venous blood was collected into tubes containing sodium citrate (0.38%) and centrifuged at 3,000 g for 3 min. Blood plasma for assessment of total LMWTs was collected and stored at –20 °C. For derivatization, 100 μL of blood plasma were added to 10 μL of 50 mM dithioteritol and 10 μL of the internal standard (0.45 mM penicillamine). Dithiothreitol and penicillamine solutions contained 10 мМ Na-EDTA. The mixture was incubated at 37 °C for 15 min. Subsequently, the 5,5'-dithiobisnitrobenzoic acid (600 μL, 20 mM) dissolved in ethanol was added, and the mixture was incubated at 4 °C for 30 min. After centrifugation at 15 000 g for 5 min, supernatant was dried under a vacuum at 60 °C for 2 h. The pellet was resuspended in 30 mM NaOH prior to analysis.

To define the levels of the LMWTs reduced forms, plasma (100 μL) was added to 25 μL of the 5-sulfosalicylic acid solution (230 g/L) immediately after plasma collection, frozen and and stored at –80 °C. The samples were centrifuged at 15,000 g for 5 min prior to derivatization. Subsequently, 40 μL of supernatant were mixed with 40 μL of 20 mM 5,5'-dithiobisnitrobenzoic acid and 2.5 μM penicillamine in 0.4 M sodium phosphate buffer (pH 8.0). Then 10 μL of 1 M NaOH were added, the solution was mixed for 5 s, and subsequently 12.5 μL of 1 M HCl with 20 mM N-ethylmaleimide were added to quench the reaction.

Analysis was performed using the Waters ACQUITY UPLC system (Waters, Milford; USA), equipped with the photodiode array (λPDA) UV detector (absorbance 330 nm; resolution 10.8 nm; frequency 5 s-1) and the Poroshell 120 SBC18 column (2.8 μm, 150 μm × 2 mm) (Agilent; USA). The temperature of the column and samples of 50 and 10 °C, respectively, was maintained. The volume of the sample injection was 10 μL, and the flow rate was 0.2 mL/min. Eluent A: 0.1 M ammonium acetate with 0.12% (v/v) HCOOH; eluent B: acetonitrile. Chromatography involved gradient elution using a linear gradient of solvent B of 2.5–10% for 5 min. Regeneration was performed with the use of 70% B for 1.5 min, and equilibration was carried out using 2.5% B for 4 min.

Statistical data processing was performed with the IBM SPSS Statistics Version 20.0 software package (IBM Corp.; USA). The Descriptive Statistics module was used to obtain the discriminative model. The quantitative characteristics were presented as median, 25th and 75th percentiles (Me (Q_1–Q_3%)), qualitative data were presented as absolute frequencies and percentage. The Kruskal–Wallis test and Mann–Whitney U test were used to compare the groups based on their quantitative characteristics. The logistic regression procedures were used to identify the prognostic factors. The variables were selected by conditional inclusion. The quality of the logistic regression model was assessed by ROC analysis and calculation of statistical characteristics of the tests (sensitivity, specificity). To evaluate the predictive power of the model, the Area Under Curve (AUC) was assessed. To define the optimal cutoff value, the importance of maintaining the sensitivity-specificity balance was taken into account. The two-tailed critical p-value, used in all comparisons and tests, was set at 0.05.

RESULTS

The main characteristics of patients with IS and CCVD are presented in Table 1. The groups of patients showed no differences in age, gender, and indicators of lipid and protein metabolism. The patients with IS had been constantly taking antihypertensive drugs in 46 cases (26.3%), antiplatelet drugs in 22 cases (12.6%), anticoagulants in 11 cases (6.3%), and statins in 8 cases (4.6%) before being included in the study. The group with CCVD received no preventive therapy before inclusion in the study.

Stroke, caused by the ICA atherothrombosis, was diagnosed in 35 cases (20%), cardioembolic stroke was diagnosed in 50 cases (28.6%), and lacunar stroke due to small-artery disease was diagnosed in 90 cases (51.4%).

In patients with atherothrombotic stroke, the developing step-by-step neurological deficits and the occurrence of single large infarctions affecting the cortical and subcortical regions outside the neighboring vascular territories were observed.

The heart-related causes of the cerebral artery thrombosis were as follows: embologenic forms of CAD (paroxysmal atrial fibrillation in 29 cases (58%), permanent atrial fibrillation in 17 cases (34%), postinfarction cardiosclerosis in 4 cases (8%)). In 34 patients, atrial fibrillation was diagnosed for the first time during the acute period of IS. Sudden emergence of persistent neurological symptoms was a clinical feature typical for cardioembolic stroke. Based on the MRI data, the cortical and subcortical infarctions were localized mostly in the middle cerebral artery basin.

IS, resulting from the hypertensive, small, deep cerebral infarctions, was characterised by the gradually increasing

Table 1. Characteristics of patients with IS and chronic cerebrovascular disease

Parameter	Patients with IS (*n* = 175)	Non-diabetic patients with CCVD (*n* = 31)	*p*
Age, years; Me (Q_1–Q_3)	62 (55–69)	63 (58–69)	0.583
Gender (males/females) (%)	89/86 (50.9/49.1)	17/14 (54.8/45.2)	0.702
IS subtype:			
Atherothrombotic stroke (ATS), *n* (%)	35 (20.0%)		
Cardioembolic stroke (CES), *n* (%)	50 (28.6%)		
Lacunar stroke (LS), *n* (%)	90 (51.4%)		
Stroke severity on admission:			
NIHSS < 7 (mild)/	92 (52.6%)		
7 ≤ NIHSS < 14 (moderate)/	67 (38.3%)		
14 ≤ NIHSS (severe)	16 (9.1%)		
NIHSS on admission; Me (Q_1–Q_3)	6 (3–11)		
NIHSS on day 21; Me (Q_1–Q_3)	3 (2–7)		
mRs on admission; Me (Q_1–Q_3)	3 (2–4)		
mRs on day 21; Me (Q_1–Q_3)	2 (1–3)		
Bartel Index on admission; Me (Q_1–Q_3)	70 (20–90)		
Bartel Index on day 21; Me (Q_1–Q_3)	85 (60–98)		
Good recovery (mRs 0–1), *n* (%)	79 (45.1%)		
Glucose, mmol/L (on admission); Me (Q_1–Q_3)	6.50 (6.22–7.72)	5.6 (5.3–6.0)	< 0.0001
Total cholesterol, mmol/L (on admission); Me (Q_1–Q_3)	5.9 (5.0–6.9)	5.9 (4.9–6.6)	0.277
LDL cholesterol, mmol/L (on admission); Me (Q_1–Q_3)	2.33 (1.80–2.97)	2.2 (1.4–3.0)	0.433
Creatinine, μmol/L	91.0 (79.0–103.0)	86.0 (75.0–97.0)	0.059
Urea, mmol/L (on admission); Me (Q_1–Q_3)	6.5 (5.9–6.9)	6.2 (5.6–6.8)	0.841
Fibrinogen, g/L (on admission); Me (Q_1–Q_3)	3,40 (2,90–4,13)	3,58 (2,97–4,06)	0,119

Table 2. Comparative analysis of the low molecular weight aminothiols plasma levels (μM) and redox status (%) in patients with IS and controls (Mann–Whitney U test)

Indicator	Patients with IS (n = 175); Me (Q_1–Q_3)	Non-diabetic patients with CCVD (n = 31); Me (Q_1–Q_3)	p
tCys (μM)	332.3 (226.8–375.9)	267.1 (230.4–321.5)	0.72
tGSH (μM)	1.64 (1.02–2.52)	3.09 (2.10–3.66)	< 0.0001
tHcy (μM)	13.54 (8.64–18.93)	13.01 (11.45–15.93)	0.932
rCys (μM)	6.28 (4.98–7.19)	6.32 (5.57–8.36)	0.33
rGSH (μM)	0.038 (0.024–0.058)	0.242 (0.177–0.374)	< 0.0001
rHcy (μM)	0.16 (0.13–0.23)	0.14 (0.10–0.17)	0.018
Cys RS, %	2.03 (1.64–2.67)	2.49 (1.98–2.97)	0.066
GSH RS, %	2.04 (1.51–3.47)	8.36 (6.68–15.96)	< 0.0001
Hcy RS, %	1.18 (0.90–1.91)	1.09 (0.83–1.33)	0.041

intensity of neurological deficits in the form of lacunar syndromes. Small, deep cerebral infarctions were localized in the basal ganglia, white matter of cerebral hemispheres, and internal capsule. Stage III hypertension was found in 71 patients (78.9%) with lacunar stroke, and stage II hypertension was observed in 19 patients (21.1%).

The baseline IS severity assessment made it possible to reveal mild neurological impairment (NIHSS < 7) in 92 cases (52.6%), moderate neurological impairment (7 ≤ NIHSS < 14) in 67 cases (38.3%), and severe neurological impairment (14 ≤ NIHSS) in 16 cases (9.1%) (see Table 1).

The admission blood glucose level in patients with IS was 6.50 (6.22–7.72) mmol/L.

Analysis of LMWTs showed that the tGSH, rGSH, and GSH RS levels in the group with IS were significantly decreased (p < 0.0001), and the rHcy and Hcy RS values were significantly increased (p = 0,018 and p = 0.041) compared to the group with CCVD (Table 2).

Analysis of the total sample revealed higher rHcy values in males with RS compared to females (0.17 (0.14–0.24) μM vs. 0.15 (0.12–0.21) μM; p = 0.026).

In the group of IS patients enrolled, T2D was diagnosed in 68 cases, and stress hyperglycemia was diagnosed in 107 cases (Table 3). The duration of T2D of less than 5 years was observed in 22 patients (32.4%), and the disease duration exceeding 5 years was observed in 46 patients (67.6%). In the group of patients with a combination of IS and T2D, the HbA1c level was 7.8% (6.8–9.6). The levels of less than 6.5% were defined in 107 patients (61.1%), the levels of 6.5–6.9% were found in 32 patients (18.3%), 20 patients (11.4%) had the

Table 3. Characteristics of patients with a combination of IS and T2D, and patients with a combination of IS and stress hyperglycemia (Mann–Whitney U test)

Parameter	Patients with a combination of IS and T2D (n = 68)	Patients with IS and stress hyperglycemia (n = 107)	p
Age, years; Me (Q_1–Q_3)	68 (55–75)	62 (54–67)	0.046
Gender (males/females) (%)	28/40 (41.2/58.8)	61/46 (57.0/43.0)	0.045
IS subtype:			
Atherothrombotic stroke (ATS), n (%)	4 (5.9%)	31 (29.0%)	< 0.0001
Cardioembolic stroke (CES), n (%)	34 (50.0%)	16 (15,0%)	< 0.0001
Lacunar stroke (LS), n (%)	30 (44,1%)	60 (56.1%)	0.162
Stroke severity on admission:			
NIHSS < 7 (mild)/	32 (47.1%)	60 (56.1%)	0.278
7 ≤ NIHSS < 14 (moderate)/	30 (44.1%)	37 (34.6%)	0.264
14 ≤ NIHSS (severe)	6 (8.8%)	10 (9.3%)	1.000
NIHSS on admission; Me (Q_1–Q_3)	7 (4–11)	6 (3–10)	0.238
NIHSS on day 21; Me (Q_1–Q_3)	3 (2–8)	3 (2–7)	0.390
mRs on admission; Me (Q_1–Q_3)	70 (28–81)	70 (20–90)	0.790
mRs on day 21; Me (Q_1–Q_3)	85 (60–100)	85 (60–95)	0.957
Bartel Index on admission; Me (Q_1–Q_3)	3 (2–4)	3 (2–4)	0.922
Bartel Index on day 21; Me (Q_1–Q_3)	2 (1–3)	2 (1–3)	0.762
Good recovery (mRs 0-1), n (%); Me (Q_1–Q_3)	30 (44.1%)	49 (45.8%)	0.877
Duration of T2D, years; Me (Q_1–Q_3)	7 (5–10)	–	
Glucose, mmol/L (on admission); Me (Q_1–Q_3)	6.50 (6.18–8.11)	6.40 (6.16–7.08)	0.083
HbA1c, %; Me (Q_1–Q_3)	7.8 (6.8–9.6)	5.5 (5.4–5.8)	< 0.0001
Total cholesterol, mmol/L (on admission); Me (Q_1–Q_3)	5.50 (5.00–6.63)	6.00 (5.00–7.00)	0.353
LDL cholesterol, mmol/L (on admission); Me (Q_1–Q_3)	2.33 (2.16–2.94)	2.27 (1.72–2.98)	0.432
Creatinine, μmol/L (on admission); Me (Q_1–Q_3)	94.0 (80.0–107.0)	88.0 (78.0–100.0)	0.075
Urea, mmol/L (on admission); Me (Q_1–Q_3)	6.40 (5.25–6.93)	6.60 (6.10–6.90)	0.233
Fibrinogen, g/L (on admission); Me (Q_1–Q_3)	3.61 (3.05–4.11)	3.39 (2.83–4.13)	0.267

Table 4. Comparison of the low molecular weight aminothiols plasma levels (μM) and redox status (%) in patients with a combination of IS and T2D, and in patients with a combination of IS and stress hyperglycemia (Mann–Whitney U test)

Indicator	Patients with IS and T2D (n = 68); Me (Q_1–Q_3)	Patients with IS and stress hyperglycemia (n = 107); Me (Q_1–Q_3)	p
tCys (μM)	135.6 (126.7–150.5)	342.6 (307.0–390.0)	< 0.0001
tGSH (μM)	0.84 (0.55–1.1)	2.13 (1.32–2.71)	< 0.0001
tHcy (μM)	5.48 (4.75–6.5)	15.24 (12.97–20.61)	< 0.0001
rCys (μM)	6.57 (4.44–7.72)	6.24 (5.03–7.14)	0.904
rGSH (μM)	0.038 (0.017–0.051)	0.036 (0.025–0.06)	0.223
rHcy (μM)	0.15 (0.12–0.19)	0.17 (0.13–0.24)	0.099
Cys RS, %	4.53 (2.85–5.69)	1.87 (1.46–2.27)	< 0.0001
GSH RS, %	4.47 (2.09–6.02)	1.96 (1.45–2.74)	< 0.0001
Hcy RS, %	2.61 (1.47–3.35)	1.08 (0.84–1.42)	<0.0001

HbA1c levels of 7–7.9%, and the levels exceeding 8% were found in 16 patients (9.2%).

Stroke, resulting from cerebral artery thrombosis with a cardiac source of embolism, was more common in patients with T2D (p < 0.0001), and atherothrombotic stroke was more common in patients with stress hyperglycemia (p < 0.0001). No intergroup differences in the prevalence of lacunar stroke were found (p = 0.162). The examined groups of patients were comparable in the neurological impairment severity and their functional status during the acute period of stroke (see Table 3).

In the group of patients with a combination of IS and T2D, the significantly decreased tCys, tGSH, and tHcy levels were observed compared to the group of patients with IS and stress hyperglycemia (p < 0.0001). However, there were no significant differences in the rCys, rGSH, and rHcy levels between the groups of patients with T2D and stress hyperglycemia. Probably, this entails higher Cys RS, GSH RS, and Hcy RS values in the group of patients with IS and T2D (p < 0.0001) (Table 4).

No significant correlations between the blood glucose levels and the levels of LMWTs were revealed both in the total group of patients with IS and in the distinct groups of patients (T2D and stress hyperglycemia).

When the patients with a combination of IS and T2D were divided based on the degree of functional recovery by day 21, analysis of LMWTs showed that in the group of patients with slight limitations in performing the activities of daily living (mRS score 0–2), the Cys RS and GSH RS were significantly higher compared to patients with severe functional limitations (Cys RS 5.26 vs. 3.51 μM, p = 0.043; GSH RS 4.92 vs. 2.79 μM, p = 0.018) (Table 5).

The logistic regression procedures were used to identify the markers of poor outcome (mRS ≥ 3) in patients with a combination of IS and T2D. The predictive value of GSH RS is presented in Fig. 1. ROC analysis of 68 patients with IS in the ICA basin and T2D showed that the threshold level GSH RS ≤ 4.06% during the first 24 h of IS is a predictor of poor IS outcome (mRS ≥ 3, 21 days after IS). Sensitivity of the model was 63.6%, specificity was 69.6%, and AUC was 0.74 ± 0.09, which corresponds to the good quality in predicting the functional recovery in patients with IS.

DISCUSSION

Chronic hyperglycemia, associated with T2D, is considered one of the risk factors for IS. Glucose is a chemical compound, which actively interacts with proteins and lipids, forming the advanced glycation end products [20, 21]. Hyperglycemia, chronic oxidative stress, and mitochondrial dysfunction, associated with T2D, result in endothelial dysfunction, impaired angiogenesis, activation of hemostasis, and the increased blood-brain barrier permeability [22]. Hyperglycemia enhances oxidative processes by lowering the levels of vitamins E, C, and other antioxidants (uric acid) [11], it is also an additional factor that stimulates and facilitates the reactive oxygen species formation [23].

Chronic hyperglycemia is defined based on the degree of glucose binding to hemoglobin, and the percentage of HbA1c. The higher the level of HbA1, the higher blood glucose levels were observed in the patient during the last 3 months. The normal levels do not exceed 6.5%. The increase in HbA1c by 1% increases the risk of stroke by 17% [24]. In our study, the duration of T2D was 7 years, and the level of HbA1c was 7.8 %.

In individuals with IS, the effects of hyperglycemia on the brain are mediated by both impaired cerebral microcirculation, and the toxic effects on brain tissue. Lactate accumulation, free radical formation, development of cytotoxic cerebral edema, and abnormal blood-brain barrier permeability are attributed to hyperglycemia [25, 26].

Table 5. Low molecular weight aminothiols plasma levels (μM) and redox status (%) in patients with a combination of IS and T2D taking into account the functional recovery (Mann–Whitney U test)

Indicator	Patients with IS and T2D (mRS 0–2 on day 21). n = 28; Me (Q_1–Q_3)	Patients with IS and T2D (mRS 3 or more on day 21); n = 40; Me (Q_1–Q_3)	p
tCys (μM)	132.8 (125.7–140.0)	139.2 (132.2–57)	0.09
tGSH (μM)	0.85 (0.74–1.02)	0.61 (0.35–1.16)	0.416
tHcy (μM)	5.87 (4.78–6.38)	5.33 (4.53–7.01)	0.823
rCys (μM)	6.57 (4.18–8.53)	6.55 (4.72–7.72)	0.959
rGSH (μM)	0.042 (0.02–0.053)	0.026 (0.014–0.042)	0.129
rHcy (μM)	0.15 (0.12–0.17)	0.15 (0.12–0.23)	1,000
Cys RS, %	5.26 (3.20–6.10)	3.51 (2.06–5.04)	0.043
GSH RS, %	4.92 (3.40–6.43)	2.79 (1.97–4.63)	0.018
Hcy RS, %	2.7 (1.97–3.57)	2.17 (1.13–3.18)	0.158

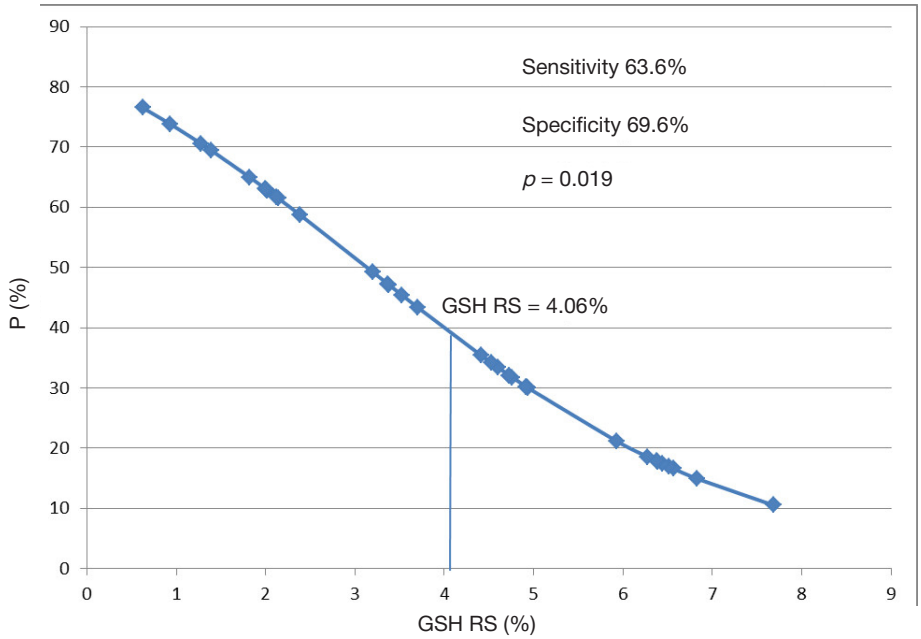

Fig. ROC curve for poor functional outcome (mRS ≥ 3) in patients with a combination of IS and T2D when assessing the glutathione redox status

Hyperglycemia in individuals with T2D and IS results in depletion of the antioxidant system and disorders of all types of tissue metabolism. The thiol/disulfide ratio (SH/SS) is the indicator of cellular and tissue redox homeostasis, as well as of the blood plasma antioxidant capacity [11, 27].

Glutathione is an endogenous thiol tripeptide, composed of cysteine, glutamic acid, and glycine. It is being synthesized continuously, but at a relatively low rate [28]. Glutathione is also a factor involved in regulation of glucose metabolism in patients with cardiovascular disorders [13]. Polymorphism of glutathione S-transferase, the enzyme, involved in the glutathione-mediated detoxification of xenobiotics, contributes to the early cardiovascular complications of diabetes mellitus [29].

In individuals with acute oxidative stress, the total content of glutathione (GSH) is decreased, and the levels of oxidized glutathione (GSSG) are increased, which results in the accelerated GSH/GSSG cycle [27].

Hyperglycemia during the acute period of IS is associated with poor functional outcome [4], however, the efficacy of insulin-based glucose lowering therapy and its effects on the severity and outcome of stroke have not been proven [1].

The findings show that T2D in patients with IS is associated with the rapid decrease in plasma tCys, tGSH, tHcy, rGSH, and GSH RS, along with the increase in Cys RS and Hcy RS.

Perhaps the chronic oxidative stress results in depletion of LMWTs in blood plasma. Irreversible disposal of GSH may be associated with intense oxidative stress, when GSH is exported from cells in order to prevent the significant shift in the redox equilibrium [28]. Presumably, it is the main mechanism explaining the lack of correlations between tGSH, tCys and tHcy, as well as between tGSH and rGSH. No significant correlations between plasma glucose levels and LMWTs have been revealed. This indicates that alterations in the metabolism of LMWTs associated with T2D are mediated by non-glycemic mechanisms.

The GSH RS value of 4.06% or lower during the first 24 h of IS is a predictor of poor IS outcome (mRS ≥ 3, three weeks after IS). Therefore, the search for approaches to glutathione metabolism correction in patients with T2D may be regarded as the potential therapeutic objective during the acute period of IS.

CONCLUSIONS

T2D is a factor having a major impact on the metabolism of LMWTs in patients with IS. Regardless of the lack of correlations between the glucose levels and LMWTs, T2D was associated with reduced total content of homocysteine, cysteine and glutathione, and the glutathione redox status of 4.06% or lower during the first 24 h of IS was associated with poor functional outcome. Glutathione metabolism correction in individuals with a combination of IS and T2D may have a positive impact on the course of IS.

References

1. Hill MD Stroke and diabetes mellitus. Handb Clin Neurol. 2014;126:167-74. DOI: 10.1016/B978-0-444-53480-4.00012-6.
2. Sarwar N, Aspelund T, Eiriksdottir G, Gobin R, Seshasai SR, Forouhi NG, et al. Markers of dysglycaemia and risk of coronary heart disease in people without diabetes: Reykjavik prospective study and systematic review. PLoS Med. 2010; 7 (5): e1000278. DOI: 10.1371/journal.pmed.1000278.
3. Barth E, Albuszies G, Baumgart K, Matejovic M, Wachter U, Vogt J, et al. Glucose metabolism and catecholamines. Crit Care Med. 2007; 35 (9 Suppl): S508–18. DOI: 10.1097/01.CCM.0000278047.06965.20.
4. Zhu B, Pan Y, Jing J, Meng X, Zhao X, Liu L, et al. Stress Hyperglycemia and Outcome of Non-diabetic Patients After Acute Ischemic Stroke. Front Neurol. 2019; 10: 1003. DOI: 10.3389/fneur.2019.01003.
5. Tuttolomondo A, Pinto A, Salemi G, Di Raimondo D, Di Sciacca R, Fernandez P, et al. Diabetic and non-diabetic subjects with ischemic stroke: differences, subtype distribution and outcome. Nutr Metab Cardiovasc Dis. 2008; 18 (2): 152–7. DOI: 10.1016/j.numecd.2007.02.003.
6. Zhao H, Han Z, Ji X, Luo Y. Epigenetic regulation of oxidative stress in ischemic stroke. Aging Dis. 2016; 2016; 7 (3): 295–306. DOI: 10.14336/AD.2015.1009.
7. Khoshnam SE, Winlow W, Farzaneh M, Farbood Y, Moghaddam

HF Pathogenic mechanisms following ischemic stroke. Neurol Sci. 2017; 38 (7): 1167–86. DOI: 10.1007/s10072-017-2938-1.
8. Ivanov AV, Alexandrin VV, Paltsyn AA, Nikiforova KA, Virus ED, Luzyanin BP, et al. Plasma low-molecular-weight thiol/disulphide homeostasis as an early indicator of global and focal cerebral ischaemia. Redox Rep. 2017; 22 (6): 460–6. DOI: 10.1080/13510002.2017.1311464.
9. Maksimova MY, Ivanov AV, Virus ED, Alexandrin VV, Nikiforova KA, Bulgakova PO, et al. Disturbance of thiol/disulfide aminothiols homeostasis in patients with acute ischemic stroke stroke: Preliminary findings. Clin Neurol Neurosurg. 2019; 183: 105393. DOI: 10.1016/j.clineuro.2019.105393.
10. Duman BS, Oztürk M, Yilmazeri S, Hatemi H. Thiols, malonaldehyde and total antioxidant status in the Turkish patients with type 2 diabetes mellitus. Tohoku J Exp Med. 2003; 201 (3): 147–55. DOI: 10.1620/tjem.201.147.
11. Tessier D, Khalil A, Fülöp T. Effects of an oral glucose challenge on free radicals/antioxidants balance in an older population with type II diabetes. J Gerontol A Biol Sci Med Sci. 1999; 54 (11): M541–5. DOI: 10.1093/gerona/54.11.m541.
12. Forrester TE, Badaloo V, Bennett FI, Jackson AA. Excessive excretion of 5-oxoproline and decreased levels of blood glutathione in type II diabetes mellitus. Eur J Clin Nutr. 1990; 44 (11): 847–50. PMID: 2086214.
13. Karolczak K, Kubalczyk P, Głowacki R, Pietruszyński R, Watała C. An inverse relationship between plasma glutathione concentration and fasting glycemia in patients with coronary artery disease and concomitant type 2 diabetes: A pilot study. Adv Clin Exp Med. 2017; 26 (9): 1359–66. DOI: 10.17219/acem/65441.
14. Lutchmansingh FK, Hsu JW, Bennett FI, Badaloo AV, McFarlane-Anderson N, Gordon-Strachan GM, et al. Glutathione metabolism in type 2 diabetes and its relationship with microvascular complications and glycemia. PLoS One. 2018; 13 (6): e0198626. DOI: 10.1371/journal.pone.0198626.
15. Fussner J, Velasco C. Stroke Coordinator Boot Camp. Assessing Stroke — Scores and Scales — American Heart Association. Available from: https://www.heart.org.
16. Quinn TJ, Langhorne P, Stott DJ. Barthel index for stroke trials: development, properties, and application. Stroke. 2011; 42 (4): 1146–51. DOI: 10.1161/STROKEAHA.110.598540.
17. Harrison JK, McArthur KS, Quinn TJ. Assessment scales in stroke: clinimetric and clinical considerations. Clin Interv Aging. 2013; 8: 201–11. DOI: 10.2147/CIA.S32405.
18. Adams HP, Bendixen BH, Kappelle LJ, et al. Classification of subtype of acute ischemic stroke. Definitions for use in a multicenter clinical trial. TOAST. Trial of Org 10172 in Acute Stroke Treatment. Stroke 1993; 24: 35–41. DOI: 10.1161/01.STR.24.1.35.
19. American Diabetes Association. Diagnosis and classification of diabetes mellitus. Diabetes Care. 2013; 36: S67–S74. PMID:15618111.
20. Brownlee M. Biochemistry and molecular cell biology of diabetic complications. Nature. 2001; 414 (6865): 813–20. DOI: 10.1038/414813a.
21. Nishikawa T, Kukidome D, Sonoda K, Fujisawa K, Matsuhisa T, Motoshima H, et al. Impact of mitochondrial ROS production on diabetic vascular complications. Diabetes Res Clin Pract. 2007; 77 Suppl 1: S41–5. DOI: 10.1016/j.diabres.2007.01.031.
22. Smith CJ, Lawrence CB, Rodriguez-Grande B, Kovacs KJ, Pradillo JM, Denes A. The immune system in stroke: clinical challenges and their translation to experimental research. J Neuroimmune Pharmacol. 2013; 8 (4): 867–87. DOI: 10.1007/s11481-013-9469-1.
23. Poulsen RC, Knowles HJ, Carr AJ, Hulley PA. Cell differentiation versus cell death: extracellular glucose is a key determinant of cell fate following oxidative stress exposure. Cell Death Dis. 2014; 5 (2): e1074. DOI: 10.1038/cddis.2014.52.
24. Stratton IM, Adler AI, Neil HA, Matthews DR, Manley SE, Cull CA, et al. Association of glycaemia with macrovascular and microvascular complications of type 2 diabetes (UKPDS 35): prospective observational study. BMJ. 2000; 321 (7258): 405–12. DOI: 10.1136/bmj.321.7258.405.
25. Bruno A, Liebeskind D, Hao Q, Raychev R; UCLA Stroke Investigators. Diabetes mellitus, acute hyperglycemia, and ischemic stroke. Curr Treat Options Neurol. 2010; 12 (6): 492–503. DOI: 10.1007/s11940-010-0093-6.
26. Venkat P, Chopp M, Chen J. Blood-Brain Barrier Disruption, Vascular Impairment, and Ischemia/Reperfusion Damage in Diabetic Stroke. J Am Heart Assoc. 2017; 6 (6): e005819. DOI: 10.1161/JAHA.117.005819.
27. Jones DP. Redox potential of GSH/GSSG couple: assay and biological significance. Methods Enzymol. 2002; 348: 93–112. DOI: 10.1016/s0076-6879(02)48630-2.
28. Wu G, Fang YZ, Yang S, Lupton JR, Turner ND. Glutathione metabolism and its implications for health. J Nutr. 2004; 134 (3): 489–92. DOI: 10.1093/jn/134.3.489.
29. Etemad A, Vasudevan R, Aziz AF, Yusof AK, Khazaei S, Fawzi N, et al. Analysis of selected glutathione S-transferase gene polymorphisms in Malaysian type 2 diabetes mellitus patients with and without cardiovascular disease. Genet Mol Res. 2016; 15 (2). DOI: 10.4238/gmr.15025845.

Литература

1. Hill MD Stroke and diabetes mellitus. Handb Clin Neurol. 2014;126:167-74. DOI: 10.1016/B978-0-444-53480-4.00012-6.
2. Sarwar N, Aspelund T, Eiriksdottir G, Gobin R, Seshasai SR, Forouhi NG, et al. Markers of dysglycaemia and risk of coronary heart disease in people without diabetes: Reykjavik prospective study and systematic review. PLoS Med. 2010; 7 (5): e1000278. DOI: 10.1371/journal.pmed.1000278.
3. Barth E, Albuszies G, Baumgart K, Matejovic M, Wachter U, Vogt J, et al. Glucose metabolism and catecholamines. Crit Care Med. 2007; 35 (9 Suppl): S508–18. DOI: 10.1097/01.CCM.0000278047.06965.20.
4. Zhu B, Pan Y, Jing J, Meng X, Zhao X, Liu L, et al. Stress Hyperglycemia and Outcome of Non-diabetic Patients After Acute Ischemic Stroke. Front Neurol. 2019; 10: 1003. DOI: 10.3389/fneur.2019.01003.
5. Tuttolomondo A, Pinto A, Salemi G, Di Raimondo D, Di Sciacca R, Fernandez P, et al. Diabetic and non-diabetic subjects with ischemic stroke: differences, subtype distribution and outcome. Nutr Metab Cardiovasc Dis. 2008; 18 (2): 152–7. DOI: 10.1016/j.numecd.2007.02.003.
6. Zhao H, Han Z, Ji X, Luo Y. Epigenetic regulation of oxidative stress in ischemic stroke. Aging Dis. 2016; 2016; 7 (3): 295–306. DOI: 10.14336/AD.2015.1009.
7. Khoshnam SE, Winlow W, Farzaneh M, Farbood Y, Moghaddam HF Pathogenic mechanisms following ischemic stroke. Neurol Sci. 2017; 38 (7): 1167–86. DOI: 10.1007/s10072-017-2938-1.
8. Ivanov AV, Alexandrin VV, Paltsyn AA, Nikiforova KA, Virus ED, Luzyanin BP, et al. Plasma low-molecular-weight thiol/disulphide homeostasis as an early indicator of global and focal cerebral ischaemia. Redox Rep. 2017; 22 (6): 460–6. DOI: 10.1080/13510002.2017.1311464.
9. Maksimova MY, Ivanov AV, Virus ED, Alexandrin VV, Nikiforova KA, Bulgakova PO, et al. Disturbance of thiol/disulfide aminothiols homeostasis in patients with acute ischemic stroke stroke: Preliminary findings. Clin Neurol Neurosurg. 2019; 183: 105393. DOI: 10.1016/j.clineuro.2019.105393.
10. Duman BS, Oztürk M, Yilmazeri S, Hatemi H. Thiols, malonaldehyde and total antioxidant status in the Turkish patients with type 2 diabetes mellitus. Tohoku J Exp Med. 2003; 201 (3): 147–55. DOI: 10.1620/tjem.201.147.
11. Tessier D, Khalil A, Fülöp T. Effects of an oral glucose challenge on free radicals/antioxidants balance in an older population with type II diabetes. J Gerontol A Biol Sci Med Sci. 1999; 54 (11): M541–5. DOI: 10.1093/gerona/54.11.m541.
12. Forrester TE, Badaloo V, Bennett FI, Jackson AA. Excessive excretion of 5-oxoproline and decreased levels of blood

glutathione in type II diabetes mellitus. Eur J Clin Nutr. 1990; 44 (11): 847–50. PMID: 2086214.
13. Karolczak K, Kubalczyk P, Głowacki R, Pietruszyński R, Watała C. An inverse relationship between plasma glutathione concentration and fasting glycemia in patients with coronary artery disease and concomitant type 2 diabetes: A pilot study. Adv Clin Exp Med. 2017; 26 (9): 1359–66. DOI: 10.17219/acem/65441.
14. Lutchmansingh FK, Hsu JW, Bennett FI, Badaloo AV, McFarlane-Anderson N, Gordon-Strachan GM, et al. Glutathione metabolism in type 2 diabetes and its relationship with microvascular complications and glycemia. PLoS One. 2018; 13 (6): e0198626. DOI: 10.1371/journal.pone.0198626.
15. Fussner J, Velasco C. Stroke Coordinator Boot Camp. Assessing Stroke — Scores and Scales — American Heart Association. Available from: https://www.heart.org.
16. Quinn TJ, Langhorne P, Stott DJ. Barthel index for stroke trials: development, properties, and application. Stroke. 2011; 42 (4): 1146–51. DOI: 10.1161/STROKEAHA.110.598540.
17. Harrison JK, McArthur KS, Quinn TJ. Assessment scales in stroke: clinimetric and clinical considerations. Clin Interv Aging. 2013; 8: 201–11. DOI: 10.2147/CIA.S32405.
18. Adams HP, Bendixen BH, Kappelle LJ, et al. Classification of subtype of acute ischemic stroke. Definitions for use in a multicenter clinical trial. TOAST. Trial of Org 10172 in Acute Stroke Treatment. Stroke 1993; 24: 35–41. DOI: 10.1161/01.STR.24.1.35.
19. American Diabetes Association. Diagnosis and classification of diabetes mellitus. Diabetes Care. 2013; 36: S67–S74. PMID:15618111.
20. Brownlee M. Biochemistry and molecular cell biology of diabetic complications. Nature. 2001; 414 (6865): 813–20. DOI: 10.1038/414813a.
21. Nishikawa T, Kukidome D, Sonoda K, Fujisawa K, Matsuhisa T, Motoshima H, et al. Impact of mitochondrial ROS production on diabetic vascular complications. Diabetes Res Clin Pract. 2007; 77 Suppl 1: S41–5. DOI: 10.1016/j.diabres.2007.01.031.
22. Smith CJ, Lawrence CB, Rodriguez-Grande B, Kovacs KJ, Pradillo JM, Denes A. The immune system in stroke: clinical challenges and their translation to experimental research. J Neuroimmune Pharmacol. 2013; 8 (4): 867–87. DOI: 10.1007/s11481-013-9469-1.
23. Poulsen RC, Knowles HJ, Carr AJ, Hulley PA. Cell differentiation versus cell death: extracellular glucose is a key determinant of cell fate following oxidative stress exposure. Cell Death Dis. 2014; 5 (2): e1074. DOI: 10.1038/cddis.2014.52.
24. Stratton IM, Adler AI, Neil HA, Matthews DR, Manley SE, Cull CA, et al. Association of glycaemia with macrovascular and microvascular complications of type 2 diabetes (UKPDS 35): prospective observational study. BMJ. 2000; 321 (7258): 405–12. DOI: 10.1136/bmj.321.7258.405.
25. Bruno A, Liebeskind D, Hao Q, Raychev R; UCLA Stroke Investigators. Diabetes mellitus, acute hyperglycemia, and ischemic stroke. Curr Treat Options Neurol. 2010; 12 (6): 492–503. DOI: 10.1007/s11940-010-0093-6.
26. Venkat P, Chopp M, Chen J. Blood-Brain Barrier Disruption, Vascular Impairment, and Ischemia/Reperfusion Damage in Diabetic Stroke. J Am Heart Assoc. 2017; 6 (6): e005819. DOI: 10.1161/JAHA.117.005819.
27. Jones DP. Redox potential of GSH/GSSG couple: assay and biological significance. Methods Enzymol. 2002; 348: 93–112. DOI: 10.1016/s0076-6879(02)48630-2.
28. Wu G, Fang YZ, Yang S, Lupton JR, Turner ND. Glutathione metabolism and its implications for health. J Nutr. 2004; 134 (3): 489–92. DOI: 10.1093/jn/134.3.489.
29. Etemad A, Vasudevan R, Aziz AF, Yusof AK, Khazaei S, Fawzi N, et al. Analysis of selected glutathione S-transferase gene polymorphisms in Malaysian type 2 diabetes mellitus patients with and without cardiovascular disease. Genet Mol Res. 2016; 15 (2). DOI: 10.4238/gmr.15025845.

EFFECTS OF VIRTUAL REALITY EXERGAME ON PSYCHOPHYSIOLOGICAL AND POSTURAL DISORDERS IN ELDERLY PATIENTS

Khizhnikova AE ✉, Klochkov AS, Fuks AA, Kotov-Smolenskiy AM, Suponeva NA, Piradov MA

Research Center of Neurology, Moscow, Russia

Balance impairment at advanced age is a serious medical problem that often has significant implications and affects the quality of the patient's life. Among the underlying causes are overall slowness of motor response and vestibular syndrome. Virtual reality exergames, including reaction and balance training, hold promise for managing balance dysfunction. The aim of this study was to investigate the effects of a combination rehabilitation program containing elements of virtual reality exergame on the postural and psychophysiological parameters of elderly patients with small vascular disease The study was conducted in 24 patients with small vascular disease (median age: 66 years). All patients underwent a virtual reality rehabilitation program. Psychophysiological, postural and clinical evaluations were performed at baseline and after the program was completed. Balance function measured on the Berg scale improved significantly and was 53 [52; 55] after the training program vs 50 [45; 54] at baseline ($p < 0.05$). The strategy of balance control also changed: the Romberg ratio was 266 [199.5; 478.5] before rehabilitation and 221 [149.25; 404] after the program was completed ($p < 0.05$). The most pronounced changes in the measured psychophysiological parameters occurred in the simple audiomotor reaction, which improved from 210 [174.25; 245.5] at baseline to 180.5 [170.5; 208] after rehabilitation ($p < 0.05$). Thus, the combination balance and reaction virtual reality training is an effective rehabilitation method for advanced-age patients with balance impairment.

Keywords: neurorehabilitation, virtual reality, balance impairment, reaction time

Funding: the study was supported by the Presidential Grant MK-118.2020.7.

✉ **Correspondence should be addressed:** Anastasia E. Khizhnikova
Volokolamskoe shosse, 80, Moscow, 125367, Russia; nastushkapal@gmail.com

Received: 26.10.2021 **Accepted:** 24.11.2021 **Published online:** 09.12.2021

DOI: 10.24075/brsmu.2021.058

ВЛИЯНИЕ ТРЕНИРОВОК В ВИРТУАЛЬНОЙ РЕАЛЬНОСТИ НА ПСИХОФИЗИОЛОГИЧЕСКИЕ И ПОСТУРАЛЬНЫЕ НАРУШЕНИЯ У ПОЖИЛЫХ

А. Е. Хижникова ✉, А. С. Клочков, А. А. Фукс, А. М. Котов-Смоленский, Н. А. Супонева, М. А. Пирадов

Научный центр неврологии, Москва, Россия

Нарушение равновесия в пожилом возрасте является острой проблемой в современной медицине и часто приводит к серьезным последствиям, снижающим качество жизни. К основным причинам такого нарушения относят замедление скорости реакции и вестибуло-атактический синдром. Для коррекции нарушений равновесия у данной категории больных наибольший интерес представляет технология виртуальной реальности, в частности с комбинированной тренировкой скорости реакции и равновесия. Целью исследования было изучить влияние комбинированных тренировок в виртуальной среде на постуральные и психофизиологические показатели у пожилых пациентов с хронической ишемией головного мозга (ХИГМ). В исследование было включено 24 пациента с диагнозом ХИГМ (медиана возраста составила 66 лет). Все пациенты проходили тренировку в виртуальной реальности. До и после тренировки пациентам проводили психофизиологическое и стабилометрическое тестирование, а также клиническую оценку. Выявлено, что у пациентов значимо улучшается функция равновесия по шкале баланса Берг до 50 [45; 54], после 53 [52; 55] ($p < 0,05$), а также изменяется стратегия поддержания равновесия по результатам стабилометрии, что подтверждено уменьшением коэффициента Ромберга после реабилитации: до 266 [199,5; 478,5], после 221 [149,25; 404] ($p < 0,05$). Среди психофизиологических показателей наиболее значимые изменения наблюдали в улучшении простой слухо-моторной реакции: до 210 [174,25; 245,5], после 180,5 [170,5; 208] ($p < 0,05$). Таким образом, комбинированная тренировка скорости реакции и равновесия в виртуальной среде является эффективным методом реабилитации пациентов пожилого возраста с нарушением функции равновесия.

Ключевые слова: нейрореабилитация, виртуальная реальность, постуральные нарушения, время реакции

Финансирование: исследование выполнено при финансовой поддержке гранта Президента РФ МК-118.2020.7.

✉ **Для корреспонденции:** Анастасия Евгеньевна Хижникова
ул. Волоколамское шоссе, д. 80, г. Москва, 125367, Россия; nastushkapal@gmail.com

Статья получена: 26.10.2021 **Статья принята к печати:** 24.11.2021 **Опубликована онлайн:** 09.12.2021

DOI: 10.24075/vrgmu.2021.058

Motor and balance dysfunction is the primary cause of increased risk for falling at advanced age. More than one-third of elderly people over 60 years have a gait disturbance. At 60–69 years, the prevalence of gait disorders is about 10.7%, increasing to 61.7% in 80-year-old patients. Gait disturbances are rooted in neurological causes in 75% of cases [1]. Among the leading causes of motor dysfunction are sensory ataxia, parkinsonism, brain damage, and cerebrovascular diseases such as Small vessel disease [2]. The latter usually manifests as gait disturbance (in up to 85% of patients with stage 2 small vascular disease), pyramidal disorders, akinetic rigid syndrome, loss of coordination, including declining ability to maintain balance, etc. [3].

The slowness of postural response to external stimuli is one of the factors affecting balance at advancing age. It is difficult for elderly patients to adequately cope with an unexpected balance disturbance; they typically respond with increased muscle coactivation and joint stiffening, which cannot ensure effective amortization [4]. In another study, elderly patients demonstrated a slow motor response when asked to lift a foot following a visual cue, and often shifted their body weight erroneously in preparation for a step. The difference in reaction times between the groups waned when the preparation stage was excluded from the analysis. Thus, a slow motor response may be associated not only with overall slowness but also with incorrect preparation to movement [5]. Apart from longer reaction time, postural stability is affected by slow braking. In an experiment involving a series of forward and backward movements, elderly participants demonstrated a higher forward velocity (2nd movement) to compensate for overall motor slowness. Besides,

their strategy of movement control was different from that of the young participants, and the braking process took longer. The authors concluded that attempts to adapt to overall motor slowness may lead to increased postural instability [6].

The risk of falls can be prevented or reduced through rehabilitation programs. Over the past two decades, a variety of high-tech methods have been introduced into routine rehabilitation. A substantial body of evidence has been accumulated confirming the effectiveness of robotic technologies, exoskeletons, brain-computer interfaces, non-invasive methods for brain stimulation, etc. [7–12]. In the age of technological abundance, a personalized approach to rehabilitation and the search for predictors of effectiveness of the applied technology and rehabilitation as such are becoming increasingly important [13]. In this light, it would be useful to identify methods for determining the effectiveness of the chosen rehabilitation approach for an individual patient. The aim of this study was to evaluate effects of the integrated rehabilitation program for better balance and faster motor response on postural and psychophysiological parameters.

METHODS

The study was conducted in 24 patients with small vascular disease (5 men and 19 women). The median age was 66 years (61; 72).

The following inclusion criteria were applied: patients of both sexes aged 60 to 70 years with Small vessel disease. Exclusion criteria: severe visual impairment preventing the patients from discriminating images on the screen; severe cognitive impairment preventing the patients from following the instructions; Montreal Cognitive Assessment (MoCA) score < 20 points; severe sensory or motor aphasia; co-morbidities causing static and dynamic balance impairments.

The patients underwent rehabilitation on a virtual reality Rehabunculus system (Intelligence and Innovations; Russia) fitted with a non-contact Kinect sensor (Microsoft; USA).

The rehabilitation course lasted for 10 days and comprised 5 30-min-long sessions per week. Exercises included in the course aimed at training static and dynamic balance function and the speed of motor reaction (Darts, Stepping over the board with the left and right legs, Dodging the ball by bending sideways, Dodging the ball by stepping sideways, Football for the left and right legs, Barley-Brick [14].

Psychophysiological parameters were evaluated using a Psychophysiologist UPFT-1/30 device (Medicom MTD; Russia).

Evaluation was based on the following battery of tests:

1. *A simple visuomotor reaction test* (SVMR). The patient was tasked to press Yes or No in response to a visual cue (a flashing LED indicator on the handheld console) as quickly as possible using their dominant hand.

2. *A complex visuomotor reaction test* (CVMR). The patient was tasked to press Yes (green light) or No (red light) in response to a visual cue as quickly as possible using their dominant hand.

3. *A simple visuomotor reaction to the movement of the pointer indicator* (SVMR -IM). The patient was tasked to press Yes or No as quickly as possible in response to the onset of pointer indicator movement on the “dial face”.

4. *A simple audiomotor reaction test* (SAMR). Headphones were not worn during the test; the patient was tasked to press Yes or No as quickly as possible in response to a loud audio stimulus emitted from the console.

5. *A complex visuomotor reaction to a combination of colors* (CVMR-CC). The patient was tasked to press Yes or No as quickly as possible in response to a certain combination of 3 flashing light stimuli (green leftmost light, red rightmost light).

6. *A functional activity of nervous processes test* (FMNP). The patient was tasked to press Yes or No as quickly as possible in response to a rapidly flashing light (red light — yes, green light or skipped yellow light — no).

7. *A reaction to a moving object test* (RMO). The patient was tasked to press Yes or No with their dominant hand to stop the pointer indicator before it reached the target position (indicated by the flashing light).

The total duration of psychophysiological testing was 30 min. Prior to each test, the patients received the instructions and verbally confirmed that the instructions were understood. The patients put their fingers in a comfortable position above the console. The stimuli were delivered at different time intervals to exclude the possibility of adjusting.

Static and dynamic balance at baseline and after the rehabilitation course was measured using a Stabilan-01-2 system (RITM OKB; Russia) and the Berg balance scale [15].

The obtained data were processed in Statistica v. 7.0 (StatSoft; USA) using the Mann–Whitney U test for independent samples, Wilcoxon test for dependent samples, and Spearman’s correlation coefficient. The results are presented below as medians and lower and upper quartiles (25%, 75%). Differences were considered significant at $p < 0.05$.

RESULTS

Effects of virtual reality training on balance function in elderly patients

The median Berg score was 50 [45; 54] points at baseline, increasing by 3 ($p < 0.05$) points after the rehabilitation course and thus reaching 53 [52; 55] points. The baseline Berg score was negatively correlated with the Berg score after rehabilitation (the correlation coefficient was 0.823 at $p = 0.000005$).

Body sway was analyzed using standard parameters listed in Table 1.

After the rehabilitation course, the Romberg ratio (KoefRomb) was significantly lower ($p < 0.05$) than at baseline (Fig. 1); there was a significant increase in the LFS_c value (length to area ratio in the eyes-closed test) and the strength of correlation between COP position in the sagittal plane relative to the line connecting the lateral and medial malleoli and COP velocity in the eyes-open test (VFY_o).

The eyes-open test revealed a significant ($p < 0.05$) increase (in comparison with baseline values) in the mean COP velocity (V_o), an increase in the velocity index (IV_o), an increase in the time-normalized statokinesigram length on the Y axis (LY_o), a decline in the balance function quality (BFQ_o), an increase in the normalized vectorgram area (VA_o), an increase in the mean linear velocity (MLV_o), especially in the sagittal plane (MLV_o_sag), a trending increase in the COP excursion index (OD_o; $p = 0.055$) and in the time-normalized statokinesigram length on the X axis (LX_o; $p = 0.058$).

The eyes-closed test revealed a significant ($p < 0.05$) increase in the COP excursion index (OD_c), an increase in LFS_c, an increase in the coefficient of sharp velocity vector directional change (CSVVDC_c), an increase in the mean angular velocity (MAV_c), an increase in the mean angular velocity variation amplitude (MAVVA_c), an increase in the angular velocity asymmetry coefficient (AVAC_c), and an increase in total angular displacement (TAD_c).

Table 1. Romberg and stability tests

Parameter	Definition
Romberg test	
Romberg ratio (KoefRomb)	The ratio of the confidence ellipse areas in the eyes-open and eyes-closed tests. This parameter is used to quantify the extent to which the patient uses their vision for standing balance control
Statokinesigram density (LFS_c)	The ratio of the COP path (the length of the statokinesigram) to its area in the eyes-open test. The parameter reflects COP excursion per unit area
VFY_o	The correlation between COP position in the sagittal plane relative to the line connecting the lateral and medial malleoli and COP velocity in the eyes-open test. The parameter describes the distance from the experimental regression curve between the COP coordinate in the sagittal plane and COP velocity
Mean COP velocity (V_o)	Mean COP velocity during the trial
COP velocity index (IV_o)	This parameter is used to calculate mean COP velocity in the sagittal or frontal planes
Time-normalized length of the statokinesigram on the Y axis (LY_o)	The total COP sway path in the vertical plane during the trial
Time-normalized length of the statokinesigram on the X axis (LX_o)	The total COP sway path in the horizontal plane during the trial
Balance function quality (BFQ_o)	This parameter is calculated as the percentage ratio of the area confined by the velocity vector length distribution function and the constant equaling to the area of the square confined by the X and Y axes, the horizontal asymptote of the velocity vector length distribution function and the vertical line. The parameter is used to evaluate how minimal COP velocity is
Vectorgram area (VA_o)	The total area of the vectorgram during signal recording. The higher COP velocity and the sharper velocity vector turns, the higher VA
Mean linear velocity (MLV_o)	Mean linear velocity during the trial
COP excursion index (OD_o)	The ratio of statokinesigram length to the mean COP excursion range during the trial
Coefficient of sharp velocity vector directional change (CSVVDC_c)	Percentage of sharp COP velocity vector turns (over 45°) relative to the total number of vectors
Mean angular velocity (MAV_c)	Mean rate of COP velocity directional changes
Mean angular velocity variation amplitude (MAVVA_c)	Mean absolute value of angular velocity changes at local peaks
Angular velocity asymmetry coefficient (AVAC_c)	Average direction of COP velocity vector rotation
Total angular displacement of vectors (TAD_c)	Total angular displacement of the velocity vector during the trial
Stability test	
Total sway zone (SZone)	The area of the squares with sides equaling to the sum of A/P and M/L displacements
Frontal displacement (MO)	COP displacement in the frontal plane
Mean COP displacement radius (R)	Mean radius of COP displacements
Mean COP velocity (V)	Mean COP velocity during the trial
Rate of statokinesigram area change (SV)	Mean rate of statokinesigram area change
COP velocity index (IV)	Mean COP velocity index
Coefficient of displacement asymmetry in the frontal plane (KAssM(x))	Shows histogram deviation relative to the independent value (the mid-point of the histogram interval which covers most of the values)
Mean linear velocity (MLV)	Mean linear velocity during the trial
Total angular displacement of vectors (TAD_c)	Total angular displacement of the velocity vector during the trial

The stability test revealed a significant ($p < 0.05$) increase in SZone (Fig. 2), an increase in frontal displacement (MO) ($p < 0.01$), an increase in the mean COP displacement radius (R), an increase in the mean COP velocity (V), an increase in the rate of statokinesigram area change (SV), an increase in the velocity index (IV), a reduction in the coefficient of displacement asymmetry in the frontal plane (KAssM(x)), an increase in the mean linear velocity (MLV), and an increase in the total angle of vector displacement (TAD_c).

Effects of virtual reality training on psychophysiological parameters in elderly patients

The simple visuomotor response test showed a trending decrease ($p = 0.052$) in the average reaction time (SVMR_MO) and a trending reduction ($p = 0.061$) in the squared deviation of the reaction time (SVMR_SD). According the statistical analysis, there was a trending increase ($p = 0.069$) in the error rate, which is below referred to as the integrated reliability index (SVMR_IRI) after the training program.

The complex visuomotor response test revealed a significant ($p < 0.05$) increase in sensorimotor performance (CVMR_CNSAL), quantitative CNS activation index (CVMR_P) and reaction time mode amplitude representing the percentage of the shortest reaction times (CVMR_AMODA).

The test of the simple visuomotor reaction to the movement of the pointer indicator demonstrated a trending increase ($p = 0.053$) in the integrated reliability index after the training course (SVMR-IM _IRI).

Changes were the most pronounced for the simple audiomotor reaction ($p < 0.05$): there was an increase in the integral reliability index (SAMR_ IRI), a reduction in the mean

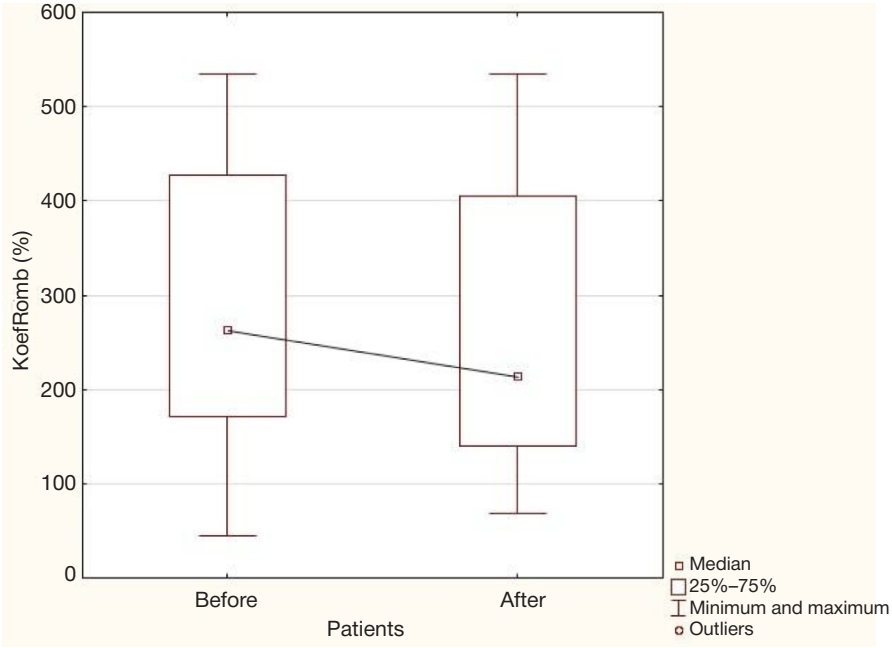

Fig. 1. Romberg ratio before (266 [199.5; 478.5]) and after (221 [149.25; 404]) rehabilitation ($p < 0.05$)

reaction time (SAMR_MO) (Fig. 3) and a reduction in the median value (SAMR_Me).

The reaction to a moving object test conducted after the training course demonstrated a significant ($p < 0.01$) rise in the number (RMO_NS) and percentage (RMO_PS) of successes and a reduction in the number (RMO_ND) and percentage (RMO_PD) of delays (Table 2).

No significant differences were observed between the results of the tests evaluating the complex visuomotor reaction to a combination of colors and the functional activity of nervous processes at baseline and after training.

The correlation analysis showed that the initial number and percentage of delayed RMO were positively correlated with changes the angular velocity asymmetry coefficient ($r = 0.53$; $p < 0.05$) and total angular displacement ($r = 0.57$; $p < 0.05$) measured in the Romberg eyes-closed test. This indicates that patients with initially slower response to a moving object had to adjust their COP position to maintain their balance more frequently and to a greater extent.

Changes in the Berg score were significantly ($p < 0.05$) correlated with the baseline integrated reliability index in the SAMR test (SAMR_IRI), CNS activation level (SAMR_CNSAL), quantitative CNS activation index (SAMR_QCNSAI), number of the classification square (SAMR_CSN), mean SAMR time (SAMR_MO), quickness of response (SAMR_QR), quickness of response in relative units (SAMR_QRR), mean squared deviation of speed (SAMR_MSD), median SAMR time (SAMR_Me), SAMR time mode (SAMR_Mo), and the longest SAMR time (SAMR_MaxT) (Table 3).

These correlations may be explained by the fact that the most pronounced changes on the Berg scale were observed in patients with the worst baseline balance parameters; according

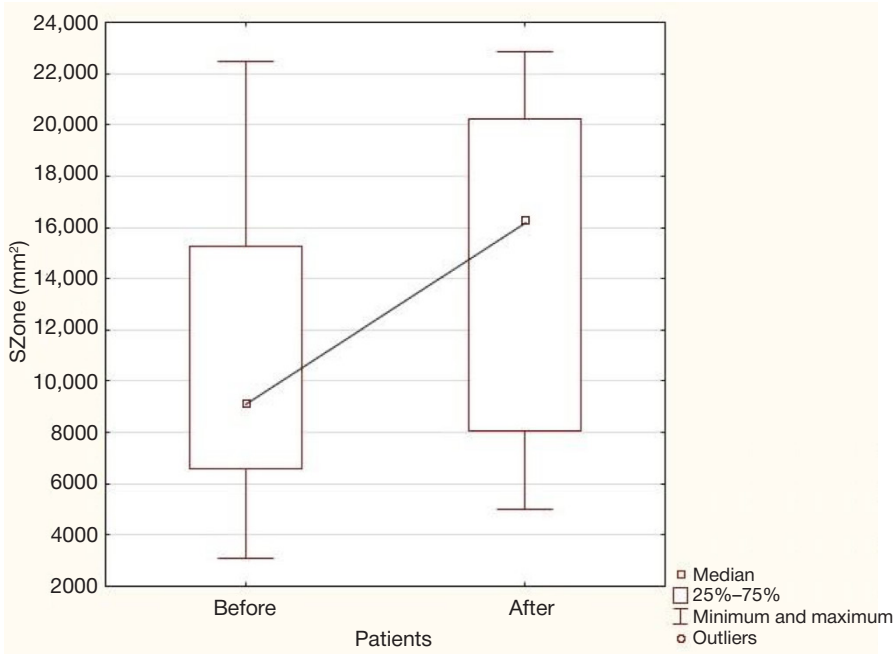

Fig. 2. Total sway zone before (9153 [7251.5; 14,805]) and after (16,289 [9006.5; 19,830]) rehabilitation ($p < 0.05$)

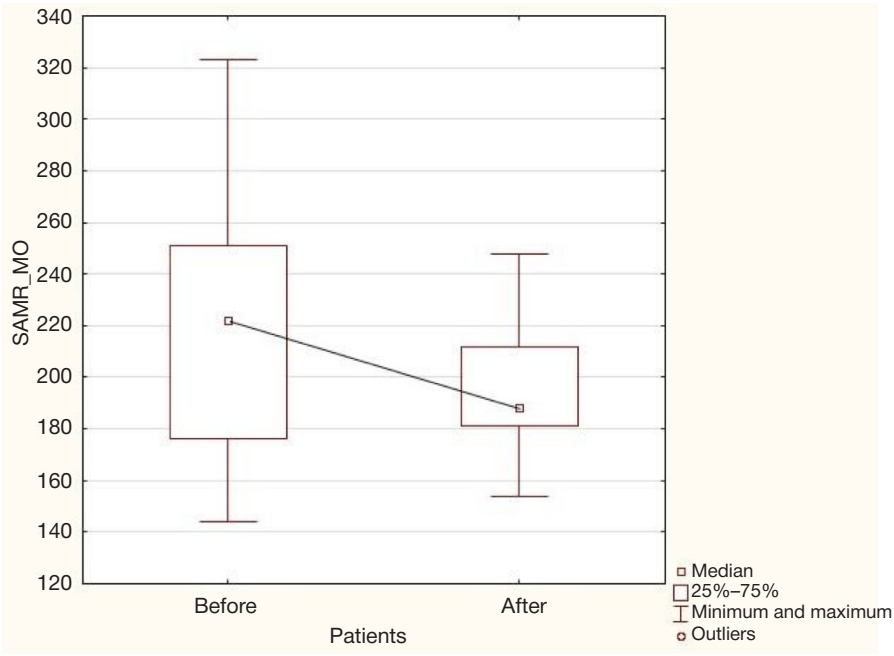

Fig. 3. Mean SAMR time before (210 [174.25; 245.5]) and after (180.5 [170.5; 208]) rehabilitation ($p < 0.05$)

to the SAMR test, the initial functional CNS state was also worse in these patients.

No correlations were established between the changes in the psychophysiological parameters and sway dynamics in the Romberg and stability tests.

The change in the Berg score was significantly ($p < 0.05$) correlated with the SAMR_IRI value ($r = 0.72$; $p < 0.05$), changes in the mean reaction time ($r = –0.73$, $p < 0.05$) and the SAMR median ($r = –0.69$; $p < 0.05$).

DISCUSSION

Based on the dynamics of the Romberg ratio, we conclude that after the rehabilitation course the patients were guided less by their vision and more by their proprioception to maintain balance. This can be explained by the necessity to use biological feedback in the virtual reality environment, which required that the patients compared proprioceptive inputs with the current position of their COP projected on the screen. The 3-D avatar on the screen allowed the patient to use the horizon in the virtual reality environment as a feedback source and to improve proprioception.

The increase in statokinesigram density (LFS_c) indicates a higher density of COP positions within a smaller area, suggesting an improvement in balance function. The correlation between COP positions in the sagittal plane relative to the line connecting the lateral and medial malleoli and COP velocity (VFY) changed from negative to positive, suggesting a change in the balance control strategy. The positive values indicate a reduction in triceps surae muscle tension and a forward COP displacement, which is a sign of a more physiologically sound strategy for balance control.

The increased values of various velocity parameters in the Romberg test may be linked to a reduction in rigidity and adoption of a more robust balance control strategy instead of a compensatory one. Giving up the compensatory strategy is essential for gaining the sufficient degree of freedom for COP movement needed to improve balance. As seen from the results of the stability test, motor control significantly improved after the rehabilitation course; the velocity and magnitude of COP excursions were much greater and easier to achieve after the course [16, 17].

The higher Berg score after the rehabilitation program suggests an improvement in the static, dynamic and functional balance. The patients with the worst balance parameters at baseline made the greatest progress during the course.

Thus, the proposed 10-day rehabilitation program had a positive impact on balance function in patients with small vascular disease, which is consistent with the findings of other studies [18–20] and corroborates the effectiveness of virtual reality as a tool for balance training [21].

The applied psychophysiological tests demonstrated that VR-based rehabilitation led to a reduction in mean SAMR and SVMR times and an increase in the integrated reliability index. The latter estimates the percentage of errors for each response. It is calculated as a mean of the reliability coefficients (RC1) for each response. No rehabilitation-related improvement in response times was registered during complex sensorimotor response tests, but the number of different error types became lower and the functional state of CNS improved. Complex sensorimotor reactions studied in the experiment were represented by recognition and choice behaviors. Not all of the applied tests revealed statistically significant changes after the rehabilitation course: changes were not while testing

Table 2. Results of the RDO test

Parameter	Baseline	After training	*p*
RMO_NS	7,5 [4,75; 9,25]	9 [7,75; 11,25]	0,003
RMO_PS (%)	25 [16; 30,75]	30 [26; 37,75]	0,002
RMO_ND	2 [1; 5]	1 [0; 2]	0,007
RMO_PD	7 [3; 17]	3 [0; 7]	0,005

Table 3. Correlations of SAMR parameters at baseline with score changes on the Berg scale

Parameter	SAMR_IRI (%)	SAMR_CNSAL	SAMR_ QCNSAI (rel.un.)	SAMR_CSN
Changes on the Berg scale	–0,72323	–0,731143	–0,694082	–0,694082
	SAMR_MO (ms)	SAMR_QR	SAMR_QRR (rel.un.)	SAMR_MSD (ms)
Changes on the Berg scale	0,659752	–0,731143	–0,731143	0,529675
	SAMR_Me (ms)	SAMR_Mo (ms)	SAMR_MaxT (ms)	
Changes on the Berg scale	0,662874	0,507568	0,554416	

Note: Significance level $p < 0.05$

the functional activity of nervous processes and the complex visuomotor reaction to a combination of colors. Perhaps, this may be due to the fact that these tests were the most difficult and required involvement of substantial cognitive resources. Overall, improved reaction time after the rehabilitation program is consistent with the literature data [22–24]. However, some researchers report slower reaction times [25] while others do not detect any effect of training on the quickness of motor response [26]. To our knowledge, there has been no analysis of correlations between VR-based rehabilitation and the reliability of testing, erroneous responses and other similar parameters. This is probably due to the choice of the device used for psychophysiological testing.

The patients with the best progress on the Berg scale (i.e., those who had worse results at baseline) also demonstrated a greater improvement in SAMR IRI, mean SAMR speed and median. This suggests that the VR-based rehabilitation program is effective in improving both balance and cognitive functions and demonstrates a predictive value of the SAMR test. The integrated reliability index and the mean SAMR speed allow identification of patients with initially worse parameters who may benefit the most from VR-based rehabilitation.

It is known that balance control depends on the afferent integration of visual, vestibular and proprioceptive inputs. Although the auditory system provides the patient with accurate and precise spatial reference, its auxiliary role in balance control is not acknowledged [27]. Nevertheless, some authors hypothesize that the role of auditory stimuli may increase if one of other involved systems is impaired [28]. The established correlation between changes in audiomotor response speed and the dynamics of balance function after rehabilitation may be linked to the increased role of auditory afferentation associated with changes in the compensatory strategy.

So far, no reliable predictors of motor recovery have been identified; however, the SAMR test may be a potential candidate. Perhaps, the absence of a unified predictor in our study may be linked to the diversity of balance impairment mechanisms in the included patients. Besides cognitive impairment, balance disorders can be caused by sarcopenia, motor deficit, proprioceptive disorders, etc.

Further research should be conducted on a larger patient sample; subgroups should be formed based on the cause of balance impairment. Larger patient samples and the analysis of vestibular function accounting for the physiological characteristics of study participants will allow us to identify different patterns of balance impairment and develop a working tool for determining therapeutic targets in balance training.

CONCLUSIONS

Based on the preliminary results, we conclude that 1) balance impairment in elderly patients may be associated with both CNS activation and inhibition impairments and postural or motor disorders; 2) a combination balance and reaction virtual reality training is an effective rehabilitation method for elderly patients that improves static and dynamic balance control; the training program helps the patient to give up the compensatory strategy and adopt a new, more physiologically robust one (in terms of biomechanics); 3) virtual reality-based balance training improves balance control and CNS activation and stimulates the patient to use additional afferent sources for balance control; 4) patients with initially more pronounced balance disorders make better progress in improving the accuracy and speed of response to visual and auditory cues during the program. Thus, the combination balance and reaction virtual reality training has a potential to become an effective rehabilitation method. However, in order to identify reliable psychophysiological and stabilometric predictors of its effectiveness, further research is needed involving patient grouping by the cause and degree of balance impairment.

References

1. Tkacheva ON.Narushenija pohodki v pozhilom i starcheskom vozraste: Metodicheskie rekomendacii. M.: Izd-vo Prometej, 2019; 48 c.
2. Mahlknecht P, Kiechl S, Bloem BR, Willeit J, Scherfler C, Gasperi A et al. Prevalence and Burden of Gait Disorders in Elderly Men and Women Aged 60–97 Years: A Population-Based Study. PLoS ONE. 2013; 8 (7): 1–7.
3. Antipenko EA. Hronicheskaja ishemija golovnogo mozga (kliniko-jeksperimental'noe issledovanie). M.: 2015.
4. Sanders O, Hsiao HY, Savin DN, Creath RA, Rogers MW. Aging changes in protective balance and startle responses to sudden drop perturbations. Journal of neurophysiology. 2019; 122 (1): 39–50.
5. Verrel J, Lisofsky N, Kühn S, Lindenberger U. Normal aging increases postural preparation errors: Evidence from a two-choice response task with balance constraints. Gait and Posture. 2016; 44: 143–148.
6. Kasahara S, Saito H. The effect of aging on termination of voluntary movement while standing: A study on community-dwelling older adults. Human Movement Science. 2019; 64 (August 2018): 347–354.
7. Ahmadeeva LR, Urazbahtina YuO, Kamalova KR, Shajmuhametova FH, Ahmadeeva YeN, Bataev HM, i dr. Transkranial'naja magnitnaja stimuljacija v nevrologii i nejroreabilitacii. Mediko-farmacevticheskij zhurnal «Pul's». 2019; 21 (12): 55–59.
8. Chernikova LA. Robotizirovannye sistemy v nejroreabilitacii. Annaly klinicheskoj i jeksperimental'noj nevrologii. 2009; 3 (3):

30–36.
9. Fasoli SE. Rehabilitation technologies to promote upper limb recovery after stroke. Elsevier Ltd.; 2016. 510 p.
10. Hatem SM, Saussez G, Della Faille M, Prist V, Zhang X, Dispa D et al. Rehabilitation of motor function after stroke: A multiple systematic review focused on techniques to stimulate upper extremity recovery. Frontiers in Human Neuroscience. 2016; (10): 1–22.
11. Oña ED, Cano-de la Cuerda., Sánchez-Herrera P, Balaguer C, Jardón AA. review of Robotics in Neurorehabilitation: Towards an automated process for upper limb. Journal of Healthcare Engineering. 2018; 2018: 1–19.
12. Paolo M, Salvo FDe, Peccini MC, Sfaldaroli A, Cadri S, Caserio M, et al. Exoskeleton in the neurorehabilitation process: Neuropsychological effects in patients affected by spinal cord injury and stroke. Digital Medicine. 2018; 4 (4): 76–85.
13. Donath L, Rössler R, Faude O. Effects of Virtual Reality Training (Exergaming) Compared to Alternative Exercise Training and Passive Control on Standing Balance and Functional Mobility in Healthy Community-Dwelling Seniors: A Meta-Analytical Review. Sports Medicine. 2016; 46 (9): 1293–309.
14. Khizhnikova AE, Klochkov AS, Kotov-Smolenskii AM, Fuks AA, Suponeva NA, Piradov MA. The effect of virtual reality based cognitive-motor training on psychophysiological parameters and balance function in the elderl. Physical and Rehabilitation Medicine Medical Rehabilitation. 2020; 2 (4): 292–302.
15. Suponeva NA, Yusupova DG, Zimin AA, Zaitsev AB, Yatsko KA, Melchenko DA, et al. Validation of a Russian version of the Berg Balance Scale. Neurology, Neuropsychiatry, Psychosomatics. 2021; 13 (3): 12–18.
16. Safonova YuA, Emelyanov VD. Analiz stabilometricheskih pokazatelej u ljudej starshe 65 let. Vestnik Severo-Zapadnogo gosudarstvennogo medicinskogo universiteta im. I. I. Mechnikova. 2017; 9 (1): 89–95.
17. Skvortsov DV. Stabilometricheskoe issledovanie: kratkoe rukovodstvo. M.: Mera-TSP, 2010; 176 c.
18. Laatar R, Kachouri H, Borji R, Rebai H, Sahli S. Combined physical-cognitive training enhances postural performances during daily life tasks in older adults. Experimental Gerontology. 2018; 107: 91–97.
19. Lacroix A, Kressig RW, Muehlbauer T, Gschwind YJ, Pfenninger B, Bruegger O, et al. Effects of a supervised versus an unsupervised combined balance and strength training program on balance and muscle power in healthy older adults: A randomized controlled trial. Gerontology. 2016; 62 (3): 275–88.
20. van het Reve E, de Bruin ED. De Strength-balance supplemented with computerized cognitive training to improve dual task gait and divided attention in older adults: A multicenter randomized-controlled tria. BMC Geriatrics. 2014; 14 (1): 1–15.
21. Kamińska MS, Miller A, Rotter I, Szylińska A, Grochans E. The effectiveness of virtual reality training in reducing the risk of falls among elderly people. Clinical Interventions in Aging. 2018; 13: 2329–38.
22. Fu AS, Gao KL, Tung AK, Tsang WW, Kwan MM. Effectiveness of Exergaming Training in Reducing Risk and Incidence of Falls in Frail Older Adults with a History of Falls. Archives of Physical Medicine and Rehabilitation. 2015; 96 (12): 2096–102.
23. Gschwind YJ, Schoene D, Lord SR, Ejupi A, Valenzuela T, Aal K, et al. The effect of sensor-based exercise at home on functional performance associated with fall risk in older people - A comparison of two exergame interventions. European Review of Aging and Physical Activity. 2015; 12 (1): 1–9.
24. Neri SGR, Cardoso JR, Cruz L, Lima RM, de Oliveira RJ, Iversen MD, et al. Do virtual reality games improve mobility skills and balance measurements in community-dwelling older adults? Systematic review and meta-analysis. Clinical Rehabilitation. 201; 31 (10): 1292–304.
25. Gschwind YJ, Eichberg S, Ejupi A, de Rosario H, Kroll M, Marston HR, et al. ICT-based system to predict and prevent falls (iStoppFalls): Results from an international multicenter randomized controlled trial. European Review of Aging and Physical Activity. 2015; 12 (1): 1–11.
26. Bootsman NJM, Skinner TL, Lal R., Glindemann D, Lagasca C, Peeters GMEEG. The relationship between physical activity, and physical performance and psycho-cognitive functioning in older adults living in residential aged care facilities. Journal of Science and Medicine in Sport. 2018; 21 (2): 173–8.
27. Palm HG, Strobel J, Achatz G, von Luebken F, Friemert B. The role and interaction of visual and auditory afferents in postural stability. Gait Posture. 2009; 30 (3): 328–33.
28. Stevens MN, Barbour DL, Gronski MP, Hullar TE. Auditory contributions to maintaining balance. J Vestib Res. 2016; 26 (5–6): 433–8.

Литература

1. Ткачева О. Н. Нарушения походки в пожилом и старческом возрасте: Методические рекомендации. М.: Изд-во Прометей, 2019; 48 с.
2. Mahlknecht P, Kiechl S, Bloem BR, Willeit J, Scherfler C, Gasperi A et al. Prevalence and Burden of Gait Disorders in Elderly Men and Women Aged 60–97 Years: A Population-Based Study. PLoS ONE. 2013; 8 (7): 1–7.
3. Антипенко Е. А. Хроническая ишемия головного мозга (клинико-экспериментальное исследование). М.: 2015.
4. Sanders O, Hsiao HY, Savin DN, Creath RA, Rogers MW. Aging changes in protective balance and startle responses to sudden drop perturbations. Journal of neurophysiology. 2019; 122 (1): 39–50.
5. Verrel J, Lisofsky N, Kühn S, Lindenberger U. Normal aging increases postural preparation errors: Evidence from a two-choice response task with balance constraints. Gait and Posture. 2016; 44: 143–148.
6. Kasahara S, Saito H. The effect of aging on termination of voluntary movement while standing: A study on community-dwelling older adults. Human Movement Science. 2019; 64 (August 2018): 347–354.
7. Ахмадеева Л. Р., Уразбахтина Ю. О., Камалова К. Р., Шаймухаметова Ф. Х., Ахмадеева Э. Н., Батаев Х. М. и др. Транскраниальная магнитная стимуляция в неврологии и нейрореабилитации. Медико-фармацевтический журнал «Пульс». 2019; 21 (12): 55–59.
8. Черникова Л. А. Роботизированные системы в нейрореабилитации. Анналы клинической и экспериментальной неврологии. 2009; 3 (3): 30–36.
9. Fasoli SE. Rehabilitation technologies to promote upper limb recovery after stroke. Elsevier Ltd.; 2016. 510 p.
10. Hatem SM, Saussez G, Della Faille M, Prist V, Zhang X, Dispa D et al. Rehabilitation of motor function after stroke: A multiple systematic review focused on techniques to stimulate upper extremity recovery. Frontiers in Human Neuroscience. 2016; (10): 1–22.
11. Oña ED, Cano-de la Cuerda., Sánchez-Herrera P, Balaguer C, Jardón AA. review of Robotics in Neurorehabilitation: Towards an automated process for upper limb. Journal of Healthcare Engineering. 2018; 2018: 1–19.
12. Paolo M, Salvo FDe, Peccini MC, Sfaldaroli A, Cadri S, Caserio M, et al. Exoskeleton in the neurorehabilitation process: Neuropsychological effects in patients affected by spinal cord injury and stroke. Digital Medicine. 2018; 4 (4): 76–85.
13. Donath L, Rössler R, Faude O. Effects of Virtual Reality Training (Exergaming) Compared to Alternative Exercise Training and Passive Control on Standing Balance and Functional Mobility in Healthy Community-Dwelling Seniors: A Meta-Analytical Review. Sports Medicine. 2016; 46 (9): 1293–309.
14. Хижникова А. Е., Клочков А. С., Котов-Смоленский А. М., Фукс А. А., Супонева Н. А., Пирадов М. А. Влияние когнитивно-моторных тренировок в виртуальной среде на психофизиологические параметры и функцию равновесия в пожилом возрасте. Физическая и реабилитационная медицина, медицинская реабилитация. 2020; 2 (4): 292–302.
15. Супонева Н. А., Юсупова Д. Г., Зимин А. А., Зайцев А. Б.,

Яцко К. А., Мельченко Д. А. и др. Валидация шкалы баланса Берг в России. Неврология, нейропсихиатрия, психосоматика. 2021; 13 (3): 12–18.
16. Сафонова Ю. А., Емельянов В. Д. Анализ стабилометрических показателей у людей старше 65 лет. Вестник Северо-Западного государственного медицинского университета им. И. И. Мечникова. 2017; 9 (1): 89–95.
17. Скворцов Д. В. Стабилометрическое исследование: краткое руководство. М.: Мера-ТСП, 2010; 176 с.
18. Laatar R, Kachouri H, Borji R, Rebai H, Sahli S. Combined physical-cognitive training enhances postural performances during daily life tasks in older adults. Experimental Gerontology. 2018; 107: 91–97.
19. Lacroix A, Kressig RW, Muehlbauer T, Gschwind YJ, Pfenninger B, Bruegger O, et al. Effects of a supervised versus an unsupervised combined balance and strength training program on balance and muscle power in healthy older adults: A randomized controlled trial. Gerontology. 2016; 62 (3): 275–88.
20. van het Reve E, de Bruin ED. De Strength-balance supplemented with computerized cognitive training to improve dual task gait and divided attention in older adults: A multicenter randomized-controlled tria. BMC Geriatrics. 2014; 14 (1): 1–15.
21. Kamińska MS, Miller A, Rotter I, Szylińska A, Grochans E. The effectiveness of virtual reality training in reducing the risk of falls among elderly people. Clinical Interventions in Aging. 2018; 13: 2329–38.
22. Fu AS, Gao KL, Tung AK, Tsang WW, Kwan MM. Effectiveness of Exergaming Training in Reducing Risk and Incidence of Falls in Frail Older Adults with a History of Falls. Archives of Physical Medicine and Rehabilitation. 2015; 96 (12): 2096–102.
23. Gschwind YJ, Schoene D, Lord SR, Ejupi A, Valenzuela T, Aal K, et al. The effect of sensor-based exercise at home on functional performance associated with fall risk in older people - A comparison of two exergame interventions. European Review of Aging and Physical Activity. 2015; 12 (1): 1–9.
24. Neri SGR, Cardoso JR, Cruz L, Lima RM, de Oliveira RJ, Iversen MD, et al. Do virtual reality games improve mobility skills and balance measurements in community-dwelling older adults? Systematic review and meta-analysis. Clinical Rehabilitation. 201; 31 (10): 1292–304.
25. Gschwind YJ, Eichberg S, Ejupi A, de Rosario H, Kroll M, Marston HR, et al. ICT-based system to predict and prevent falls (iStoppFalls): Results from an international multicenter randomized controlled trial. European Review of Aging and Physical Activity. 2015; 12 (1): 1–11.
26. Bootsman NJM, Skinner TL, Lal R., Glindemann D, Lagasca C, Peeters GMEEG. The relationship between physical activity, and physical performance and psycho-cognitive functioning in older adults living in residential aged care facilities. Journal of Science and Medicine in Sport. 2018; 21 (2): 173–8.
27. Palm HG, Strobel J, Achatz G, von Luebken F, Friemert B. The role and interaction of visual and auditory afferents in postural stability. Gait Posture. 2009; 30 (3): 328–33.
28. Stevens MN, Barbour DL, Gronski MP, Hullar TE. Auditory contributions to maintaining balance. J Vestib Res. 2016; 26 (5–6): 433–8.

ULTRASOUND IMAGING OF VAGUS NERVES IN PATIENTS WITH PARKINSON'S DISEASE

Chechetkin AO ✉, Moskalenko AN, Fedotova EYu, Illarioshkin SN

Research Center of Neurology, Moscow, Russia

Parkinson's disease (PD) is a neurodegenerative multisystem disorder characterized by pathologic α-synuclein aggregation affecting, among other things, vagal fibers. The aim of this study was to investigate the cross-sectional area (CSA) of the vagus nerve (VN) in patients with PD using ultrasound imaging. The study was conducted in 32 patients with PD (15 men and 17 women; mean age 58 ± 10 years) and 32 healthy controls comparable with the main group in terms of sex and age. All study participants underwent ultrasound examination of the VN using a high-resolution transducer. Left VN CSA was significantly smaller in patients with PD than in the control group (1.78 ± 0.52 mm^2 vs 2.11 ± 0.41 mm^2; $p = 0.007$). A similar result was obtained for right VN CSA at the trend level. ROC analysis demonstrated that the threshold CSA value of < 2.10 mm^2 for the left VN has low diagnostic sensivity (59%) for VN atrophy in patients with PD. Right VN CSA was significantly larger than left VN CSA in both groups ($p < 0.001$). The analysis of the PD group did not reveal any associations between VN CSA and age, duration and stage of the disease, motor (UPDRS III) and non-motor (NMSQ) scores. Patients with akinetic-rigid form of PD had smaller left VN CSA than patients with the mixed form of the disease ($p < 0.05$). A moderate inverse correlation was established between left VN CSA and the area of substantia nigra hyperechogenicity on both sides ($p < 0.04$); for the right VN a similar correlation was established at the trend level. High-resolution ultrasound of patients with PD demonstrated atrophy of the VN and the association of VN CSA with the clinical form of the disease and the ultrasound features of the substantia nigra.

Keywords: Parkinson's disease, vagus nerve, ultrasound, cross-sectional area.

Author contribution: Chechetkin AO — study design, acquisition of ultrasound imaging data, data interpretation, manuscript preparation; Moskalenko AN — clinical data acquisition, analysis and interpretation; Fedotova EYu, Illarioshkin SN — study design, manuscript editing.

Compliance with ethical standards: the study was approved by the Ethics Committee of the Research Center of Neurology (Protocol No. 2-6/20 dated March 18, 2020)

✉ **Correspondence should be addressed:** Andrey O. Chechetkin
Volokolamskoe shosse, 80, Moscow, 125367, Russia; andreychechetkin@gmail.com

Received: 25.10.2021 **Accepted:** 11.11.2021 **Published online:** 24.11.2021

DOI: 10.24075/brsmu.2021.054

УЛЬТРАЗВУКОВОЕ ИССЛЕДОВАНИЕ БЛУЖДАЮЩИХ НЕРВОВ У ПАЦИЕНТОВ С БОЛЕЗНЬЮ ПАРКИНСОНА

А. О. Чечеткин ✉, А. Н. Москаленко, Е. Ю. Федотова, С. Н. Иллариошкин

Научный центр неврологии, Москва, Россия

Болезнь Паркинсона (БП) является мультисистемным заболеванием, при котором нейродегенеративные изменения с накоплением α-синуклеина затрагивают волокна блуждающих нервов (БлН). Целью данной работы было провести ультразвуковое исследование (УЗИ) площади поперечного сечения (ППС) БлН у пациентов с БП. В исследование вошли 32 больных БП (15 мужчин и 17 женщин; средний возраст 58 ± 10 лет) и 32 человека контрольной группы, сопоставимые по полу и возрасту. Всем исследуемым проводили ультразвуковую оценку ППС БлН датчиком высокого разрешения. ППС левого БлН у пациентов с БП была меньше по сравнению с лицами контрольной группы (1,78 ± 0,52 мм^2 против 2,11 ± 0,41 мм^2; $p = 007$), для правого БлН аналогичное различие получено на уровне тенденции. ROC-анализ показал, что пороговая величина ППС для левого БлН менее 2,10 мм^2 имеет низкий показатель чувствительности (59%) для диагностики атрофии нерва при БП. ППС правого БлН была достоверно выше, чем левого БлН для пациентов обеих групп ($p < 0,001$). При анализе группы больных БП не выявлено зависимости ППС БлН от возраста, продолжительности и стадии заболевания, количества баллов при оценке по моторной (UPDRS III) и немоторной (NMSQ) шкалам. При этом у пациентов с акинетико-ригидной формой ППС левого БлН была значимо меньше по сравнению с пациентами со смешанной формой БП ($p < 0,05$). Выявлена умеренная обратная корреляция ППС левого БлН с площадью гиперэхогенности черной субстанции с обеих сторон ($p < 0,04$) и на уровне тенденции — для правого БлН. УЗИ пациентов с БП показало атрофические изменения БлН при данном заболевании, а также взаимосвязь ППС БлН с клинической формой БП и ультразвуковыми изменениями черной субстанции головного мозга.

Ключевые слова: болезнь Паркинсона, блуждающий нерв, ультразвук, площадь поперечного сечения

Вклад авторов: А. О. Чечеткин — разработка дизайна исследования, сбор ультразвуковых данных, анализ и интерпретация данных, написание рукописи; А. Н. Москаленко — сбор клинических данных, анализ и интерпретация данных; Е. Ю. Федотова, С. Н. Иллариошкин — разработка дизайна исследования, редактирование рукописи.

Соблюдение этических стандартов: исследование одобрено этическим комитетом Научного центра неврологии (протокол № 2-6/20 от 18 марта 2020 г.)

✉ **Для корреспонденции:** Андрей Олегович Чечеткин
Волоколамское шоссе, д. 80, г. Москва, 125367, Россия; andreychechetkin@gmail.com

Статья получена: 25.10.2021 **Статья принята к печати:** 11.11.2021 **Опубликована онлайн:** 24.11.2021

DOI: 10.24075/vrgmu.2021.054

Parkinson's disease (PD) is the second most common neurodegenerative disorder after Alzheimer's disease. Its annual incidence varies from 5 to over 35 cases per 100, 000 population [1]. In PD, autonomic dysfunction can develop years before the main motor symptoms set in. The prodromal period of PD is often characterized by gastrointestinal dysfunction manifesting as constipation, gastroparesis or nausea [2].

There is a hypothesis that pathologic deposition of α-synuclein in CNS observed in PD may start in the enteric nervous system and then spread rostrocranially via the vagus nerve (VN) [3]. According to pathomorphological reports, neuronal loss in the dorsal motor vagal nucleus can be as high as 50% [4]. Aggregates of α-synuclein are detected in some VN nuclei in the very early stages of the disease [5]. Importantly, subdiaphragmatic vagotomy is associated with a reduction in the subsequent risk of PD [6, 7]. A study conducted on an animal model has shown that α-synuclein derived from the brain lysate of patients with PD and recombinant α-synuclein injected into the intestinal wall are transported to CNS via the VN [8]. Abnormal α-synuclein aggregates have been detected in the glossopharyngeal and vagal

roots and in the cervical and pharyngeal segments of the VN of patients with PD [9, 10]. 11C-donepezil PET has found decreased acetylcholinesterase density in the gastrointestinal tract of patients with PD [11, 12]. This is believed to reflect parasympathetic denervation largely due to VN damage. Thus, adequate assessment of VN degeneration may serve as an additional tool to aid PD diagnosis. However, it is still unknown whether neurodegeneration observed in patients with PD is associated with VN atrophy that can be measured *in vivo*.

High-resolution ultrasound (HR-US) is a method of choice for visualizing peripheral and cranial nerves: ultrasound is often employed to detect peripheral nerve damage and polyneuropathy. For example, HR-US is capable of detecting mild and moderate VN atrophy in patients with lateral amyotrophic sclerosis and diabetic neuropathy [13–15]. A study reported that the cross-sectional area (CSA) of both VNs measured during HR-US was smaller in patients with PD than in the control group; this finding corroborates the hypothesis about the presence of nerve atrophy in PD patients [16]. There is ongoing debate about using high-resolution ultrasonography for estimating VN atrophy, a potential PD biomarker. The literature data on this problem are scarce and controversial [4, 16–23].

This study aimed to examine VNs in patients with PD using HR-US and to investigate possible associations between the obtained measurements, the clinical picture of the disease and the intensity of the hyperechoic signal from the substantia nigra of the middle cerebral peduncles.

METHODS

Patients

The study was conducted at the Research Center of Neurology from March 2020 to March 2021. Thirty-two patients with PD (15 men and 17 women) were included in the study. The mean age of the participants was 58 ± 10 years. Their clinical characteristics are provided in Table 1. The clinical history of PD varied from 1 to 26 years. The group was dominated by the mixed and akinetic-rigid forms of the disease (78%). The stage of the disease was determined using the Hoehn & Yahr scale. The severity of the patients' overall condition and motor function were assessed based on the total score on Part III of the Unified Parkinson's Disease Rating Scale (UPDRS). Non-motor symptoms were assessed using the Non-motor Symptoms Questionnaire (NMSQ). Four patients without clinically manifested polyneuropathy had type 2 diabetes mellitus controlled by adequate therapy. The following inclusion criteria were applied: any form of Hoehn & Yahr stage 1–3 PD. Exclusion criteria: severe diabetes mellitus with clinically manifested polyneuropathy; the absence of temporal bone acoustic window for transcranial ultrasound.

The control group consisted of 32 individuals comparable with the study group in terms of sex (16 men and 16 women) and age (mean age: 59 ± 6 years), without a medical history of diabetes mellitus, impaired glucose tolerance and neurological (including neurodegenerative) diseases.

Ultrasound examination

Transverse scans of the VN were performed using the iU 22 scanner (Philips; Netherlands) equipped with a L17-5 high-frequency linear array transducer. To measure CSA of the VN, the nerve was manually traced inside the hyperechoic epineural rim at the level of the distal portion of the common carotid artery, proximal to the bifurcation point (Fig. 1). During the scan, the pressure applied to the transducer was minimal to prevent nerve compression. The color Doppler mode was activated when necessary, so as not to confuse a small blood vessel in this hypervascularized region for VN. CSA was measured with 0.1 mm^2 precision. The average value derived from the sum of 3 measurements on each side was used in the subsequent statistical analysis.

Transcranial ultrasound of the substantia nigra was performed using the same scanner, an S5-1 sector array transducer and the standard technique described in [24]. Longitudinal scans were performed bilaterally using the transtemporal approach (temporal bone acoustic window). The images of the middle cerebral peduncles, which are visualized as a hypoechoic structure resembling a butterfly and surrounded by the hyperechoic basal cisterns, were captured and zoomed in 200% or 300%. If a hyperechoic signal was registered from the anatomic location of the substantia nigra (substantia nigra hyperechogenicity, SNH), that region was delineated with a cursor and CSA (cm^2) was calculated automatically.

Statistical analysis

Statistical analysis was carried out in StatTech v. 2.3.0 (StatTech; Russia). For quantitative variables, normality of distribution was tested using the Shapiro–Wilk test. Normally distributed quantitative variables were described as arithmetic means (M) and standard deviations (SD). Non-normally distributed quantitative variables were described as medians (Me) and the upper and lower quartiles (Q_1; Q_3). Intergroup differences in normally distributed quantitative variables with equal variances were estimated using Student's t-test. Intergroup differences in non-normally distributed quantitative variables were estimated in the Mann–Whitney U test. The direction and strength of correlations between two quantitative variables were assessed using Spearmen's correlation coefficient. ROC-curve analysis was applied to assess the diagnostic significance of quantitative parameters in predicting a given clinical outcome. The optimal cutoff point was calculated based on the maximum value of the Youden index. The significance threshold was assumed to be $p < 0.05$.

Table 1. Clinical characteristics of patients with PD included in the study

Disease characteristics	Patients with PD
Duration (Me [Q_1; Q_3])	3 [2; 8] years
Form	Akinetic-rigid — 7 (22%) Mixed — 25 (78%)
Hoehn & Yahr stage	1 — 8 (25%) 2 — 10 (31%) 3 — 14 (44%)
Severity of overall condition, UPDRS-III	37.0 ± 16.1 points
Severity of non-motor symptoms, NMSQ	8.2 ± 3.8 points

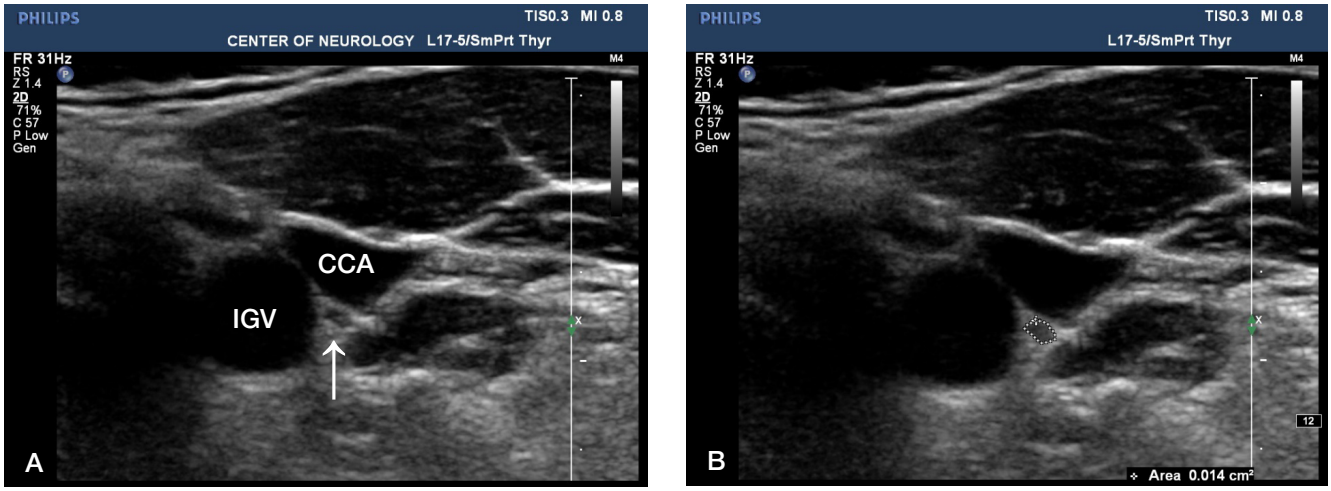

Fig. 1. A transverse ultrasound image of the vagus nerve. **A**. The left vagus nerve (indicated by the *white arrow*) is located between the common carotid artery (CCA) and the internal jugular vein (IGV). **B**. The same image showing delineation of the vagus nerve along the internal contour of the hyperechoic epineural rim. CSA (cross-sectional area) of the nerve = 0.014 cm^2, or 1.4 mm^2

RESULTS

The analysis revealed that CSA of the right VN was reliably larger than that of the left VN in both groups ($p < 0.001$; Table 2).

No significant sex-related differences between right and left VN CSAs were detected within the group of patients with PD ($p = 0.16$ and $p = 0.19$, respectively), although CSA tended to be bilaterally smaller in women (Table 2). In the control group, left VN CSA was smaller in women than in men ($p = 0.03$) but right VN CSA did not differ between the sexes ($p = 0.08$; Table 2).

The analysis also showed that left VN CSA was smaller in patients with PD than in the control group ($p = 0.007$). Right VN CSA did not differ significantly between the groups ($p = 0.13$) although it tended to be smaller in PD patients. Men with PD had smaller left VN CSA than men in the control group; by contrast, no significant difference in the right VN CSA was observed between the groups ($p = 0.09$). The right and left VN CSA did not differ between female participants ($p = 0.61$ and $p = 0.39$, respectively).

Considering the differences in the left VN CSA between the PD and the control groups, we conducted ROC analysis to determine a threshold value for the left VN CSA and assessed the model's sensitivity and specificity (Fig. 2). The threshold value of left VN CSA (the cutoff point) corresponded to the maximum value of the Youden index and was 2.10 mm^2; sensitivity and specificity of the model were 59.4% and 75.0%, respectively.

The analysis of the PD group data did not detect any associations between CSA and age, clinical duration or stage of the disease, UPDRS-III and NMSQ scores ($p > 0.05$). However, there was an association between the form of the disease and left VN CSA: the latter was smaller in patients with akinetic rigid PD ($p = 0.043$). Right VN CSA only tended to be smaller for this form of the disease ($p = 0.064$; Table 3).

During transcranial ultrasound, SNH was detected in 27 (84%) patients. The hyperechoic area was 0.23 (0.15; 0.26) cm2 on the right side and 0.22 (0.15; 0.27) cm2 on the left side. The analysis of possible associations between CSA and SNH areas on both sides demonstrated a moderate inverse correlation between left VN CSA and SNH areas on the left ($R = –0.38$; $p = 0.03$) and right ($R = –0.36$; $p = 0.04$) sides (Fig. 3). At the trend level, a similar association was observed for the right VN CSA: $R = –0.352$, $p = 0.05$ on the right and $R = –0.28$, $p = 0.12$ on the left side.

DISCUSSION

In our study, right VN CSA was reliably larger than CSA of the left VN in both groups. This pattern was observed for both male and female participants. Similar findings are reported by another study proposing reference VN CSA values for healthy populations [25] and by almost all publications on the HR-US-based assessment of the VN in patients with PD [4, 17–20, 22]. This is consistent with the difference between the right and left VNs observed during a morphological examination [26]. The amount of nerve fibers in the right VN is ~20% higher than in the left nerve [27]. This asymmetry may result from unequal innervation of unpaired organs in the abdominal cavity [28]. The right VN innervates a part of the small bowel, the colon and the anterior gastric plexus; the left VN ends in the anterior gastric plexus and branches off to the stomach, liver and the superior duodenum.

Table 2. CSA of the right and left vagus nerves in patients with PD and healthy controls

Group	Right VN CSA (mm^2)	Left VN CSA (mm^2)
PD ($n = 32$)	2.03 ± 0.50	1.78 ± 0.52 *
men ($n = 15$)	2.20 ± 0.44	2.03 ± 0.46 *
women ($n = 17$)	2.04 ± 0.46	1.87 ± 0.52
Control ($n = 32$)	2.21 ± 0.39	2.11 ± 0.41
men ($n = 16$)	2.33 ± 0.37	2.26 ± 0.37
women ($n = 16$)	2.09 ± 0.38	1.96 ± 0.39

Note: CSA — cross-sectional area; VN — vagus nerve; PD — Parkinson's disease; * — $p < 0.05$, comparison with the control group.

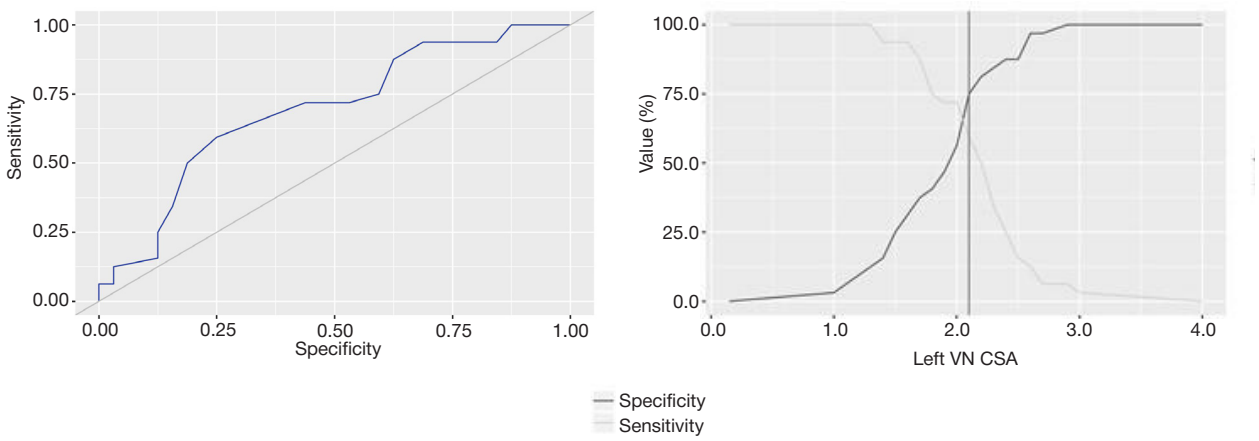

Fig. 2. Analysis of the model's sensitivity and specificity depending on the threshold values of the left VN CSA. CSA — cross-sectional area; VN — vagus nerve

According to our observations, VN CSA was smaller in women than in men in both groups ($p < 0.001$). These findings are consistent with the results of the largest study on the subject [4] in which HR-US of the VN was performed on 63 patients with PD and 56 healthy individuals. However, in another study VN CSA was larger in men than in women [19].

According to our measurements, left VN CSA was smaller in patients with PD than in the control group ($p < 0.05$); right VN CSA did not differ significantly between the groups although it did tend to be smaller in patients with PD. Eight identified publications on HR-US-based VN assessment in patients with PD yielded conflicting data despite the use of high-frequency high-resolution transducers (linear array transducer frequencies ranged from 12 to 19 MHz; Table 4). Significant atrophy of the right and left VNs of patients with PD was reported by 4 studies [16, 19, 20, 23]. Another 4 studies included in the analysis reported no differences between the VNs of patients with PD and healthy individuals [4, 18, 21, 22]. But although no differences in VN CSA between patients with PD and the control group were initially observed in the study [4], once the obtained data were corrected for sex, right (as opposed to left), VN CSA turned to be considerably smaller for female patients with PD ($p = 0.041$). In our study, left VN CSA was reliably smaller in men with PD than in healthy male controls, but no significant differences were found for right VBN CSA.

In our study, the average VN CSA was 8% smaller on the right side and 15% smaller on the left side in patients with PD than in the control group. Other studies report a reduction of 10% to 30% [16, 17, 19, 20, 23]. In order to determine the threshold value for left VN CSA, which, according to our data, was reliably smaller in the PD group, ROC analysis was carried out. Based on its results, a value below 2.10 mm^2 may serve as a VN atrophy indicator for patients with PD with 59% sensitivity and 75% specificity. In an earlier study conducted on 60 healthy volunteers, VN CSA was 3.0 ± 0.7 (1.7–4.3) mm^2 on the right and 2.3 ± 0.6 (1.1–3.5) mm^2 on the left side [25]. Knowing that typical VN CSA varies from 1 to 4 mm^2 and considering the low sensitivity of this indicator, we think that the obtained threshold value cannot be used in clinical practice for such small anatomical structures as VN. It should be noted that in all of the publications we included in the analysis, the area of the nerve was measured at different levels, which may have affected the results because there is some anatomical variability in nerve thickness in its cervical segment. Similar to our strategy, some researchers measured VN CSA at the level of the distal end of the common carotid artery [16, 21]; others took measurements at the level of the thyroid cartilage [4, 19]; some studies did not specify the level at which the measurements were taken [18]. However, the difference in the applied methodologies alone cannot explain why significant atrophy of the VN was observed in some studies and was undetected in others. The conflicting results may be explained by the fact that differences in the obtained measurements were minor and generally depend on the technical specifications of the scanner, transducer frequency and the experience of the sonographer.

We did not find any correlations between VN CSA and most of the clinical characteristics of PD. There were no reports of correlations between VN CSA and the patient's age, Hoehn & Yahr stage, duration of the disease, UPDRS-III scores, cognitive scores, gastrointestinal and other non-motor symptoms in almost all of the analyzed publications [4, 17, 18, 20–23]. The absence of correlations may be linked to the progressive degeneration of the dorsal motor vagal nucleus at the early stages of the disease [29]. However, there are publications suggesting an association between the VN caliber and the clinical manifestations of PD. For instance, left VN CSA is reported to correlate with the severity of PD symptoms on the UPDRS-III scale ($r = 0.58$; $p = 0.007$), in contrast with right VN CSA ($p = 0.53$) [19]. Besides, right VN CSA is correlated with bradykinesia assessed on the UPDRS-III scale ($r = 0.53$; $p = 0.003$) [18]. The authors of the cited studies hypothesize that bradykinesia-dominant PD subtypes seem to be associated with more advanced Lewy body pathology. Our findings corroborate this conclusion. In our study, the nerve caliber was associated with the form of the disease: left VN CSA was smaller in patients with akinetic rigid PD ($p = 0.05$) whereas a similar pattern for right VN CSA was observed at the trend level ($p = 0.06$).

Table 3. 3VN CSA in patients with different forms of PD

Parameter	Form of PD	
	Akinetic rigid	Mixed
Right CSA (mm^2)	1.70 ± 0.47	2.13 ± 0.48
Left CSA (mm^2)	1.46 ± 0.35 *	1.87 ± 0.53

Note: * — indicates statistically significant differences ($p < 0.05$).

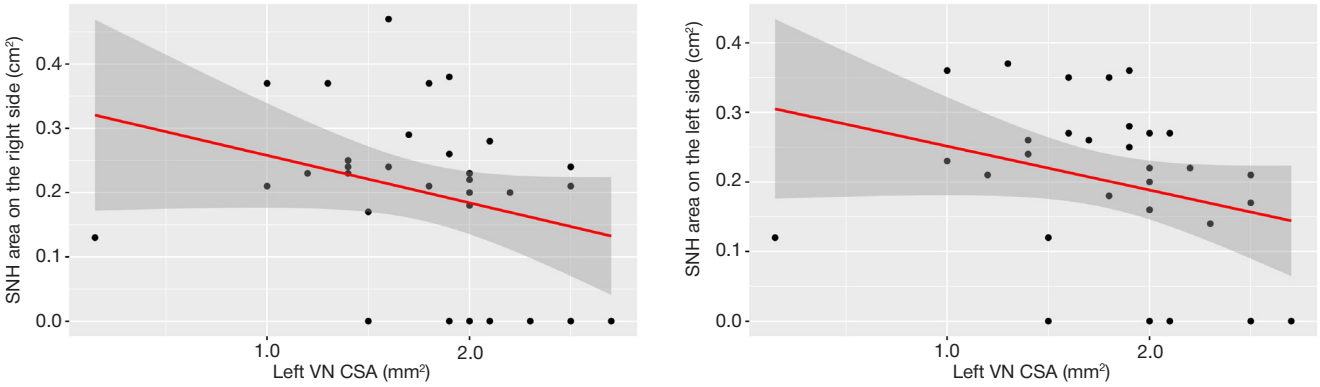

Fig. 3. The regression function graph for the association between the left VN CSA and SNH area on the right (**A**) and left (**B**). CSA — cross-sectional area; VN — vagus nerve; SNH — substantia nigra hyperechogenicity

Table 4. Ultrasonography findings in patients with PD

Reference study	Number of patients with PD/control	Number of men and women with PD	Transducer frequency	VN CSA on HR-US, (mm²) PD / control		Significant differences between PD and control groups
				Right VN	Left VN	
[16, 17]	19 / 21	6 / 13	12 MHz	1.58 / 2.35	1.45 / 1.91	yes
[18]	32 / 15	20 / 12	15 MHz	2.9 ± 0.7 / 2.7 ± 0.7	2.6 ± 0.7 / 2.4 ± 0.7	no
[19]	20 / 61	13 / 7	15 MHz	0.64 ± 0.17 / 1.04 ± 0.20	0.69 ± 0.18 / 0.87 ± 0.15	yes
[20]	35 / 35	19 / 16	15 MHz	2.1 ± 0.4 / 2.3 ± 0.5	1.5 ± 0.4 / 1.8 ± 0.4	yes
[21]	20 / 20	10 / 10	12 MHz	1.17 / 1.13#		no
[22] *	31 / 51	16 / 15	n/a	2.54 / 2.24	2.10 / 1.90	no
[23]	20 / 20	12 / 8	19 MHz	2.37 + 0.91 / 6.0 + 1.33	1.87 ± 1.35 / 5.6 ± 1.26	yes
[4]	63 / 56	43 / 20	12 MHz	2.23 / 2.37	1.89 / 1.97	no / yes¥
Our data	32 / 32	14 / 16	17 MHz	2.03 ± 0.50 / 2.21 ± 0.39	1.78 ± 0.52 / 2.11 ± 0.41	yes

Note: PD — Parkinson's disease; HR-US — high-resolution ultrasound; CSA — cross-sectional area; VN — vagus nerve; * preprint, not peer reviewed yet; # — average diameter (mm); ¥ — reduction of right VN CSA in the PD group corrected for sex.

While conducting literature analysis, we found a single report of a significant inverse correlation between right/left VN CSA and the severity of autonomic dysfunction in PD measured on the NMSQ scale (r = –0.46; p = 0.003) [19]. Besides, right (but not left) VN CSA was directly correlated with parasympathetic heart-rate variability (r = 0.58; p = 0.001) whereas left VN CSA was correlated with the severity of PD symptoms on the UPDRS-III scale (r = 0.58; p = 0.007). This inconsistency between our findings and the results of other studies might be explained by the applied study selection criteria: patients with comorbidities that could be associated with VN neuropathy were excluded.

In the course of the study, we investigated possible associations between VN CSA and SNH in the middle cerebral peduncles assessed by transcranial ultrasound. The analysis revealed a moderate inverse correlation between the left VN CSA and SNH area on both sides ($p < 0.04$). A similar correlation for the right VN was observed at the trend level. These findings seem to reflect the neurodegenerative process in the VN and dopaminergic neurons of the substantia nigra in patients with PD. Previously, we had demonstrated that SNH area (similar to VN CSA investigated in this study) did not correlate with the duration or severity of the disease. This marker stability suggests that changes can occur at the very early stages of the disease [23, 30].

CONCLUSIONS

HR-US of patients with PD has revealed atrophy of the VN and associations of VN CSA with the clinical form of PD and the changed echogenicity of the substantia nigra. However, the low sensitivity of the described VN assessment method prevents using HR-US as a diagnostic modality in wide clinical practice. Thus, VN CSA is not a reliable marker of VN damage.

References

1. Poewe W, Seppi K, Tanner CM, Halliday GM, Brundin P, Volkmann J, et al. Parkinson disease. Nat Rev Dis Primers. 2017; 3 (1): 1–21. DOI: 10.1038/nrdp.2017.13.
2. Klingelhoefer L, Reichmann H. Pathogenesis of Parkinson disease–the gutbrain axis and environmental factors. Nat Rev Neurol. 2015. 11; 625–36. DOI: 10.1038/nrneurol.2015.197.
3. Hawkes CH, Del Tredici K, Braak H. Parkinson's disease: a dualhit hypothesis. Neuropathol Appl Neurobiol. 2007; 33: 599–614. DOI: 10.1111/j.1365-2990.2007.00874.x.
4. Horsager J, Walter U, Fedorova TD, Andersen KB, Skjærbæk C, Knudsen K, et al. Vagus Nerve Cross-Sectional Area in Patients With Parkinson's Disease-An Ultrasound Case-

Control Study. Front Neurol. 2021; 12: 681413. DOI: 10.3389/fneur.2021.681413.
5. Del Tredici K, Braak H. Review: Sporadic Parkinson's disease: development and distribution of α-synuclein pathology. Neuropathol Appl Neurobiol. 2016; 42: 33–50. DOI: 10.1111/nan.12298.
6. Svensson E, Horváth-Puhó E, Thomsen RW, Djurhuus JC, Pedersen L, Borghammer P, et al. Vagotomy and subsequent risk of Parkinson's disease. Ann Neurol. 2015; 78: 522–29. DOI: 10.1002/ana.24448.
7. Liu B, Fang F, Pedersen NL, Tillander A, Ludvigsson JF, Ekbom A, et al. Vagotomy and Parkinson disease: a Swedish register-based matchedcohort study. Neurology. 2017; 88: 1996–2002. DOI: 10.1212/WNL.0000000000 003961.
8. Holmqvist S, Chutna O, Bousset L, Aldrin-Kirk P, Li W, Björklund T., et al. Direct evidence of Parkinson pathology spread from the gastrointestinal tract to the brain in rats. Acta Neuropathol. 2014; 128: 805–20. DOI: 10.1007/s00401-014-1343-6.
9. Mu L, Sobotka S, Chen J, Su H, Sanders I, Adler C, et al. Alphasynuclein pathology and axonal degeneration of the peripheral motor nerves innervating pharyngeal muscles in Parkinson disease. J Neuropathol Exp Neurol. 2013. 72; 119–29. DOI: 10.1097/NEN.0b013e3182 801cde.
10. Nakamura K, Mori F, Tanji K, Miki Y, Toyoshima Y, Kakita A, et al. α-Synuclein pathology in the cranial and spinal nerves in Lewy body disease. Neuropathology. 2016; 36: 262–69. DOI: 10.1111/neup. 12269.
11. Gjerloff T, Fedorova T, Knudsen K, Munk O, Nahimi A, Jacobsen S, et al. Imaging acetylcholinesterase density in peripheral organs in Parkinson's disease with 11C-donepezil PET. Brain. 2015; 138 (Pt 3): 653–63. DOI: 10.1093/brain/awu369.
12. Fedorova T, Seidelin L, Knudsen K, Schacht A, Geday J, Pavese N, et al. Decreased intestinal acetylcholinesterase in early Parkinson disease: An (11)C-donepezil PET study. Neurology. 2017. 88: 775–81. DOI: 10.1212/WNL.0000000000003633.
13. Grimm A, Décard B, Athanasopoulou I, Schweikert K, Sinnreich M, Axer H. Nerve ultrasound for differentiation between amyotrophic lateral sclerosis and multifocal motor neuropathy. J Neurol. 2015; 262: 870–80. DOI: 10.1007/s00415-015-7648-0.
14. Hong M, Baek J, Kim D, Ha E, Choi W, Choi Y, et al. Spinal accessory nerve: ultrasound findings and correlations with neck lymph node levels. Ultraschall Med. 2016; 37: 487–91. DOI: 10.1055/s-0034-1385673.
15. Tawfik E, Walker F, Cartwright M, El-Hilaly R. Diagnostic ultrasound of the vagus nerve in patients with diabetes. J Neuroimaging. 2017; 27: 589–93. DOI: 10.1111/jon.12452.
16. Tsukita K, Taguchi T, Sakamaki-Tsukita H, Tanaka K, Suenaga T. Vagus nerve atrophy in Parkinson's disease detected by ultrasonography. Journal of the Neurological Sciences. 2017; 365, 129. DOI: 10.1016/j.jns.2017.08.391.
17. Tsukita K, Taguchi T, Sakamaki-Tsukita H, Tanaka K, Suenaga T. The vagus nerve becomes smaller in patients with Parkinson's disease: a preliminary cross-sectional study using ultrasonography. Parkinsonism Relat Disord. 2018; 55: 148–49. DOI: 10.1016/j.parkreldis.2018.06.002.
18. Fedtke N, Witte O, Prell T. Ultrasonography of the vagus nerve in Parkinson's disease. Front Neurol. 2018; 9: 525. DOI: 10.3389/fneur.2018.00525.
19. Walter U, Tsiberidou P, Kersten M, Storch A, Lohle M. Atrophy of the vagus nerve in Parkinson's Disease revealed by high-resolution ultrasonography. Front Neurol. 2018; 9: 805. DOI: 10.3389/fneur.2018.00805.
20. Pelz J, Belau E, Fricke C, Classen J, Weise D. Axonal degeneration of the vagus nerve in Parkinson's disease-a high-resolution ultrasound study. Front Neurol. 2018; 9: 951. DOI: 10.3389/fneur.2018.00951.
21. Laucius O, Balnyte R, Petrikonis K, Matijosaitis V, Juceviciute N, Vanagas T, et al. Ultrasonography of the vagus nerve in the diagnosis of Parkinson's disease. Parkinsons Dis. 2020; 2020: 2627471. DOI: 10.1155/2020/2627471.
22. Sijben L, Mess W, Walter U, Janssen A, Kuijf M, Oosterloo M. The cross-sectional area of the vagus nerve is not reduced in Parkinson's Disease patients. medRxiv [Preprint]. 2020. DOI: 10.1101/2020.10.19.20214973.
23. Sartucci F, Bocci T, Santin M, Bongioanni P, Orlandi G. High-resolution ultrasound changes of the vagus nerve in idiopathic Parkinson's disease (IPD): a possible additional index of disease. Neurol Sci. 2021. DOI: 10.1007/s10072-021-05183-5.
24. Fedotova EYu, Chechetkin AO, Shadrina MI, Slominsky PA, Ivanova-Smolenskaya IA, Illarioshkin SN. Transcranial sonography in Parkinson's disease. Zh Nevrol Psikhiatr Im SS Korsakova. 2011; 1: 49–55.
25. Pelz J, Belau E, Henn P, Hammer N, Classen J, Weise D. Sonographic evaluation of the vagus nerves: protocol, reference values, and side-to-side differences. Muscle Nerve. 2018; 57 (5): 766–71. DOI: 10.1002/mus.25993.
26. Verlinden T, Rijkers K, Hoogland G, Herrler A. Morphology of the human cervical vagus nerve: implications for vagus nerve stimulation treatment. Acta Neurol Scand. 2016; 133: 173–82. DOI: 10.1111/ane.12462.
27. Hoffman H, Schnitzlein H. The numbers of nerve fibers in the vagus nerve of man. Anat Rec. 1961; 139: 429–35. DOI: 10.1002/ar.1091390312.
28. Cheng Z, Powley T, Schwaber J, Doyle F. Projections of the dorsal motor nucleus of the vagus to cardiac ganglia of rat atria: an anterograde tracing study. J Comp Neurol. 1999; 410: 320–41.
29. Braak H, Del Tredici K, Rub U, de Vos R, Steur J, Braak E. Staging of brain pathology related to sporadic Parkinson's disease. Neurobiol Aging. 2003; 24: 197–211. DOI: 10.1016/S0197-4580(02)00065-9.
30. Fedotova EYu, Chechetkin AO, Abramycheva NYu, Chigaleychik LA, Baziyan BKh, Ponomareva TA, et al. Identification of people at the latent stage of Parkinson's disease (the PARKINLAR study): first results and an optimization of the algorithm. Zh Nevrol Psikhiatr Im S S Korsakova. 2015; 115 (6): 4–11. DOI: 10.17116/jnevro2015115614-11.

Литература

1. Poewe W, Seppi K, Tanner CM, Halliday GM, Brundin P, Volkmann J, et al. Parkinson disease. Nat Rev Dis Primers. 2017; 3 (1): 1–21. DOI: 10.1038/nrdp.2017.13.
2. Klingelhoefer L, Reichmann H. Pathogenesis of Parkinson disease–the gutbrain axis and environmental factors. Nat Rev Neurol. 2015. 11; 625–36. DOI: 10.1038/nrneurol.2015.197.
3. Hawkes CH, Del Tredici K, Braak H. Parkinson's disease: a dualhit hypothesis. Neuropathol Appl Neurobiol. 2007; 33: 599–614. DOI: 10.1111/j.1365-2990.2007.00874.x.
4. Horsager J, Walter U, Fedorova TD, Andersen KB, Skjærbæk C, Knudsen K, et al. Vagus Nerve Cross-Sectional Area in Patients With Parkinson's Disease-An Ultrasound Case-Control Study. Front Neurol. 2021; 12: 681413. DOI: 10.3389/fneur.2021.681413.
5. Del Tredici K, Braak H. Review: Sporadic Parkinson's disease: development and distribution of α-synuclein pathology. Neuropathol Appl Neurobiol. 2016; 42: 33–50. DOI: 10.1111/nan.12298.
6. Svensson E, Horváth-Puhó E, Thomsen RW, Djurhuus JC, Pedersen L, Borghammer P, et al. Vagotomy and subsequent risk of Parkinson's disease. Ann Neurol. 2015; 78: 522–29. DOI: 10.1002/ana.24448.
7. Liu B, Fang F, Pedersen NL, Tillander A, Ludvigsson JF, Ekbom A, et al. Vagotomy and Parkinson disease: a Swedish register-based matchedcohort study. Neurology. 2017; 88: 1996–2002. DOI: 10.1212/WNL.0000000000 003961.
8. Holmqvist S, Chutna O, Bousset L, Aldrin-Kirk P, Li W, Björklund T., et al. Direct evidence of Parkinson pathology spread from the gastrointestinal tract to the brain in rats. Acta Neuropathol. 2014; 128: 805–20. DOI: 10.1007/s00401-014-1343-6.

9. Mu L, Sobotka S, Chen J, Su H, Sanders I, Adler C, et al. Alphasynuclein pathology and axonal degeneration of the peripheral motor nerves innervating pharyngeal muscles in Parkinson disease. J Neuropathol Exp Neurol. 2013. 72; 119–29. DOI: 10.1097/NEN.0b013e3182 801cde.
10. Nakamura K, Mori F, Tanji K, Miki Y, Toyoshima Y, Kakita A, et al. α-Synuclein pathology in the cranial and spinal nerves in Lewy body disease. Neuropathology. 2016; 36: 262–69. DOI: 10.1111/neup. 12269.
11. Gjerloff T, Fedorova T, Knudsen K, Munk O, Nahimi A, Jacobsen S, et al. Imaging acetylcholinesterase density in peripheral organs in Parkinson's disease with 11C-donepezil PET. Brain. 2015; 138 (Pt 3): 653–63. DOI: 10.1093/brain/awu369.
12. Fedorova T, Seidelin L, Knudsen K, Schacht A, Geday J, Pavese N, et al. Decreased intestinal acetylcholinesterase in early Parkinson disease: An (11)C-donepezil PET study. Neurology. 2017. 88: 775–81. DOI: 10.1212/WNL.0000000000003633.
13. Grimm A, Décard B, Athanasopoulou I, Schweikert K, Sinnreich M, Axer H. Nerve ultrasound for differentiation between amyotrophic lateral sclerosis and multifocal motor neuropathy. J Neurol. 2015; 262: 870–80. DOI: 10.1007/s00415-015-7648-0.
14. Hong M, Baek J, Kim D, Ha E, Choi W, Choi Y, et al. Spinal accessory nerve: ultrasound findings and correlations with neck lymph node levels. Ultraschall Med. 2016; 37: 487–91. DOI: 10.1055/s-0034-1385673.
15. Tawfik E, Walker F, Cartwright M, El-Hilaly R. Diagnostic ultrasound of the vagus nerve in patients with diabetes. J Neuroimaging. 2017; 27: 589–93. DOI: 10.1111/jon.12452.
16. Tsukita K, Taguchi T, Sakamaki-Tsukita H, Tanaka K, Suenaga T. Vagus nerve atrophy in Parkinson's disease detected by ultrasonography. Journal of the Neurological Sciences. 2017; 365, 129. DOI: 10.1016/j.jns.2017.08.391.
17. Tsukita K, Taguchi T, Sakamaki-Tsukita H, Tanaka K, Suenaga T. The vagus nerve becomes smaller in patients with Parkinson's disease: a preliminary cross-sectional study using ultrasonography. Parkinsonism Relat Disord. 2018; 55: 148–49. DOI: 10.1016/j.parkreldis.2018.06.002.
18. Fedtke N, Witte O, Prell T. Ultrasonography of the vagus nerve in Parkinson's disease. Front Neurol. 2018; 9: 525. DOI: 10.3389/fneur.2018.00525.
19. Walter U, Tsiberidou P, Kersten M, Storch A, Lohle M. Atrophy of the vagus nerve in Parkinson's Disease revealed by high-resolution ultrasonography. Front Neurol. 2018; 9: 805. DOI: 10.3389/fneur.2018.00805.
20. Pelz J, Belau E, Fricke C, Classen J, Weise D. Axonal degeneration of the vagus nerve in Parkinson's disease-a high-resolution ultrasound study. Front Neurol. 2018; 9: 951. DOI: 10.3389/fneur.2018.00951.
21. Laucius O, Balnyte R, Petrikonis K, Matijosaitis V, Juceviciute N, Vanagas T, et al. Ultrasonography of the vagus nerve in the diagnosis of Parkinson's disease. Parkinsons Dis. 2020; 2020: 2627471. DOI: 10.1155/2020/2627471.
22. Sijben L, Mess W, Walter U, Janssen A, Kuijf M, Oosterloo M. The cross-sectional area of the vagus nerve is not reduced in Parkinson's Disease patients. medRxiv [Preprint]. 2020. DOI: 10.1101/2020.10.19.20214973.
23. Sartucci F, Bocci T, Santin M, Bongioanni P, Orlandi G. High-resolution ultrasound changes of the vagus nerve in idiopathic Parkinson's disease (IPD): a possible additional index of disease. Neurol Sci. 2021. DOI: 10.1007/s10072-021-05183-5.
24. Fedotova EYu, Chechetkin AO, Shadrina MI, Slominsky PA, Ivanova-Smolenskaya IA, Illarioshkin SN. Transcranial sonography in Parkinson's disease. Zh Nevrol Psikhiatr Im SS Korsakova. 2011; 1: 49–55.
25. Pelz J, Belau E, Henn P, Hammer N, Classen J, Weise D. Sonographic evaluation of the vagus nerves: protocol, reference values, and side-to-side differences. Muscle Nerve. 2018; 57 (5): 766–71. DOI: 10.1002/mus.25993.
26. Verlinden T, Rijkers K, Hoogland G, Herrler A. Morphology of the human cervical vagus nerve: implications for vagus nerve stimulation treatment. Acta Neurol Scand. 2016; 133: 173–82. DOI: 10.1111/ane.12462.
27. Hoffman H, Schnitzlein H. The numbers of nerve fibers in the vagus nerve of man. Anat Rec. 1961; 139: 429–35. DOI: 10.1002/ar.1091390312.
28. Cheng Z, Powley T, Schwaber J, Doyle F. Projections of the dorsal motor nucleus of the vagus to cardiac ganglia of rat atria: an anterograde tracing study. J Comp Neurol. 1999; 410: 320–41.
29. Braak H, Del Tredici K, Rub U, de Vos R, Steur J, Braak E. Staging of brain pathology related to sporadic Parkinson's disease. Neurobiol Aging. 2003; 24: 197–211. DOI: 10.1016/S0197-4580(02)00065-9.
30. Fedotova EYu, Chechetkin AO, Abramycheva NYu, Chigaleychik LA, Baziyan BKh, Ponomareva TA, et al. Identification of people at the latent stage of Parkinson's disease (the PARKINLAR study): first results and an optimization of the algorithm. Zh Nevrol Psikhiatr Im S S Korsakova. 2015; 115 (6): 4–11. DOI: 10.17116/jnevro2015115614-11.

EFFECTS OF HIS-PHE-ARG-TRP-PRO-GLY-PRO PEPTIDE ON FREE-RADICAL OXIDATION PROCESSES IN CONDITIONS OF CHRONIC RESTRAINT STRESS

Vorvul AO[1] ✉, Bobyntsev II[1], Medvedeva OA[1], Azarova YuE[1], Belykh AE[1], Andreeva LA[2]

[1] Kursk State Medical University, Kursk, Russia

[2] Institute of Molecular Genetics, RAS, Moscow, Russia

Studying the effects of regulatory peptides on the stress-induced shifts in the bodily processes is of great fundamental and applied significance. Currently, a wide range of peptide neurotropic drugs, affecting the stress response development, are used in medicine, and new promising molecules are being studied. The study was aimed to assess the effects of the adrenocorticotropic hormone (ACTH) synthetic analog, ACTH(6-9)-Pro-Gly-Pro, administered at a dose of 5, 50 and 500 μg/kg, on the free-radical oxidation processes in Wistar rats, subjected to chronic restraint stress (CRS) during two weeks. Serum levels of 8-oxo-2'-deoxyguanosine (8-OHdG) and superoxide dismutase 3 (SOD3) were assessed by enzyme immunoassay, and the levels of thiobarbituric acid reactive substances (TBARS) were assessed by fluorimetric method. CRS lead to the significant increase in the 8-OHdG levels by 18.4% (p = 0.01) and the decrease in the SOD3 levels by 14.3% (p = 0.01), however, it had no effect on the levels of TBARS. ACTH(6-9)-Pro-Gly-Pro, administered at a dose of 5 and 50 μg/kg, significantly decreased the levels of 8-OHdG by 19.8% (p = 0.03) and 30% (p = 0.001), respectively. Thus, it was found that CRS resulted in oxidative stress in animals. ACTH(6-9)-Pro-Gly-Pro administration at a dose of 5 and 50 μg/kg inhibits the stress-induced free-radical oxidation processes.

Keywords: regulatory peptides, His-Phe-Arg-Trp-Pro-Gly-Pro, ACTH(6-9)-Pro-Gly-Pro, free-radical oxidation, oxidative stress, chronic restraint stress

Author contribution: Vorvul AO — performing experiments, quantification of oxidative stress markers, data acquisition and statistical processing, manuscript writing; Bobyntsev II — study concept and design, manuscript writing; Medvedeva OA — study concept and design; Azarova YuE — quantification of oxidative stress markers; Belykh AE — manuscript writing; Andreeva LA — study concept and design, peptide synthesis.

Compliance with ethical standards: the study was approved by the Ethics Committee of the Kursk State Medical University (protocol № 3 dated November 16, 2020). All the experiments were in line with the ARRIVE guidelines and were performed in accordance with the Directive 2010/63/EU of the European Parliament and of the Council on the protection of animals used for scientific purposes.

✉ **Correspondence should be addressed:** Anton O. Vorvul
Karla Marxa, 3, Kursk, 305041, Russia; vorvul1996@mail.ru

Received: 28.10.2021 **Accepted:** 14.11.2021 **Published online:** 28.11.2021

DOI: 10.24075/brsmu.2021.056

ВЛИЯНИЕ ПЕПТИДА HIS-PHE-ARG-TRP-PRO-GLY-PRO НА ПРОЦЕССЫ СВОБОДНОРАДИКАЛЬНОГО ОКИСЛЕНИЯ В УСЛОВИЯХ ХРОНИЧЕСКОГО ИММОБИЛИЗАЦИОННОГО СТРЕССА

А. О. Ворвуль[1] ✉, И. И. Бобынцев[1], О. А. Медведева[1], Ю. Э. Азарова[1], А. Е. Белых[1], Л. А. Андреева[2]

[1] Курский государственный медицинский университет, Курск, Россия

[2] Институт молекулярной генетики РАН, Москва, Россия

Изучение влияния регуляторных пептидов на развитие стресс-индуцированных сдвигов в организме имеет важное фундаментальное и прикладное значение. В настоящее время в медицине используют целый ряд нейротропных препаратов пептидной природы, оказывающих влияние на развитие стрессорной реакции, а также ведут исследование новых перспективных молекул. Целью работы было изучить эффекты синтетического аналога адренокортикотропного гормона (АКТГ) АКТГ(6-9)-Pro-Gly-Pro в дозах 5, 50 и 500 мкг/кг на процессы свободнорадикального окисления у крыс Вистар в условиях двухнедельного хронического иммобилизационного стресса (ХИС). Уровни 8-оксо-2'-дезоксигуанозина (8-OHdG) и супероксиддисмутазы 3 (СОД3) в сыворотке крови оценивали с применением иммуноферментного анализа, а уровни продуктов, реагирующих с тиобарбитуровой кислотой (ТБК-РП), оценивали флуориметрическим методом. ХИС приводил к значимому повышению уровня 8-OHdG на 18,4% (p = 0,01) и снижению СОД3 на 14,3% (p = 0,01), но не влиял на уровень ТБК-РП. Применение АКТГ(6-9)-Pro-Gly-Pro в дозах 5 и 50 мкг/кг значимо снижало содержание 8-OHdG на 19,8% (p = 0,03) и 30% (p = 0,001) соответственно. Таким образом, установлено, что ХИС приводит к развитию окислительного стресса у животных. Введение АКТГ(6-9)-Pro-Gly-Pro в дозах 5 и 50 мкг/кг оказывает ингибирующее влияние на стресс-индуцированные процессы свободнорадикального окисления.

Ключевые слова: регуляторные пептиды, His-Phe-Arg-Trp-Pro-Gly-Pro, АКТГ(6-9)-Pro-Gly-Pro, свободнорадикальное окисление, окислительный стресс, хронический иммобилизационный стресс

Вклад авторов: А. О. Ворвуль — выполнение экспериментов, количественная оценка маркеров окислительного стресса, сбор и статистическая обработка данных, написание рукописи; И. И. Бобынцев — концепция и дизайн исследования, написание рукописи; О. А. Медведева — концепция и дизайн исследования; Ю. Э. Азарова — количественная оценка маркеров окислительного стресса; А. Е. Белых — написание рукописи; Л. А. Андреева — концепция и дизайн исследования, синтез пептида.

Соблюдение этических стандартов: исследование одобрено этическим комитетом Курского государственного медицинского университета (протокол № 3 от 16 ноября 2020 г.). Все эксперименты соответствовали руководящим принципам ARRIVE и были проведены в соответствии с директивой 2010/63/EU Европейского парламента и Совета Европейского союза по охране животных, используемых в научных целях.

✉ **Для корреспонденции:** Антон Олегович Ворвуль
ул. К. Маркса, д. 3 г. Курск, 305041, Россия; vorvul1996@mail.ru

Статья получена: 28.10.2021 **Статья принята к печати:** 14.11.2021 **Опубликована онлайн:** 28.11.2021

DOI: 10.24075/vrgmu.2021.056

Activation of free-radical oxidation is one of the main mechanisms, underlying cell damage, resulting from the organism's exposure to stressor [1, 2], which determines the relevance of searching for effective approaches to cytoprotection under the condition of stress.

The use of peptide molecules could be one of the promising directions for solving the mentioned above problems [3, 4]. No toxicity and allergenic capacity along with the broad spectrum of physiological and pharmacological activity is the advantage of using the drug products based on regulatory peptides [5].

These molecules include regulatory peptides, belonging to the group of N-terminal analogs of adrenocorticotropic hormone (ACTH). It is well known that Semax, containing the ACTH(4-7)-Pro-Gly-Pro synthetic peptide as an active substance, corrects histoarchitectonics and free-radical oxidation processes in the liver, as well as serum transaminases levels in the stressed rats [6]. Furthermore, Semax exhibits neuroprotective effects due to increased expression of brain-derived neurotrophic factor (BDNF) in the conditions of brain ischemia [7].

The His-Phe-Arg-Trp-Pro-Gly-Pro peptide (ACTH(6-9)-Pro-Gly-Pro) is structurally and functionally related to Semax. The His-Phe-Arg-Trp sequence, matching the ACTH(6-9) region, is an active center of ACTH, which interacts with melanocortin receptors (MCR) of all types, except MC2R [8]. However, attachment of the Pro-Gly-Pro tripeptide to the C-terminus of this molecule increases the molecule resistance to carboxypeptidases against the background of preserved neurotropic effects. Like Semax, ACTH(6-9)-Pro-Gly-Pro exhibits a broad range of neurotropic effects, including in the stressor load models, and is capable of exhibiting the more prominent activity when administered at comparable doses [9].

Therefore, the study was aimed to assess the effects of the ACTH(6-9)-Pro-Gly-Pro peptide on the free-radical oxidation processes in rats subjected to chronic restraint stress (CRS).

METHODS

Animals

The experiment involved 55 male Wistar rats weighting 280–300 g. The temperature of 22 ± 2 °C, humidity of 60 ± 5%, and the 12-hour light/dark cycle (light on from 8:00 to 20:00) were maintained in the room where the animals were kept. The animals were provided ad libitum access to food and water. The rats were divided into five groups, 11 rats per group: 1 — intact animals (administration of normal saline (NS) with no stress applied), 2 — control group (CRS + NS), 3 — CRS + ACTH(6-9)-Pro-Gly-Pro 5 μg/kg, 4 — CRS + ACTH(6-9)-Pro-Gly-Pro 50 μg/kg, 5 — CRS + ACTH(6-9)-Pro-Gly-Pro 500 μg/kg.

Chronic restraint stress

The CRS model was modeled by placing the rats in the tight transparent plastic boxes with ventilation holes, the size of which was adjusted individually for each animal. The animals were subjected to stress for 2 h (from 11:00 to 13:00) during 14 days (Fig. 1) [10].

Peptide

The N-terminal analog of ACTH, ACTH(6-9)-Pro-Gly-Pro (His-Phe-Arg-Trp-Pro-Gly-Pro), synthesized in the Institute of Molecular Genetics of the National Research Centre “Kurchatov Institute” (RAS), was used during the study, which was dissolved in NS and administered intraperitoneally at a dose of 5, 50 and 500 μg/kg daily 12–15 min before stress exposure in a volume of 1 mL per 1 kg of body weight. Intact animals and controls received equivalent amounts of NS on a daily basis. The peptide doses and the procedure for administration, used during the experiment, were selected in accordance with the available literature data on their efficacy [9, 11].

Blood serum collection

The animals were euthanized 24 h after the final stress exposure by blood withdrawal from the right ventricle of the heart after performing parasternal bilateral thoracotomy under ether anesthesia using the S-Monovette vacuum system with procoagulant (SARSTEDT; Germany). A total of 7.0–7.5 mL of blood was collected; the vacuum system needle position was assessed visually. The blood samples collected were centrifuged at 1500 g for 15 min. The serum obtained was distributed in 200 μL aliquotes in the clean individual microtubes, frozen at –20 °C, and then stored at –80 °C for further study. Aliquotes were thawed at room temperature for 4 h prior to analysis.

Assessing the intensity of free radical processes and the stress response intensity

The nucleic acid metabolite 8-oxo-2'-deoxyguanosine (8-OHdG) was selected as a marker of oxidative damage to cellular DNA, it was assessed by enzyme immunoassay (ELISA) using the DNA/RNA Oxidative Damage (High Sensitivity) ELISA Kit (589320, Cayman Chemical; USA). Moreover, the concentration of extracellular superoxide dismutase (SOD3) was defined by ELIZA using the ELISA Kit For Superoxide Dismutase 3, Extracellular (SEA117Ra, Cloud-Clone Corp.; USA); thiobarbituric acid reactive substances (TBARS) were assessed by fluorimetric method using the TBARS (TCA Method) Assay Kit (700870, Cayman Chemical; USA).

To evaluate the stress response intensity, corticosterone serum levels were defined by enzyme immunoassay using the Corticosterone ELISA kit (ADI-900-097, Enzo Life Sciences; USA).

All the assays were performed in accordance with the manufacturers' procedures. Absorbance and fluorescence were registered and analyzed using the Varioskan Flash advanced spectral scanning multimode reader (Thermo Fisher Scientific; USA) and the SkanIt software (Thermo Fisher Scientific; USA).

Statistical analysis

Statistical processing of the data obtained was performed using v.4.1.0 of R language [12] in the RStudio Desktop v. 1.4.1717 integrated development environment (RStudio, PBC; USA; https://www.rstudio.com). The Shapiro–Wilk test was used for the normality hypothesis test, and equality of variances was tested using the Levene’s test. In case of the hypothesis confirmation, two groups were compared using the Welch's t-test, and four groups were compared using one-way ANOVA with post hoc Newman–Keuls test. In case of the hypothesis rejection, the Mann–Whitney U test was used for two groups, and the Kruskal–Wallis test with post hoc Dunn's test were used for four groups. The Benjamini–Hochberg procedure was applied to reduce the false discovery rate. The differences were considered significant when $p < 0.05$.

RESULTS

The study found that CRS resulted in oxidative stress (Fig. 2). Thus, a significant increase in the levels of 8-OHdG by 18.4% ($p = 0.01$) along with the significant decrease in the levels of SOD3 by 14.3% ($p = 0.01$) against the background of CRS were observed. However, the concentration of TBARS did not change ($p = 0.43$).

At the same time, it has been shown that ACTH(6-9)-Pro-Gly-Pro corrects the CRS-induced oxidative stress. The significant differences in the serum 8-OHdG levels ($p = 0.0004$) between the controls, subjected to stress, and the animals, receiving the peptide, have been revealed. However, no significant differences in the levels of SOD3 ($p = 0.2$) have been found.

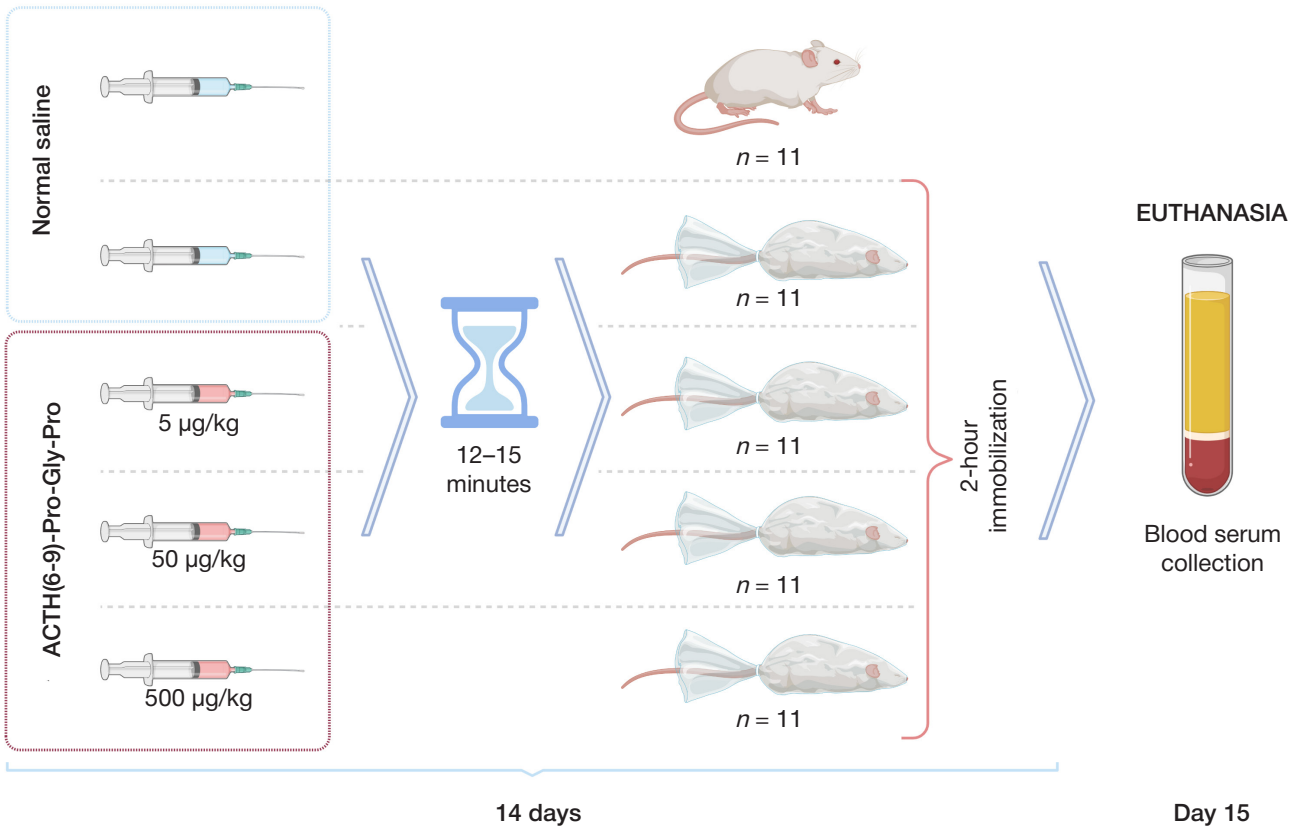

Fig. 1. Study design

The post hoc analysis has found that the serum 8-OHdG levels significantly decreased by 19.8% (p = 0.03) and 30% (p = 0.001), respectively, after the ACTH(6-9)-Pro-Gly-Pro administration at a dose of 5 and 50 μg/kg. However, peptide administration at a maximum dose of 500 μg/kg had no effect on the 8-OHdG levels (p = 0.72).

Based on the data obtained, it was also found that the significant increase in the levels of corticosterone by 27% (p = 0.009) was observed in the CRS model. The use of ACTH(6-9)-Pro-Gly-Pro resulted in significanly altered levels of the hormone (p = 0.003). The post hoc analysis showed that ACTH(6-9)-Pro-Gly-Pro administration at a dose of 5, 50, 500 μg/kg resulted in the significant decrease in the levels of corticosterone by 34.9% (p = 0.004), 16.4% (p = 0.04), and 28.6% (p = 0.01), respectively.

DISCUSSION

The effects of the ACTH(6-9)-Pro-Gly-Pro peptide on the free-radical oxidation processes in rats against the background of CRS were assessed during the study. The free-radical oxidation markers, which were used in the study, were selected based on their diagnostic and pathophysiology value. Thus, 8-OHdG is a reliable biomarker of the generalized and cellular oxidative stress, and an important indicator of oxidative brain damage in acute ischemic stroke, atherosclerosis, cardiovascular diseases, neurodegenerative disorders, such as Alzheimer's disease and Parkinson's disease, as well as in mental disorders, such as schizophrenia, etc. [13]. The other selected marker of oxidative stress is malondialdehyde (MDA), resulting from peroxidation of polyunsaturated fatty acids, which is used as an indicator of the reactive oxygen species-mediated damage to cell membranes. The levels of MDA are measured by TBARS assessment [14]. SOD is a first-line antioxidant, which initiates activation of protection against the reactive oxygen species [15]. Three isoforms of SOD have been reported, however, extracellular SOD3 is a predominant antioxidant enzyme of blood serum, and the role of SOD3 is not confined to free-radical scavenging, but also involves the impact on the immune response and cell signaling [16]. Consequently, ELISA was used as a reliable and specific research method, allowing one to identify this exact isoform of the enzyme, in order to evaluate the SOD3 level changes in the conditions of CRS and peptide administration.

The study found that CRS resulted in significantly increased concentrations of the DNA/RNA free-radical oxidation products in blood serum of experimental animals. These results were obtained in the similar C57BL/6J murine model of chronic stress [17]. Furthermore, CRS resulted in the decreased SOD3 levels. It should be noted that free-radical oxidation activation and the decrease in the SOD3 concentration occurred against the background of the elevated corticosterone blood levels. It is known that elevated corticosterone levels are accompanied by a decline in the antioxidant enzyme system activity [18]. Thus, the chronic stress model, which was used in the study, induced activation of the free radical oxidation processes.

It was found that CRS caused no significant changes in the levels of TBARS. However, there are contradictory data in the literature regarding the serum levels of this marker under prolonged stressor exposure. Thus, in a number of studies, chronic stress resulted in significantly increased serum concentrations of TBARS [19, 20]. However, the changes observed occurred against the background of chronic unpredictable stress, characterized by exposure to stressors of various intensity, while we used a model involving exposure to monotonous stress. At the same time, there are some papers, reporting no significant changes in the serum levels of TBARS in the experimental conditions similar to ours, regardless of the significantly increased MDA concentration in the organs and tissues [18, 21]. It is also important to mention that, despite their speed and simplicity, fluorometric and spectrophotometric

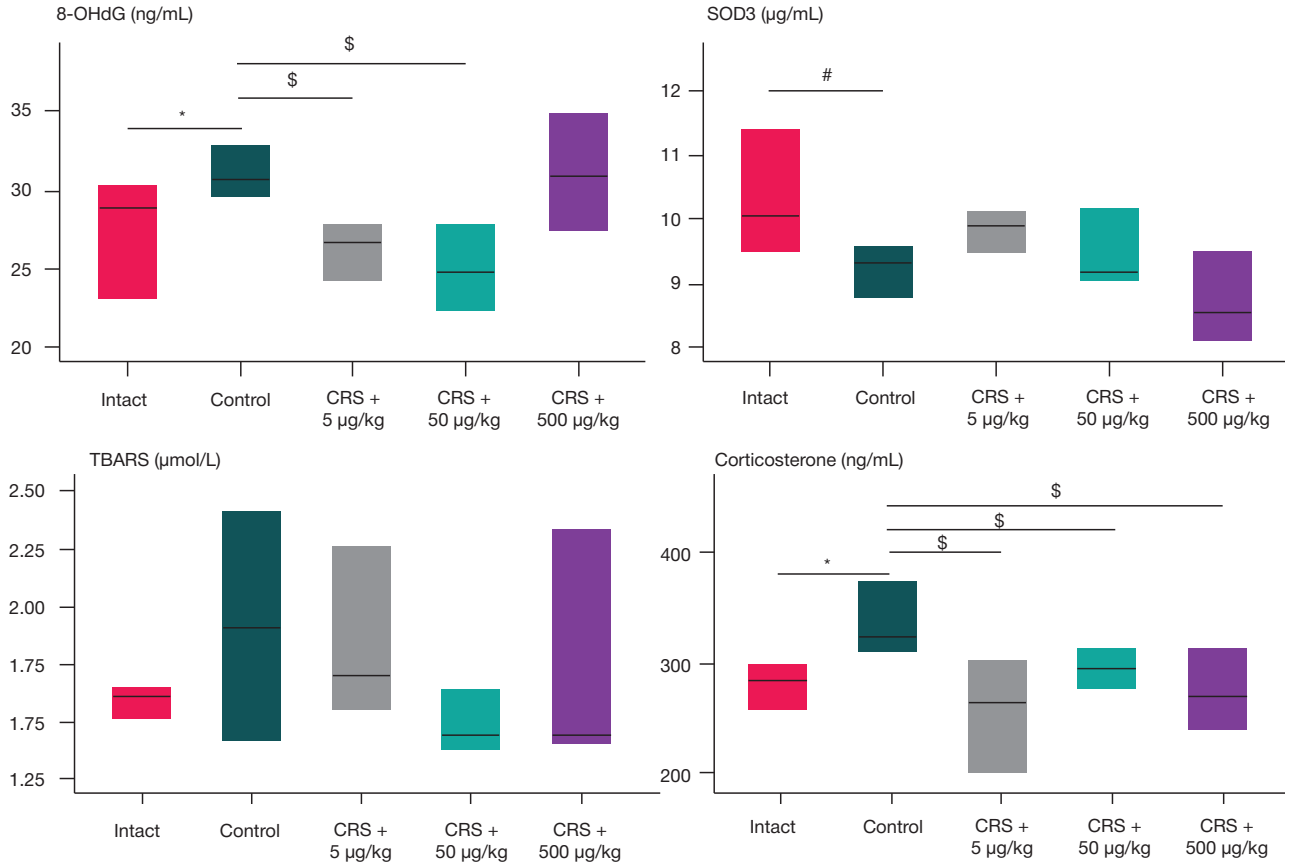

Fig. 2. Effects of the ACTH(6-9)-Pro-Gly-Pro peptide on the intensity of free-radical processes and stress response intensity against the background of CRS. * — $p < 0.05$, significance level of the differences compared with the control group not subjected to stress (based on Welch's *t*-test); # — $p < 0.05$, significance level of the differences compared with the control group (based on Mann–Whitney U-test); $ — $p < 0.05$, significance level of the differences compared with the control group subjected to stress (based on one-way ANOVA with post hoc Newman–Keuls test); semi-bold bar — median; box — interquartile range.

methods for TBARS assessment are not always reliable in heterogeneous systems due to the potential of aldehydes other than MDA to produce derivatives, absorbing light in the same wavelength range [14]. At the same time, the lack of significant changes in the serum concentrations of TBARS may be also due to the increase in the activity of the antioxidant mechanisms, unexplored during our study, by the end of the experiment. Therefore, clarifying the mechanisms, underlying alterations in the free-radical oxidation processes, identified during our study, requires further identification of a number of additional markers in blood serum.

ACTH(6-9)-Pro-Gly-Pro, administered at a dose of 5 and 50 μg/kg, reduced the intensity of free-radical oxidation processes, as reflected in the significantly decreased 8-OHdG levels. In this regard, it should be pointed out that ACTH(4-7)-Pro-Gly-Pro (Semax), which is similar to ACTH(6-9)-Pro-Gly-Pro based on its structural and functional properties, administered at comparable doses, has a cytoprotective effect on the neurons of the brain in the conditions of ischemia, in particular, due to the elevated neuronal expression of BDNF [6, 22, 23]. Considering the fact that stroke involves activation of oxidative stress [24, 25], correction of free-radical oxidation processes by administration of ACTH(6-9)-Pro-Gly-Pro, found during our study, may be also of some significance for cytoprotection.

Furthermore, the mechanisms, underlying cytoprotective effects of the peptide, may be associated with modulation of NF-κB activity and activation of the redox-sensitive NRF2 signaling pathway, which have been defined when studying the protective effects of ACTH(6-9)-Pro-Gly-Pro on the SH-SY5Y cells in the conditions of hydrogen peroxide-induced cytotoxicity [26].

Moreover, it is well known that hypothalamic-pituitary-adrenal axis, involved in both production and release of cortisol, is capable of increasing oxidative stress due to modulation of the reactive oxygen species production together with mitochondrial calcium homeostasis. However, cortisol levels correlate positively with plasma 8-OHdG concentrations [27]. Given the neurotropic activity, exhibited by ACTH(6-9)-Pro-Gly-Pro [9], it can be assumed that the anti-stress effects of the substance may be also associated with modulation of stress response in the central nervous system, as evidenced by simultaneous decrease in the levels of cortisol and 8-OHdG, observed during our study.

The differences in the effects of ACTH(6-9)-Pro-Gly-Pro depending on the dose, in particular, the lack of activity when using the maximum dose (500 μg/kg), is typical for regulatory peptides [5, 9]. Thus, as it has been shown for melanocortins, the signal is transduced from MCR via interaction with adenylyl cyclase and activation of the cAMP signaling pathway [28]. However, the signal transduction pathways may depend on the ligand concentration and the transduction may involve other secondary messenger systems, which may affect the effects direction and severity. For example, the signal from MC3R may be transmitted via phosphoinositol pathway [29], and the signal transduction from MC5R may involve Jak/STAT [30].

CONCLUSIONS

The study showed that in animals, chronic (14-day) restraint stress resulted in activation of the free-radical oxidation processes. Administration of ACTH(6-9)-Pro-Gly-Pro at a dose of 5 и 50 μg/kg reduced the intensity of stress response and inhibited the stress-induced free-radical oxidation processes.

Our findings and the data of other studies, focused on the effects of the N-terminal ACTH analogs, indicate the need for further investigation of the mechanisms underlying the effects of those on the stress-induced free-radical oxidation with the use of more complex evaluation of the wider range of prooxidant and antioxidant system markers.

References

1. Sies H, Berndt C, Jones DP. Oxidative stress. Annu Rev Biochem. 2017; 86: 715–48. DOI: 10.1146/annurev-biochem-061516-045037. PubMed PMID: 28441057.
2. Sies H. Oxidative stress: concept and some practical aspects. Antioxidants (Basel). 2020; 9 (9): 852. DOI: 10.3390/antiox9090852. PubMed PMID: 32927924.
3. Khavinson VKh. Peptide medicines: past, present, future. Klinicheskaia meditsina. 2020; 98(3): 165–77. DOI: https://doi.org/10.30629/0023-2149-2020-98-3-165-177. Russian.
4. Perlikowska R. Whether short peptides are good candidates for future neuroprotective therapeutics? Peptides. 2021; 140: 170528. DOI: 10.1016/j.peptides.2021.170528. PMID: 33716091.
5. Koroleva SV, Myasoedov NF. Semax as a universal drug for therapy and research. Biol Bull. 2018; (45): 589–600. DOI:10.1134/S1062359018060055.
6. Bobyntsev II, Kryukov AA, Shepeleva OM, Ivanov AV. The effect of ACTH-4-7-PGP peptide on lipid peroxidationin liver and activity of serum transaminases in rats under acute and chronic immobilization stress conditions. Eksperimentalnaya i Klinicheskaya Farmakologiya. 2015; 78 (8): 18–21. DOI: https://doi.org/10.30906/0869-2092-2015-78-8-18-21. Russian.
7. Dmitriyeva VG, Dergunova LV, Povarova OV, Skvortsova VI, Limborskaya SA, Myasoyedov NF. Deystviye semaksa i ego S-kontsevogo tripeptida PGP na ekspressiyu genov faktorov rosta i ikh retseptorov v usloviyakh eksperimental'noy ishemii mozga krys. Doklady Akademii Nauk. 2008; 422 (2): 258–61. Russian.
8. Levitskaya NG, Kamensky AA. Melanocortin system. Progress in physiological science. 2009; 40 (1): 44–65. Russian.
9. Dodonova SA, Bobyntsev II, Belykh AE, Vorvul AO. ACTH6-9-PGP improves memory consolidation processes in rats. Research Results in Pharmacology. 2021; 7 (1): 27–32. DOI: 10.3897/rrpharmacology.7.62479.
10. Zheng J, Dobner A, Babygirija R, Ludwig K, Takahashi T. Effects of repeated restraint stress on gastric motility in rats. Am J Physiol Regul Integr Comp Physiol. 2009; 296 (5): R1358–65. DOI: 10.1152/ajpregu.90928.2008.
11. Mukhina AY, Mishina ES, Bobyntsev II, Medvedeva OA, Svishcheva MV, Kalutskii PV, et al. Morphological changes in the large intestine of rats subjected to chronic restraint stress and treated with Selank. Bull Exp Biol Med. 2020; 169 (2): 281–5. DOI: https://doi.org/: 10.1007/s10517-020-04868-9. PubMed PMID: 32651826.
12. R Core Team. R: A language and environment for statistical computing. R Foundation for Statistical Computing, Vienna, Austria. 2020. Available from: https://www.R-project.org/.
13. Liu Z, Cai Y, He J. High serum levels of 8-OHdG are an independent predictor of post-stroke depression in Chinese stroke survivors. Neuropsychiatr Dis Treat. 2018; 14: 587–96. DOI: 10.2147/NDT.S155144. PubMed PMID: 29497302.
14. Katerji M, Filippova M, Duerksen-Hughes P. Approaches and methods to measure oxidative stress in clinical samples: research applications in the cancer field. Oxid Med Cell Longev. 2019; 2019: 1279250. DOI: 10.1155/2019/1279250. PubMed PMID: 30992736.
15. Ighodaro OM, Akinloye OA. First line defence antioxidants-superoxide dismutase (SOD), catalase (CAT) and glutathione peroxidase (GPX): Their fundamental role in the entire antioxidant defence grid. Alexandria Journal of Medicine. 2018; 54 (4): 287–93. DOI: https://doi.org/10.1016/j.ajme.2017.09.001.
16. Ściskalska M, Ołdakowska M, Marek G, Milnerowicz H. Changes in the Activity and concentration of superoxide dismutase isoenzymes (Cu/Zn SOD, MnSOD) in the blood of healthy subjects and patients with acute pancreatitis. Antioxidants (Basel). 2020; 9 (10): 948. DOI: 10.3390/antiox9100948. PubMed PMID: 33019780.
17. Yisireyili M, Alimujiang A, Aili A, Li Y, Yisireyili S, Abudureyimu K. Chronic restraint stress induces gastric mucosal inflammation with enhanced oxidative stress in a murine model. Psychol Res Behav Manag. 2020; 13: 383–93. DOI: 10.2147/PRBM.S250945. PubMed PMID: 32440237.
18. Ranjbar H, Radahmadi M, Reisi P, Alaei H. Effects of electrical lesion of basolateral amygdala nucleus on rat anxiety-like behaviour under acute, sub-chronic, and chronic stresses. Clin Exp Pharmacol Physiol. 2017; 44 (4): 470–9. DOI: 10.1111/1440-1681.12727. PubMed PMID: 28063155.
19. Gokul M, Arun Kumar N, Durgadas Kini R, et al. Evaluation of biomarkers of stress in chronic stress-exposed comorbid depression model Wistar rats. J Basic Clin Physiol Pharmacol. 2019; 30 (5). DOI: 10.1515/jbcpp-2018-0215. PubMed PMID: 31469653.
20. Ghalwash M, Elmasry A, Omar NMA. Possible cardioprotective role of NaHS on ECG and oxidative stress markers in an unpredictable chronic mild stress model in rats. Can J Physiol Pharmacol. 2021; 99 (3): 321–7. DOI: 10.1139/cjpp-2019-0646. PubMed PMID: 33175584.
21. Gorodetskaya IV, Korenevskaya NA Thyroid hormones influence on lipid peroxidation changes due to the acute and chronic stress. Izvestiya Natsional'noy akademii nauk Belarusi. Seriya meditsinskikh nauk. 2010; 1: 78–84. Russian.
22. Stavchansky VV, Tvorogova TV, Botsina AY, Skvortsova VI, Limborska SA, Mysoedov NF, Dergunova LV. Effect of semax and its C-terminal peptide PGP on expression of neurotrophins and their receptors in rat brain during incomplete global ischemia. Mol Biol. 2011; 45 (6): 941–9. DOI: https://doi.org/10.1134/S0026893311050128.
23. Kulaga EA, Gavrilova SA, Buravkov SV, Koshelev VB. Dynamics of the brain-derived neurotrophic factor (BDNF) expression in the rats cerebral cortex and the effect of the drug "Semax" for BDNF production after ischemic stroke. Regional blood circulation and microcirculation. 2013; 12 (3): 39–46. DOI: https://doi.org/10.24884/1682-6655-2013-12-3-39-46. Russian.
24. Chugunov AV, Kamchatnov PV, Mikhailova NA. Correction of free-radical oxidation as a pathogenetic approach to the treatment of acute ischemic stroke. Zhurnal nevrologii i psikhiatrii. 2009; 10 (2): 65–8. Russian.
25. Levichkin VD, Remenyakina EI, Pavlyuchenko II, Kade AKh, Trofimenko AI, Zanin SA. Influence of TES-therapy on indicators of system of pro/antioksidanty at rats with the experimental ischemic stroke. Sovremennyye problemy nauki i obrazovaniya. 2014; (2): 332. Russian.
26. Akimov MG, Fomina-Ageeva EV, Dudina PV, Andreeva LA, Myasoyedov NF, Bezuglov VV. ACTH(6-9)PGP peptide protects SH-SY5Y cells from H2O2, tert-butyl hydroperoxide, and cyanide cytotoxicity via stimulation of proliferation and induction of prosurvival-related genes. Molecules. 2021; 26 (7): 1878. DOI: 10.3390/molecules26071878. PubMed PMID: 33810344.
27. Black CN, Bot M, Révész D, Scheffer PG, Penninx B. The association between three major physiological stress systems and oxidative DNA and lipid damage. Psychoneuroendocrinology. 2017; 80: 56–66. DOI: 10.1016/j.psyneuen.2017.03.003.
28. Clark AJ, Forfar R, Hussain M, Jerman J, McIver E, Taylor D, Chan L. ACTH antagonists. Front Endocrinol (Lausanne). 2016; (7): 101. DOI: 10.3389/fendo.2016.00101. PubMed PMID: 27547198.
29. Konda Y, Gantz I, DelValle J, Shimoto Y, Miwa H, Yamada T. Interaction of dual intracellular signaling pathways activated by the

melanocortin-3 receptor. J Biol Chem. 1994; 269 (18): 13162–6. PubMed PMID: 8175743.
30. Buggy JJ. Binding of alpha-melanocyte-stimulating hormone to its G-protein-coupled receptor on B-lymphocytes activates the Jak/STAT pathway. Biochem J. 1998; 331 (Pt 1) (Pt 1): 211–6. DOI: 10.1042/bj3310211. PubMed PMID: 9512481.

Литература

1. Sies H, Berndt C, Jones DP. Oxidative stress. Annu Rev Biochem. 2017; 86: 715–48. DOI: 10.1146/annurev-biochem-061516-045037. PubMed PMID: 28441057.
2. Sies H. Oxidative stress: concept and some practical aspects. Antioxidants (Basel). 2020; 9 (9): 852. DOI: 10.3390/antiox9090852. PubMed PMID: 32927924.
3. Хавинсон В. Х. Лекарственные пептидные препараты: прошлое, настоящее, будущее. Клиническая медицина. 2020; 98 (3): 165–77. DOI: https://doi.org/10.30629/0023-2149-2020-98-3-165-177.
4. Perlikowska R. Whether short peptides are good candidates for future neuroprotective therapeutics? Peptides. 2021; 140: 170528. DOI: 10.1016/j.peptides.2021.170528. PMID: 33716091.
5. Koroleva SV, Myasoedov NF. Semax as a universal drug for therapy and research. Biol Bull. 2018; (45): 589–600. DOI:10.1134/S1062359018060055.
6. Бобынцев И. И., Крюков А. А., Шепелева О. М., Иванов А. В. Влияние пептида АКТГ4-7-ПГП на перекисное окисление липидов в печени крыс и активность сывороточных трансаминаз в условиях иммобилизационного стресса. Экспериментальная и клиническая фармакология. 2015; 78 (8): 18–21. DOI: https://doi.org/10.30906/0869-2092-2015-78-8-18-21.
7. Дмитриева В. Г., Дергунова Л. В., Поварова О. В., Скворцова В. И., Лимборская С. А., Мясоедов Н. Ф. Действие семакса и его С-концевого трипептида PGP на экспрессию генов факторов роста и их рецепторов в условиях экспериментальной ишемии мозга крыс. Доклады Академии Наук. 2008; 422 (2): 258–61.
8. Левицкая Н. Г., Каменский А. А. Меланокортиновая система. Успехи физиологических наук. 2009; 40 (1): 44–65.
9. Dodonova SA, Bobyntsev II, Belykh AE, Vorvul AO. ACTH6-9-PGP improves memory consolidation processes in rats. Research Results in Pharmacology. 2021; 7 (1): 27–32. DOI: 10.3897/rrpharmacology.7.62479.
10. Zheng J, Dobner A, Babygirija R, Ludwig K, Takahashi T. Effects of repeated restraint stress on gastric motility in rats. Am J Physiol Regul Integr Comp Physiol. 2009; 296 (5): R1358–65. DOI: 10.1152/ajpregu.90928.2008.
11. Mukhina AY, Mishina ES, Bobyntsev II, Medvedeva OA, Svishcheva MV, Kalutskii PV, et al. Morphological changes in the large intestine of rats subjected to chronic restraint stress and treated with Selank. Bull Exp Biol Med. 2020; 169 (2): 281–5. DOI: https://doi.org/: 10.1007/s10517-020-04868-9. PubMed PMID: 32651826.
12. R Core Team. R: A language and environment for statistical computing. R Foundation for Statistical Computing, Vienna, Austria. 2020. Available from: https://www.R-project.org/.
13. Liu Z, Cai Y, He J. High serum levels of 8-OHdG are an independent predictor of post-stroke depression in Chinese stroke survivors. Neuropsychiatr Dis Treat. 2018; 14: 587–96. DOI: 10.2147/NDT.S155144. PubMed PMID: 29497302.
14. Katerji M, Filippova M, Duerksen-Hughes P. Approaches and methods to measure oxidative stress in clinical samples: research applications in the cancer field. Oxid Med Cell Longev. 2019; 2019: 1279250. DOI: 10.1155/2019/1279250. PubMed PMID: 30992736.
15. Ighodaro OM, Akinloye OA. First line defence antioxidants-superoxide dismutase (SOD), catalase (CAT) and glutathione peroxidase (GPX): Their fundamental role in the entire antioxidant defence grid. Alexandria Journal of Medicine. 2018; 54 (4): 287–93. DOI: https://doi.org/10.1016/j.ajme.2017.09.001.
16. Ściskalska M, Ołdakowska M, Marek G, Milnerowicz H. Changes in the Activity and concentration of superoxide dismutase isoenzymes (Cu/Zn SOD, MnSOD) in the blood of healthy subjects and patients with acute pancreatitis. Antioxidants (Basel). 2020; 9 (10): 948. DOI: 10.3390/antiox9100948. PubMed PMID: 33019780.
17. Yisireyili M, Alimujiang A, Aili A, Li Y, Yisireyili S, Abudureyimu K. Chronic restraint stress induces gastric mucosal inflammation with enhanced oxidative stress in a murine model. Psychol Res Behav Manag. 2020; 13: 383–93. DOI: 10.2147/PRBM.S250945. PubMed PMID: 32440237.
18. Ranjbar H, Radahmadi M, Reisi P, Alaei H. Effects of electrical lesion of basolateral amygdala nucleus on rat anxiety-like behaviour under acute, sub-chronic, and chronic stresses. Clin Exp Pharmacol Physiol. 2017; 44 (4): 470–9. DOI: 10.1111/1440-1681.12727. PubMed PMID: 28063155.
19. Gokul M, Arun Kumar N, Durgadas Kini R, et al. Evaluation of biomarkers of stress in chronic stress-exposed comorbid depression model Wistar rats. J Basic Clin Physiol Pharmacol. 2019; 30 (5). DOI: 10.1515/jbcpp-2018-0215. PubMed PMID: 31469653.
20. Ghalwash M, Elmasry A, Omar NMA. Possible cardioprotective role of NaHS on ECG and oxidative stress markers in an unpredictable chronic mild stress model in rats. Can J Physiol Pharmacol. 2021; 99 (3): 321–7. DOI: 10.1139/cjpp-2019-0646. PubMed PMID: 33175584.
21. Городецкая И. В., Кореневская Н. А. Влияние тиреоидных гормонов на изменения перекисного окисления липидов, вызванные острым и хроническим стрессом. Известия Национальной академии наук Беларуси. Серия медицинских наук. 2010; 1: 78–84.
22. Stavchansky VV, Tvorogova TV, Botsina AY, Skvortsova VI, Limborska SA, Mysoedov NF, Dergunova LV. Effect of semax and its C-terminal peptide PGP on expression of neurotrophins and their receptors in rat brain during incomplete global ischemia. Mol Biol. 2011; 45 (6): 941–9. DOI: https://doi.org/10.1134/S0026893311050128.
23. Кулага Е. А., Гаврилова С. А., Буравков С. В., Кошелев В. Б. Динамика экспрессии мозгового нейротрофического фактора (BDNF) в коре головного мозга крыс и влияние препарата «Семакс» на его продукцию при моделировании ишемического инсульта. Регионарное кровообращение и микроциркуляция. 2013; 12 (3): 39–46. DOI: https://doi.org/10.24884/1682-6655-2013-12-3-39-46.
24. Чугунов А. В., Камчатнов П. В., Михайлова Н. А. Коррекция свободнорадикального окисления — патогенетический подход к лечению острого ишемического инсульта. Журнал неврологии и психиатрии. 2009; 10 (2): 65–8.
25. Левичкин В. Д., Ременякина Е. И., Павлюченко И. И., Каде А. Х., Трофименко А. И., Занин С. А. Влияние ТЭС-терапии на показатели системы про/антиоксиданты у крыс с экспериментальным ишемическим инсультом. Современные проблемы науки и образования. 2014; (2): 332.
26. Akimov MG, Fomina-Ageeva EV, Dudina PV, Andreeva LA, Myasoyedov NF, Bezuglov VV. ACTH(6-9)PGP peptide protects SH-SY5Y cells from H2O2, tert-butyl hydroperoxide, and cyanide cytotoxicity via stimulation of proliferation and induction of prosurvival-related genes. Molecules. 2021; 26 (7): 1878. DOI: 10.3390/molecules26071878. PubMed PMID: 33810344.
27. Black CN, Bot M, Révész D, Scheffer PG, Penninx B. The association between three major physiological stress systems and oxidative DNA and lipid damage. Psychoneuroendocrinology. 2017; 80: 56–66. DOI: 10.1016/j.psyneuen.2017.03.003.
28. Clark AJ, Forfar R, Hussain M, Jerman J, McIver E, Taylor D, Chan L. ACTH antagonists. Front Endocrinol (Lausanne). 2016; (7): 101. DOI: 10.3389/fendo.2016.00101. PubMed PMID: 27547198.
29. Konda Y, Gantz I, DelValle J, Shimoto Y, Miwa H, Yamada T. Interaction of dual intracellular signaling pathways activated by the melanocortin-3 receptor. J Biol Chem. 1994; 269 (18): 13162–6. PubMed PMID: 8175743.
30. Buggy JJ. Binding of alpha-melanocyte-stimulating hormone to its G-protein-coupled receptor on B-lymphocytes activates the Jak/STAT pathway. Biochem J. 1998; 331 (Pt 1) (Pt 1): 211–6. DOI: 10.1042/bj3310211. PubMed PMID: 9512481.

NOVEL *KLEBSIELLA PNEUMONIAE* VIRULENT BACTERIOPHAGE KPPK108.1 CAPABLE OF INFECTING THE K108 SEROTYPE STRAINS

Evseev PV[1], Shneider MM[1] ✉, Mikhailova YuV[2], Shelenkov AA[2], Yanushevich YuG[3], Karlova MG[4], Moiseenko AV[4], Sokolova OS[4], Shagin DA[3]

[1] Shemyakin-Ovchinnikov Institute of Bioorganic Chemistry, Moscow, Russia

[2] Central Research Institute of Epidemiology of Rospotrebnadzor, Moscow, Russia

[3] Pirogov Russian National Research Medical University, Moscow, Russia

[4] Lomonosov Moscow State University, Moscow, Russia

Multidrug-resistant *Klebsiella pneumoniae* strains are one of the major causes of nosocomial infections caused by the antibiotic-resistant bacteria. There are different options for dealing with this threat, among which is the clinical application of bacteriophages. The study was aimed to isolate and describe a virulent bactriophage, having the potential for therapeutic use. The standard phage biology and bioinformatic methods were used, which included the advanced techniques for protein structure prediction (AlphaFold software), and electron microscopy. The virulent podovirus KPPK108.1, being the member of genus *Drulisvirus*, which is able to specifically infect the *K. pneumoniae* strains with the KL108 type capsular polysaccharide, has been isolated from the wastewater. The sequence of the bactriophage genome has been defined, the biological properties have been investigated, and the genetic features have been described.

Keywords: bacteriophage, *Klebsiella pneumoniae*, capsular polysaccharide, depolymerase

Funding: the study was funded by the Ministry of Health of the Russian Federation (EGISU R&D № 121052800048-3).

Acknowledgements: the authors wish to thank the Center for Precision Genome Editing and Genetic Technologies for Biomedicine, Pirogov Russian National Research Medical University, for advice on research methods.

Author contribution: Shagin DA — research conceptualization, study management, manuscript writing; Evseev PV, Shelenkov AA — formal analysis of sequencing data, manuscript editing; Shneider MM — methodology, study management; Mikhailova YuV — sequencing, data validation; Yanushevich YuG, Moiseenko AV, Karlova MG — methodology; Sokolova OS — electron microscopy, methodology.

✉ **Correspondence should be addressed:** Mikhail M. Shneider
Miklukho-Maklaya, 16/10, Moscow, 117997, Russia; mm_shn@mail.ru

Received: 08.12.2021 **Accepted:** 22.12.2021 **Published online:** 30.12.2021

DOI: 10.24075/brsmu.2021.068

НОВЫЙ ВИРУЛЕНТНЫЙ БАКТЕРИОФАГ *KLEBSIELLA PNEUMONIAE* KPPK108.1, ИНФИЦИРУЮЩИЙ ШТАММЫ СЕРОТИПА K108

П. В. Евсеев[1], М. М. Шнейдер[1] ✉, Ю. В. Михайлова[2], А. А. Шеленков[2], Ю. Г. Янушевич[3], М. Г. Карлова[4], А. В. Моисеенко[4], О. С. Соколова[4], Д. А. Шагин[3]

[1] Институт биохимии имени М. М. Шемякина и Ю. А. Овчинникова, Москва, Россия

[2] Центральный научно-исследовательский институт эпидемиологии Роспотребнадзора, Москва, Россия

[3] Российский национальный исследовательский медицинский университет имени Н. И. Пирогова, Москва, Россия

[4] Московский государственный университет имени М. В. Ломоносова, Москва, Россия

Мультирезистентные штаммы *Klebsiella pneumoniae* являются одной из самых серьезных причин внутрибольничных инфекций, вызванных бактериями, устойчивыми к антибиотикам. Существуют различные варианты борьбы с этой угрозой, один из них — клиническое использование бактериофагов. Целью работы было выделить и детально охарактеризовать вирулентный бактриофаг, имеющий потенциал для терапевтического применения. Использовали стандартные методы фаговой биологии, биоинформатики, включая современные способы предсказания белковых структур (программа AlphaFold), электронную микроскопию. Из образцов сточных вод был выделен вирулентный подовирус KPPK108.1, относящийся к роду *Drulisvirus*, специфично инфицирующий штаммы *K. pneumoniae*, имеющие капсулярный полисахарид типа KL108, определена последовательность его генома, исследованы его биологические свойства и дана генетическая характеристика.

Ключевые слова: бактериофаг, *Klebsiella pneumoniae*, капсулярный полисахарид, деполимераза

Финансирование: работа выполнена при финансовой поддержке Министерства здравоохранения Российской Федерации (ЕГИСУ НИОКТР № 121052800048-3).

Благодарности: авторы благодарят Центр высокоточного редактирования и генетических технологий для биомедицины РНИМУ им. Н. И. Пирогова за консультации по методической части исследования.

Вклад авторов: Д. А. Шагин — концептуализация, руководство исследованием, редактирование рукописи; П. В. Евсеев, А. А. Шеленков — формальный анализ данных секвенирования, редактирование рукописи; М. М. Шнейдер — методология, руководство исследованием; Ю. В. Михайлова — секвенирование, валидация данных; Ю. Г. Янушевич, А. Моисеенко, М. Г. Карлова — методология; О. С. Соколова — электронная микроскопия, методология.

✉ **Для корреспонденции:** Михаил Маркович Шнейдер
ул. Миклухо-Маклая, д. 16/10, г. Москва, 117997, Россия; mm_shn@mail.ru

Статья получена: 08.12.2021 **Статья принята к печати:** 22.12.2021 **Опубликована онлайн:** 30.12.2021

DOI: 10.24075/vrgmu.2021.068

The modern personalized approach to phage therapy is based on the detailed assessment of the interaction between phages and bacterial cells. Bacterial carbohydrates exposed on the cell surface, O-antigens and capsular polysaccharides, are one of the most important specificity determinants in the phage–cell interaction. Capsular polysaccharides of K. pneumoniae, being the virulence factors [1], are highly diverse in their structure. Currently, bioinformatics databases indicate the existence of at least 134 genetic variants [2]. To meet the challenges of clinical practice it is necessary to create the collection of phages with

the defined specificity, inter alia based on their capacity of adsorption through recognition of capsular polysaccharides with certain structure. The study was aimed to isolate the virulent phage, which specifically infected the previously described *K. pneumoniae* strains with the KL108 capsular polysaccharide, as well as to fully explore the biological and genetic features of the phage. Standard phage biology methods, electron microscopy, and bioinformatics, including the advanced methods for protein structure prediction (AlphaFold software) were used in order to provide the comprehensive description of the phage.

METHODS

The P224 (1732) and P225 (1333) clinical strains of *K. pneumoniae* with the K108 type capsular polysaccharide were obtained from the collection of the Institute of Epidemiology (Moscow, Russia). The wastewater samples, collected from the wastewater treatment facilities in Moscow, were used for bacteriophage isolation. Dry components of the bacterial culture medium (trypton, 10 g/L, yeast extract, 5 g/L, NaCl, 5 g/L) were added to the wastewater samples previously clarified by centrifugation, then the media were inoculated with the bacterial cells culture being in the phase of exponential growth. Cultivation was carried out at 37 °C for 16 h. The bacterial culture was subsequently inactivated with chloroform, and the samples were clarified by centrifugation. Phages were detected by titration using the double-layer agar plate method. The isolated phage was titrated twice in a row in order to obtain single phage plaques. Preparative bacteriophage growth was performed in 1 L of the P224 strain culture at 37 °C. Bacteriophage was precipitated with polyethylene glycol and purified by caesium chloride density gradient ultracentrifugation [3].

Genomic DNA of the phage was extracted from the purified phage preparation by incubation with the solution, containing 100 mM Tris-HCl (pH 7.5), 25 mM EDTA, 1.5 M NaCl, 2% (w/v) CTAB buffer, 0.3% (v/v) β- mercaptoethanol, and 50 mg/mL of proteinase K, at 50 °C for 30 min, with subsequent chloroform DNA extraction, and precipitated by adding 0.6 volume of isopropyl alcohol. Genome sequencing was performed on the MiSeq platform using the Nextera DNA library preparation kit (Illumina; USA). A single contig was assembled from the resulting sequences using v. 3.13 of the SPAdes software [4].

The experiment aimed at assessing the phage particle production was performed in accordance with the previously reported protocol [5].

Negative contrast electron microscopy was utilized to visualize the phage particles. Phage preparation with a volume of 3 μL was applied to a carbon-coated 400 mesh grid. The negatively contrasted preparation was obtained by 1% uranyl acetate staining for 30 s. Imaging was performed with the JEOL JEM-2100 200 kV transmission electron microscope (JEOL USA Inc.; USA) at 30,000x magnification.

The *Klebsiella* bacteriophage KPPK108.1 was annotated with the Prokka tool [6] using the embedded databases. The functions of the genome protein products were predicted with the BLAST search tool [7] based on the known homologs, and by the HMM-HMM comparison, performed with the Hhpred [8] and Phyre2 [9] web-based tools using the SCOPe70_2.07, ECOD_ECOD_F70, and UniProt-SwissProt-viral70 databases. E value < 10^{-5} was used as a criterion of significant similarity in BLAST analysis; the Phyre2 “confidence” and HHpred “probability” values exceeding 95% were used as the criteria of significant similarity for the HMM-HMM comparison. Genetic mapping was carried out with the Geneious Prime software [10].

Genome sequences of bacteriophages to be used for comparison with the KPPK108.1 phage were downloaded from the NCBI Genome database [11]. The average nucleotide identity was calculated using the VIRIDIC online service [12] and the orthoANIu software [13]. Phylogenetic analysis was performed by the maximum likelihood method implemented in the RaxML program [14] with the use of the GAMMA LG amino acid substitution model [15] and the concatenated amino acid sequence alignment of the major capsid protein, terminase large subunit, DNA polymerase, and RNA polymerase. The sequences were aligned with the MAFFT program [16] and concatenated with the Geneious Prime software [10]. The intergenomic comparison diagram was created with the Easyfig application [17] using the TBLASTX tool [7] to find the homologous regions within genomes.

The models of the gene 8 product tertiary structure and the tailspike protein quaternary structure for the *Klebsiella* bacteriophage KPPK108.1 were constructed with the AlphaFold-Multimer application [18, 19]. The tailspike protein structure of the *Enterobacteria* phage –92 was dowloaded from the PDB database [20]. Electrostatic surface charge of the tailspike protein was calculated using the APBS program [21]. The UCSF Chimera program was used for structure alignment and visualization [22].

RESULTS

The KPPK108.1 bacteriophage forms clear plaques, 5 mm in diameter, surrounded by the translucent halos, in the bacterial cultures grown on the agar plates (Fig. 1). The presence of a halo typically indicate the presence of phage-derived depolymerase, which has been confirmed by further research. The one-step growth curve showed a latent period of 15 min and burst size of 46 phage particles per one infected cell.

Klebsiella bacteriophage KPPK108.1 has a genome, typical for the *Autographiviridae* phages, which consists of double-stranded DNA 43,755 bp in length with the direct terminal repeats 244 bp in size. The GC-content is 53.6%, somewhat lower than the value of 57.5%, characteristic of the sequenced *K. pneumoniae* strain HS11286 (GenBank Accession

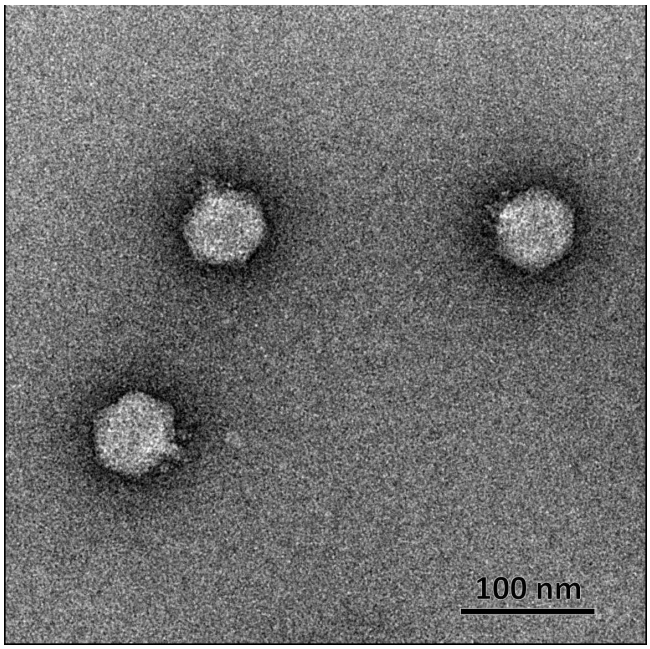

Fig. 1. Electron microscopy of *Klebsiella* bacteriophage KPPK108.1. Negative staining with 1% uranyl acetate, magnification ×30,000

CP003200.1). The search for coding sequences revealed a total of 56 protein-coding genes and no tRNA-encoding genes in the genome (Fig. 2). The search for homologous and similar sequences using the BLAST algorithm and the HMM-HMM comparison in public databases and web servers made it possible to predict the functions of 29 proteins, encoded in the genome. It was not possible to identify the functions of 27 proteins. No genes, encoding integrases or other proteins specific to temperate phages, were found in the genome.

Comparison of the average nucleotide identity (ANI), involving all 14,923 genes of tailed bacteriophages, deposited in the NCBI Genome database, revealed a group of *Klebsiella* bacteriophages of the genus *Drulisvirus*, being the most close to phage KPPK108.1 based on this parameter (Fig . 3). The ANI values of phage KPPK108.1 and a typical phage of the genus *Drulisvirus*, *Klebsiella* phage KP34, are 73.0%. Phylogenetic analysis, performed with the use of the concatenated amino acid sequences of the major capsid protein, large terminase subunit, DNA polymerase, and RNA polymerase, shows that *Drulisvirus* bacteriophages and KPPK108.1 phage form a monophyletic group (Fig. 4). The genetic makeup and genomic organization of the phage KPPK108.1 are generally similar to those of the other *Autographiviridae* phages (Fig. 5), and are almost identical to those of other members of the genus *Drulisvirus*. An interesting feature of the gene 8 product was found. Protein structural modeling revealed unusual L-shape of the protein with a tubular C-terminal region (Fig. 6.1). This region was characterized by the number of positively charged amino acid residues above the average. Electrostatic field simulation showed that the C-terminal region of the gene 8 product had a significant negative surface charge (up to –5) (Fig. 6.2).

Bioinformatic analysis of the KPPK108.1 phage genome revealed genes, encoding the head-tail connector and tailspike proteins. Modeling and analysis of the tailspike protein structure was performed (Fig. 6). The search for similar structures revealed a high degree of similarity between the tailspike of the phage KPPK108.1 and the tailspike of the *Enterobacteria* phage –92 (PDB entry 6E0V) (Fig. 6) exhibiting colanidase activity confirmed by experimental data [23].

DISCUSSION

The genome-wide similarity score of the phages KPPK108.1 and KP34 exceeding 70% of the genus boundary, together with the results of the phylogenetic analysis performed based on the concatenated sequences of conservative genes, show that the *Klebsiella* phage KPPK108.1 belongs to the genus *Drulisvirus*, subfamily *Slopekvirinae*, family *Autographiviridae*. Intergenomic comparisons support this finding. Minor differences in genome organization can be explained by the recombination events that took place during the *Klebsiella* bacteriophages' evolution, as confirmed by the presence of NHN endonuclease genes in the genomes of KPPK108.1 and other related bacteriophages. The genome structure of the KPPK108.1 phage is typical for bacteriophages of the *Autographivirinae* family and is characterized by the presence of the early gene region [24], comprising gene 8, encoding a hypothetical protein with an unusual L-shaped tertiary structure. Regardless of the fact that

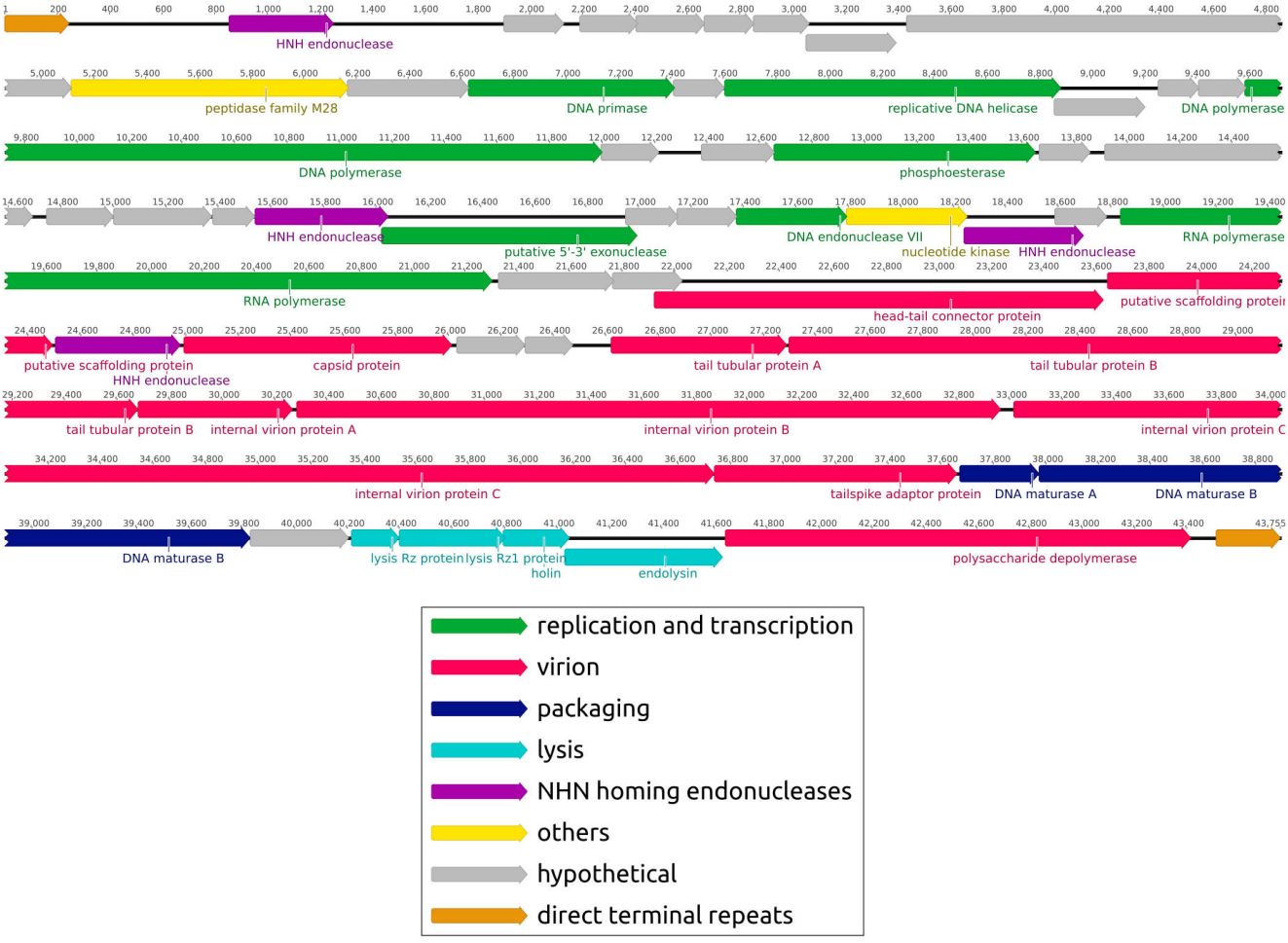

Fig. 2. Genetic map of *Klebsiella* bacteriophage KPPK108.1. Genes are colored in accordance with the functions of their products (see caption). Arrows indicate gene directions in accordance with their encoding functions

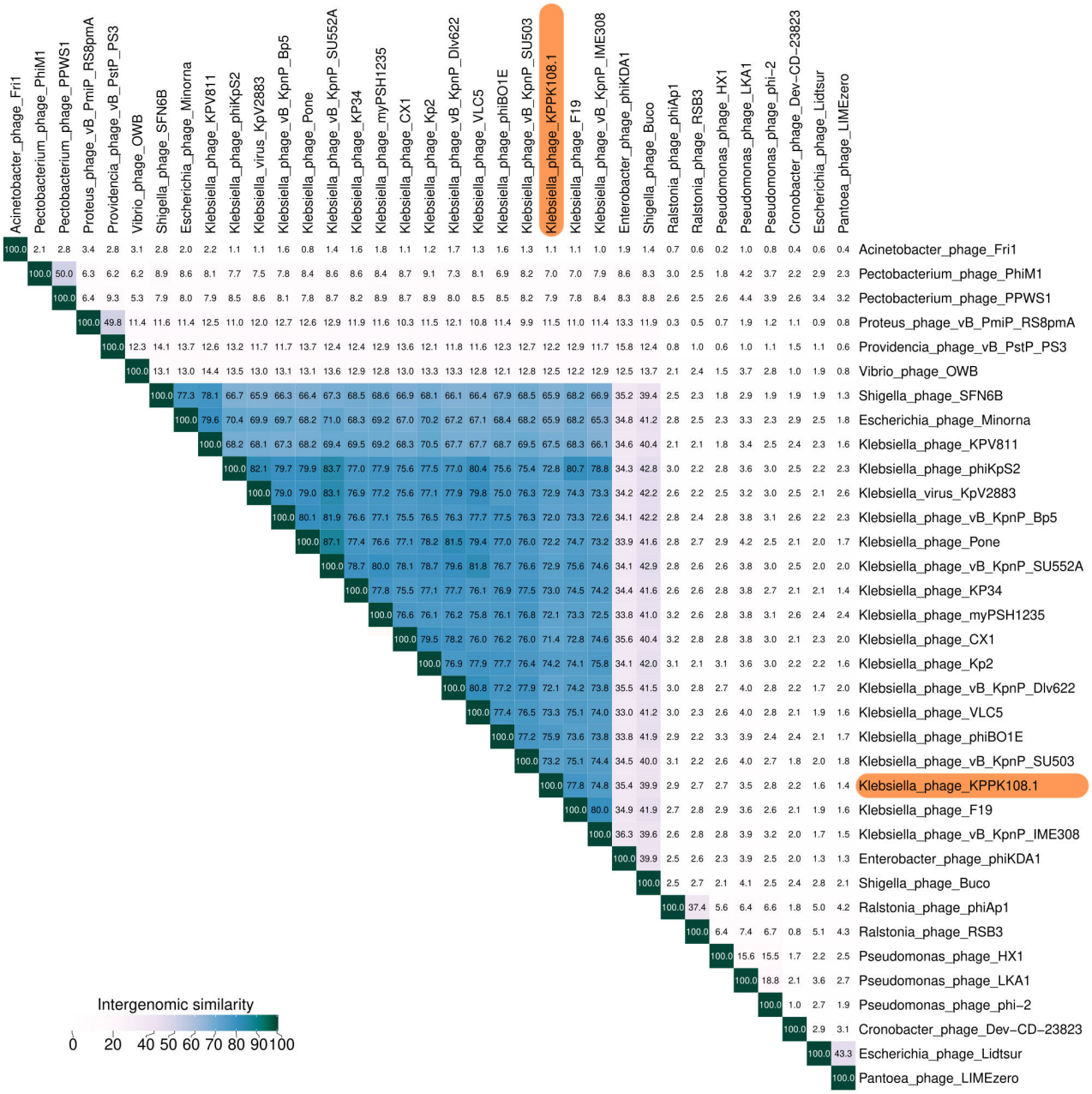

Fig. 3. Average nucleotide identity (ANI) distance matrix of the *Klebsiella* phage KPPK108.1 generated with the VIRIDIC web-based tool using the genomes of various *Autographiviridae* family members

the function of this protein has not been defined by searching for homologues using BLAST, or searching for similar proteins by HMM-HMM comparison, the surface charge distribution makes it possible to assume that this protein mimics nucleic acid, like Ocr proteins, which are also located within the early gene regions in the genomes of other *Autographiviridae*, and are capable of DNA mimicking [25, 26]. It has been shown that Ocr protein effectively inhibits the BREX restriction modification system, facilitating phage infection [27].

Bioinformatic analysis of the KPPK108.1 phage genome makes it possible to predict the organizational structure of the adsorption apparatus comprised of the head-tail connector and the tailspike protein, possessing enzymatic properties. The tailspike protein seems to be the receptor-binding protein (RBP), which determines host specificity and the host spectrum of the phage [28]. The tailspike protein structure analysis indicates the presence of depolymerizing activity against the polysaccharide, presumed to be related to the *E. coli* colanic acid. Colanic acid, the extracellular polysaccharide, consisting of several types of carbohydrate residues (such as L-fucose, D-glucose, D-galactose, and D-glucuronic acid), which is released into the extracellular environment by bacteria of the *Enterobacteriaceae* family, is the colanidase substrate [29]. Colanidases have been relatively recently discovered in phage RBPs [30]. Colanidases are present in a number of virulent bacteriophages of the evolutionarily distant groups, such as podoviruses and myoviruses [23, 30], some of which have proven to be effective when used in phage cocktails for phage therapy [30]. It is essential to define the structure of the type K108 *K. pneumoniae* capsular polysaccharide to clarify the question of the similarity of this polymer to colanic acid.

CONCLUSIONS

Klebsiella bacteriophage KPPK108.1 is a virulent bacteriophage of the genus *Drulisvirus*, family *Autographiviridae*. Thorough

Fig. 4. Phylogenetic tree of *Klebsiella* phage KPPK108.1 and other *Autographiviridae* phages generated with the RaxML program using the concatenated amino acid sequences of the major capsid protein, terminase large subunit, DNA polymerase, and RNA polymerase

bioinformatic analysis has revealed the lytic nature of the phage infection cycle. The analysis makes it possible to predict the structure of the phage adsorption apparatus comprised of the head-tail connector and the tailspike protein, exhibiting colanidase activity. The predicted characteristics of KPPK108.1 bacteriophage indicate the feasibility of using KPPK108.1 in phage cocktails for phage therapy. As far as we know, KPPK108.1 is the first fully described phage specific for capsular type KL108.

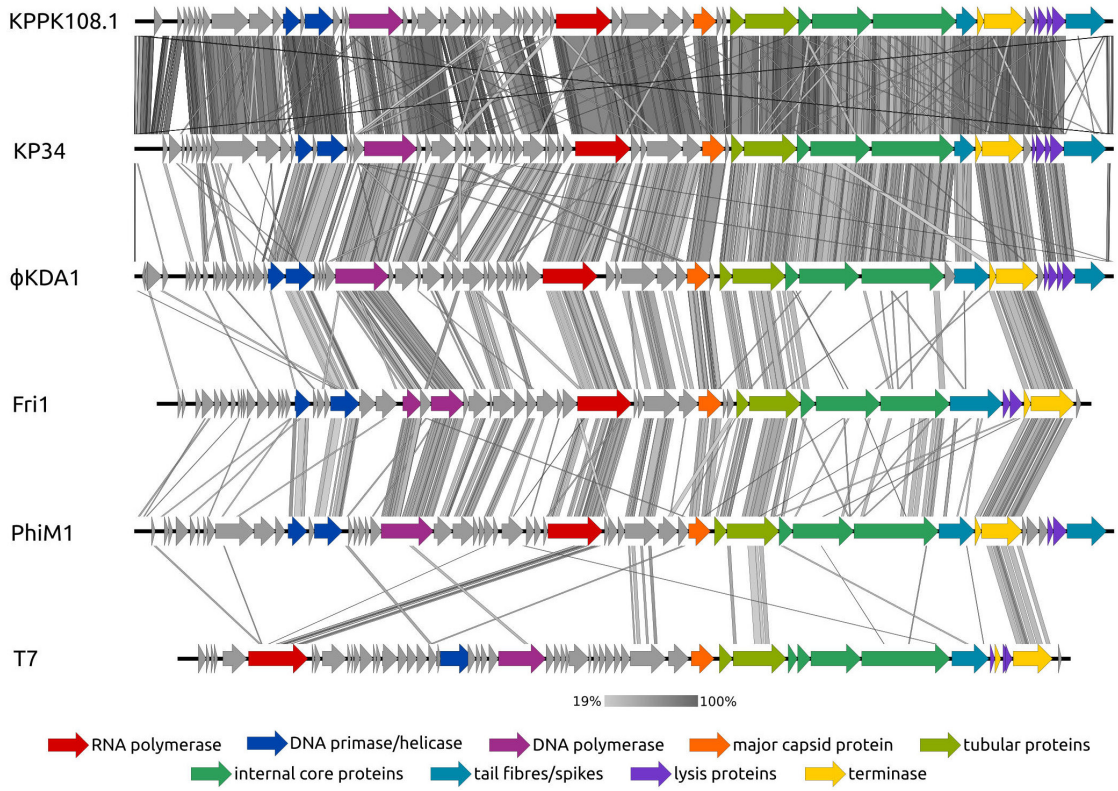

Fig. 5. Intergenomic comparison diagram created with EasyFig and TBLASTX using the genomes of *Klebsiella* phage KPPK108.1 and other *Autographiviridae* phages. The vertical lines are colored in accordance with the color scale showing the degree of similarity

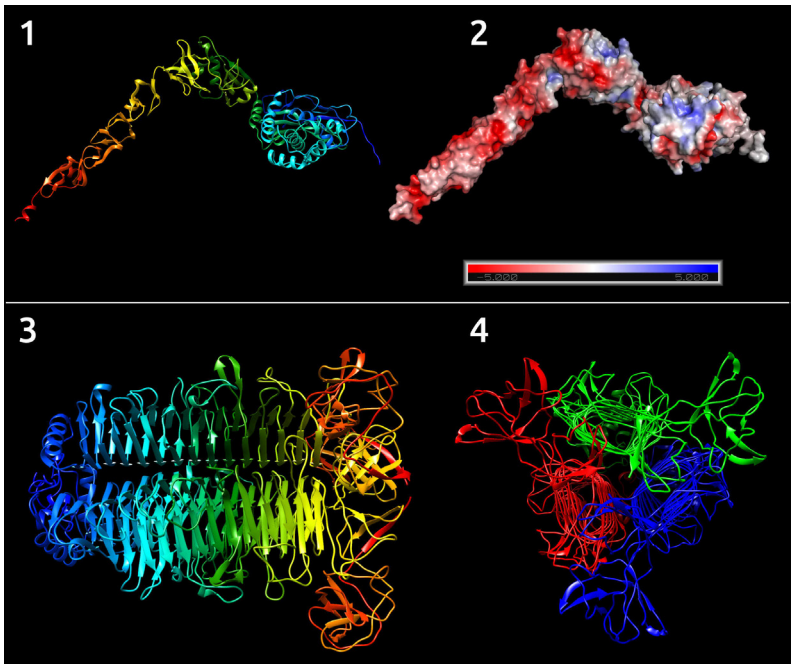

Fig. 6. Predicted tertiary structure of the KPPK108.1 phage gene 8 product painted with rainbow colors, where *blue* indicates N-terminal region, and *red* indicates C-terminal region of the protein (**1**). Predicted tertiary structure of the gene 8 product painted in accordance with the charge of the protein surface electrostatic field (**2**). Predicted tertiary structure of the KPPK108.1 phage tailspike trimer painted with rainbow colors, where *blue* indicates N-terminal region, and *red* indicates C-terminal region of the protein, longitudinal view (**3**). Predicted tertiary structure of the KPPK108.1 phage tailspike trimer with monomers painted with different colors, view along transverse axis (**4**)

References

1. Paczosa MK, Mecsas J. Klebsiella pneumoniae: Going on the Offense with a Strong Defense. Microbiol Mol Biol Rev. 2016; 80 (3): 629–61.
2. Wyres KL, Wick RR, Gorrie C, Jenney A, Follador R, Thomson NR, et al. Identification of Klebsiella capsule synthesis loci from whole genome data. Microb Genom. 2016; 2 (12): e000102.
3. Colombet J, Robin A, Lavie L, Bettarel Y, Cauchie HM, Sime-Ngando T. Virioplankton "pegylation": use of PEG (polyethylene glycol) to concentrate and purify viruses in pelagic ecosystems. J Microbiol Methods. 2007; 71 (3): 212–9.
4. Bankevich A, Nurk S, Antipov D, Gurevich AA, Dvorkin M, Kulikov AS, et al. SPAdes: a new genome assembly algorithm and its applications to single-cell sequencing. J Comput Biol. 2012; 19 (5): 455–77.
5. Drulis-Kawa Z, Mackiewicz P, Kęsik-Szeloch A, Maciaszczyk-Dziubinska E, Weber-Dąbrowska B, Dorotkiewicz-Jach A, et al. Isolation and characterisation of KP34 — a novel φKMV-like bacteriophage for Klebsiella pneumoniae. Appl Microbiol Biotechnol. 2011; 90 (4): 1333–45.
6. Seemann T. Prokka: rapid prokaryotic genome annotation. Bioinformatics. 2014; 30 (14): 2068–9.
7. Altschul SF, Gish W, Miller W, Myers EW, Lipman DJ. Basic local alignment search tool. J Mol Biol. 1990; 215 (3): 403–10.
8. Gabler F, Nam S-Z, Till S, Mirdita M, Steinegger M, Söding J, et al. Protein Sequence Analysis Using the MPI Bioinformatics Toolkit. Current Protocols in Bioinformatics. 2020; 72 (1): e108.
9. Kelley LA, Mezulis S, Yates CM, Wass MN, Sternberg MJE. The Phyre2 web portal for protein modeling, prediction and analysis. Nat Protoc. 2015; 10 (6): 845–58.
10. Geneious. Bioinformatics Software for Sequence Data Analysis. Geneious [cited 2021 Nov 11]. Available from: https://www.geneious.com/
11. Home — Genome — NCBI [cited 2021 Nov 11]. Available from: https://www.ncbi.nlm.nih.gov/genome.
12. Moraru C, Varsani A, Kropinski AM. VIRIDIC — A Novel Tool to Calculate the Intergenomic Similarities of Prokaryote-Infecting Viruses. Viruses. 2020; 12 (11): 1268.
13. Lee I, Ouk Kim Y, Park S-C, Chun J. OrthoANI: An improved algorithm and software for calculating average nucleotide identity. Int J Syst Evol Microbiol. 2016; 66 (2): 1100–3.
14. Stamatakis A. RAxML version 8: a tool for phylogenetic analysis and post-analysis of large phylogenies. Bioinformatics. 2014; 30 (9): 1312–3.
15. Le SQ, Gascuel O. An improved general amino acid replacement matrix. Mol Biol Evol. 2008; 25 (7): 1307–20.
16. Katoh K, Misawa K, Kuma K, Miyata T. MAFFT: a novel method for rapid multiple sequence alignment based on fast Fourier transform. Nucleic Acids Research. 2002; 30 (14): 3059–66.
17. Sullivan MJ, Petty NK, Beatson SA. Easyfig: a genome comparison visualizer. Bioinformatics. 2011; 27 (7): 1009–10.
18. Jumper J, Evans R, Pritzel A, Green T, Figurnov M, Ronneberger O, et al. Highly accurate protein structure prediction with AlphaFold. Nature. 2021; 596 (7873): 583–9.
19. Evans R, O'Neill M, Pritzel A, Antropova N, Senior A, Green T, et al. Protein complex prediction with AlphaFold-Multimer. 2021 [cited 2021 Dec 6]. 2021.10.04.463034. Available from: https://www.biorxiv.org/content/10.1101/2021.10.04.463034v1.
20. Berman HM, Westbrook J, Feng Z, Gilliland G, Bhat TN, Weissig H, et al. The Protein Data Bank. Nucleic Acids Research. 2000; 28 (1): 235–42.
21. Jurrus E, Engel D, Star K, Monson K, Brandi J, Felberg LE, et al. Improvements to the APBS biomolecular solvation software suite. Protein Science. 2018; 27 (1): 112–28.
22. Pettersen EF, Goddard TD, Huang CC, Couch GS, Greenblatt DM, Meng EC, et al. UCSF Chimera--a visualization system for exploratory research and analysis. J Comput Chem. 2004; 25 (13): 1605–12.
23. Schwarzer D, Buettner FFR, Browning C, Nazarov S, Rabsch W, Bethe A, et al. A Multivalent Adsorption Apparatus Explains the Broad Host Range of Phage phi92: a Comprehensive Genomic and Structural Analysis. Journal of Virology. 2012; 86 (19): 10384–98.
24. Evseev PV, Lukianova AA, Shneider MM, Korzhenkov AA, Bugaeva EN, Kabanova AP, et al. Origin and Evolution of Studiervirinae Bacteriophages Infecting Pectobacterium: Horizontal Transfer Assists Adaptation to New Niches. Microorganisms. 2020; 8 (11): 1707.
25. Roberts GA, Stephanou AS, Kanwar N, Dawson A, Cooper LP, Chen K, et al. Exploring the DNA mimicry of the Ocr protein of phage T7. Nucleic Acids Res. 2012; 40 (16): 8129–43.
26. Zavilgelsky GB, Rastorguev SM. Antirestriction proteins ArdA and Ocr as efficient inhibitors of type I restriction-modification enzymes. Mol Biol. 2009; 43 (2): 241.
27. Isaev A, Drobiazko A, Sierro N, Gordeeva J, Yosef I, Qimron U, et al. Phage T7 DNA mimic protein Ocr is a potent inhibitor of BREX defence. Nucleic Acids Res. 2020; 48 (10): 5397–406.
28. Zampara A, Sørensen MCH, Grimon D, Antenucci F, Vitt AR, Bortolaia V, et al. Exploiting phage receptor binding proteins to enable endolysins to kill Gram-negative bacteria. Sci Rep. 2020; 10 (1): 12087.
29. Stevenson G, Andrianopoulos K, Hobbs M, Reeves PR. Organization of the Escherichia coli K-12 gene cluster responsible for production of the extracellular polysaccharide colanic acid. J Bacteriol. 1996; 178 (16): 4885–93.
30. Kim H, Kim M, Bai J, Lim J-A, Heu S, Ryu S. Colanic Acid Is a Novel Phage Receptor of Pectobacterium carotovorum subsp. carotovorum Phage POP72. Frontiers in Microbiology. 2019; 10: 143.

Литература

1. Paczosa MK, Mecsas J. Klebsiella pneumoniae: Going on the Offense with a Strong Defense. Microbiol Mol Biol Rev. 2016; 80 (3): 629–61.
2. Wyres KL, Wick RR, Gorrie C, Jenney A, Follador R, Thomson NR, et al. Identification of Klebsiella capsule synthesis loci from whole genome data. Microb Genom. 2016; 2 (12): e000102.
3. Colombet J, Robin A, Lavie L, Bettarel Y, Cauchie HM, Sime-Ngando T. Virioplankton "pegylation": use of PEG (polyethylene glycol) to concentrate and purify viruses in pelagic ecosystems. J Microbiol Methods. 2007; 71 (3): 212–9.
4. Bankevich A, Nurk S, Antipov D, Gurevich AA, Dvorkin M, Kulikov AS, et al. SPAdes: a new genome assembly algorithm and its applications to single-cell sequencing. J Comput Biol. 2012; 19 (5): 455–77.
5. Drulis-Kawa Z, Mackiewicz P, Kęsik-Szeloch A, Maciaszczyk-Dziubinska E, Weber-Dąbrowska B, Dorotkiewicz-Jach A, et al. Isolation and characterisation of KP34 — a novel φKMV-like bacteriophage for Klebsiella pneumoniae. Appl Microbiol Biotechnol. 2011; 90 (4): 1333–45.
6. Seemann T. Prokka: rapid prokaryotic genome annotation. Bioinformatics. 2014; 30 (14): 2068–9.
7. Altschul SF, Gish W, Miller W, Myers EW, Lipman DJ. Basic local alignment search tool. J Mol Biol. 1990; 215 (3): 403–10.
8. Gabler F, Nam S-Z, Till S, Mirdita M, Steinegger M, Söding J, et al. Protein Sequence Analysis Using the MPI Bioinformatics Toolkit. Current Protocols in Bioinformatics. 2020; 72 (1): e108.
9. Kelley LA, Mezulis S, Yates CM, Wass MN, Sternberg MJE. The Phyre2 web portal for protein modeling, prediction and analysis. Nat Protoc. 2015; 10 (6): 845–58.
10. Geneious. Bioinformatics Software for Sequence Data Analysis. Geneious [cited 2021 Nov 11]. Available from: https://www.geneious.com/
11. Home — Genome — NCBI [cited 2021 Nov 11]. Available from: https://www.ncbi.nlm.nih.gov/genome.

12. Moraru C, Varsani A, Kropinski AM. VIRIDIC — A Novel Tool to Calculate the Intergenomic Similarities of Prokaryote-Infecting Viruses. Viruses. 2020; 12 (11): 1268.
13. Lee I, Ouk Kim Y, Park S-C, Chun J. OrthoANI: An improved algorithm and software for calculating average nucleotide identity. Int J Syst Evol Microbiol. 2016; 66 (2): 1100–3.
14. Stamatakis A. RAxML version 8: a tool for phylogenetic analysis and post-analysis of large phylogenies. Bioinformatics. 2014; 30 (9): 1312–3.
15. Le SQ, Gascuel O. An improved general amino acid replacement matrix. Mol Biol Evol. 2008; 25 (7): 1307–20.
16. Katoh K, Misawa K, Kuma K, Miyata T. MAFFT: a novel method for rapid multiple sequence alignment based on fast Fourier transform. Nucleic Acids Research. 2002; 30 (14): 3059–66.
17. Sullivan MJ, Petty NK, Beatson SA. Easyfig: a genome comparison visualizer. Bioinformatics. 2011; 27 (7): 1009–10.
18. Jumper J, Evans R, Pritzel A, Green T, Figurnov M, Ronneberger O, et al. Highly accurate protein structure prediction with AlphaFold. Nature. 2021; 596 (7873): 583–9.
19. Evans R, O'Neill M, Pritzel A, Antropova N, Senior A, Green T, et al. Protein complex prediction with AlphaFold-Multimer. 2021 [cited 2021 Dec 6]. 2021.10.04.463034. Available from: https://www.biorxiv.org/content/10.1101/2021.10.04.463034v1.
20. Berman HM, Westbrook J, Feng Z, Gilliland G, Bhat TN, Weissig H, et al. The Protein Data Bank. Nucleic Acids Research. 2000; 28 (1): 235–42.
21. Jurrus E, Engel D, Star K, Monson K, Brandi J, Felberg LE, et al. Improvements to the APBS biomolecular solvation software suite. Protein Science. 2018; 27 (1): 112–28.
22. Pettersen EF, Goddard TD, Huang CC, Couch GS, Greenblatt DM, Meng EC, et al. UCSF Chimera--a visualization system for exploratory research and analysis. J Comput Chem. 2004; 25 (13): 1605–12.
23. Schwarzer D, Buettner FFR, Browning C, Nazarov S, Rabsch W, Bethe A, et al. A Multivalent Adsorption Apparatus Explains the Broad Host Range of Phage phi92: a Comprehensive Genomic and Structural Analysis. Journal of Virology. 2012; 86 (19): 10384–98.
24. Evseev PV, Lukianova AA, Shneider MM, Korzhenkov AA, Bugaeva EN, Kabanova AP, et al. Origin and Evolution of Studiervirinae Bacteriophages Infecting Pectobacterium: Horizontal Transfer Assists Adaptation to New Niches. Microorganisms. 2020; 8 (11): 1707.
25. Roberts GA, Stephanou AS, Kanwar N, Dawson A, Cooper LP, Chen K, et al. Exploring the DNA mimicry of the Ocr protein of phage T7. Nucleic Acids Res. 2012; 40 (16): 8129–43.
26. Zavilgelsky GB, Rastorguev SM. Antirestriction proteins ArdA and Ocr as efficient inhibitors of type I restriction-modification enzymes. Mol Biol. 2009; 43 (2): 241.
27. Isaev A, Drobiazko A, Sierro N, Gordeeva J, Yosef I, Qimron U, et al. Phage T7 DNA mimic protein Ocr is a potent inhibitor of BREX defence. Nucleic Acids Res. 2020; 48 (10): 5397–406.
28. Zampara A, Sørensen MCH, Grimon D, Antenucci F, Vitt AR, Bortolaia V, et al. Exploiting phage receptor binding proteins to enable endolysins to kill Gram-negative bacteria. Sci Rep. 2020; 10 (1): 12087.
29. Stevenson G, Andrianopoulos K, Hobbs M, Reeves PR. Organization of the Escherichia coli K-12 gene cluster responsible for production of the extracellular polysaccharide colanic acid. J Bacteriol. 1996; 178 (16): 4885–93.
30. Kim H, Kim M, Bai J, Lim J-A, Heu S, Ryu S. Colanic Acid Is a Novel Phage Receptor of Pectobacterium carotovorum subsp. carotovorum Phage POP72. Frontiers in Microbiology. 2019; 10: 143.

DEGENERATIVE DISC DISEASE IN YOUNG ADULTS: CYTOKINE PROFILE AND ANGIOGENIC FACTORS

Novikova AV[1]✉, Pravdyuk NG[1], Saklakova VS[2], Lolomadze EA[2], Feniksov VM[3], Nikolaev DA[3], Davygora KS[1], Timofeev VT[1], Shostak NA[1]

[1] Pirogov Russian National Research Medical University, Moscow, Russia

[2] Kulakov National Medical Research Center for Obstetrics, Gynecology and Perinatology, Moscow, Russia

[3] Pirogov City Clinical Hospital № 1, Moscow, Russia

Back pain (BP), associated with the degenerative disc disease (DDD), poses a heavy social and economic burden due to early disability and indications to surgery, emerging in young adults. Pathophysiological basis of premature intervertebral disc (IVD) degeneration is being actively studied. The study was aimed to define the profiles of inflammatory cytokines in DDD, as well as their relationship to the structural spine diseases. The molecular genetic analysis of the mRNA gene abundance in patients with BP and herniated IVD after discectomy and healthy individuals was performed by the quantitative polymerase chain reaction method. High expression of TNFα, IL17 was revealed in the IVD tissues of the affected patients ($p < 0.01$); the levels of TNFα and IL1β correlated with the DDD severity ($r = 0.301$ and 0.37; $p < 0.05$). Elevated expression of IL1β, IL6 was found in peripheral white blood cells ($p < 0.01$); the levels of IL6 negatively correlated with Modic type 1 and 2 changes ($r = –0.31$; $p < 0.05$), and the levels of IL17 positively correlated with the IVD herniation in combination with erosions of the adjacent vertebral body endplates and Modic changes ($r = 0.401$; $p < 0.05$). The expression of VEGF-A in the IVD tissues and white blood cells negatively correlated with the DDD grades ($r = –0.85$; $p < 0.001$), indicating reduced vascularization in the terminal phase of the disease. The findings on DDD demonstrate the contribution of the local low-immune inflammation, coupled with the intense disc vascularization at the earlier stages, and associated with the reactive inflammation in vertebral bodies. The results are prerequisites for developing the anti-inflammatory and reparative therapy based on the DDD grade and the presence of Modic changes in young adults with BP.

Keywords: back pain, degenerative disc disease, young age, discectomy, cytokine expression, mRNA TNFα, IL1β, IL6, IL17, VEGF-A, Modic-changes

Acknowledgements: we would like to thank neurosurgeons of the Department of Neurosurgery, Nekrasova MA, Babenkova VV, Isaeva AN, Smirnova VA, Glukhova DS, Gabechiya GV, Choriyeva DB, Kozheva AKh, for assistance in our research.

Author contribution: Novikova AV — literature analysis, clinical data acquisition and biomaterial collection, preanalytical phase of the study, data analysis and interpretation, preparation of figures and graphs; Pravdyuk NG — literature analysis, task definition, study design, data analysis and interpretation; Saklakova VS — literature analysis, analytic phase of laboratory testing, definition and statistical analysis of mRNA abundance in biomaterial, scheduling; Lolomadze EA — analysis of laboratory work, analysis of mRNA abundance in biomaterial; Feniksov VM and Nikolaev DA — admission to clinical data acquisition, neurological examination of patients, discectomy, biomaterial collection; Davygora KS — literature analysis, analysis of laboratory work; Timofeev VT — study planning, preanalytical phase of the study, evaluation of the data obtained; Shostak NA — research management, study design, data interpretation, manuscript editing.

Compliance with ethical standards: the study was approved by the Ethics Committee of Pirogov Russian National Research Medical University (protocol № 181 dated January 28, 2019); the informed consent to blood testing and investigation of intervertebral disc was obtained from all participants.

✉ **Correspondence should be addressed:** Anna V. Novikova
Ostrovitianova, 1, Moscow, 117997, Russia; annove2008@mail.ru

Received: 22.11.2021 **Accepted:** 06.12.2021 **Published online:** 19.12.2021

DOI: 10.24075/brsmu.2021.061

ДЕГЕНЕРАТИВНАЯ БОЛЕЗНЬ ДИСКА У МОЛОДЫХ: ЦИТОКИНОВЫЙ ПРОФИЛЬ И ФАКТОРЫ АНГИОГЕНЕЗА

А. В. Новикова[1]✉, Н. Г. Правдюк[1], В. С. Саклакова[2], Е. А. Ломадзе[2], В. М. Фениксов[3], Д. А. Николаев[3], К. С. Давыгора[1], В. Т. Тимофеев[1], Н. А. Шостак[1]

[1] Российский национальный исследовательский медицинский университет имени Н. И. Пирогова, Москва, Россия

[2] Национальный медицинский исследовательский центр акушерства, гинекологии и перинатологии имени В. И. Кулакова, Москва, Россия

[3] Городская клиническая больница № 1 имени Н. И. Пирогова, Москва, Россия

Боль в спине (БС), ассоциированная с дегенеративной болезнью диска (ДБД), — тяжелое социальное и экономическое бремя вследствие ранней инвалидизации и возникновения показаний к оперативному вмешательству уже в молодом возрасте. Патофизиологические основы преждевременной дегенерации межпозвонкового диска (МПД) находятся на стадии активного изучения. Целью исследования было определить профиль воспалительных цитокинов при ДБД и их связь со структурными нарушениями в позвоночнике. У пациентов молодого возраста с БС и грыжей МПД, подвергшихся дискэктомии, и у здоровых лиц проводили молекулярно-генетический анализ представленности генов мРНК методом количественной полимеразной цепной реакции. У больных в ткани МПД выявлен высокий уровень экспрессии TNFα, IL17 ($p < 0,01$); уровни TNFα и IL1β коррелировали с тяжестью ДБД ($r = 0,301$ и 0,37; $p < 0,05$). В лейкоцитах периферической крови обнаружена повышенная экспрессия IL1β, IL6 ($p < 0,01$); уровень IL6 отрицательно коррелировал с I и II стадиями Modic-изменений ($r = –0,31$; $p < 0,05$), IL17 прямо коррелировал с грыжей МПД в сочетании с эрозией замыкательных пластин и Modic ($r = 0,401$; $p < 0,05$). Экспрессия VEGF-A в ткани МПД и в лейкоцитах крови отрицательно коррелировала со стадией ДБД ($r = –0,85$; $p < 0,001$), указывая на снижение активности васкуляризации в терминальной стадии. Данные, выявленные при ДБД, говорят о вкладе локального низкоиммунного воспаления, сопряженного с активной васкуляризацией диска на более ранних стадиях и ассоциированного с реактивным воспалением тел позвонков. Полученные результаты служат предпосылкой к разработке противовоспалительной и репаративной терапии в зависимости от стадии ДБД и наличия Modic-изменений у лиц молодого возраста с БС.

Ключевые слова: боль в спине, дегенеративная болезнь диска, молодой возраст, дискэктомия, экспрессия цитокинов, мРНК TNFα, IL1β, IL6, IL17, VEGF-A, Modic-изменения

Благодарности: врачам-нейрохирургам нейрохирургического отделения М. А. Некрасову, В. В. Бабенкову, А. Н. Исаеву, В. А. Смирнову, Д. С. Глухову, Г. В. Габечия, Д. Б. Чориеву, А. Х. Кожеву за помощь в исследовании.

Вклад авторов: А. В. Новикова — анализ литературы, сбор клинических данных и набор биоматериала, выполнение преаналитического этапа работы, анализ и интерпретация данных, подготовка рисунков и графиков; Н. Г. Правдюк — анализ литературы, постановка задачи, разработка дизайна исследования, анализ и интерпретация данных; В. С. Саклакова — анализ литературы, выполнение аналитической части лабораторной работы, определение и статистический анализ уровня представленности мРНК в биоматериале, составление графиков; Е. А. Ломадзе — анализ лабораторной работы, анализ уровня представленности мРНК в биоматериале; В. М. Фениксов и Д. А. Николаев — допуск к набору клинического материала, неврологический осмотр пациентов, дискэктомия, получение биоматериала; К. С. Давыгора — анализ литературы, анализ лабораторной работы; В. Т. Тимофеев — планирование исследования, выполнение преаналитического этапа работы, оценка полученных данных; Н. А. Шостак — руководство проведением исследования, разработка дизайна исследования, интерпретация данных, редактирование рукописи.

Соблюдение этических стандартов: исследование одобрено этическим комитетом РНИМУ им. Н. И. Пирогова (протокол № 181 от 28 января 2019 г.); от всех участников получено информированное согласие на проведение исследования образцов крови и межпозвонкового диска.

✉ **Для корреспонденции:** Анна Владимировна Новикова
ул. Островитянова, д. 1, г. Москва, 117997, Россия; annove2008@mail.ru

Статья получена: 22.11.2021 **Статья принята к печати:** 06.12.2021 **Опубликована онлайн:** 19.12.2021

DOI: 10.24075/vrgmu.2021.061

Back pain (BP) is one of the main causes of the patients' disability in the developed world, resulting in permanent disability. BP is found in all age groups. Thus, according to a Polish study, BP recurrence within 34 years was observed in 85% of males and 86% of females with the BP onset at the age of 14 [1]. Degenerative disc disease (DDD), resulting from degradation and inflammation of the intervertebral disc (IVD) tissues, is one of the BP variants, associated with unfavourable outcomes [2]. DDD is a chronic condition with a trend towards progression. Despite the fact that there are still no explicit criteria for distinguishing between the "natural" physiological disc ageing and the pathological degeneration, also found in young adults, the term "DDD" is used by both clinicians and pathologists to define the disc extracellular matrix disruption with impaired homeostasis and the inflammatory process induction in the IVD space [3]. The DDD clinical manifestations are well documented: these are BP of mechanical origin associated with axial load (getting worse with physical activity, moving heavy objects, flexion, and improving at rest) and/or with spinal stenosis, radiculopathy, and less often with myelopathy. DDD is one of the causes of chronic segmental instability and early disability in the working age patients. Studies have shown that the IVD degeneration is a multifaceted process, involving apoptosis, inflammation, ageing, and biomechanical dysfunction [4]. Recently, considerable attention has been paid to studying the effects of inflammatory cytokines on the DDD development, as well as to the imbalance between the pro-inflammatory and anti-inflammatory cytokines [5].

It is shown, that inflammatory pattern triggers the catabolic processes in the cartilage matrix of the compromized functional spinal unit, together with further degeneration of extracellular matrix and dehydratation of nucleus pulposus (NP) and annulus fibrosus (AF) [5, 6]. The loss of the disc structural integrity and the AF microcracks cause the prolapse of the NP content into the AF tissue and outwards with the formation of protrusion, extrusion, and sequestration. The role of TNFα, IL1β, overexpression of IL6, and CD16 monocytes in the development and progression of degenerative changes is being discussed in literature. It is important to mention that the cytokine expression may be correlated with the IVD degeneration severity. The role of IL6 in the disc degeneration and herniation was studied by many researchers [7]. The hypothesis about the IL6 involvement in the human IVD degeneration was confirmed by the fact that the abundance of the catabolic gene transcript increased, and the expression of genes encoding proteoglycans was suppressed with the increase in the IL6 expression [8]. Studying the role of IL17 in the DDD-associated inflammatory cascade showed that the exposure of human NP cells to IL17 and TNFα contributed to the increased release of IL6 in vitro and the increased expression of intercellular adhesion molecules (ICAM-1) on the surface of cells in NP and AF [9]. The association between pain intensity, IVD herniation, and inflammatory response was defined. It was suggested to treat the listed above biomarkers as the potential markers of the disease onset, severity, and progression.

The possibility of using the analysis of serum inflammatory biomarkers for identification of degeneration and inflammation of the IVD tissues in patients with DDD was demonstrated [7, 10]. Molecular patterns of degeneration and inflammation in the disc tissued were assessed in order to develop the approaches to the reparative therapy of DDD [3]. IL1β, TNFα, and VEGF were verified by immunohistochemistry in individuals of various ages having no symptoms of BP [11]; the expression of these markers in the disc tissues showed almost no differences between the groups of young and elderly individuals having no symptoms of the disease. Accordingly, measuring the cytokine levels in the damaged disc is an important challenge in terms of searching for the pathogenetically substantiated anti-inflammatory and reparative therapy. Recently, the role of the vascular endothelial growth factor (VEGF, VFA) in the disc tissue vascularization (the disc is normally avascular) at all stages of the IVD degeneration was shown. The VEGF activity is realized via regulation of the soluble vascular endothelial growth factor receptor 1 expression [12].

When studying the pattern of the hernia resorption in patients with DDD (confirmed by MRI), Japanese researchers assessed the interaction sequence TNFα–VEGF–MMP (matrix metalloproteinases MMP-3 and MMP-7 involved in degradation of the extracellular matrix proteins, aggrecan and collagen) and found that the expression of mRNA and VEGF protein increased in the situation of the contact between macrophages and human disc tissues in vitro, and positively correlated with the TNFα expression levels [13]. Thus, it was shown that neovascularization promoted the reverse development of intervertebral hernias. The process of the capillary ingrowth into the IVD tissue was confirmed by magnetic resonance imaging (MRI) with the use of gadolinium-based contrast agents, and could serve as an additional determinant of the extrusion resorption [14].

The relationship between the markers of aseptic inflammation and IVD reparation in the disk tissues, and the abundance of those in peripheral blood of young patients with advanced grade DDD have not been fully defined. Various data are available on the preponderant role in altering the IVD immune homeostasis, played by one or another cytokine. Studying the cytokine profile (together with the features of the functional spinal unit lesion) would make it possible to define the immune phenotypes of patients in order to develop the biological targets for therapy and prognosis of the disease. The study was aimed to define the profiles of the key biomarkers of inflammatory damage (TNFα, IL6, IL17, IL1β) and angiogenesis (isoforms of the vascular endothelial growth factor A, VEGF121, VEGF165, and VEGF189) in the cartilage tissue of IVDs and white blood cells of young patients with DDD, who underwent discectomy, compared to controls.

METHODS

The study was carried out at the Department of Neurosurgery, Pirogov City Clinical Hospital № 1, and A.I. Nesterov Department of Faculty Therapy, Pirogov Russian National Research Medical University, in 2019–2021. A total of 87 young (aged 18–44 in accordance with the WHO classification, 2012) adults were enrolled (40 males and 48 females). Index group inclusion criteria: young patients (median age 37.01 years [35.54–38.49]) having BP associated with DDD, confirmed by instrumental evaluation (MRI) (Table). Exclusion criteria: history of spinal injury or spinal injury at the time of the study, tumors and infections affecting the spine and other organs, inflammatory spondyloarthropathy, surgical interventions in the previous 30 days. All individuals in the index group underwent surgery (microdiscectomy) due to the spinal disc herniation at the corresponding level in the lumbar spine. Pain intensity was measured in millimeters using the Visual Analogue Scale (VAS). The functional limitations in the lumbar spine were assessed based on the Backache Index (BAI) [15]. The control group was represented by healthy volunteers with no BP (20 individuals), comparable in gender and age. All patients and controls underwent MRI of the lumbar spine prior to surgery. IVD degeneration was assessed based on the reduced IVD

Table. Demographic, clinical and instrumental characteristics of the studied groups

Characteristics of patients	Index group		Control group		P I–II
Number of patients	67		20		
females	30		10		
males	37		10		
Average age, years	Me	LQ–UQ	Me	LQ–UQ	
	37,01	[35,54–38,49]	34,5	[29,26–39,74]	< 0,01
Pfirrmann degeneration grade at the level of L1–L5 (mean value)	2,62	[2,4–3,0]	1,2	[1,1–1,8]	< 0,01
Pfirrmann degeneration grade at the level of operated IVD (mean value)	M	σ	M	σ	
	4,26	±0,59	2,15	±1,18	< 0,01
Number of patients with herniated IVDs	Abs. (%)		Abs. (%)		
at the level of L4–L5	24 (43)		1 (5)		< 0,01
at the level of L5–S1	36 (64)		0		
Number of patients with Modic changes (total)	47 (70)		1 (5)		< 0,01
Modic 1	21 (45)		0		< 0,01
Modic 2	26 (55)		1 (5)		< 0,01
Modic 3	0		0		

Index group		
Characteristics of patients	Me	LQ–UQ
Disease duration, years	5	[2,0–10,0]
Duration of the last painful episode, weeks	6	[3,0–12,0]
Pain intensity (VAS, mm)	68	[48,0–88,0]
Variant of pain syndrome	Abs.	%
acute	12	18
chronic	55	82
Functional impairment severity (Backache Index (BAI))		
mild	11	18
moderate	16	24
severe	40	58

signal intensity, disc space narrowing, structural changes in the disk, and blurring between the nucleus pulposus (NP) and the annulus fibrosus (AF). IVD degeneration was graded in accordance with the C.W. Pfirmann grading system (2001) (grades 1–5). Grades 3, 4, 5 were treated as irreversible damage to the disc, and grades 4, 5 were interpreted as severe DDD.

The fragments of degenerative IVDs were obtained during discectomy. Microparticles of IVD smaller than 1 mm^3 were immediately immersed in the IntactRNA stabilization solution (non-toxic aqueous fixative solution for rapid stabilization of cellular RNA in tissues and cell cultures, preserving the cell integrity), and the disc tissue samples were assigned a barcode, identical to the barcode of the patient's blood samples. The same molecular markers were identified in blood and cartilalage tissue samples, selected in accordance with the recent data based on the review articles and technical accessibility of the laboratory diagnosis (DNA-Technology; Russia). The abundance of mRNAs of the studied genes in blood cells (white blood cells) and IVD tissue was defined by the reverse transcription-quantitative polymerase chain reaction method with the use of the reagent kits (DNA-Technology; Russia). Amplification was performed in the DTprime 4 PCR system (DNA-Technology; Russia).

Obtaining IVD tissue samples (1 mm^3): RNA was extracted after cutting the cartilage with surgical blade (sterile disposable surgical scalpel, manufactured by Huaiyin Medikal Instruments Co. Ltd., China). After cutting, the fragment sized 1 mm was obtained, which was further grinded by the rubbing the conus of the microcentrifuge tube against the Petri dish bottom in order to obtain fine particles and molds. Then 320 μL of the lysing solution from the Proba-NK kit (DNA-Technology; Russia) were added to the dish. The contents of the dish together with the crushed sample were transferred to the Axygen microcentrifuge tubes (Axygen, Inc.; USA), and then mixed using the Micro-Spin FV-2400 centrifuge/vortex (Biosan; Latvia) for 5 s, and sedimented. Subsequently, this was left to lyse for 1 h. After that RNA was isolated using the Proba-NK kit (DNA-Technology; Russia) in accordance with the manufacturer's guidelines. The extracted RNA in the amount of 16.5 μL was immediately used for reverse transcription, which was performed at a temperature of 40 °C for 30 min, with subsequent inactivation of reverse transcriptase at 95 °C for 5 min. The resulting cDNA solution was either immediately used for quantitative PCR, or stored at –20 °C. The volume of 35 μL was used for amplification with the real-time registration of the results in accordance with the following program: 50 cycles 94 °C — 10 s, 64 °C — 20 s, 72 °C — 10 s. Fluorescence was measured during each cycle at a temperature of 64 °C.

The 4 ml blood samples were collected into the disposable Vacutainer EDTA tubes (Becton Dickinson; USA) 24 hours before surgery with subsequent blood processing in order to extract white blood cells. To obtain the buffy coat, the Proba-Ficoll kit for extraction of lymphocytes from the whole blood was used.

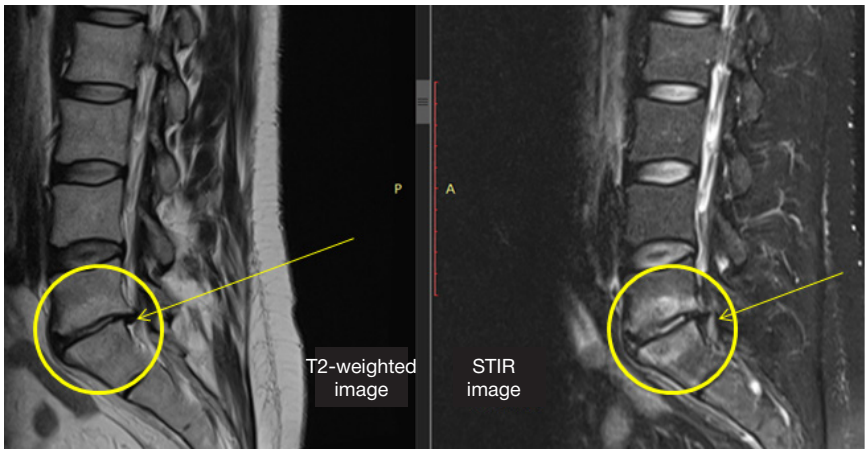

Fig. 1. Patient K. aged 37 with BP and Pfirrmann grade 4 DDD at the level of L5–S1, with IVD herniation (*arrow*) and Modic type 1 changes in vertebral bodies (*yellow contour*). T2-weighted and STIR images

RNA was isolated using the Proba-NK kit (DNA-Technology; Russia) in accordance with the manufacturer's guidelines. RNA extracted in the amount of 16.5 μL was immediately used for reverse transcription, which was performed at a temperature of 40 °C for 30 min, with subsequent inactivation of reverse transcriptase at 95 °C for 5 min. The resulting cDNA solution was either immediately used for quantitative PCR, or stored at –20 °C. The volume of 35 μL was used for amplification with the real-time registration of the results in accordance with the following program: 50 cycles 94 °C — 10 s, 64 °C — 20 s, 72 °C — 10 s. Fluorescence was measured during each cycle at a temperature of 64 °C.

The studied genes included TNFα, IL6, IL17, IL1β, and isoforms of vascular endothelial growth factor A (VEGF121, VEGF165, VEGF189). Normalization genes were represented by β2-microglobulin (B2m), and β-glucuronidase (GUSB). Normalization values for each gene mRNA were calculated by the ΔΔCt method [16]. The expression levels of the gene mRNAs were expressed in arbitrary units in relation to normalization genes (B2m, GUSB), which had the relatively stable expression levels.

Statistical analysis

The nonparametric method (Mann–Whitney U test) was used to assess the statistical significance of the differences obtained. Quantitative indicators were tested for normality using the Shapiro–Wilk test. Qualitative indicators were compared using the chi-squared test and the two-tailed Fisher's test for small samples. The differences between groups were considered significant when $p < 0.01$ and $p < 0.05$. Data analysis was performed using the Statistica v 8.0, SPSS v.10, and Graph Pad Prism software.

RESULTS

Clinical and instrumental characteristics of patients

Clinical characteristics of the young patients with BP are presented in Table. The average pain intensity value corresponded to 68 mm [48.0–88.0]. Acute pain (lasting for a maximum of 12 weeks) was found in 18% of patients, and 82% of patients had chronic pain. The median disease

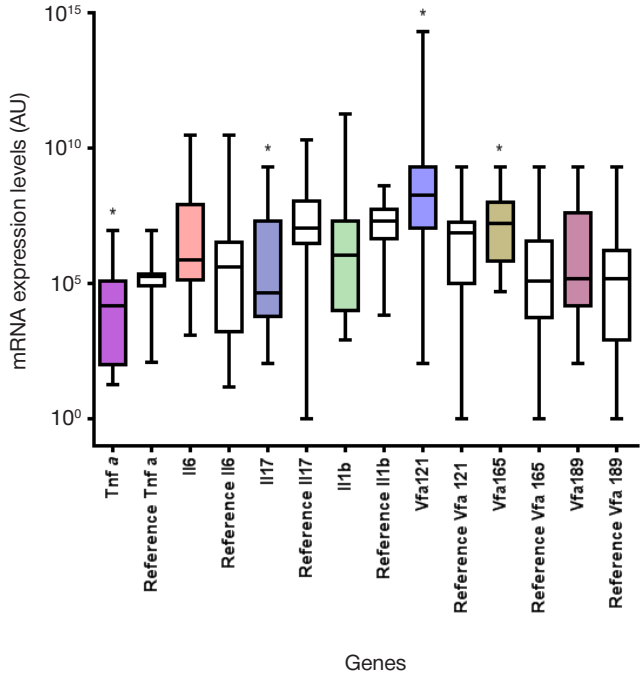

Fig. 2. Expression levels of mRNAs of the studied genes in relation to normalization genes (B2m, GUSB) in the IVD tissues of the index group patients and controls (* — $p < 0.01$)

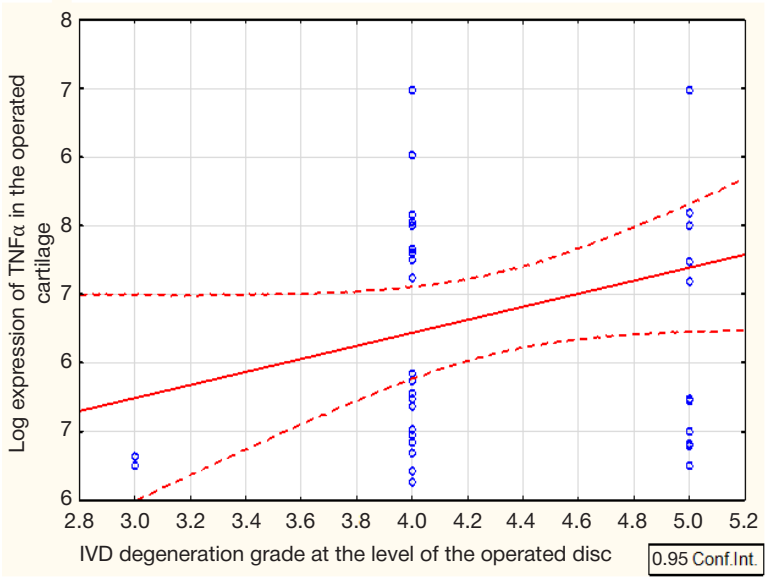

Fig. 3. Correlation between the TNFα mRNA expression levels in the IVD tissues and the Pfirrmann degeneration grades in the index group patients

duration in the latter was 5 years [2.0–10.0]. Based on BAI values, 82% of patients had moderate and severe functional impairment. The lumbar spine MRI showed the significant disc space narrowing, blurring between NP and AF, and reduced NP signal intensity. At the level of the operated disc, the IVD degeneration grade corresponded to grades 4 and 5 of the Pfirrmann grading system in 66% and 33% of the index group patients, respectively. Herniation was localized at the levels of L4–L5, L5–S1 at a ratio of 36 and 64%, respectively. In 70% of patients, MRI at the level of the operated disc revealed the altered intensity of the bone marrow MR signal on the T2-weighted and STIR (short tau inversion recovery) images, which indicated Modic type 1 changes, the bone marrow edema (45% of patients) (Fig. 1), and Modic type 2 changes, the fatty degeneration (55 %), in almost equal proportions. In the control group, Modic changes were found in only one patient (5%) out of 20, and these changes were also associated with severe DDD and asymptomatic IVD herniation. MRI revealed the combination of IVD herniation with erosions of the adjacent vertebral body endplates and Modic changes in 37 index group patients (53.6%). Such a "triple combination" was associated with longer BP duration (years), morning pain, and persistent chronic pain with no "lucid intervals" ($p < 0.05$) compared to patients with no erosions of the vertebral body endplates and/or Modic changes. The index group patients and the controls showed significant differences in the average Pfirrmann DDD grades and the prevalence of Modic changes (4.4 and 2.8 for DDD grades, 70 and 5% for Modic changes; $p < 0.01$). The findings confirm the correlation of Modic changes with IVD herniation and severe DDD.

Abundance of mRNAs of cytokines and vascular endothelial growth factor isoforms in IVD tissues

Of all mRNAs of the studied genes, encoding cytokines and vascular endothelial growth factor isoforms, the TNFα, IL17, VEGF121, and VEGF165 expression in the cartilage tissue was significantly elevated ($p < 0.01$) compared to the control group (Fig. 2). Juxtaposing the mRNA expression levels of all genes, studied in the index group patients, with the IVD degeneration Pfirrmann grades revealed a positive correlation between the expression of TNFα and the IVD degeneration grades ($r = 0.301$; $p < 0.05$) (Fig. 3). Despite the fact that the expression of the IL1β mRNA showed no significant differences with the control group, the abundance of this gene in the disc tissue correlated with the disc degeneration severity ($r = 0.37$; $p < 0.05$) (Fig. 4).

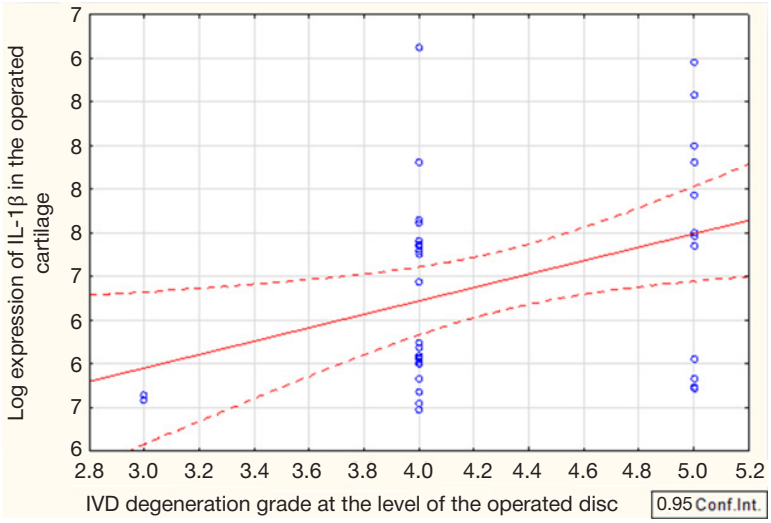

Fig. 4. Correlation between the IL1β mRNA expression levels in the IVD tissues and the Pfirrmann degeneration grades in the index group patients

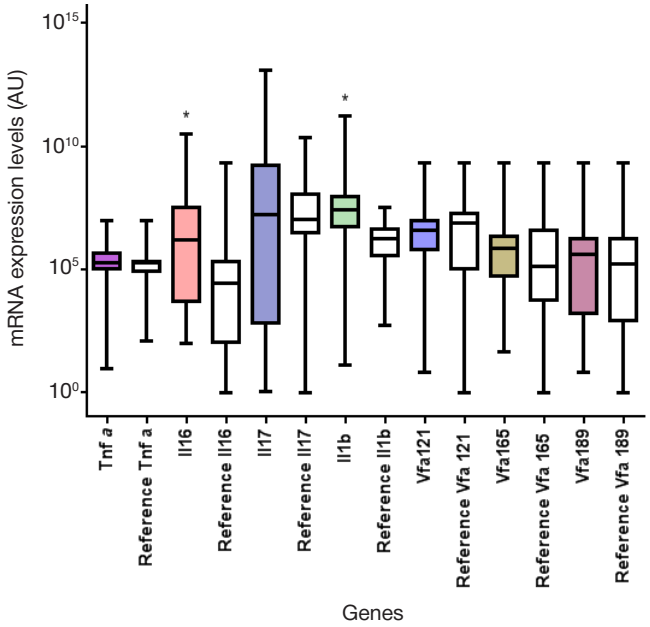

Fig. 5. Expression levels of mRNAs of the studied genes in relation to normalization genes (B2m, GUSB) in the white blood cells of the index group patients and controls ($p < 0.01$)

From the perspective of the IVD matter disorganization progression, it was interesting to assess the cartilage vascularization markers in IVDs with grade 4 or 5 degeneration. The significant negative correlation between the levels of VEGF121 and the IVD degeneration grades ($r = –0.85$; $p < 0.001$) was identified for vascular endothelial growth factors, which could indicate the decreased angiogenesis intensity in the discs of patients with the advanced stage DDD.

Analysis of gene abundance in blood cells

Further analysis was aimed to identify mRNAs of cytokines and growth factors in peripheral white blood cells. Our study revealed the significantly increased abundance of the genes, encoding interleukins IL1β, IL6 ($p < 0.01$) (Fig. 5). Analysis of the relationship between the expression of the IL6 cytokine mRNA in peripheral blood and the IVD degeneration grade showed the dicrease in the cytokine levels in the discs with the advanced IVD Pfirrmann degeneration grades ($r = –0.347$; $p < 0.05$), which was indicative of the cytokine significant contribution to degeneration at earlier stages.

Taking into account the high prevalence of Modic changes in the vertebral bodies (70%) of the index group patients, we assessed the relationship between the cytokine expression levels and the presence of Modic changes. A significant negative correlation between the IL6 levels in blood cells and Modic type 1 and 2 changes was revealed ($r = –0.31$; $p < 0.05$), which was indicative of the elevated cytokine expression at the stage of inflammatory bone marrow edema compared to the stage of fatty transformation within the adjacent vertebral bodies. Individuals with a more severe lesion in their functional spinal units, the triple combination (herniation + erosions of the vertebral body endplates + Modic) ($r = 0.401$; $p < 0.05$), had a higher expression of IL17 in their peripheral blood compared to individuals having herniation only. Regardless of the low abundance of angiogenic biomarkers in blood of patients with BP, we decided to see whether the vascular endothelial growth factor (isoforms 121, 165, 189) expression levels changed depending on the IVD degeneration grades: significant negative correlations were obtained for all three isoforms ($r = –0.44$; –0.33, and –0.45, respectively; $p < 0.05$).

DISCUSSION

Studying the BP pathophysiology in young patients confirmed the involvement of immune and inflammatory mechanisms in disc degeneration. High expression of TNFα and TNFα receptors, especially in the AF tissue, in patients with DDD, was also reported by other authors [17, 18]. This specific cytokine was described in experiments as an apparent inducer of matrix degradation, especially at the early stages, compared to other mediators [19]. The coupled expression of TNFα and IL17, identified during our study, was found in two studies, conducted by Chinese researchers, and confirmed by the effects of etanercept (inhibitor of TNFα receptor), which was capable of quenching the entire inflammatory cascade in the disc NP tissue [20, 21]. Pathogenetic relationships between the immune inflammation and the disc vascularization, observed during our study, were shown in the overseas human and animal studies [22, 23].

Association of the elevated IL6 gene expression in peripheral blood with Modic changes, and specifically with the inflammatory bone marrow edema grade, was also shown within the framework of the study, performed by Chinese researchers: the expression of IL6 was significantly increased in elderly patients with DDD and Modic type 1 changes compared to patients with Modic type 2 changes [24]. The assessment of changes confirmed the fact of the reactive aseptic spondylitis in patients with severe DDD. Detection of the elevated IL17 expression in idividuals with the triple combination of lesions in their functional spinal units suggests the existence of the adverse clinical and instrumental phenotype of BP with the immune marker at the systemic level.

It is known that, in accordance with the Pfirrmann grading system, grade 5 of the IVD degeneration is characterized by the dramatically decreased IVD height, hypointense and nonhomogeneous signal from NP, which corresponds to severe, almost total dehydration of NR together with the extracellular matrix disintegration, replacement of the disc central space with type I collagen, and blurring between NP and AF [25]. When distinguishing between the natural age-related disc degeneration process and the abnormal disc degeneration, we wish to emphasize the key role of inflammatory markers in the second scenario, being particularly evident and manifesting

as severe degeneration in young adults [26]. By the age of 4, blood vessels and capillaries of the disc vanish, and the disc becomes a completely avascular structure [27]. As the "low-immune" inflammation develops in the IVD tissues, neovascularization becomes the way of the immunocompetent cells delivery from the systemic blood flow to the cartilage tissue with subsequent activation of catabolic pathways [28] and resorption of the tissue fragment that has fallen out of AF. The vascular endothelial growth factor A (VEGF) is one of the major regulators of angiogenesis. VEGF plays an important role in physiological and pathological neovascularization [29]. The VEGF expression is promoted by the activity of chondrocytes, which form clusters within the NP. In grade 5 DDD, the disc might no longer have the NP along with the rest of the NP cellular content, which is likely to disrupt the angiogenesis stimulation pathway in this settings. These data are consistent with the study, which has shown that the VEGF angiogenic factor expression levels in IVD samples with mild degenerative changes are significantly higher compared to advanced degeneration grades [12]. Taking into account the low reparative capacity of the disc with grade 5 degenerative changes, the use of therapeutic bioengineering, involving the application of tissue engineering and 3D IVD scaffold fabrication with subsequent cellular therapy, is the most promising.

CONCLUSIONS

The study sheds light on the range of activated genes, which express cytokines, and shows the inflammatory profiles of those in IVD tissues and peripheral blood depending on the DDD severity and the area of the functional spinal unit lesion. The abundance of mRNAs of the studied cytokines and vascular endothelial growth factor isoforms in the IVD tissues (TNFα, IL17, VEGF121, VEGF165) was higher in individuals with BP and DDD. The vascular endothelial growth factor expression levels, reflecting the possible processes of neovascularization, dramatically decreased in patients with the terminal grade DDD, both in the IVD tissues and in peripheral blood. However, the levels of TNFα and IL1β cytokines in the cartilage tissue positively correlated with the severity of the IVD degeneration, which was in line with the concept of immune inflammation, associated with DDD. The IL6 gene expression levels in white blood cells turned out to be increased in patients with Modic changes and were to a greater extent associated with inflammatory bone marrow edema in adjacent vertebral bodies at the level of the compromized segments, and the levels of IL17 turned out to be increased in patients with a combination of herniation, erosions of the adjacent vertebral body endplates, and Modic changes. The findings would help to identify the molecular targets and new directions for the anti-inflammatory and reparative therapy of DDD.

References

1. Zwierzchowska A, Tuz J. Evaluation of the impact of sagittal spinal curvatures on musculoskeletal disorders in young people. Med Pr. 2018; 69 (1): 29–36. DOI: 10.13075/mp.5893.00558.
2. Fujii K, Yamazaki M, Kang JD, Risbud MV, Cho SK, Qureshi SA, et al. Discogenic Back Pain: Literature Review of Definition, Diagnosis, and Treatment JBMR Plus. 2019; 3 (5): e10180. DOI: 10.1002/jbm4.10180.
3. Anitua E, Padilla S. Biologic therapies to enhance intervertebral disc repair. RegenMed. 2018; 13 (1): 55–72. DOI: 10.2217/rme-2017-0111.
4. Hu S, Fu Y, Yan B, Shen Z, Lan T. Analysis of key genes and pathways associated with the pathogenesis of intervertebral disc degeneration. J Orthop Surg Res. 2020; 15 (1): 371. DOI: 10.1186/s13018-020-01902-4.
5. Li Y, Liu J, Liu Z, Duan D. Inflammation in low back pain may be detected from the peripheral blood: suggestions for biomarker. Biosci Rep. 2016; 36 (4): e00361. DOI: 10.1042/BSR20160187.
6. Hodgkinson T, Shen B, Diwan A, Hoyland JA, Richardson SM. Therapeutic potential of growth differentiation factors in the treatment of degenerative disc diseases. Spine. 2019; 2 (1): e1045. DOI: 10.1002/jsp2.1045.
7. Kraychete DC, Sakata RK, Issy AM, Bacellar O, Santos-Jesus R, Carvalho EM. Serum cytokine levels in patients with chronic low back pain due to herniated disc: analytical cross-sectional study. Sao Paulo Med J. 2010; 128 (5): 259–62. DOI: 10.1590/s1516-31802010000500003.
8. Studer RK, Vo N, Sowa G, Ondeck C, Kang J. Human nucleus pulposus cells react to IL6: independent actions and amplification of response to IL1 and TNFα. Spine. 36: 593–9. DOI: 10.1097/BRS.0b013e3181da38d5
9. Gabr MA, Jing L, Helbling AR, Sinclair SM, Allen KD, Shamji MF, et al. Interleukin-17 synergizes with IFNγ or TNFα to promote inflammatory mediator release and intercellular adhesion molecule-1 (ICAM-1) expression in human intervertebral disc cells. J Orthop Res. 2011; 29 (1): 1–7. DOI: 10.1002/jor.21206.
10. Rodrigues LMR, Oliveira LZ, Silva MBRD, Accardo CM, Giglio ABD, Pinhal MADS. Inflammatory biomarkers in sera of patients with intervertebral disc degeneration. Einstein (Sao Paulo). 2019; 17 (4): eAO4637. DOI: 10.31744/einstein_journal/2019AO4637.
11. Baptista JS, Traynelis VC, Liberti EA, Fontes RBV. Expression of degenerative markers in intervertebral discs of young and elderly asymptomatic individuals. PLoS One. 2020; 15 (1): e0228155. DOI: 10.1371/journal.pone.0228155.
12. Capossela S, Bertolo A, Gunasekera K, Pötzel T, Baur M, Stoyanov JV. VEGF vascularization pathway in human intervertebral disc does not change during the disc degeneration process. BMC Res Notes. 2018; 11: 333 DOI: 10.1186/s13104-018-3441-3.
13. Haro H, Kato T, Komori H, Osada M, Shinomiya K. Vascular endothelial growth factor (VEGF)-induced angiogenesis in herniated disc resorption. J Orthop Res. 2002; 20 (3): 409–15. DOI: 10.1016/S0736-0266(01)00150-4
14. Autio RA, Karppinen J, Niinimäki J, Ojala R, Kurunlahti M, Haapea M, et al. Determinants of spontaneous resorption of intervertebral disc herniations. Spine. 2006; 31 (11): 1247–52. DOI: 10.1097/01.brs.0000217681.83524.4a.
15. Longo UG, Loppini M, Denaro L, Maffulli N, Denaro V. Rating scales for low back pain. Br Med Bull. 2010; 94: 81–144. DOI: 10.1093/bmb/ldp052.
16. Farasyn A, Meeusen R. Validity of the new Backache Index (BAI) in patients with low back pain. Spine J. 2006; 6 (5): 565–71. DOI: 10.1016/j.spinee.2006.01.021.
17. Rebrikov DV, Samatov GA, Trofimov DYu. PCR v real'nom vremeni. M.: Laboratorija znanij, 2019; 216s.
18. Andrade P, Visser-Vandewalle V, Philippens M, Daemen MA, Steinbusch HWM, Buurman WA, et al. TNF-alpha levels correlate with postoperative pain severity in lumbar disc hernia patients: opposite clinical effects between TNF receptor 1 and 2. Pain. 2011; 152: 2645–52. DOI: 10.1016/j.pain.2011.08.012.
19. Altun I. Cytokine profile in degenerated painful intervertebral disc: variability with respect to duration of symptoms and type of disease. Spine J. 2016; 16 (7): 857–61. DOI: 10.1016/j.spinee.2016.03.019.
20. Kang R, Li H, Rickers K, Ringgaard S, Xie L, Bünger C. Intervertebral disc degenerative changes after intradiscal injection of TNFα in a porcine model. Eur Spine J. 2015; 24 (9): 2010–6. DOI: 10.1007/s00586-015-3926-x.
21. Wang S, Wei J, Fan Y, Ding H, Tian H, Zhou X, et al. Progranulin Is Positively Associated with Intervertebral Disc Degeneration

by Interaction with IL10 and IL17 Through TNF Pathways. Inflammation. 2018; 41 (5): 1852–63. DOI: 10.1007/s10753-018-0828-1.
22. Wang SS, Zhang W, Zhang YQ, Zhao Y, Liu Y, Li JK, et al. IL17A enhances ADAMTS-7 expression through regulation of TNFα in human nucleus pulposus cells. J Mol Histol. 2015; 46 (6): 475–83. DOI: 10.1007/s10735-015-9640-5.
23. Ohba T, Haro H, Ando T, Wako M, Suenaga F, Aso Y, et al. TNF-alpha-induced NF-kappaB signaling reverses age-related declines in VEGF induction and angiogenic activity in intervertebral disc tissues. J Orthop Res. 2009; 27 (2): 229–35. DOI: 10.1002/jor.20727.
24. Binch AL, Cole AA, Breakwell LM, Michael AL, Chiverton N, Cross AK, et al. Expression and regulation of neurotrophic and angiogenic factors during human intervertebral disc degeneration. Arthritis Res Ther. 2014; 16 (5): 416. DOI: 10.1186/s13075-014-0416-1.
25. Zhang JF, Wang GL, Zhou ZJ, Fang XQ, Chen S, Fan SW. Expression of Matrix Metalloproteinases, Tissue Inhibitors of Metalloproteinases, and Interleukins in Vertebral Cartilage Endplate. Orthop Surg. 2018; 10 (4): 306–11. DOI: 10.1111/os.12409.
26. Oh CH, Yoon SH. Whole Spine Disc Degeneration Survey according to the Ages and Sex Using Pfirrmann Disc Degeneration Grades. Korean J Spine. 2017; 14 (4): 148–54. DOI: 10.14245/kjs.2017.14.4.148.
27. Akyol S, Eraslan BS, Etyemez H, Tanriverdi T, Hanci M. Catabolic cytokine expressions in patients with degenerative disc disease. Turk Neurosurg. 2010; 20 (4): 492–9. DOI: 10.5137/1019-5149.JTN.3394-10.1.
28. Takeno K, Kobayashi S, Negoro K, Uchida K, Miyazaki T, Yayama T, et al. Physical limitations to tissue engineering of intervertebral disc cells: effect of extracellular osmotic change on glycosaminoglycan production and cell metabolism. Laboratory investigation. J Neurosurg Spine. 2007; 7 (6): 637–44. DOI: 10.3171/SPI-07/12/637.
29. Chung SA, Khan SN, Diwan AD. The molecular basis of intervertebral disk degeneration. Orthop Clin North Am. 2003; 34 (2): 209–19. DOI: 10.1016/s0030-5898(03)00026-9.

Литература

1. Zwierzchowska A, Tuz J. Evaluation of the impact of sagittal spinal curvatures on musculoskeletal disorders in young people. Med Pr. 2018; 69 (1): 29–36. DOI: 10.13075/mp.5893.00558.
2. Fujii K, Yamazaki M, Kang JD, Risbud MV, Cho SK, Qureshi SA, et al. Discogenic Back Pain: Literature Review of Definition, Diagnosis, and Treatment JBMR Plus. 2019; 3 (5): e10180. DOI: 10.1002/jbm4.10180.
3. Anitua E, Padilla S. Biologic therapies to enhance intervertebral disc repair. RegenMed. 2018; 13 (1): 55–72. DOI: 10.2217/rme-2017-0111.
4. Hu S, Fu Y, Yan B, Shen Z, Lan T. Analysis of key genes and pathways associated with the pathogenesis of intervertebral disc degeneration. J Orthop Surg Res. 2020; 15 (1): 371. DOI: 10.1186/s13018-020-01902-4.
5. Li Y, Liu J, Liu Z, Duan D. Inflammation in low back pain may be detected from the peripheral blood: suggestions for biomarker. Biosci Rep. 2016; 36 (4): e00361. DOI: 10.1042/BSR20160187.
6. Hodgkinson T, Shen B, Diwan A, Hoyland JA, Richardson SM. Therapeutic potential of growth differentiation factors in the treatment of degenerative disc diseases. Spine. 2019; 2 (1): e1045. DOI: 10.1002/jsp2.1045.
7. Kraychete DC, Sakata RK, Issy AM, Bacellar O, Santos-Jesus R, Carvalho EM. Serum cytokine levels in patients with chronic low back pain due to herniated disc: analytical cross-sectional study. Sao Paulo Med J. 2010; 128 (5): 259–62. DOI: 10.1590/s1516-31802010000500003.
8. Studer RK, Vo N, Sowa G, Ondeck C, Kang J. Human nucleus pulposus cells react to IL6: independent actions and amplification of response to IL1 and TNFα. Spine. 36: 593–9. DOI: 10.1097/BRS.0b013e3181da38d5
9. Gabr MA, Jing L, Helbling AR, Sinclair SM, Allen KD, Shamji MF, et al. Interleukin-17 synergizes with IFNγ or TNFα to promote inflammatory mediator release and intercellular adhesion molecule-1 (ICAM-1) expression in human intervertebral disc cells. J Orthop Res. 2011; 29 (1): 1–7. DOI: 10.1002/jor.21206.
10. Rodrigues LMR, Oliveira LZ, Silva MBRD, Accardo CM, Giglio ABD, Pinhal MADS. Inflammatory biomarkers in sera of patients with intervertebral disc degeneration. Einstein (Sao Paulo). 2019; 17 (4): eAO4637. DOI: 10.31744/einstein_journal/2019AO4637.
11. Baptista JS, Traynelis VC, Liberti EA, Fontes RBV. Expression of degenerative markers in intervertebral discs of young and elderly asymptomatic individuals. PLoS One. 2020; 15 (1): e0228155. DOI: 10.1371/journal.pone.0228155.
12. Capossela S, Bertolo A, Gunasekera K, Pötzel T, Baur M, Stoyanov JV. VEGF vascularization pathway in human intervertebral disc does not change during the disc degeneration process. BMC Res Notes. 2018; 11: 333 DOI: 10.1186/s13104-018-3441-3.
13. Haro H, Kato T, Komori H, Osada M, Shinomiya K. Vascular endothelial growth factor (VEGF)-induced angiogenesis in herniated disc resorption. J Orthop Res. 2002; 20 (3): 409–15. DOI: 10.1016/S0736-0266(01)00150-4
14. Autio RA, Karppinen J, Niinimäki J, Ojala R, Kurunlahti M, Haapea M, et al. Determinants of spontaneous resorption of intervertebral disc herniations. Spine. 2006; 31 (11): 1247–52. DOI: 10.1097/01.brs.0000217681.83524.4a.
15. Longo UG, Loppini M, Denaro L, Maffulli N, Denaro V. Rating scales for low back pain. Br Med Bull. 2010; 94: 81–144. DOI: 10.1093/bmb/ldp052.
16. Farasyn A, Meeusen R. Validity of the new Backache Index (BAI) in patients with low back pain. Spine J. 2006; 6 (5): 565–71. DOI: 10.1016/j.spinee.2006.01.021.
17. Ребриков Д. В., Саматов Г. А., Трофимов Д. Ю. ПЦР в реальном времени. М.: Лаборатория знаний, 2019; 216 с.
18. Andrade P, Visser-Vandewalle V, Philippens M, Daemen MA, Steinbusch HWM, Buurman WA, et al. TNF-alpha levels correlate with postoperative pain severity in lumbar disc hernia patients: opposite clinical effects between TNF receptor 1 and 2. Pain. 2011; 152: 2645–52. DOI: 10.1016/j.pain.2011.08.012.
19. Altun I. Cytokine profile in degenerated painful intervertebral disc: variability with respect to duration of symptoms and type of disease. Spine J. 2016; 16 (7): 857–61. DOI: 10.1016/j.spinee.2016.03.019.
20. Kang R, Li H, Rickers K, Ringgaard S, Xie L, Bünger C. Intervertebral disc degenerative changes after intradiscal injection of TNFα in a porcine model. Eur Spine J. 2015; 24 (9): 2010–6. DOI: 10.1007/s00586-015-3926-x.
21. Wang S, Wei J, Fan Y, Ding H, Tian H, Zhou X, et al. Progranulin Is Positively Associated with Intervertebral Disc Degeneration by Interaction with IL10 and IL17 Through TNF Pathways. Inflammation. 2018; 41 (5): 1852–63. DOI: 10.1007/s10753-018-0828-1.
22. Wang SS, Zhang W, Zhang YQ, Zhao Y, Liu Y, Li JK, et al. IL17A enhances ADAMTS-7 expression through regulation of TNFα in human nucleus pulposus cells. J Mol Histol. 2015; 46 (6): 475–83. DOI: 10.1007/s10735-015-9640-5.
23. Ohba T, Haro H, Ando T, Wako M, Suenaga F, Aso Y, et al. TNF-alpha-induced NF-kappaB signaling reverses age-related declines in VEGF induction and angiogenic activity in intervertebral disc tissues. J Orthop Res. 2009; 27 (2): 229–35. DOI: 10.1002/jor.20727.
24. Binch AL, Cole AA, Breakwell LM, Michael AL, Chiverton N, Cross AK, et al. Expression and regulation of neurotrophic and angiogenic factors during human intervertebral disc degeneration. Arthritis Res Ther. 2014; 16 (5): 416. DOI: 10.1186/s13075-014-0416-1.
25. Zhang JF, Wang GL, Zhou ZJ, Fang XQ, Chen S, Fan SW. Expression of Matrix Metalloproteinases, Tissue Inhibitors of Metalloproteinases, and Interleukins in Vertebral Cartilage

Endplate. Orthop Surg. 2018; 10 (4): 306–11. DOI: 10.1111/os.12409.
26. Oh CH, Yoon SH. Whole Spine Disc Degeneration Survey according to the Ages and Sex Using Pfirrmann Disc Degeneration Grades. Korean J Spine. 2017; 14 (4): 148–54. DOI: 10.14245/kjs.2017.14.4.148.
27. Akyol S, Eraslan BS, Etyemez H, Tanriverdi T, Hanci M. Catabolic cytokine expressions in patients with degenerative disc disease. Turk Neurosurg. 2010; 20 (4): 492–9. DOI: 10.5137/1019-5149.JTN.3394-10.1.
28. Takeno K, Kobayashi S, Negoro K, Uchida K, Miyazaki T, Yayama T, et al. Physical limitations to tissue engineering of intervertebral disc cells: effect of extracellular osmotic change on glycosaminoglycan production and cell metabolism. Laboratory investigation. J Neurosurg Spine. 2007; 7 (6): 637–44. DOI: 10.3171/SPI-07/12/637.
29. Chung SA, Khan SN, Diwan AD. The molecular basis of intervertebral disk degeneration. Orthop Clin North Am. 2003; 34 (2): 209–19. DOI: 10.1016/s0030-5898(03)00026-9.

LONG-TERM EFFECTS OF MULTIMODALITY LASER THERAPY IN PATIENT WITH DRUSENOID PIGMENT EPITHELIAL DETACHMENT

Takhchidi KhP, Takhchidi NKh, Kasmynina TA, Mahno NA ✉

Pirogov Russian National Research Medical University, Moscow, Russia

Drusenoid pigment epithelial detachment is a condition characterized by separation of the retinal pigment epithelium from the underlying Bruch's membrane due to formation of drusenoid deposits. The disorder represents the intermediate stage of the age-related macular degeneration, and is a risk factor for the age-related macular degeneration progression to late stage characterized by geographic atrophy, which results in the irreversible central vision loss. Management of patients with this disorder is in most cases limited to follow-up. The feasibility of using the multimodality low power mode laser therapy for treatment of drusenoid pigment epithelial detachment is reported. The results of laser photocoagulation of the retina demonstrate the morphological and functional recovery: retinal pigment epithelial detachment sealing, improvement of visual function, and restored retinal architecture.

Keywords: age-elated macular degeneration, drusenoid pigment epithelial detachment, retina, micropulse laser

Author contribution: Takhchidi KhP — study concept and design, manuscript editing; Takhchidi NKh — literature analysis; Kasmynina TA — laser therapy; Mahno NA — data acquisition and processing, manuscript writing.

Compliance with ethical standards: the patients submitted the informed consent to laser therapy and personal data processing.

✉ **Correspondence should be addressed:** Nadezhda A. Mahno
Volokolamskoe shosse, 30, korp. 2, Moscow, 123182, Russia; nadezda.mahno7@gmail.com

Received: 24.11.2021 **Accepted:** 16.12.2021 **Published online:** 29.12.2021

DOI: 10.24075/brsmu.2021.067

ОТДАЛЕННЫЕ РЕЗУЛЬТАТЫ ПРИМЕНЕНИЯ КОМБИНИРОВАННОГО ЛАЗЕРНОГО ЛЕЧЕНИЯ ДРУЗЕНОИДНОЙ ОТСЛОЙКИ РЕТИНАЛЬНОГО ПИГМЕНТНОГО ЭПИТЕЛИЯ

Х. П. Тахчиди, Н. Х. Тахчиди, Т. А. Касмынина, Н. А. Махно ✉

Российский национальный исследовательский медицинский университет имени Н. И. Пирогова, Москва, Россия

Друзеноидная отслойка ретинального пигментного эпителия — патологическое состояние, при котором ретинальный пигментный эпителий отделяется от подлежащей мембраны Бруха вследствие образования и накопления друзеноидного материала. Заболевание представляет собой промежуточную стадию возрастной макулярной дегенерации, является фактором риска прогрессирования возрастной макулярной дегенерации до поздней стадии с развитием географической атрофии, что приводит к необратимой потере центрального зрения. В основном ведение пациентов с данной патологией сводится к динамическому наблюдению. Представлена возможность использования комбинированного лазерного лечения с низкоэнергетическими параметрами при лечении друзеноидной отслойки ретинального пигментного эпителия сетчатки. Полученные результаты применения лазерной коагуляции сетчатки свидетельствуют о восстановлении морфофункциональных показателей: ликвидации отслойки ретинального пигментного эпителия, повышении зрительных функций и восстановлении микроархитектоники сетчатки.

Ключевые слова: возрастная макулярная дегенерация, друзеноидная отслойка ретинального пигментного эпителия, сетчатка, микроимпульсное лазерное воздействие

Вклад авторов: Х. П. Тахчиди — концепция и дизайн исследования, редактирование текста; Н. Х. Тахчиди — анализ литературных данных; Т. А. Касмынина — лазерное лечение пациента; Н. А. Махно — сбор и обработка материала, написание текста.

Соблюдение этических стандартов: от пациента получено добровольное информированное согласие на лазерное лечение и обработку персональных данных.

✉ **Для корреспонденции:** Надежда Александровна Махно
Волоколамское шоссе, д. 30, корпус 2, г. Москва, 123182, Россия; nadezda.mahno7@gmail.com

Статья получена: 24.11.2021 **Статья принята к печати:** 16.12.2021 **Опубликована онлайн:** 29.12.2021

DOI: 10.24075/vrgmu.2021.067

Currently, age-related macular degeneration (AMD) is among the leading causes of the irreversible central vision loss, occurring predominantly in the elderly. According to literature, the prevalence of AMD among individuals aged 45–85 is 8.96%, with a predominance of the early stages of the disease (8.01%) [1].

In accordance with the generally accepted classification of the Age-Related Eye Disease Study (AREDS), AMD is subdivided into four categories. The AREDS Category 1 (no AMD) is characterized by no drusen or small drusen of less than 63 μm in diameter. The AREDS Category 2 (early stage AMD) corresponds to numerous small drusen, and/or a small number of medium-sized drusen of 63–124 μm in diameter, or initial changes in the retinal pigment epithelium (RPE). The AREDS Category 3 (intermediate stage AMD) is characterized by numerous medium-sized drusen, and/or one large druse of more than 125 μm in diameter, or RPE atrophy, not affecting the retinal center. The AREDS Category 4 (late stage AMD) is characterized by atrophy of RPE and choriocapillaris layer in the retinal center, and/or neovascular maculopathy [2].

Drusenoid pigment epithelial detachment (DPED), in which RPE and its basement membrane are separated from the inner collagen layer of the underlying Bruch's membrane due to formation and accumulation of drusenoid material, represents the intermediate stage of AMD. This form of PED was originally described by A. G. Casswell in 1985 [3, 4].

To date, pathophysiological mechanisms of DPED have not been fully explored. It is believed that this disorder results from the gradual increase and merging of the large number of pre-existing soft drusen, which results in the focal retinal detachment of at least 350 μm in diameter. With increasing DPED, the prolonged dissociation between the RPE cells and the Bruch's membrane/choriocapillaris complex leads on the one hand to the RPE cells' migration into the outer retinal layer,

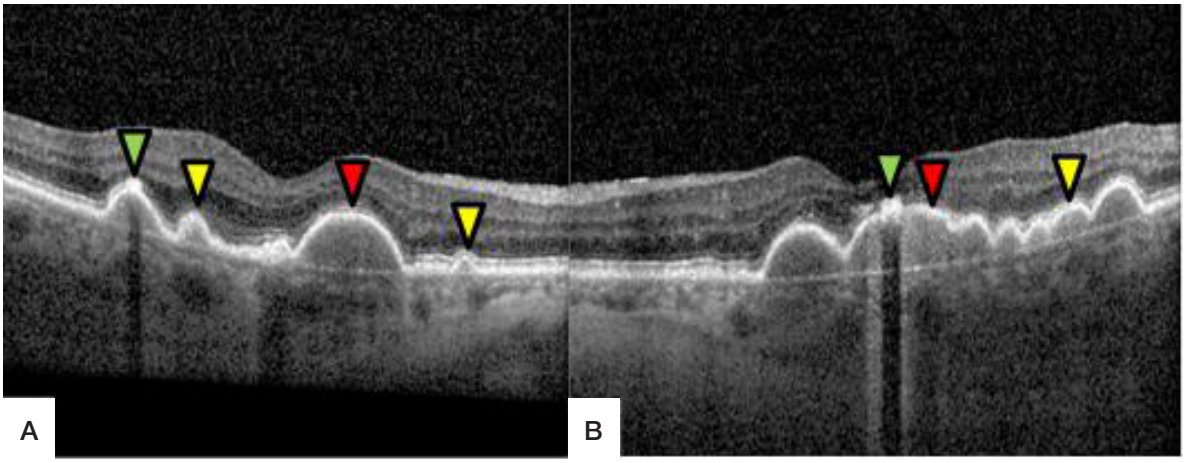

Fig. 1. Spectral-domain optical coherence tomography image of the fovea. **A**. Right eye: RPE detachment (*red arrow*) with the height of 166 μm and the length of 1126 μm, with homogeneously hyperreflective deposits. Coalescent soft drusen (*yellow arrow*), accumulation of subretinal hyperreflective deposits (*green arrow*). **B**. Left eye: RPE detachment (red arrow) with the height of 173 μm and the length of 2348 μm, with homogeneously hyperreflective deposits. Coalescent soft drusen (*yellow arrow*), accumulation of subretinal hyperreflective deposits (*green arrow*)

and on the other hand to these cells' apoptosis. The long-lasting DPED, associated with the decreased number and alteration of RPE cells, results in photoreceptor dysfunction and subsequent atrophy. Eventually, in case of DPED collapse, the zone of complete RPE atrophy is registered, with the outer neurosensory retina atrophy [5, 6].

In case of the long-lasting DPED with its subsequent regression, the most common symptoms are as follows: decreased visual acuity, metamorphopsia, difficulty or inability to read up close. However, RPE detachment, identified at an early stage, is characterized by preserved visual functions [5–8].

The use of the spectral-domain optical coherence tomography (SD-OCT) in morphometric assessment of the retinal layer changes in patients with DPED made it possible to distinguish the risk factors for the disease progression, such as height, volume, and diameter of the detached RPE, as well as the presence of intraretinal and subretinal hyperreflective material above the RPE detachment. These risks were studied with regard to DPED located within 500 μm of the fovea [6, 7].

Currently, there are no efficient and safe treatment methods for DPED. If this disorder is diagnosed, the management of patients is in most cases limited to follow-up. However, progression to late AMD is observed in the natural course of the disease within 5 years (42% of cases), with the development of geographic atrophy in the macular zone (19% of cases), which results in irreversible vision loss, as well as in declined quality of life, disability, and poor work ability prognosis [3, 7, 8].

Conservative treatment, which involves the use of antioxidant medications, vitamins and minerals, fails to prevent the AMD progression to advanced stages, which was confirmed by research, and requires the constant use of these medications throughout the patient's life [9].

The majority of studies on assessing the efficacy and safety of using laser technologies in patients with intermediate AMD were focused mostly on finding ways to slow down the disease progression and to reduce the number of various soft drusen types [10–15].

With regard to the high risk of DPED progression to late AMD, with subsequent significant decline in the patients' visual functions, finding the efficient and safe treatment method for this disorder is relevant. The study was aimed to demonstrate and assess the long-term morphological and functional effects of multimodality laser therapy in a patient with DPED, observed during the 5-year follow-up period.

Clinical case

In June 2017, patient Sh. aged 74 presented with complaints of diminished visual acuity in both eyes, metamorphopsia, and trouble with close-up reading using both eyes at the Research Center of Ophthalmology, Pirogov Russian National Research Medical University. According to medical history, the above symptoms have been troubling the patient for a year. In 2015, cataract surgery, phacoemulsification and intraocular lens implantation, was performed in the right and left eye.

Once admitted to the Center, the patient underwent a comprehensive ophthalmic examination, which included the standard diagnostic tests (visometry for uncorrected visual acuity (UCVA) and best corrected visual acuity (BCVA), indirect ophthalmoscopy with a MaxField indirect lens (Ocular Inc.; USA)), specific assessment methods (microperimetry (MAIA microperimeter, CenterVue Inc.; Italy), SD-OCT, and optical coherence tomography angiography (OCTA) performed using a Spectralis HRA+OCT, OCT-2 module at 85,000 Hz (Heidelberg Engineering, Inc.; Germany)).

Laser photocoagulation was performed with the IRIDEX IQ 577 ophthalmic laser system (IRIDEX Corporation, MountainView; USA).

During the initial assessment the patient complained of diminished visual acuity in both eyes, metamorphopsia, and trouble with close-up reading using both eyes; UCVA of the right eye (OD) was 0.3; BCVA was 0.7 OD, and those of the left eye (OS) were 0.2 and 0.7, respectively. According to micropirometry, the average central retinal sensitivity was 23.3 dB OD and 21.6 dB OS.

Slit lamp biomicroscopy and indirect ophthalmoscopy in both eyes (OU) showed that the anterior segment was intact; the well-centered intraocular lens was in the capsular bag. The optic disc was pale pink, with well-defined margins. Hypertensive angiopathy was revealed. There were numerous prominent small yellowish round-shaped lesions with well-defined margins in the macular zone. In the foveal zone, expanding downwards into the parafoveal region, the there was a large prominent pale-yellow oval-shaped lesion 1.5 times the diameter of the optic disc with blurry margins and redistribution of pigment, surrounded by large yellowish lesions with blurry margins. Retinal periphery was intact.

SD-OCT OD revealed macular deformation. In the foveal zone, the RPE detachment was visible with the height of 166 μm and the length of 1126 μm, with downward expansion into

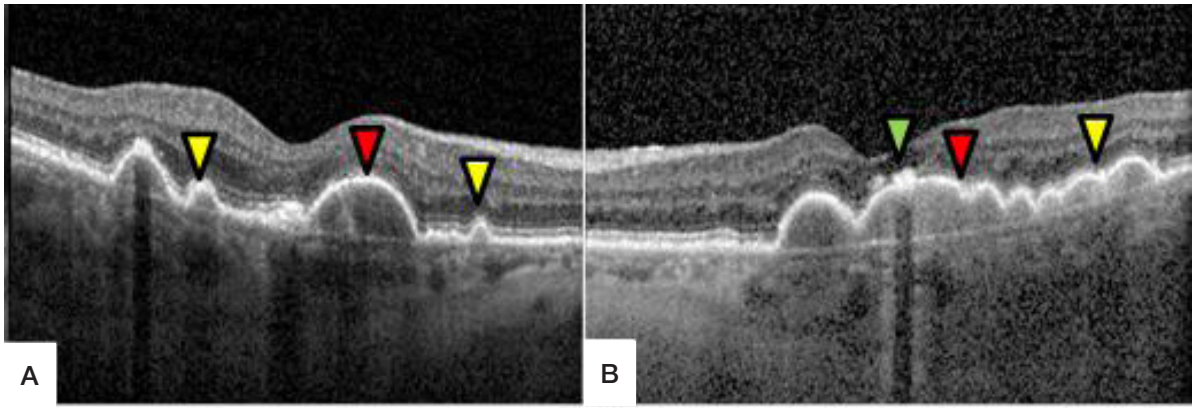

Fig. 2. Spectral-domain optical coherence tomography image of the fovea. **A**. Right eye: RPE detachment (*red arrow*) with the height of 164 μm and the length of 1081 μm, with homogeneously hyperreflective deposits. Coalescent soft drusen (*yellow arrow*), accumulation of subretinal hyperreflective deposits (*green arrow*). **B**. Left eye: RPE detachment with the height of 154 μm and the length of 2286 μm, with homogeneously hyperreflective deposits. Coalescent soft drusen (*yellow arrow*), accumulation of subretinal hyperreflective deposits (*green arrow*)

the parafoveal region with the height of 218 μm and the length of 1852 μm, with homogeneously hyperreflective deposits, together with the undulating RPE line, and the coalescent soft drusen up to 125 μm in diameter. Subretinal hyperreflective deposits were found above the detached RPE (Fig. 1A).

SD-OCT OS revealed macular deformation. In the foveal zone, the RPE detachment was visible with the height of 173 μm and the length of 2348 μm, with downward expansion into the parafoveal region with the height of 190 μm and the length of 1039 μm, with homogeneously hyperreflective deposits, together with the undulating RPE line, and the coalescent soft drusen up to 125 μm in diameter. Subretinal hyperreflective deposits were found above the detached RPE (Fig . 1B).

OCTA image (OU) analysis revealed no evidence supporting the choroidal neovascularization.

The following diagnosis was established based on the patient's complaints, medical history, and the results of the comprehensive ophthalmic examination: OU Age-related macular degeneration, dry form, intermediate stage (according to AREDS classification). Drusenoid pigment epithelial detachment. Pseudophakia.

It was decided to perform the multimodality laser therapy, which included grid laser photocoagulation with the lowest possible energy settings to form the first degree coagulum. After 10 days the patient received three sessions of micropulse laser therapy (every four weeks). Grid laser photocoagulation was performed using the following settings: wavelength 577 nm, power 50 mW, pulse duration 0.1 s, spot size 100 μm; coagula were applied throughout the area of the detached RPE, except avascular zone, with a spacing of 150 μm. Micropulse laser therapy was performed with the following settings: wavelength 577 nm, burst duration 30 ms, micropulse duration 50 μs, pulse ratio 4.7%, spot size 100 μm, power 50 mW; coagula were applied throughout the area of the detached RPE, the avascular zone was avoided.

One month after the multimodality laser therapy the patient reported the improvement of visual acuity, however, metamorphopsia persisted.

Ophthalmic examination showed that UCVA OD was 0.3, BCVA OD had improved to 0.8, UCVA OS had improved to 0.3, and BCVA OS was 0.7. According to micropirometry, the average central retinal sensitivity had improved to 24.1 dB OD, and to 23.0 dB OS. Slit lamp biomicroscopy and indirect ophthalmoscopy OU revealed no improvement: in the foveal zone, expanding downwards into the parafoveal region, there was still a large prominent pale-yellow oval-shaped lesion 1.5 times the diameter of the optic disc with blurry margins and redistribution of pigment, surrounded by the large yellowish lesions with blurry margins; the lightly pigmented coagula were visible across the surface of the detached RPE.

According to SD-OCT OD, the macular deformation persisted, and the RPE detachment reduction was observed. In the foveal zone, the height of the RPE detachment reduced from 166 to 164 μm, and the RPE detachment length reduced from 1126 to 1081 μm. In the lower parafoveal region the height reduced from 218 to 211 μm, and the RPE detachment length reduced from 1852 to 1826 μm. The homogeneously hyperreflective deposits, together with the undulating RPE line, and the coalescent soft drusen up to 125 μm in diameter were found below the detached RPE. Subretinal hyperreflective deposits were found above the detached RPE (Fig. 2A).

According to SD-OCT OS, the macular deformation persisted, and the RPE detachment reduction was observed. In the foveal zone, the height of the RPE detachment reduced from 173 to 154 μm, and the RPE detachment length reduced from 2348 to 2286 μm. In the lower parafoveal region the height reduced from 190 to 171 μm, and the RPE detachment length reduced from 1039 to 982 μm. The homogeneously hyperreflective deposits, together with the undulating RPE line, and the coalescent soft drusen up to 125 μm in diameter were found below the detached RPE. Subretinal hyperreflective deposits were found above the detached RPE (Fig. 2B).

Three months after the laser treatment on the follow-up examination the patient reported the improvement of visual acuity, no metamorphopsia, and no trouble with the close-up reading. Ophthalmic examination showed that UCVA OD and OS was stable (0.3); BCVA OD and OS was 0.8. The average central retinal sensitivity was stable (24.1 dB OD, 23.4 dB OS). Slit lamp biomicroscopy and indirect ophthalmoscopy OU revealed the following features: small yellowish round-shaped lesions with well-defined margins in the macular zone, sporadic large yellowish lesions with blurry margins, redistribution of pigment; the lightly pigmented coagula were visible, the DPED was completely regressed.

SD-OCT OD and OS revealed the restored macula, the completely regressed DPED, undulating RPE line, sporadic soft drusen, and accumulation of subretinal hyperreflective deposits (Fig. 3A, B).

A year after the multimodality laser therapy the patient had no complaints. Ophthalmic examination showed that UCVA OD and OS was 0.3, BCVA OD had reached 0.9, and BCVA OS was stable (0.8). According to micropirometry, the average central retinal sensitivity OD improved to 25.7 dB, and the average central retinal sensitivity OS was stable (23.9 dB). Slit

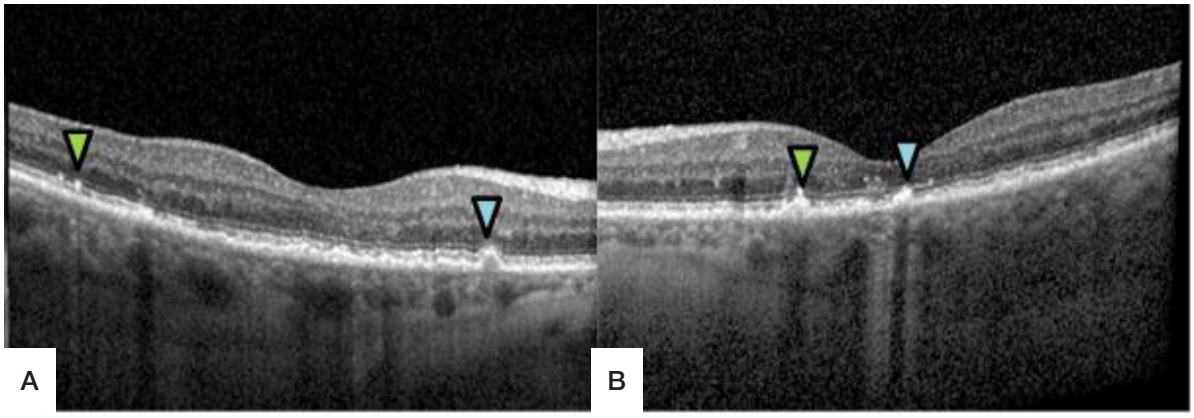

Fig. 3. Spectral-domain optical coherence tomography image of the fovea. **A**. Right eye: macula remains intact, undulating RPE line, sporadic hard drusen (*blue arrow*), accumulation of subretinal hyperreflective deposits (*green arrow*). **B**. Left eye: macula remains intact, undulating RPE line, sporadic hard drusen (*blue arrow*), accumulation of subretinal hyperreflective deposits (*green arrow*)

lamp biomicroscopy and indirect ophthalmoscopy OU revealed small yellowish round-shaped lesions with well-defined margins and redistribution of pigment in the macular zone, the lightly pigmented coagula were visible.

SD-OCT OD and OS revealed the intact macula, the integrity of retinal layers, and no evidence supporting the atrophy of the retinal outer layer and RPE.

Ophthalmic examination performed three years later showed that UCVA OD had improved to 0.4, UCVA OS had improved to 0.3, and BCVA was stable (0.9 OD, 0.8 OS, respectively). The average central retinal sensitivity OD was stable (25.7 dB), and the average central retinal sensitivity OS had improved to 24.0 dB. Slit lamp biomicroscopy and indirect ophthalmoscopy OU revealed small yellowish round-shaped lesions with well-defined margins, redistribution of pigment, and the lightly pigmented coagula in the macular zone.

SD-OCT OD and OS revealed the intact macula, the integrity of retinal layers, and no atrophy of the retinal outer layer and RPE.

Five years after the multimodality laser treatment the follow-up examination revealed stable morphological and functional effects, the patient had no complaints. Ophthalmic examination showed that UCVA OD was 0.4, UCVA OS was 0.3, BCVA OD was 0.9, and BCVA OS was 0.8. According to micropirometry, the average central retinal sensitivity OD was 24.8 dB, and the average central retinal sensitivity OS was 24.3 dB. Slit lamp biomicroscopy and indirect ophthalmoscopy OU small yellowish round-shaped lesions with well-defined margins, redistribution of pigment, and the lightly pigmented coagula in the macular zone.

SD-OCT OD and OS revealed the intact macula, the integrity of retinal layers, and no atrophy of the retinal outer layer and RPE (Fig 4A, B).

OCTA image (OU) analysis revealed no evidence supporting the choroidal neovascularization.

Clinical case discussion

Currently, there is no generally accepted treatment strategy for drusenoid pigment epithelial detachment. Literature analysis has shown that the disorder is the risk factor for AMD progression to late stage characterized by geographic atrophy, which results in the irreversible central vision loss.

A number of authors reported the cases of using photodynamic therapy with verteporfin [16], intravitreal injections of angiogenesis inhibitors [17], high-dose statin therapy [18] for treatment of DPED. These methods contributed to the reduction and regression of RPE detachment throughout the one-year follow-up period. However, the long-term efficacy and safety of the methods had not been explored.

The clinical trials on using the laser technologies in patients with the intermediate stage AMD were focused on assessing the feasibility of reducing the number of drusen and slowing the progression of the disease; in the majority of cases the follow-up period was three years. According to a number of authors, encouraging results in the form of the reduced drusen volume were achieved when using laser photocoagulation. However, side effects can develop when using the high energy laser treatment, such as photoreceptor layer death, formation of central and paracentral scotomas, progression to geographic atrophy, choroidal neovascularization, and subretinal fibrosis [10, 11]. Low power mode laser therapy was used in the reported case in order to prevent the listed above complications and provide a positive clinical impact.

Currently, a number of subthreshold laser therapy methods are used allowing one to selectively and precisely affect the RPE

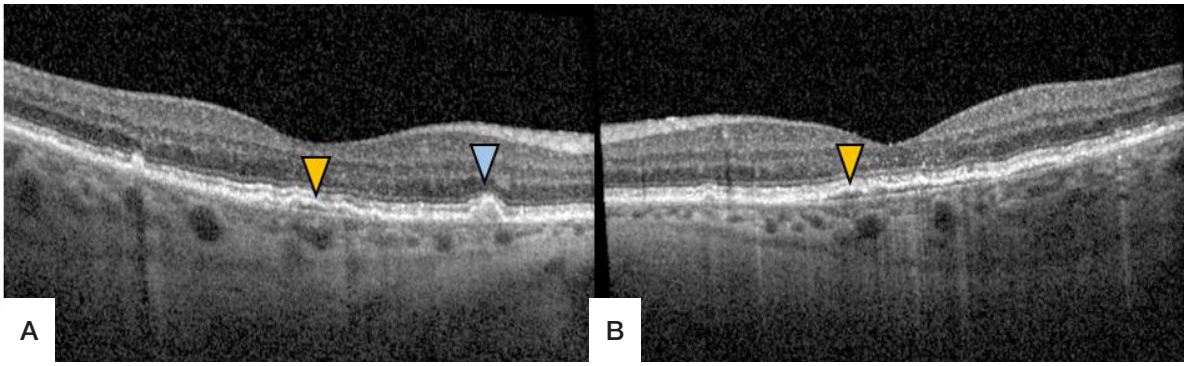

Fig. 4. Spectral-domain optical coherence tomography image of the fovea. **A**. Right eye: macula remains intact, undulating RPE line (*orange arrow*), sporadic hard drusen (*blue arrow*). **B**. Left eye: macula remains intact, undulating RPE line (*orange arrow*)

cells only and thus reduce the risk of adverse alterations in the retina and choriocapillaries. The use of these laser therapy methods in patients with the intermediate stage disorder reduced the number of drusen, contributed to drusen resorption and visual acuity improvement, but did not seem to have much effect in terms of slowing the disease progression to geographic atrophy or choroidal neovascularization. According to the LEAD study, no correlations between the use of laser technologies and the complications, such as retinal hemorrhages, nascent geographic atrophy, and photoreceptor layer atrophy, were revealed [12, 13].

We used a combination of two laser procedures with different mechanisms of action in order to improve the morphological and functional treatment outcome in patients with DPED. The first step was grid laser photocoagulation aimed at activating the RPE pumping function, as well as at improving the retinal architecture and enhancing the structural support provided by Muller cells through the chorioretinal adhesion creation. The use of micropulse laser therapy allowed us to selectively target the RPE cells avoiding damage to the retinal neuroepithelium. The production of factors, maintaining and enhancing regeneration, prolonging the processes of the retinal architecture restoration and visual function improvement, was considered the main therapeutic effect.

Thus, the use of the proposed multimodality laser treatment for DPED made it possible not only to achieve good morphological and functional results, but also to maintain this level throughout the 5-year period.

CONCLUSION

The proposed multimodality laser treatment method allowed us to repair the pigment epithelial detachment (DPED), restore the retinal architecture, and improve the visual functions. The results achieved showed the potential of low-level laser microsurgery for restoring the macular morphological and functional parameters in the presence of the age-related dystrophic process. With further study, this technology may increase the potential for treatment of the intermediate age-related macular degeneration (DPED).

References

1. Wong WL, Su X, Li X, Cheung CM, Klein R, Cheng CY, Wong TY. Global prevalence of age-related macular degeneration and disease burden projection for 2020 and 2040: a systematic review and meta-analysis. Lancet Glob Health. 2014; 2 (2): 106–16.
2. Ferris FL, Wilkinson CP, Bird A, Chakravarthy U, Chew E, Csaky K, Sadda SR; Beckman Initiative for Macular Research Classification Committee. Clinical classification of age-related macular degeneration. Ophthalmology. 2013; 120 (4): 844–51.
3. Casswell AG, Kohen D, Bird AC. Retinal pigment epithelial detachments in the elderly: classification and outcome. British Journal of Ophthalmology. 1985; 69: 397–403.
4. Spaide RF, Jaffe GJ, Sarraf D, Freund KB, Sadda SR, Staurenghi G, Waheed NK; Consensus Nomenclature for Reporting Neovascular Age-Related Macular Degeneration Data: Consensus on Neovascular Age-Related Macular Degeneration Nomenclature Study Group. Ophthalmology. 2020; 127 (5): 616–36.
5. Sarks JP, Sarks SH, Killingsworth MC. Evolution of soft drusen in age-related macular degeneration. Eye (Lond). 1994; 8: 269–83.
6. Balaratnasingam C, Yannuzzi LA, Curcio CA, Morgan WH, Querques G, Capuano V, et al. Associations Between Retinal Pigment Epithelium and Drusen Volume Changes During the Lifecycle of Large Drusenoid Pigment Epithelial Detachments. Invest Ophthalmol Vis Sci. 2016; 57 (13): 5479–89.
7. Yu JJ, Agrón E, Clemons TE, Domalpally A, van Asten F, Keenan TD, et al. Age-Related Eye Disease Study 2 Research Group. Natural History of Drusenoid Pigment Epithelial Detachment Associated with Age-Related Macular Degeneration: Age-Related Eye Disease Study 2 Report No. 17. Ophthalmology. 2019; 126 (2): 261–73.
8. Roquet W, Roudot-Thoraval F, Coscas G, Soubrane G. Clinical features of drusenoid pigment epithelial detachment in age related macular degeneration. Br J Ophthalmol. 2004; 88 (5): 638–42.
9. Chew EY, Clemons TE, Agrón E, Sperduto RD, Sangiovanni JP, Kurinij N, et al. Age-Related Eye Disease Study Research Group. Long-term effects of vitamins C and E, β-carotene, and zinc on age-related macular degeneration: AREDS report no. 35. Ophthalmology. 2013; 120 (8): 1604–11.
10. Complications of Age-Related Macular Degeneration Prevention Trial Research Group. Laser treatment in patients with bilateral large drusen: the complications of age-related macular degeneration prevention trial. Ophthalmology. 2006; 113 (11): 1974–86.
11. Virgili G, Michelessi M, Parodi MB, Bacherini D, Evans JR. Laser treatment of drusen to prevent progression to advanced age-related macular degeneration. Cochrane Database Syst Rev. 2015; 10 (10): 1–67.
12. Prahs P, Walter A, Regler R, Theisen-Kunde D, Birngruber R, Brinkmann R, Framme C. Selective retina therapy (SRT) in patients with geographic atrophy due to age-related macular degeneration. Graefes Arch Clin Exp Ophthalmol. 2010; 248 (5): 651–8.
13. Guymer RH, Wu Z, HodgsonL AB, Caruso E, Brassington KH, Tindill N, et al. Laser Interventionin Early Stages of Age-Related Macular Degeneration Study Group. Subthreshold Nanosecond Laser Intervention in Age-Related Macular Degeneration: The LEAD Randomized Controlled Clinical Trial. Ophthalmology. 2019; 126 (6): 829–38.
14. Gordeeva MV, Gacu MV. Funkcional'nye rezul'taty porogovoj lazerkoaguljacii razlichnyh vidov mjagkih makuljarnyh druz. Vestnik OGU. 2013; 4 (153); 59–62. Russian.
15. Gordeeva MV. Sravnenie jeffektivnosti razlichnyh lazernyh metodik lechenija mjagkih makuljarnyh druz [dissertacija]. M., 2013. Russian.
16. Novais EA, Badaró E, Regatieri CV, Duker J, de Oliveira Bonomo PP. Regression of drusen after combined treatment using photodynamic therapy with verteporfin and ranibizumab. Ophthalmic Surg Lasers Imaging Retina. 2015; 46 (2): 275–8.
17. Gallego-Pinazo R, Marina A, Suelves-Cogollos, Francés-Muñoz E, Millán JM, Arevalo JF, et al. Intravitreal ranibizumab for symptomatic drusenoid pigment epithelial detachment without choroidal neovascularization in age-related macular degeneration. Clin Ophthalmol. 2011; 5: 161–5.
18. Vavvas DG, Daniels AB, Kapsala ZG, Goldfarb JW, Ganotakis E, Loewenstein JI, et al. Regression of Some High-risk Features of Age-related Macular Degeneration (AMD) in Patients Receiving Intensive Statin Treatment. EBioMedicine. 2016; 5: 198–203.

Литература

1. Wong WL, Su X, Li X, Cheung CM, Klein R, Cheng CY, Wong TY. Global prevalence of age-related macular degeneration and disease burden projection for 2020 and 2040: a systematic review and meta-analysis. Lancet Glob Health. 2014; 2 (2): 106–16.
2. Ferris FL, Wilkinson CP, Bird A, Chakravarthy U, Chew E, Csaky K, Sadda SR; Beckman Initiative for Macular Research Classification Committee. Clinical classification of age-related macular degeneration. Ophthalmology. 2013; 120 (4): 844–51.
3. Casswell AG, Kohen D, Bird AC. Retinal pigment epithelial detachments in the elderly: classification and outcome. British Journal of Ophthalmology. 1985; 69: 397–403.
4. Spaide RF, Jaffe GJ, Sarraf D, Freund KB, Sadda SR, Staurenghi G, Waheed NK; Consensus Nomenclature for Reporting Neovascular Age-Related Macular Degeneration Data: Consensus on Neovascular Age-Related Macular Degeneration Nomenclature Study Group. Ophthalmology. 2020; 127 (5): 616–36.
5. Sarks JP, Sarks SH, Killingsworth MC. Evolution of soft drusen in age-related macular degeneration. Eye (Lond). 1994; 8: 269–83.
6. Balaratnasingam C, Yannuzzi LA, Curcio CA, Morgan WH, Querques G, Capuano V, et al. Associations Between Retinal Pigment Epithelium and Drusen Volume Changes During the Lifecycle of Large Drusenoid Pigment Epithelial Detachments. Invest Ophthalmol Vis Sci. 2016; 57 (13): 5479–89.
7. Yu JJ, Agrón E, Clemons TE, Domalpally A, van Asten F, Keenan TD, et al. Age-Related Eye Disease Study 2 Research Group. Natural History of Drusenoid Pigment Epithelial Detachment Associated with Age-Related Macular Degeneration: Age-Related Eye Disease Study 2 Report No. 17. Ophthalmology. 2019; 126 (2): 261–73.
8. Roquet W, Roudot-Thoraval F, Coscas G, Soubrane G. Clinical features of drusenoid pigment epithelial detachment in age related macular degeneration. Br J Ophthalmol. 2004; 88 (5): 638–42.
9. Chew EY, Clemons TE, Agrón E, Sperduto RD, Sangiovanni JP, Kurinij N, et al. Age-Related Eye Disease Study Research Group. Long-term effects of vitamins C and E, β-carotene, and zinc on age-related macular degeneration: AREDS report no. 35. Ophthalmology. 2013; 120 (8): 1604–11.
10. Complications of Age-Related Macular Degeneration Prevention Trial Research Group. Laser treatment in patients with bilateral large drusen: the complications of age-related macular degeneration prevention trial. Ophthalmology. 2006; 113 (11): 1974–86.
11. Virgili G, Michelessi M, Parodi MB, Bacherini D, Evans JR. Laser treatment of drusen to prevent progression to advanced age-related macular degeneration. Cochrane Database Syst Rev. 2015; 10 (10): 1–67.
12. Prahs P, Walter A, Regler R, Theisen-Kunde D, Birngruber R, Brinkmann R, Framme C. Selective retina therapy (SRT) in patients with geographic atrophy due to age-related macular degeneration. Graefes Arch Clin Exp Ophthalmol. 2010; 248 (5): 651–8.
13. Guymer RH, Wu Z, HodgsonL AB, Caruso E, Brassington KH, Tindill N, et al. Laser Interventionin Early Stages of Age-Related Macular Degeneration Study Group. Subthreshold Nanosecond Laser Intervention in Age-Related Macular Degeneration: The LEAD Randomized Controlled Clinical Trial. Ophthalmology. 2019; 126 (6): 829–38.
14. Гордеева М. В., Гацу М. В. Функциональные результаты пороговой лазеркоагуляции различных видов мягких макулярных друз. Вестник ОГУ. 2013; 4 (153); 59–62.
15. Гордеева М. В. Сравнение эффективности различных лазерных методик лечения мягких макулярных друз [диссертация]. М., 2013.
16. Novais EA, Badaró E, Regatieri CV, Duker J, de Oliveira Bonomo PP. Regression of drusen after combined treatment using photodynamic therapy with verteporfin and ranibizumab. Ophthalmic Surg Lasers Imaging Retina. 2015; 46 (2): 275–8.
17. Gallego-Pinazo R, Marina A, Suelves-Cogollos, Francés-Muñoz E, Millán JM, Arevalo JF, et al. Intravitreal ranibizumab for symptomatic drusenoid pigment epithelial detachment without choroidal neovascularization in age-related macular degeneration. Clin Ophthalmol. 2011; 5: 161–5.
18. Vavvas DG, Daniels AB, Kapsala ZG, Goldfarb JW, Ganotakis E, Loewenstein JI, et al. Regression of Some High-risk Features of Age-related Macular Degeneration (AMD) in Patients Receiving Intensive Statin Treatment. EBioMedicine. 2016; 5: 198–203.

LASER TREATMENT OF MACULAR RETINAL FOLDS IN LATE POSTOPERATIVE PERIOD AFTER RETINAL DETACHMENT REPAIR

Takhchidi KhP, Takhchidi EKh, Kasminina TA, Tebina EP ✉

Pirogov Russian National Research Medical University, Moscow, Russia

Macular retinal folds are a rare yet grave complication of surgical rhegmatogenous retinal detachment repair. Clinical symptoms vary depending on the location and severity of folding. Fold located in the periphery of the ocular fundus can be asymptomatic, but macular retinal folds cause diminished visual acuity and metamorphopsia. Currently, the most effective treatment for retinal folds is repeat surgery. Its serious disadvantage is the risk of complications in the early postoperative period, including hemophthalmia, inflammation, secondary glaucoma, cataracts, RRD recurrence, macular tears, retinal vascular occlusion, etc. The clinical case described below demonstrates the potential of combination laser therapy for the treatment of macular retinal folds based on the use of modern diagnostic and therapeutic methods.

Keywords: macular retinal folds, laser photocoagulation, rhegmatogenous retinal detachment, micropulse laser

Author contribution: Takhchidi KhP — study concept and design, manuscript editing; Takhchidi EKh — literature analysis; Tebina EP — data acquisition, manuscript preparation; Kasminina TA — laser therapy.

Compliance with ethical standards: the patient gave informed consent to laser therapy and personal data processing.

✉ **Correspondence should be addressed:** Ekaterina P. Tebina
Volokolamskoe shosse, d. 30, korp. 2, Moscow, 123182, Russia; ekaterinatebina@mail.ru

Received: 19.11.2021 **Accepted:** 05.12.2021 **Published online:** 21.12.2021

DOI: 10.24075/brsmu.2021.060

ЛАЗЕРНОЕ ЛЕЧЕНИЕ МАКУЛЯРНОЙ РЕТИНАЛЬНОЙ СКЛАДЧАТОСТИ КАК ОСЛОЖНЕНИЯ В ОТДАЛЕННОМ ПОСЛЕОПЕРАЦИОННОМ ПЕРИОДЕ ВЕДЕНИЯ ОТСЛОЙКИ СЕТЧАТКИ

Х. П. Тахчиди, Е. Х. Тахчиди, Т. А. Касмынина, Е. П. Тебина ✉

Российский национальный исследовательский медицинский университет имени Н. И. Пирогова, Москва, Россия

Макулярная ретинальная складчатость является редким, но серьезным осложнением после оперативного лечения регматогенной отслойки сетчатки. Тяжесть проявления клинических симптомов, вызванных ретинальной складчатостью, зависит от ее расположения и степени выраженности. В случае локализации складчатости на периферии глазного дна заболевание может протекать бессимптомно, однако при расположении складок в макулярной зоне приводит к снижению остроты зрения и появлению метаморфопсий. В настоящее время наиболее эффективным методом лечения ретинальных складок является повторное оперативное лечение. Однако его недостатком является наличие рисков развития осложнений в раннем послеоперационном периоде: гемофтальма, воспалительных процессов, вторичной глаукомы, катаракты, рецидивов отслойки сетчатки, макулярных разрывов, окклюзий сосудов сетчатки и др. Представленный клинический случай демонстрирует возможность применения комбинированного лазерного лечения у пациента с осложнением в виде макулярной ретинальной складчатости, с использованием современных методов диагностики и лечения.

Ключевые слова: макулярная ретинальная складчатость, лазерная коагуляция, регматогенная отслойка сетчатки, микроимпульсное лазерное воздействие

Вклад авторов: Х. П. Тахчиди — концепция и дизайн исследования, редактирование текста; Е. Х. Тахчиди — анализ литературных данных; Е. П. Тебина — сбор и обработка материала, написание текста; Т. А. Касмынина — лазерное лечение пациента.

Соблюдение этических стандартов: от пациента получено согласие на лазерное лечение и обработку персональных данных.

✉ **Для корреспонденции:** Екатерина Павловна Тебина
Волоколамское шоссе, д. 30, корп. 2, г. Москва, 123182, Россия; ekaterinatebina@mail.ru

Статья получена: 19.11.2021 **Статья принята к печати:** 05.12.2021 **Опубликована онлайн:** 21.12.2021

DOI: 10.24075/vrgmu.2021.060

Macular retinal folds are a rare yet grave complication of surgical rhegmatogenous retinal detachment (RRD) repair [1]. Macular folds were first described by Pavan in 1984 following a scleral buckling procedure combined with intravitreal gas tamponade. The literature on retinal folds associated with RRD surgery is scarce and mostly comprises clinical case reports. In 1991 Van Meurs et al. analyzed the outcomes of RRD surgery in 137 patients; of them, 4 (2.8%) patients had developed retinal folds. According to a 2011 publication by Isaico et al., 3 (1.96%) of 153 examined patients had retinal folds after surgical RRD repair. The primary risk factors for postoperative retinal folds include intraocular gas injection, acute RRD, large wide explants, bullous RRD with tears in the superior quadrants, transscleral drainage of subretinal fluid, and RRD extending into the macular zone [1–6].

Clinical symptoms vary depending on the location and severity of retinal folding. Macular retinal folds manifest as visual field defects, diplopia, metamorphopsia, and reduced visual acuity, whereas peripheral retinal folds can be asymptomatic [3, 6–10].

Until recently, retinal folds were classified in the literature by their location (posterior and macular), shape and orientation (arcuate), pathogenesis (compression folds), clinical features (dry) or were referred to simply as retinal folds [11].

Then, retinal fold morphology was elucidated by optical coherence tomography (OCT). Two types of retinal folds were distinguished: partial-thickness (involving the inner or outer retina) and full-thickness folds. The latter involve all layers of the retinal neuroepithelium and appear as a convex, deformed retina on OCT images. OCT features of the full-thickness retinal fold include contact between the basal segments of adjacent retinal layers, disorganized retinal architecture, structural changes in the external limiting membrane, the connecting cilium between the outer and inner photoreceptor segments, the outer nuclear layer, the outer plexiform layer and not uncommonly in the overlying layers, as well as formation of hyperreflective areas

[11, 12]. Inner retinal folds involve the inner retinal layer and appear on OCT as a pronounced distortion of the retinal profile presenting as internal limiting membrane to internal limiting membrane apposition. Outer retinal folds appear as multiple small vertically oriented hyperreflective lesions over the retinal pigment epithelium (RPE), extending into the outer nuclear layer [11, 12].

According to the literature, there is no unified treatment strategy for retinal folds. The outcomes also vary, from complete resolution of the fold and visual function recovery to partial regression with minimal or moderate vision recovery to severe irreversible retinal damage. In most cases, macular retinal folds persist causing irreversible loss of visual acuity and metamorphopsia [3–6, 10, 13]. Besides, patients with previously stable retinal folds are reported to develop late recurrent retinal detachment resulting from proliferative vitreoretinopathy, which in turn may be caused by retinal folds [5].

Considering the high risk of intra- and postoperative complications after repeat vitreoretinal surgery, it is important to develop a non-invasive pathogenetic treatment for retinal folds that would minimize potential damage to the sensory retina.

Currently, laser technologies are being increasingly used for treating retinal pathology. Retinal grid laser photocoagulation with spots applied in the checkerboard pattern and spaced > 1 spot size apart is a popular technique for enhancing the structural support provided by Müller cells and improving retinal architecture by creating chorioretinal adhesions. Active and sustainable retinal tissue regeneration can be achieved through micropulse laser therapy [14, 15]. Below we report the use of combination laser therapy for the macular retinal fold developing in the late postoperative period after surgical RRD repair.

Clinical case

In October 2020, a male patient presented with complaints of metamorphopsia and diminished visual acuity in the right eye at the Research Center of Ophthalmology, Pirogov Russian National Research Medical University. According to his medical records, in August 2020 the patient had undergone microinvasive subtotal vitrectomy with intravitreal perfluorocarbon liquid (PFCL)/gas injection and received an intraocular lens implant for RRD in the right eye.

Once admitted to the Center, the patient underwent a comprehensive ophthalmic examination. Standard diagnostic tests included visometry for uncorrected visual acuity (UVA) and best corrected visual acuity (BCVA) and indirect ophthalmoscopy with a MaxField indirect lens (Ocular Inc.; USA). In addition, optical coherence tomography was performed using a Spectralis HRA+OCT platform (Heidelberg Engineering GmbH.; Germany).

Laser photocoagulation therapy was delivered using a VISULAS Trion work laser station (Carl Zeiss; Germany) operated at 577 nm wavelength.

During the initial examination the patient complained of metamorphopsia and diminished visual acuity in his right eye. UVA of the right eye (OD) was 0.05; BCVA was 0.7 for OD and 1.0 for the left eye (OS).

Ophthalmic OD biomicroscopy revealed that the anterior segment was intact and the intraocular lens was well centered. The optic disc was pale pink, with well-defined margins. A PFCL bubble was visible peripapillarily on the nasal side. Pronounced retinal folding ending with a subretinal PFCL bubble extended from the temporal optic disc margin toward the 8 o'clock plane (Fig. 1). The caliber of the retinal vessels was unchanged. Cellophane maculopathy also known as epiretinal membrane was visualized paravasally along the course of the superior and inferior temporal arcades. Laser-sealed retinal breaks were present in the upper quadrant of the peripheral

Of all OCT images of the right eye, the most informative in terms of postoperative dynamics were scan A (Fig. 2A) and the next scan B passing 250 μm higher, closer to fovea (Fig. 2B).

Considering the patient's complaints, his medical history and the results of the comprehensive ophthalmic examination, the following diagnosis was established: operated RRD in the right eye complicated with macular retinal folding; epiretinal membrane; avitria; artiphakia.

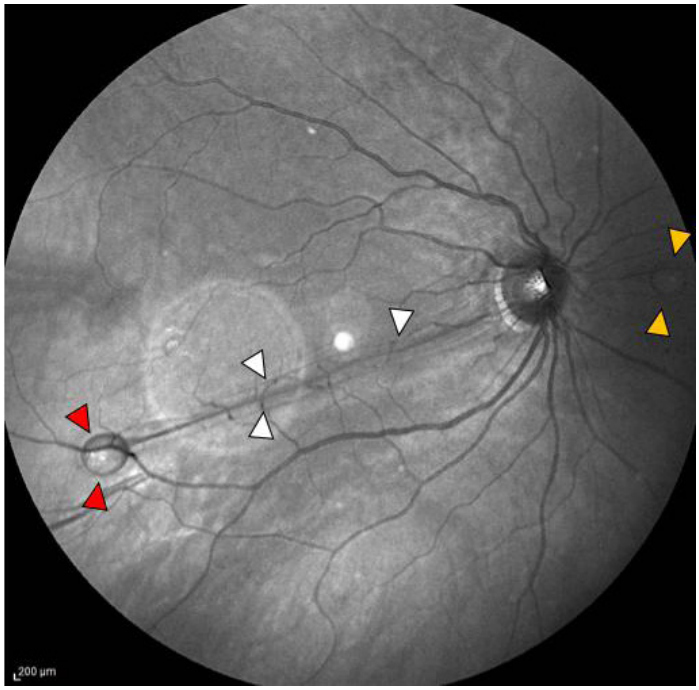

Fig. 1. The panoramic image of the right ocular fundus. A 756-μm PFCL bubble is visible peripapillarily on the nasal side (*yellow arrow*). A tight 633-μm-wide retinal fold extends from the temporal margin of the optic disc toward the 8 o'clock plane (*white arrow*) ending with a subretinal PFCL bubble sized 977 μm (*red arrow*). The fold involves half of the macular zone, predominantly its lower part

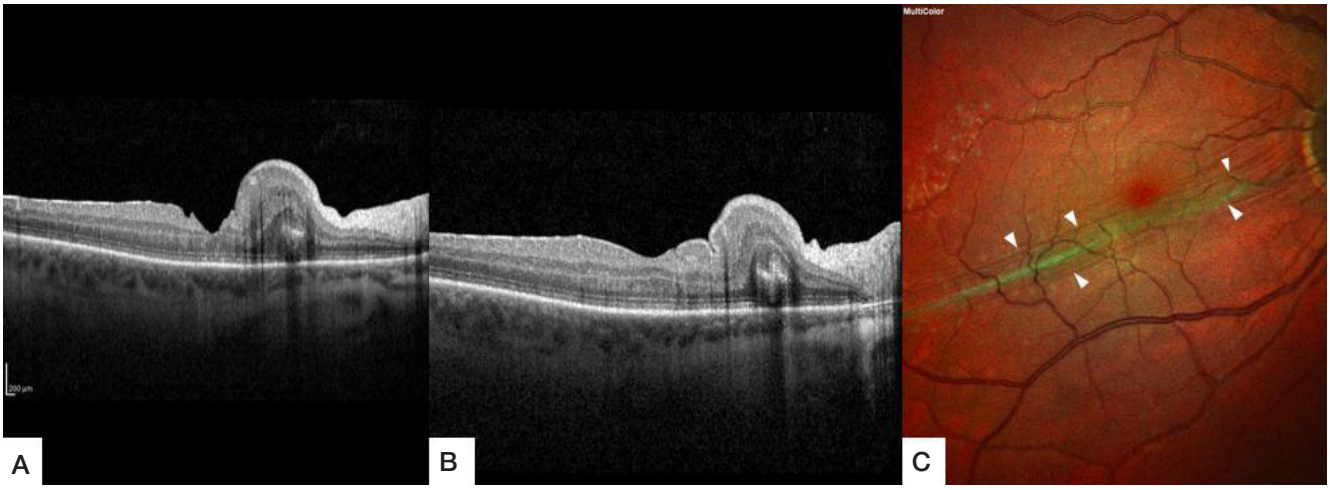

Fig. 2. Retinal spectral-domain optical coherence tomography scans of the right eye. **A.** The macula looks deformed, the foveal contour is normal (foveal depth: 185 μm, retinal thickness in the fovea: 192 μm); parafoveally, on the nasal side, the retina has a convex configuration showing a dominant retinal fold up to 637 μm in height, the retinal architecture looks grossly disorganized (changes involve the external limiting membrane, the connecting cilium between the inner and outer photoreceptor segments, the outer nuclear layer, and the outer plexiform layer). **B.** The macula is flattened; foveal depth: 106 μm, retinal thickness: 284 μm; a dominant full-thickness retinal fold up to 601 μm in height with gross retinal structure disorganization is visualized on the nasal side, further from the foveal margin. **C**. A multispectral image. Pronounced 633-μm-wide retinal folding extends from the temporal margin of the optic disc toward the 8 o'clock plane (white arrows)

In December 2020, a decision was made to perform laser microsurgery on the patient in order to restore the architecture of the macular zone, flatten the folds, and improve the morphology and function of the retina. The combination treatment was delivered in several steps. In the first step, the patient underwent grid laser photocoagulation. The burns were applied along the course of the retinal fold and under it in the checkerboard pattern in 3 to 4 rows depending on the severity of the fold; the avascular zone was avoided. The laser workstation was operated at the lowest possible settings to ensure the lowest intensity of coagulation: power 50 mW, pulse duration 0.05 s, spot diameter 100 μm, wavelength 577 nm, spacing 150 μm. Single laser spots were applied paramacularly along the upper edge of the macula. Additionally, laser coagulation was performed on the epiretinal membrane along the course of the superior and inferior temporal vascular arcades. In the second step, the patient received 3 sessions of micropulse laser therapy (wavelength 577 nm, burst duration 30 ms, micropulse duration 50 μs, pulse ratio 4.7%, spot diameter 100 μm, power 50 mW.

Two months after surgery, the comprehensive ophthalmic examination revealed a slight improvement, although no significant morphological and functional changes were observed.

Four months after the intervention, the patient reported a significant reduction of metamorphopsia. His UVA and BCVA had improved to 0.2 and 0.7, respectively. Ophthalmic biomicroscopy of the right eye revealed the intact anterior segment and the well-centered intraocular lens. The fold in the central zone had flattened and was now 921 μm wide (Fig. 3B). Paramacularly and along the retinal fold, weakly pigmented coagulation spots were visible. The caliber of the retinal vessels was unchanged. Paravasally, weakly pigmented coagulation spots were present in the epiretinal membrane area. Changes in the retina can be clearly seen on the follow-up OCT scans (Fig. 3A, B).

Six months later on another follow-up examination the patient reported the absence of metamorphopsias in the right eye; UVA: 0.2; BCVA: 0.7. On ophthalmic biomicrosopy the anterior segment was intact, the intraocular lens was well-centered. The optic disc was pale pink, with well-defined margins. The retinal folds had unfolded, the dominant retinal fold was not visualized. A slight undulation (up to 1.371 μm in width) was visualized on the retinal surface where retinal folding had been previously observed (Fig. 4B). Weakly pigmented coagulations spots were present in the epiretinal membrane area, except for the avascular zone. Changes in the retina can be clearly seen on the follow-up OCT scans (Fig. 4A, B).

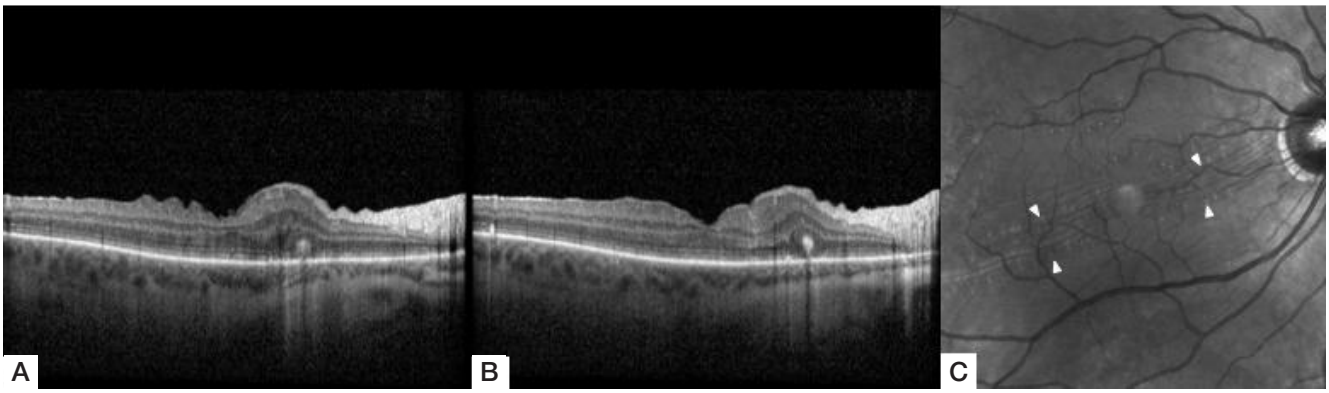

Fig. 3. Retinal spectral-domain optical coherence tomography scans of the right eye. **A**. The macular profile is restored; the fovea is flattened: foveal depth 134 μm, retinal thickness in the fovea 240 μm; parafoveally on the nasal side, the retinal fold has diminished in height from 637 to 487 μm; the structural organization of the retinal layers appears partially restored; microfolds are visualized in the inner retinal layers paramacularly on the temporal side. **B**. The foveal contour is clear; foveal depth has increased to 142 μm, retinal thickness in the fovea has decreased to 243 μm; parafoveally on the nasal side, the retinal fold has diminished in height from 601 to 473 μm, the structural organization of the retinal layers looks partially restored. **C**. Infrared image. In the central zone, the folds have become less pronounced and flattened to 921 μm in width (*white arrow*)

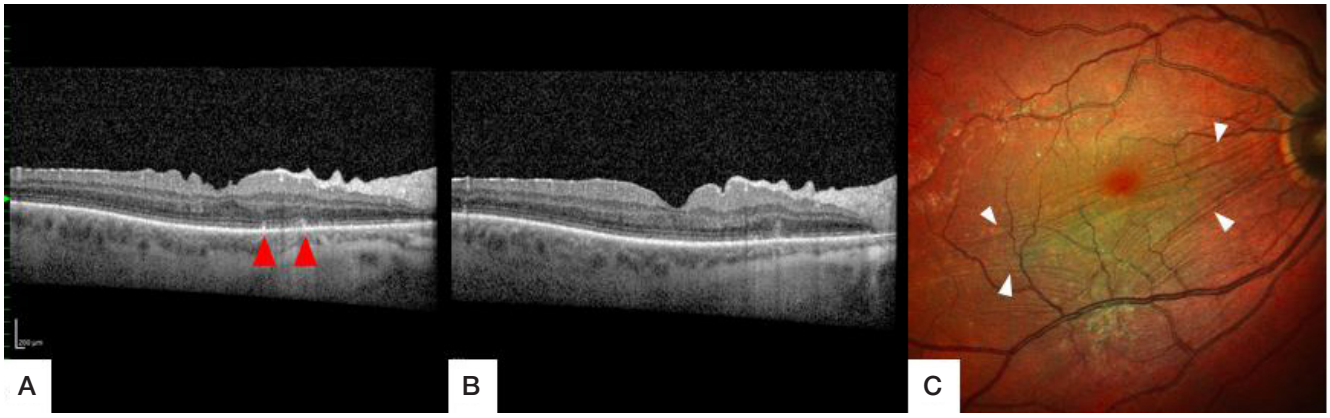

Fig. 4. Retinal spectral-domain optical coherence tomography scans of the right eye. **A.** The macular profile is restored, the fovea is flattened; foveal depth has decreased to124 μm, retinal thickness in the fovea has increased to 273 μm; paramacularly, on the nasal side, intraretinal coagulation spots are visible at the RPE level (*red arrow*). B The macular profile is restored, the fovea has a clear contour; foveal depth: 160 μm, retinal thickness in the fovea: 224 μm, the structural organization of the retinal layers is restored; paramacularly on the nasal side microfolds are visible in the inner retinal layers. **C**. A multispectral image: the retinal folds have unfolded (*white arrow*), weakly pigmented coagulation spots are visible in the macular zone, except for the avascular area, and in the epiretinal membrane area.

Clinical case discussion

Retinal folds are a clinically important complication of surgical RRD repair. Few attempts have been reported to surgically treat retinal folds, including macular folds of different etiology [2, 16, 18]. There is no clear guidance on the timeframe and indications for repeat surgery. Experiments conducted in vivo have demonstrated that apoptosis of the photoreceptor layer and thinning of the outer nuclear layer start a week after macular translocation [18].

Repeat surgery is often delayed because retinal folds can be diagnosed no sooner than gas injected in the vitreous cavity is reabsorbed. Another reason is the risk of complications in the early postoperative period, including hemophthalmia, inflammation, secondary glaucoma, cataracts, RRD recurrence, macular tears, retinal vascular occlusion, etc. [11, 17, 19].

This study describes an alternative to vitreoretinal surgery: a combination laser therapy involving 2 interventions with different mechanisms of action. The proposed treatment method has indisputable advantages like non-invasiveness, low injury rate, and lack of serious complications or adverse effects. Due to the gradual topographically directed effect of grid laser photocoagulation, we were able to unfold the retina, restore the position of the macula and its functional and morphological characteristics. Paramacular tissues (the dominant retinal fold) flattened out, and retinal thickness and structural organization were recovered. The macular profile shifted to its normal microtopographic position, becoming more clearly visible on OCT scan B (Fig. 3B); foveal depth and width also normalized. The patient's metamorphopsia (distorted vision) resolved, his uncorrected visual acuity and the ability to use binocular vision improved. In addition, micropulse laser therapy prolonged tissue regeneration.

Summing up, the coagulation effect of laser energy applied locally to achieve controlled retinal stretching causes shifting of retinal microlayers, reorganizing the architecture of the macular zone. Low-dose exposure of the affected retinal zones to micropulse laser energy activates prolonged regeneration.

The proposed method produced pronounced morphofunctional effects on macular retinal folding, which develops in the late postoperative period after retinal detachment repair.

CONCLUSION

The proposed combination laser treatment of macular folds developing in the late postoperative period after RRD repair significantly improved the morphofunctional characteristics of the eye. The application of transpupillary laser surgery to ophthalmological practice broadens the arsenal of methods for noninvasive correction of RRD associated with macular retinal folds

The study demonstrates the potential of laser microsurgery (at the micron level) for correcting the damaged microtopography and microarchitecture of the macular retina, ensuring recovery of normal functions of the eye.

References

1. Pavan PR. Retinal fold in macula following intraocular gas: an avoidable complication of retinal detachment surgery. Arch Ophthalmol. 1984; 102 (1): 83–84.
2. Gruener AM, Lee RMH, Kourtis N, Herbert L. Surgical repair of macular fold after vitrectomy for bullous rhegmatogenous retinal detachment. Retina. 2013; 33 (4): 894–7.
3. Larrison WI, Frederick AR Jr, Peterson TJ, Topping TM. Posterior retinal folds following vitreoretinal surgery. Arch Ophthalmol. 1993; 111 (5): 621–5.
4. Lewen RM, Lyon CE, Diamond JG. Scleral buckling with intraocular air injection complicated by arcuate retinal folds. Arch Ophthalmol. 1987; 105 (9): 1212–4.
5. van Meurs JC, Humalda D, Mertens DA, Peperkamp E. Retinal folds through the macula. Doc Ophthalmol. 1991;78 (3–4): 335–40.
6. Heimann H, Bopp S. Retinal Folds following Retinal Detachment Surgery. Ophthalmologica. 2011; 226 (1): 18–26.
7. Trinh L, Glacet-Bernard A, Colasse-Marthelot V, Leynaud JL, Soubrane G. Macular fold following retinal detachment surgery. J Fr Ophtalmol. 2006; 29 (9): 995–9.
8. El-Amir AN, Every S, Patel CK. Repair of macular fold following retinal detachment surgery. Clin Experiment Ophthalmol. 2007; 35 (9): 791–2.
9. Herbert EN, Groenewald C, Wong D. Treatment of retinal folds using a modified macula relocation technique with perfluorohexyloctane tamponade. Br J Ophthalmol. 2003; 87 (7): 921–2.

10. Ruiz-Moreno JM, Montero JA. Sliding macular fold following retinal detachment surgery. Graefes Arch Clin Exp Ophthalmol. 2011; 249 (2): 301–3.
11. R Rishi Gupta, Douglas S M Iaboni, Mark E Seamone, David Sarraf. Inner, outer, and full thickness retinal folds following rhegmatogenous retinal detachment repair: A Review. Surv Ophthalmol. 2019; 64 (2): 135–61.
12. Stolyarenko GE, Savostyanova NV, Doroshenko D, Salahutdinov VK. Makuljarnye skladki posle hirurgii otslojki setchatki c polnym ee prileganiem. Sovremennye tehnologii v oftal'mologii. 2020 (1): 257–63. Russian.
13. Pierro L, Sadda SR, Gagliardi M, Mantovani E, de Benedetto U., Codenotti M, Bandello F. SD OCT features of dry arcuate longstanding retinal folds. Eur J Ophthalmol. 2011; 21 (6): 215–7.
14. Fedoruk NA, Fedorov AA, Bolshunov AV. Morfologicheskie i gistohimicheskie osobennosti subporogovogo lazernogo vozdeĭstvija na struktury horioretinal'nogo kompleksa. Vestnik oftal'mologii. 2013; (5): 73–81. Russian.
15. Zheltov GI, Romanov GS, Romanov OG, Ivanova EV. Selektivnoe dejstvie lazernyh impul'sov na retinal'nyj pigmentnyj jepitelij. Fizicheskie osnovy. Novoe v oftal'mologii. 2012; (3): 37. Russian.
16. Ahn SJ, Woo SJ, Ahn J, Park KH. Spontaneous resolution of macular fold following retinal reattachment: morphologic features on SD-OCT. Ophthalmic Surg Lasers Imaging. 2011; 42 Online: e81–83.
17. Barale P, Mora P, Errera M-H, Ores R, Paques M, Sahel J-A. Treatment of macular folds complicating retinal detachment surgery using air for retinal unfolding. Retin Cases Br Reports. 2018; 12 (3): 228–30.
18. Hayashi A, Usui S, Kawaguchi K, et al. Retinal changes after retinal translocation surgery with scleral imbrication in dog eyes. Investig Ophthalmol Vis Sci. 2000; 41 (13): 4288–92.
19. Benson SE, Schlottmann PG, Bunce C, Xing W, Charteris DG. Optical Coherence Tomography Analysis of the Macula after Vitrectomy Surgery for Retinal Detachment. Ophthalmology. 2006; 113 (7): 1179–83.

Литература

1. Pavan PR. Retinal fold in macula following intraocular gas: an avoidable complication of retinal detachment surgery. Arch Ophthalmol. 1984; 102 (1): 83–84.
2. Gruener AM, Lee RMH, Kourtis N, Herbert L. Surgical repair of macular fold after vitrectomy for bullous rhegmatogenous retinal detachment. Retina. 2013; 33 (4): 894–7.
3. Larrison WI, Frederick AR Jr, Peterson TJ, Topping TM. Posterior retinal folds following vitreoretinal surgery. Arch Ophthalmol. 1993; 111 (5): 621–5.
4. Lewen RM, Lyon CE, Diamond JG. Scleral buckling with intraocular air injection complicated by arcuate retinal folds. Arch Ophthalmol. 1987; 105 (9): 1212–4.
5. van Meurs JC, Humalda D, Mertens DA, Peperkamp E. Retinal folds through the macula. Doc Ophthalmol. 1991;78 (3–4): 335–40.
6. Heimann H, Bopp S. Retinal Folds following Retinal Detachment Surgery. Ophthalmologica. 2011; 226 (1): 18–26.
7. Trinh L, Glacet-Bernard A, Colasse-Marthelot V, Leynaud JL, Soubrane G. Macular fold following retinal detachment surgery. J Fr Ophtalmol. 2006; 29 (9): 995–9.
8. El-Amir AN, Every S, Patel CK. Repair of macular fold following retinal detachment surgery. Clin Experiment Ophthalmol. 2007; 35 (9): 791–2.
9. Herbert EN, Groenewald C, Wong D. Treatment of retinal folds using a modified macula relocation technique with perfluorohexyloctane tamponade. Br J Ophthalmol. 2003; 87 (7): 921–2.
10. Ruiz-Moreno JM, Montero JA. Sliding macular fold following retinal detachment surgery. Graefes Arch Clin Exp Ophthalmol. 2011; 249 (2): 301–3.
11. R Rishi Gupta, Douglas S M Iaboni, Mark E Seamone, David Sarraf. Inner, outer, and full thickness retinal folds following rhegmatogenous retinal detachment repair: A Review. Surv Ophthalmol. 2019; 64 (2): 135–61.
12. Столяренко Г. Е., Савостьянова Н. В., Дорошенко Д., Салахутдинов В. К. Макулярные складки после хирургии отслойки сетчатки с полным ее прилеганием. Современные технологии в офтальмологии. 2020 (1): 257–63.
13. Pierro L, Sadda SR, Gagliardi M, Mantovani E, de Benedetto U., Codenotti M, Bandello F. SD OCT features of dry arcuate longstanding retinal folds. Eur J Ophthalmol. 2011; 21 (6): 215–7.
14. Федорук Н. А., Федоров А. А., Большунов А. В. Морфологические и гистохимические особенности субпорогового лазерного воздействия на структуры хориоретинального комплекса. Вестник офтальмологии. 2013; (5): 73–81.
15. Желтов Г. И., Романов Г. С., Романов О. Г., Иванова Е. В. Селективное действие лазерных импульсов на ретинальный пигментный эпителий. Физические основы. Новое в офтальмологии. 2012; (3): 37.
16. Ahn SJ, Woo SJ, Ahn J, Park KH. Spontaneous resolution of macular fold following retinal reattachment: morphologic features on SD-OCT. Ophthalmic Surg Lasers Imaging. 2011; 42 Online: e81–83.
17. Barale P, Mora P, Errera M-H, Ores R, Paques M, Sahel J-A. Treatment of macular folds complicating retinal detachment surgery using air for retinal unfolding. Retin Cases Br Reports. 2018; 12 (3): 228–30.
18. Hayashi A, Usui S, Kawaguchi K, et al. Retinal changes after retinal translocation surgery with scleral imbrication in dog eyes. Investig Ophthalmol Vis Sci. 2000; 41 (13): 4288–92.
19. Benson SE, Schlottmann PG, Bunce C, Xing W, Charteris DG. Optical Coherence Tomography Analysis of the Macula after Vitrectomy Surgery for Retinal Detachment. Ophthalmology. 2006; 113 (7): 1179–83.

USING MOTION CAPTURE ANALYSIS FOR ASSESSING LOCOMOTION AFTER ARTHROSCOPIC ANTERIOR CRUCIATE LIGAMENT RECONSTRUCTION

Mozheyko EYu[1] ✉, Pavlov AO[2], Chistov MA[1], Khramchenko MA[1], Gurevich VA[1]

[1] Voino-Yasenetsky Krasnoyarsk State Medical University, Krasnoyarsk, Russia

[2] Federal Siberian Research and Clinical Center of FMBA, Krasnoyarsk, Russia

An anterior cruciate ligament tear is one of the most common injuries to the capsular ligament apparatus of the knee necessitating operative treatment. Postoperatively, patients with anterior cruciate ligament injuries develop a pathologic gait pattern. Today, innovative diagnostic and rehabilitation methods for patients with gait disturbances associated with such injuries are in high demand. Below, we present a case of using 3D motion capture analysis for the personalized assessment of gait function in a patient with the reconstructed anterior cruciate ligament two months after surgery. The analysis revealed that the patient had a slower, shorter, wider step with longer step intervals than the healthy subject; the flexion and extension amplitude in the large joints of the operated leg was smaller than in the healthy contralateral leg. Motion capture analysis can be used to assess the postoperative dynamics in patients with anterior cruciate ligament tears.

Keywords: motion capture, anterior cruciate ligament, gait, postural disorders, rehabilitation

Author contribution: Mozheyko EYu formulated the hypothesis, proposed the design, defined the goals and objectives of the study, analyzed study results, wrote and edited the manuscript; Pavlov AO formulated the hypothesis and edited the manuscript; Chistov MA, Khramchenko MA searched the literature, analyzed study results, performed statical analysis and wrote the manuscript; Gurevich VA recruited the subjects, analyzed the results and performed statistical analysis.

Compliance with ethical standards: the study was approved by the Ethics Committee of Krasnoyarsk State Medical University (Protocol № 89/2019 dated April 17, 2019).

✉ **Correspondence should be addressed:** Elena Yu. Mozheyko
Prospekt Mira, 5, Krasnoyarsk, 660049, Russia; el_mozhejko@mail.ru

Received: 20.11.2021 **Accepted:** 13.12.2021 **Published online:** 28.12.2021

DOI: 10.24075/brsmu.2021.063

ИСПОЛЬЗОВАНИЕ ВИДЕОАНАЛИЗА ДВИЖЕНИЙ ПРИ ОЦЕНКЕ ЛОКОМОТОРНЫХ ФУНКЦИЙ ПОСЛЕ АРТРОСКОПИЧЕСКОЙ РЕКОНСТРУКЦИИ ПЕРЕДНЕЙ КРЕСТООБРАЗНОЙ СВЯЗКИ

Е. Ю. Можейко[1] ✉, А. О. Павлов[2], М. А. Чистов[1], М. А. Храмченко[1], В. А. Гуревич[1]

[1] Красноярский государственный медицинский университет имени В. Ф. Войно-Ясенецкого, Красноярск, Россия

[2] Федеральный сибирский научно-клинический центр Федерального медико-биологического агентства, Красноярск, Россия

Разрыв передней крестообразной связки — одно из наиболее часто встречающихся повреждений капсульно-связочного аппарата коленного сустава, требующий оперативного лечения. В ходе длительного периода реабилитации после реконструктивных операций при данном виде травм у пациента формируется характерный двигательный паттерн. На сегодняшний день применение инновационных объективных методов диагностики и реабилитации двигательных нарушений при таких повреждениях актуально и востребованно. Представлен пример персонализированной реабилитационной оценки функции ходьбы пациента через два месяца после пластики передней крестообразной связки методом трехмерного видеоанализа движений. Выявлено нарушение паттерна ходьбы пациента: более медленный короткий редкий широкий шаг по сравнению с шагом здорового исследуемого; амплитуда сгибания-разгибания в крупных суставах оперированной нижней конечности меньше, чем в контрлатеральной нижней конечности пациента. Метод может быть использован в анализе динамики восстановительного лечения после оперативных вмешательств при разрыве крестообразных связок коленного сустава.

Ключевые слова: видеоанализ движений, передняя крестообразная связка, ходьба, постуральные нарушения, реабилитация

Вклад авторов: Е. Ю. Можейко — анализ результатов исследования, формулировка рабочей гипотезы, разработка дизайна исследования, определение цели и задач исследования, написание и утверждение рукописи для публикации; А. О. Павлов — формулировка рабочей гипотезы, утверждение рукописи; М. А. Чистов, М. А. Храмченко — поиск литературы, анализ результатов исследования, статистический анализ, написание статьи; В. А. Гуревич — отбор единиц наблюдения, анализ результатов, статистический анализ.

Соблюдение этических стандартов: исследование одобрено этическим комитетом КрасГМУ (протокол № 89/2019 от 17 апреля 2019 г.).

✉ **Для корреспонденции:** Елена Юрьевна Можейко
ул. Проспект Мира, д. 5, г. Красноярск, 660049, Россия; el_mozhejko@mail.ru

Статья получена: 20.11.2021 **Статья принята к печати:** 13.12.2021 **Опубликована онлайн:** 28.12.2021

DOI: 10.24075/vrgmu.2021.063

An injury to the knee ligament apparatus is a pathology that involves one or more ligaments of the knee joint [1]. It is more prevalent among young able-bodied working-age men actively engaged in sports and exercise and is one of the most common traumatic and orthopedic injuries that compel the patient to seek medical help [1, 2].

The most common injury to the capsular ligament apparatus is an anterior cruciate ligament tear, affecting 30–35 people per 100,000 population [1].

Cruciate ligaments are fibrous bands of connective tissue that connect the femur and the tibia and limit excessive tibial mobility [3].

Most often, anterior cruciate ligament injuries are noncontact and occur during sudden knee joint rotation with the foot firmly planted [1, 4]. Many isolated ligament injuries are consequences of sports injuries caused by a rotational mechanism [5].

The following procedures are used to establish a diagnosis of anterior cruciate ligament tear: history taking, the Lachman test, the Anterior and posterior drawer tests of the knee, radiography of the knee joint (anterior, posterior and lateral views), and magnetic resonance imaging (MRI) of the knee joint [4].

Motion capture analysis (MCA) of gait provides valuable diagnostic data about the patient's locomotion patterns. It

Table 1. Characteristics of gait speed and rhythm in the patient with injuries to the knee ligament apparatus and the healthy subject

MCA parameters	Patient with anterior cruciate ligament tear			Healthy subject		
	Left leg	Right leg	Both legs	Left leg	Right leg	Both legs
Cadence (steps/min)	94,4 ± 2,91	96,7 ± 3,78	95,5 ± 3,51	116,88 ± 3,25	117,56 ± 4,12	117,22 ± 3,68
Lead toe off (% of the gait cycle)	62,0 ± 1,54	62,9 ± 2,87	62,4 ± 2,29	60,10 ± 1,79	60,90 ± 2,16	60,60 ± 1,97
Initial contact, lead foot (% of the gait cycle)	49,80 ± 1,62	50,10 ± 2,32	49,90 ± 1,96	49,90 ± 1,13	50,10 ± 1,75	49,9 ± 1,56
Contralateral toe off (% of the gait cycle)	12,40 ± 0,71	12,80 ± 0,96	12,60 ± 0,85	9,80 ± 0,94	10,90 ± 0,85	10,50 ± 0,96
Single support time (s)	0,48 ± 0,021	0,46 ± 0,038	0,47 ± 0,031	0,41 ± 0,026	0,44 ± 0,020	0,43 ± 0,025
Double support time (s)	0,31 ± 0,023	0,32 ± 0,020	0,32 ± 0,021	0,21 ± 0,023	0,25 ± 0,018	0,23 ± 0,021
Step time (s)	0,64 ± 0,031	0,62 ± 0,040	0,63 ± 0,036	0,51 ± 0,027	0,56 ± 0,028	0,54 ± 0,028
Stride time (s)	1,27 ± 0,042	1,24 ± 0,049	1,26 ± 0,047	1,02 ± 0,044	1,12 ± 0,040	1,08 ± 0,048
Step length (m)	0,61 ± 0,021	0,62 ± 0,016	0,61 ± 0,020	0,68 ± 0,033	0,75 ± 0,016	0,72 ± 0,027
Step width (m)	0,20 ± 0,018	0,20 ± 0,010	0,20 ± 0,015	0,07 ± 0,012	0,07 ± 0,010	0,07 ± 0,011
Stride length (m)	1,21 ± 0,023	1,23 ± 0,030	1,22 ± 0,029	1,36 ± 0,014	1,51 ± 0,0071	1,45 ± 0,011
Walking velocity (m/s)	0,95 ± 0,042	0,99 ± 0,057	0,97 ± 0,053	1,24 ± 0,028	1,44 ± 0,025	1,34 ± 0,028

relies on the computer analysis of movements in which image acquisition is performed in a cableless, noncontact fashion [6].

Today, passive markers are widely used in clinical motion capture analysis. Passive markers are reflective sensors that are attached to the patient's body; the signals emitted by the sensors are captured by the video camera. The acquired data are transmitted to the computer for further processing. Finally, a report is generated that is subsequently used to analyze the linear and angular kinematics of the patient's movements [7].

MCA requires that, since a plane is defined by 3 points, there should be at least 3 reflective markers in the field of view of at least 2 cameras [8].

To measure the physical characteristics of the studied body segments, calibrating markers are attached to the subject. So far, reference standards have been elaborated for movements of the foot, tibia, femur, pelvis, spine, wrist, forearm, and shoulder [9].

At present, MCA is being actively used to uncover the mechanisms of noncontact injuries to the anterior cruciate ligament of the knee joint [10]. 3D MCA has been proposed for adoption into clinical practice as a tool for monitoring rehabilitation in patients with knee joint injuries and assessing the risk of re-injury [11].

The clinical case described below illustrates a personalized MCA-based assessment of locomotor function in the patient with anterior cruciate ligament tear.

Clinical case

Patient I., aged 21 years, was diagnosed with a complete anterior cruciate ligament tear of the left knee joint and a partial posterior cruciate ligament tear. On January 19, 2021 the patient

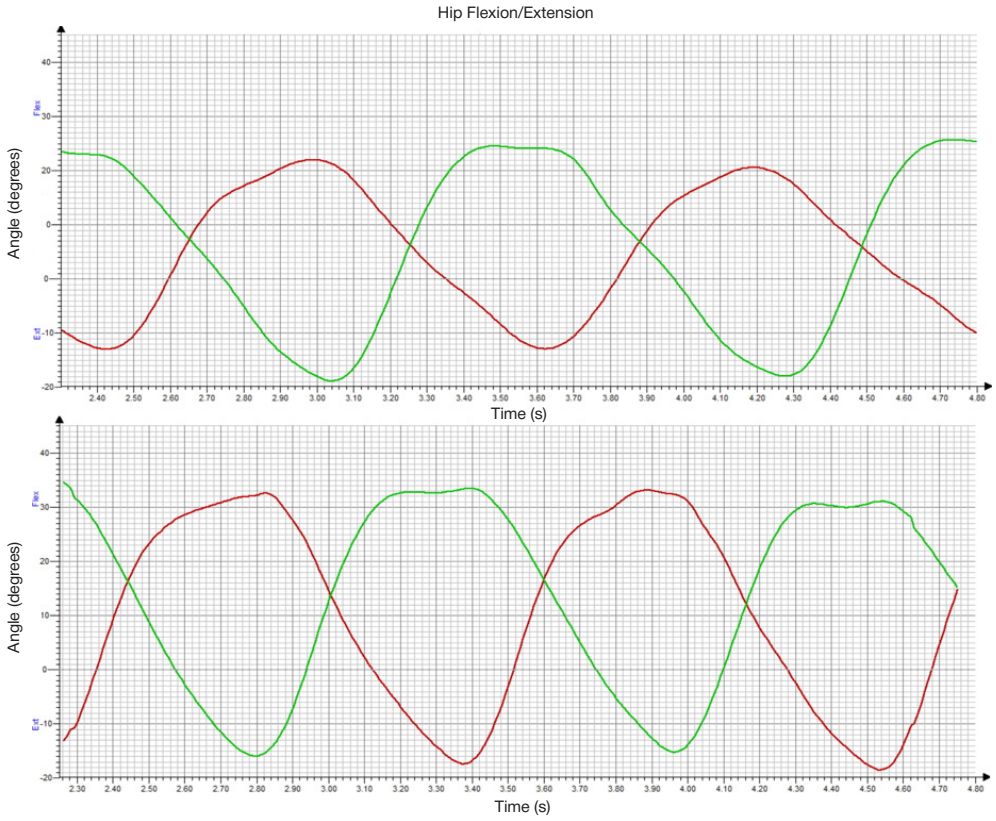

Fig. 1. Hip flexion and extension during one cycle in the patient with injuries to the knee ligament apparatus (*top*) and the healthy subject (*bottom*)

Table 2. Mean hip flexion and extension angles and amplitudes during one gait cycle in the patient with injuries to the knee ligament apparatus and the healthy subject

	Patient with injured knee ligament apparatus		Healthy subject	
	Left leg	Right leg	Left leg	Right leg
	Me [P_{25}; P_{75}]			
Angle 1	–13,71	–18,08	–17,79	–16,28
	[–15,03; –13,0]	[–18,59; –17,63]	[–16,79; –15,26]	[–16,63; –15,93]
Angle 2	23,3	24,43	34,52	32,66
	[22,27; 24,48]	[23,62; 25,84]	[33,16; 35,19]	[31,07; 33,16]
Δ	37,62	42,68	50,1	48,84
	[35,51; 38,56]	[41,09; 43,83]	[49,57; 50,72]	[47,86; 49,67]

underwent arthroscopy of the left knee joint, resection of the remnant anterior cruciate ligament tissue, reconstruction of the anterior cruciate ligament with a peroneus longus autograft and autograft fixation with 19 PEEK Interference Screws (Arthrex; USA). The postoperative course was unremarkable. The patient received conservative treatment, which included antibiotics, analgesics, anticoagulants, and dressings. The knee joint was immobilized with a knee brace; the patient was using crutches for support when walking. On discharge, the patient's condition was satisfactory.

Preoperative MRI performed on December 3, 2020 revealed an impression fracture of the lateral femoral condyle; trabecular edema of the lateral tibial condyle, the intercondylar area and the medial femoral condyle; synovitis and suprapatellar bursitis; MR features of injury to the anterior cruciate ligament and ligamentitis of the medial collateral ligament; moderate degenerative changes of the anterior and posterior horns of the medial meniscus; periarticular soft tissue edema.

Subject V., aged 22 years, had no health complaints regarding their musculoskeletal system, no medical history of lower limb surgery or injury and was comparable with patient I in terms of their anthropometric characteristics.

The patient and the healthy subject were tested at the Laboratory of MCA at the Federal Siberian Research and Clinical Center (FMBA, Russia) using a Vicon Motion Capture Systems (Vicon; UK). The system consisted of 12 infrared T20 video cameras, 3 force plates, a Vicon GigaNet connectivity device, a computer with installed software for video signal capture and processing (Nexus ver. 1.7.15) and software for generating reports (Polygon ver. 3.5.1).

The testing included several stages. First, anthropometric measurements were taken to map the sizes of the patient's body segments to the computer model. Then, reflective markers were attached to the subject's bony landmarks. The patient and the subject were asked to walk at their usual speed on 3 force plates. During the test, the video cameras captured the spatial positions of the markers and the force plates recorded the ground reaction force. Each participant performed at least 10 gait cycles on 3 force plates.

The following changes in gait characteristics were observed in the patient with an anterior cruciate ligament tear vs the

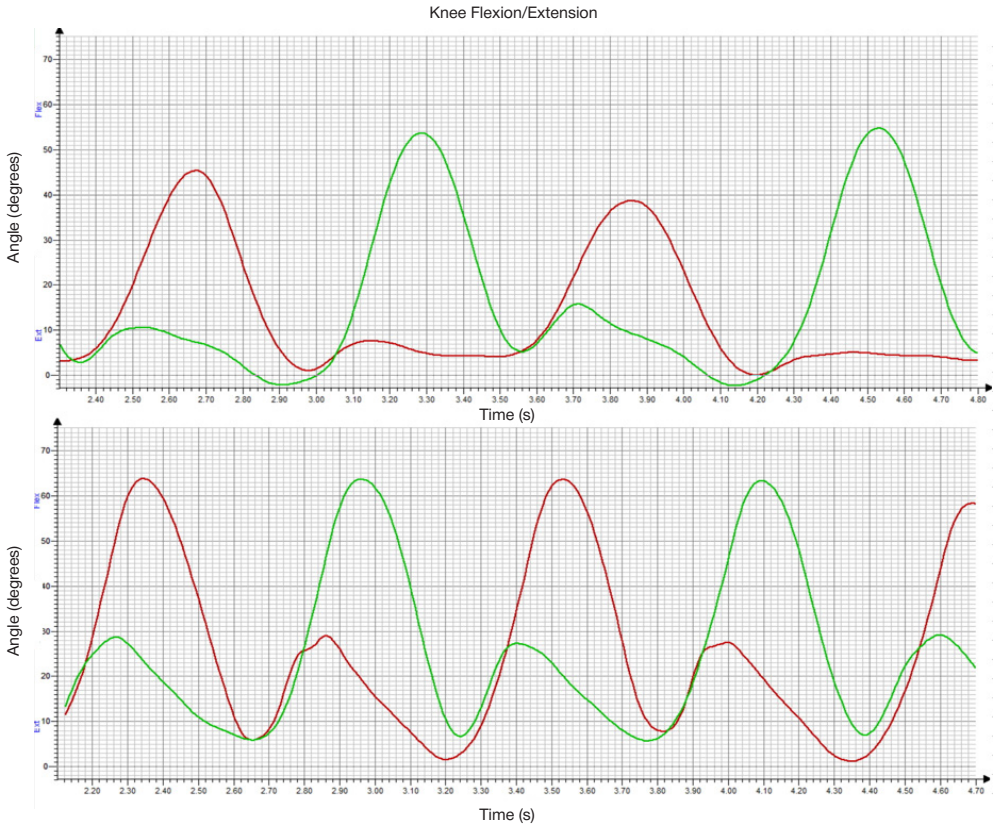

Fig. 2. Knee flexion and extension during one gait cycle in the patient with injuries to the knee ligament apparatus (*top*) and the healthy subject (*bottom*)

Table 3. Mean knee flexion and extension angles and amplitudes during one gait cycle in the patient with injuries to the knee ligament apparatus and the healthy subject

	Patient with injured knee ligament apparatus		Healthy subject	
	Left leg	Right leg	Left leg	Right leg
	Me [P_{25}; P_{75}]			
Angle 1	1,39	–2,89	1,7	5,3
	[1,04; 2,37]	[–3,32; –2,36]	[1,33; 2,26]	[5,02; 5,67]
Angle 2	45,07	52,82	61,89	63,73
	[42,61; 48,18]	[51,2; 54,59]	[60,82; 63,34]	[63,4; 64,86]
Δ	43,16	56,01	60,85	58,39
	[40,54; 46,55]	[54,89; 57,09]	[58,47; 61,57]	[57,73; 59,17]

healthy subject: significantly lower cadence and velocity, shorter step and stride lengths, longer step and stride times, longer single and double support phases, shorter toe-off phase for both lead and contralateral legs (Table 1).

The step width was significantly greater in the patient after anterior cruciate ligament reconstruction than in the healthy subject.

The initial contact time for the contralateral leg did not differ between the patient and the healthy subject.

The changes detected during the test suggest a gait pattern disturbance in the patient characterized by a slower, shorter, wider step with longer step intervals. We think that these changes are associated with 2 factors. First, the gait pattern may have undergone pathologic changes in the early postoperative period when the patient had to use crutches for locomotion and wear braces. Second, proprioception in the operated knee joint was impaired, which affected coordination in and between the muscles surrounding the knee joint.

3D MCA can be used to measure the amplitude of movement for different body parts at different stages of gait cycle and to compare the obtained data with the podometry data.

The amplitudes of movement of the hip, knee and ankle joints observed in the patient and the healthy participant are shown in the graphs (Fig. 1–4). The analysis revealed that hip flexion and extension amplitudes in the operated (left) leg were narrower than in the right leg (Fig. 1, Table 2).

The analysis showed that the amplitude of left lower leg flexion and extension at the knee joint during one gait cycle was reduced in the patient, as compared with the healthy subject (Fig. 2, Table 3).

Ankle flexion and extension amplitudes during walking were smaller for the operated leg than for the right healthy leg (Fig. 3, Table 4).

The amplitude of movement in the lower leg joints was reduced due to the impaired gait pattern and a reduction in the passive and active range of motion in the lower leg, which again could be explained by immobilization after surgery (the need to wear an orthosis/brace) and the lack of adequate movement stereotype. The range of motion in the joints may be affected by the choice of the donor site for anterior cruciate ligament reconstruction. Further research is needed to test this hypothesis.

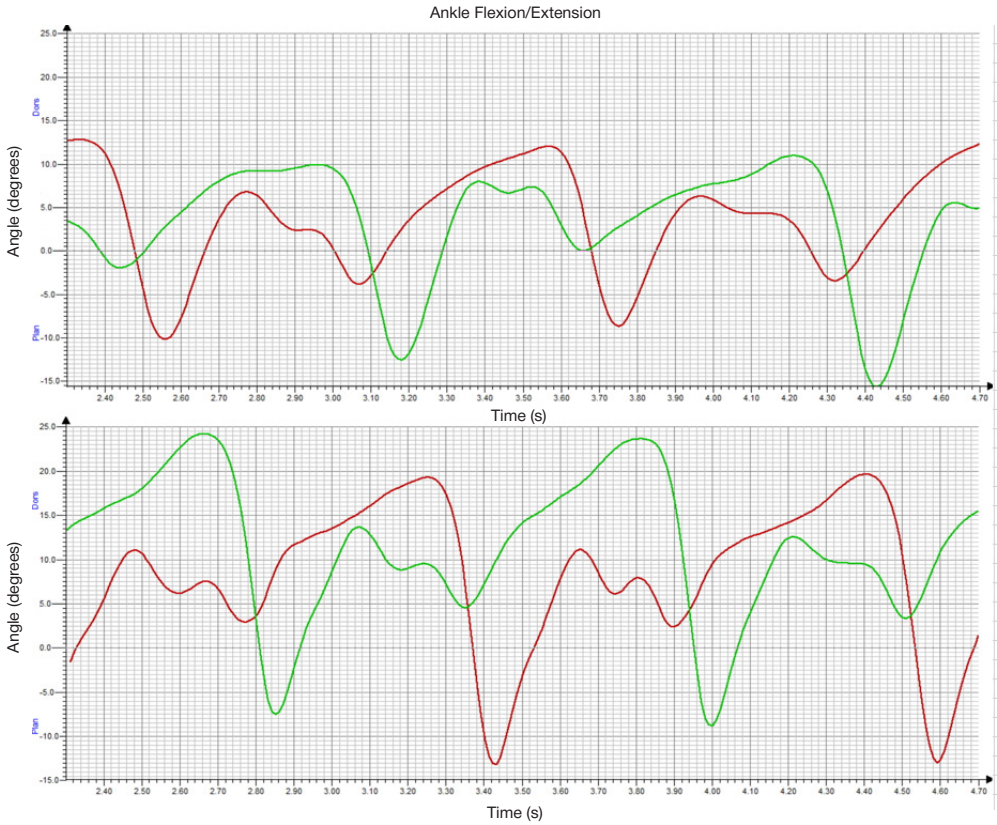

Fig. 3. Ankle flexion and extension during one cycle in the patient with injuries to the knee ligament apparatus (*top*) and the healthy subject (*bottom*)

Table 4. Mean ankle extension and flexion angles and amplitudes during one gait cycle in the patient with injuries to the knee ligament apparatus and the healthy subject

	Patient with injured knee ligament apparatus		Healthy subject	
	Left leg	Right leg	Left leg	Right leg
	Me [P_{25}; P_{75}]			
Angle 1	–8,24	–15,65	–9,59	–9,18
	[–9,41; –7,01]	[–17,19; –14,37]	[–12,05; –7,8]	[–10,39; –8,52]
Angle 2	13,48	10,79	19,76	23,52
	[12,99; 14,71]	[9,25; 11,47]	[18,26; 20,49]	[22,11; 24,22]
Δ	21,9	26,21	29,33	32,26
	[20,98; 22,85]	[25,16; 27,07]	[28,58; 30,28]	[30,83; 33,91]

We also found that the degree of left knee joint rotation was significantly lower than in the right knee joint (Fig. 4, Table 5). Rotation asymmetry in the knee joint was observed in the healthy subject, too, but it was slight.

Discussion clinical case

A study reported the use of MCA during a single leg hop test for assessing recovery of static and locomotor function in athletes after anterior cruciate ligament repair [12]. The following parameters were evaluated: knee flexion at initial contact, peak knee flexion, knee flexion range of motion, and knee valgus range of motion in the frontal and sagittal planes. The speed and rhythm of the gait were not studied. The authors concluded that MCA could be recommended as a simple and accurate method for assessing knee joint stability and predicting changes of returning to sports after anterior cruciate ligament reconstruction [12].

Another study employed MCA to assess the risk of injury in athletes following anterior cruciate ligament reconstruction [13]. The researchers performed the motion analysis of leg movements and assessed stability of the knee joint during walking, running, kicking the ball with moderate force and ball lashing. In addition to the speed and rhythm of gait, the researchers measured the ratios of flexion and extension angles in the operated and healthy knees during running and ball kicking. The angular characteristics of movements were not studied. It was concluded that MCA could be used as independently and as a complementary tool for gait analysis [13].

Another study was conducted in female athletes with anterior cruciate ligament injury; MCA was applied to analyze the mean knee flexion and the mean valgus angles during the initial contact, the internal and external rotation angles of the knee joint, and the mean peak vertical ground reaction force. The anterior cruciate ligament injury was attributed to a combination of valgus loading and internal knee joint rotation [14].

In another publication, the mechanisms of a slip-catch injury to the anterior cruciate ligament were investigated using MCA. The following parameters were analyzed: the knee

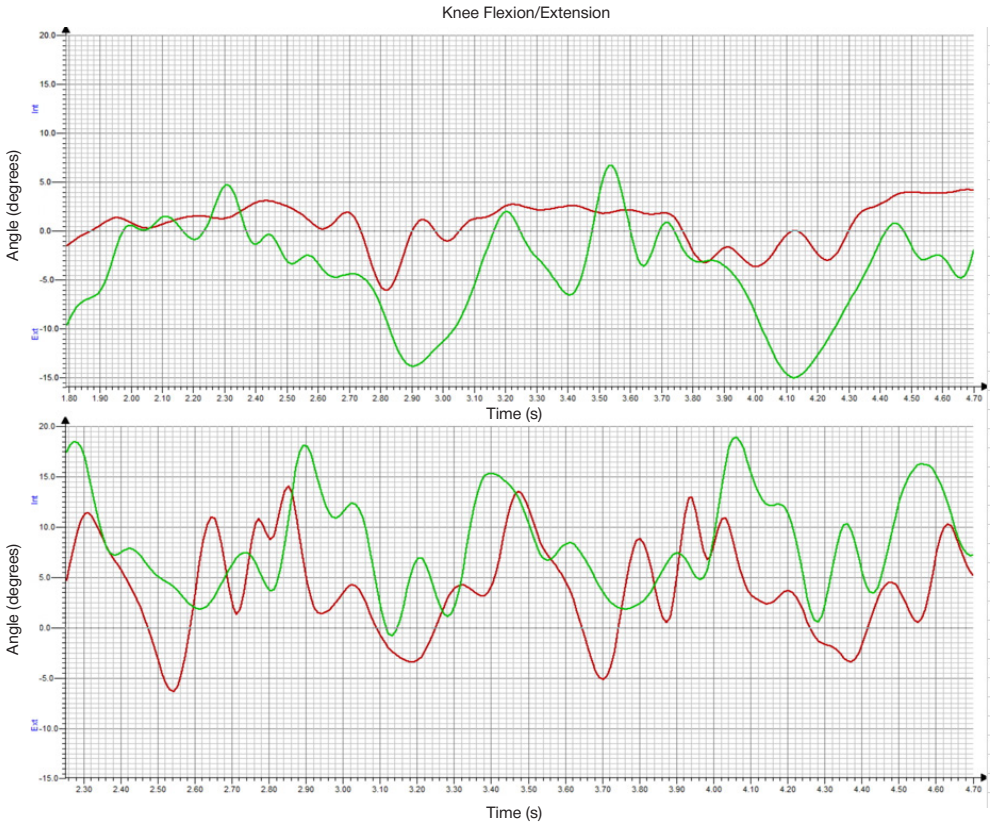

Fig. 4. Knee joint rotation during one gait cycle in the patient with injuries to the knee ligament apparatus (*top*) and the healthy subject (*bottom*)

Table 5. Mean knee rotation angles and amplitudes during one gait cycle in the patient with injuries to the knee ligament apparatus and the healthy subject

	Patient with injured knee ligament apparatus		Healthy subject	
	Left leg	Right leg	Left leg	Right leg
	Me [P_{25}; P_{75}]			
Angle 1	–5,83	–14,55	–7,28	0,57
	[–7,48; –4,96]	[–15,73; –13,37]	[–8,23; –5,12]	[–0,64; 1,16]
Angle 2	2,41	4,12	14,27	17,78
	[1,78; 2,79]	[3,13; 5,54]	[13,91; 15,17]	[17,02; 18,9]
Δ	8,15	19,01	21,59	17,05
	[7,04; 9,58]	[17,2; 20,69]	[19,54; 22,75]	[16,03; 18,8]

flexion angle, the tibial internal rotation angle, and the mean knee valgus angle. Speed, rhythm and angular parameters of motion in the hip and ankle joints were not studied. The study concluded that valgus loading, internal knee joint rotation and abduction were significant contributors to the slip-catch injury [15].

Changes in movement characteristics observed in the operated knee (reduced hip, knee and ankle flexion and extension, reduced left knee rotation) are consistent with the findings of other researchers [16, 17].

CONCLUSION

3D MCA is an informative method for the analysis of subtle changes in the biomechanics of walking in patients with anterior cruciate ligament injuries. The method generates valuable data about the amplitude and angular parameters of motion, and the speed and rhythm of gait.

Further research is needed to clarify how long the pathologic changes to the gait may persist and whether they can be managed through rehabilitation.

References

1. Povrezhdenie svjazok kolennogo sustava. Klinicheskie rekomendacii. Obshherossijskaja obshhestvennaja organizacija «Associacija travmatologov-ortopedov Rossii (ATOR)». 2020; 36 s. Russian.
2. Korolev AV, Afanasev AP, Ilin DO, Gerasimov DO, Ryazancev MS, Kadancev PM. Povrezhdenija zadnej krestoobraznoj svjazki: biomehanika, osnovnye napravlenija diagnostiki, lechenija i profilaktiki vtorichnogo osteoartrita. Genij ortopedii. 2020; 26 (3): 413–8. DOI: 10.17116/hirurgia2020091130. Russian.
3. Fedulova DV, Yamaletdinova GA. Metody ocenki processa vosstanovlenija posle rekonstrukcii perednih krestoobraznyh svjazok kolennogo sustava. Nauchno-sportivnyj vestnik Urala i Sibiri. 2018; 1 (17): 68–85. Russian.
4. Razvalyaeva DV, Razvalyaev AS, Eremushkin MA, Styazhkina EM. Sravnitel'naja ocenka jeffektivnosti konservativnoj i operativnoj taktiki lechenija pacientov posle travmy perednej krestoobraznoj svjazki s ispol'zovaniem robotizirovannoj mehanoterapevticheskoj sistemy "CON-TREX". Vestnik vosstanovitel'noj mediciny. 2019; 5: 35–39. Russian.
5. Valiev YeYu, Hakimov RN, Ubajdullaev BS. Sovremennyj vzgljad na lechenie kompleksnyh povrezhdenij svjazok kolennogo sustava. Vestnik jekstrennoj mediciny. 2015; 2: 81–84. Russian.
6. Ma Y, Soatto S, Košecká J, Sastry SS. An invitation to 3D vision. From Images to Geometric Models. Interdisciplinary Applied Mathematics. New York: Springer, 2004.
7. Wang l, Hu W, Tan T. Recent developments in human motion analysis. Pattern Recognition. 2003; 36 (3): 585–601. DOI: 10.1016/S0031-3203(02)00100-0.
8. Skvorcov DV. Metodika issledovanija kinematiki dvizhenij i sovremennye standarty. Videoanaliz. Lechebnaja fizkul'tura i sportivnaja medicina. 2012; 12: 4–10. Russian.
9. Cappozzo A, Cappello A, Croce UD, Pensalfini F. Surface-marker cluster design criteria for 3-D bone movement reconstruction. IEEE Transactions on Biomedical Engineering. 1997; 44 (12): 1165–74. DOI: 10.1109/10.649988.
10. Hewett TE, Torg JS, Boden BP. Video analysis of trunk and knee motion during non-contact anterior cruciate ligament injury in female athletes: lateral trunk and knee abduction motion are combined components of the injury mechanism. British Journal of Sports Medicine. 2009; 49 (6): 417–22. DOI: 10.1136/bjsm.2009.059162.
11. Asaeda M, Nakamae A, Hirata K, Kono Y, Uenishi H, Adachi N. Factors associated with dynamic knee valgus angle during single-leg forward landing in patients after anterior cruciate ligament reconstruction. Asia-Pacific Journal of Sports Medicine, Arthroscopy, Rehabilitation and Technology. 2020; 24 (22): 56–61. DOI: 10.1016/j.asmart.2020.07.002.
12. Welling W, Benjaminse A, Seil R, Lemmink K, Gokeler A. Altered movement during single leg hop test after ACL reconstruction: implications to incorporate 2-D video movement analysis for hop tests. Knee Surgery Sports Traumatology Arthroscopy. 2018; 26 (10): 3012–9. DOI: 10.1007/s00167-018-4893-7.
13. Preobrazhenskij VYu, Zinovev OV, Sidorenko EV, Galuhin VV, Vnukov DV, Preobrazhenskij AV, i dr. Ocenka fizicheskogo sostojanija sportsmenov posle plastiki perednej krestoobraznoj svjazki s cel'ju preduprezhdenija povtornyh travm. Doktor.ru. 2011; 8 (67): 38–41. Russian.
14. Koga H, Nakamae A, Shima Yo, Iwasa J, Myklebust G, Engebretsen L, et al. Mechanisms for noncontact anterior cruciate ligament injuries: knee joint kinematics in 10 injury situations from female team handball and basketball. The American journal of sports medicine. 2010; 38 (11): 2218–25. DOI: 10.1177/0363546510373570.
15. Bere T, Mok K, Koga H, Krosshaug T, Nordsletten L, Bahr R. Kinematics of anterior cruciate ligament ruptures in World Cup alpine skiing: 2 case reports of the slip-catch mechanism. The American journal of sports medicine. 2013; 41 (5): 1067–73. DOI: 10.1177/0363546513479341.
16. Clark N, Forshey T, Mulligan I, Kindel C. Knee mechanics during a change of direction movement in division I athletes following full return to sport from anterior cruciate ligament reconstruction. Physical Therapy in Sport. 2018; 35 (4): 75–78. DOI: 10.1016/j.ptsp.2018.11.008
17. Sharifmoradi K, Karimi M, Hoseini Y. Evaluation of the Asymmetry of Leg Muscles Forces in the Subjects with Anterior Cruciate Ligament Reconstruction. The Journal of Knee Surgery. 2019; 34 (4): 357–62. DOI: 10.1055/s-0039-1695703.

Литература

1. Повреждение связок коленного сустава. Клинические рекомендации. Общероссийская общественная организация «Ассоциация травматологов-ортопедов России (АТОР)». 2020; 36 с.
2. Королев А. В., Афанасьев А. П., Ильин Д. О., Герасимов Д. О., Рязанцев М. С., Каданцев П. М. Повреждения задней крестообразной связки: биомеханика, основные направления диагностики, лечения и профилактики вторичного остеоартрита. Гений ортопедии. 2020; 26 (3): 413–8. DOI: 10.17116/hirurgia2020091130.
3. Федулова Д. В., Ямалетдинова Г. А. Методы оценки процесса восстановления после реконструкции передних крестообразных связок коленного сустава. Научно-спортивный вестник Урала и Сибири. 2018; 1 (17): 68–85.
4. Разваляева Д. В., Разваляев А. С., Еремушкин М. А., Стяжкина Е. М. Сравнительная оценка эффективности консервативной и оперативной тактики лечения пациентов после травмы передней крестообразной связки с использованием роботизированной механотерапевтической системы "CONTREX". Вестник восстановительной медицины. 2019; 5: 35–39.
5. Валиев Э. Ю., Хакимов Р. Н., Убайдуллаев Б. С. Современный взгляд на лечение комплексных повреждений связок коленного сустава. Вестник экстренной медицины. 2015; 2: 81–84.
6. Ma Y, Soatto S, Košecká J, Sastry SS. An invitation to 3D vision. From Images to Geometric Models. Interdisciplinary Applied Mathematics. New York: Springer, 2004.
7. Wang I, Hu W, Tan T. Recent developments in human motion analysis. Pattern Recognition. 2003; 36 (3): 585–601. DOI: 10.1016/S0031-3203(02)00100-0.
8. Скворцов Д. В. Методика исследования кинематики движений и современные стандарты. Видеоанализ. Лечебная физкультура и спортивная медицина. 2012; 12: 4–10.
9. Cappozzo A, Cappello A, Croce UD, Pensalfini F. Surface-marker cluster design criteria for 3-D bone movement reconstruction. IEEE Transactions on Biomedical Engineering. 1997; 44 (12): 1165–74. DOI: 10.1109/10.649988.
10. Hewett TE, Torg JS, Boden BP. Video analysis of trunk and knee motion during non-contact anterior cruciate ligament injury in female athletes: lateral trunk and knee abduction motion are combined components of the injury mechanism. British Journal of Sports Medicine. 2009; 49 (6): 417–22. DOI: 10.1136/bjsm.2009.059162.
11. Asaeda M, Nakamae A, Hirata K, Kono Y, Uenishi H, Adachi N. Factors associated with dynamic knee valgus angle during single-leg forward landing in patients after anterior cruciate ligament reconstruction. Asia-Pacific Journal of Sports Medicine, Arthroscopy, Rehabilitation and Technology. 2020; 24 (22): 56–61. DOI: 10.1016/j.asmart.2020.07.002.
12. Welling W, Benjaminse A, Seil R, Lemmink K, Gokeler A. Altered movement during single leg hop test after ACL reconstruction: implications to incorporate 2-D video movement analysis for hop tests. Knee Surgery Sports Traumatology Arthroscopy. 2018; 26 (10): 3012–9. DOI: 10.1007/s00167-018-4893-7.
13. Преображенский В. Ю., Зиновьев О. В., Сидоренко Е. В., Галухин В. В., Внуков Д. В., Преображенский А. В., и др. Оценка физического состояния спортсменов после пластики передней крестообразной связки с целью предупреждения повторных травм. Доктор.ру. 2011; 8 (67): 38–41.
14. Koga H, Nakamae A, Shima Yo, Iwasa J, Myklebust G, Engebretsen L, et al. Mechanisms for noncontact anterior cruciate ligament injuries: knee joint kinematics in 10 injury situations from female team handball and basketball. The American journal of sports medicine. 2010; 38 (11): 2218–25. DOI: 10.1177/0363546510373570.
15. Bere T, Mok K, Koga H, Krosshaug T, Nordsletten L, Bahr R. Kinematics of anterior cruciate ligament ruptures in World Cup alpine skiing: 2 case reports of the slip-catch mechanism. The American journal of sports medicine. 2013; 41 (5): 1067–73. DOI: 10.1177/0363546513479341.
16. Clark N, Forshey T, Mulligan I, Kindel C. Knee mechanics during a change of direction movement in division I athletes following full return to sport from anterior cruciate ligament reconstruction. Physical Therapy in Sport. 2018; 35 (4): 75–78. DOI: 10.1016/j.ptsp.2018.11.008
17. Sharifmoradi K, Karimi M, Hoseini Y. Evaluation of the Asymmetry of Leg Muscles Forces in the Subjects with Anterior Cruciate Ligament Reconstruction. The Journal of Knee Surgery. 2019; 34 (4): 357–62. DOI: 10.1055/s-0039-1695703.

BIOIMPEDANCE ANALYSIS OF BODY COMPOSITION IN THE DIAGNOSIS OF PHYSICAL DEVELOPMENT DISORDERS IN CHILDREN AND ADOLESCENTS

Gavryushin MYu ✉, Sazonova OV, Gorbachev DO, Borodina LM, Frolova OV, Tupikova DS, Berezhnova OV, Trubetskaya SR

Samara State Medical University, Samara, Russia

Traditionally, anthropometric method is used in clinical practice for the diagnosis of excess body weight. Obesity is the excess development of primarily visceral and subcutaneous adipose tissue, which can be diagnosed by bioimpedance analysis (BIA). The study was aimed to assess the role of BIA of body composition in the diagnosis of the physical development disorders in children and adolescents. Anthropometric assessment and BIA were performed in 431 Samara school students aged 12–16 of the health status groups I and II (230 boys and 201 girls). The results were analyzed with the use of the regional regression scores, BAZ indices, and the body fat percentage values. The results of estimation using the regression scores showed that 22.61% of boys and 23.43% of girls were overweight, while more than 2/3 of the sample had a normal pattern of physical development. The BAZ indices revealed a significantly higher proportion of overweight children among boys (25.7%), than among girls (11.5%, $p < 0.01$). The body fat percentage fluctuations based on the BIA data were found not only in children with disharmonious physical development, but also in 60% of children with normal body weight. Moreover, the data of BIA confirmed the body weight fluctuations, revealed with the use of the regression scores, in the significantly larger number of cases compared to the low body weight and excess body weight, diagnosed based on the BAZ indices. Accordingly, anthropometric analysis with the use of the regional regression scores may be used at the baseline for the early diagnosis of the nutritional status disorders in children. To confirm overweight and obesity in children, as well as to provide further treatment, the reliable method for estimation of the body fat content is required, which may be the method of BIA.

Keywords: hygiene of children and adolescents, physical development, body mass index, regression scales, bioimpedance analysis

Funding: the study was supported by the grant from the President of the Russian Federation (MK-5809.2021.3).

Author contribution: Gavryushin MYu — research initiator, design, data acquisition; Sazonova OV — scientific management; Gorbachev DO, Borodina LM — literature analysis, manuscript writing and editing; Frolova OV, Tupikova DS, Berezhnova OV — data acquisition, processing of the results; Trubetskaya SR — processing of the results, manuscript writing.

Compliance with ethical standards: the study was approved by the Ethics Committee of the Samara State Medical University (protocol № 2 dated February 24, 2021). The informed consent was obtained from all participants (their legal representatives).

✉ **Correspondence should be addressed:** Mikhail Yu. Gavryushin
Chapayevskaya, 89, Samara, 443099, Russia; m.yu.gavryushin@samsmu.ru

Received: 01.12.2021 **Accepted:** 15.12.2021 **Published online:** 28.12.2021

DOI: 10.24075/brsmu.2021.062

БИОИМПЕДАНСНЫЙ АНАЛИЗ СОСТАВА ТЕЛА В ДИАГНОСТИКЕ НАРУШЕНИЙ ФИЗИЧЕСКОГО РАЗВИТИЯ ДЕТЕЙ И ПОДРОСТКОВ

М. Ю. Гаврюшин ✉, О. В. Сазонова, Д. О. Горбачев, Л. М. Бородина, О. В. Фролова, Д. С. Тупикова, О. В. Бережнова, С. Р. Трубецкая

Самарский государственный медицинский университет, Самара, Россия

В клинической практике для диагностики избыточной массы тела и ожирения традиционно используют антропометрический метод. Ожирение — это избыточное развитие прежде всего висцеральной и подкожной жировой ткани, которое может быть диагностировано методом биоимпедансометрии (БИА). Целью исследования было оценить роль биоимпедансного анализа состава тела в диагностике нарушений физического развития детей и подростков. Проведено антропометрическое и биоимпедансометрическое обследование 431 самарского школьника I и II групп здоровья в возрасте 12–16 лет (230 мальчиков и 201 девочка). Анализ результатов проводили по региональным шкалам регрессии, показателю BAZ и доле жировой массы. Результаты оценки по шкалам регрессии выявили 22,61% мальчиков и 23,43% девочек с избыточной массой тела, при этом более 2/3 выборки имели нормальное физическое развитие. Показатель BAZ выявил значимо большее число детей с избыточной массой тела среди мальчиков (25,7%), чем среди девочек (11,5%, $p < 0,01$). Отклонения доли жировой массы по данным БИА определены не только среди детей с дисгармоничным физическим развитием, но и среди 60% детей с нормальной массой тела. При этом выявленные по шкалам регрессии отклонения массы тела данные БИА подтверждали в большем числе случаев, нежели диагнозы избыточной или недостаточной массы тела, полученные по индексу BAZ. Исходя из этого, первоначально, для своевременной диагностики нарушений нутритивного статуса у детей, может быть использован антропометрический анализ с применением региональных шкал регрессии. Для подтверждения избыточной массы тела и ожирения у детей, а также для дальнейшей терапии необходим достоверный метод оценки жировой составляющей организма, в качестве которого может выступать метод БИА.

Ключевые слова: гигиена детей и подростков, физическое развитие, индекс массы тела, шкалы регрессии, биоимпедансный анализ

Финансирование: работа выполнена при поддержке гранта Президента РФ (МК-5809.2021.3).

Вклад авторов: М. Ю. Гаврюшин — инициатор исследования, дизайн, сбор материала; О. В. Сазонова — научное руководство; Д. О. Горбачев, Л. М. Бородина — анализ литературы, подготовка и редактирование рукописи; О. В. Фролова, Д. С. Тупикова, О. В. Бережнова — сбор материала, обработка результатов; С. Р. Трубецкая — обработка результатов, подготовка рукописи.

Соблюдение этических стандартов: исследование одобрено этическим комитетом ФГБОУ ВО СамГМУ Минздрава России (протокол № 2 от 24 февраля 2021 г.). Добровольное информированное согласие было получено для каждого участника (его законного представителя).

✉ **Для корреспонденции:** Михаил Юрьевич Гаврюшин
ул. Чапаевская, д. 89, г. Самара, 443099, Россия; m.yu.gavryushin@samsmu.ru

Статья получена: 01.12.2021 **Статья принята к печати:** 15.12.2021 **Опубликована онлайн:** 28.12.2021

DOI: 10.24075/vrgmu.2021.062

Physical development is an essential criterion of the comprehensive health assessment, performed during the routine check-ups of children and adolescents, which reflects the impact of the complex set of factors [1–3]. According to the research, carried out in the regions of our country, a little over 60% of boys and about 67% of girls are characterized by the harmonious physical development. Disharmonious physical development is due more to the excess body weight, which is found in 18% of boys and 14% of girls [3–6]. The importance of the excess body weight issue is defined by high prevalence of pathological conditions and complications, high risk of obesity with comorbidities, resulting in the young patients' disability [7, 8]. Traditionally, anthropometric method, involving the analysis of the results obtained by the standard measurement of height and body weight, as well as the calculation of the estimation indices, mostly the body mass index (BMI), is used in clinical practice for the diagnosis of excess body weight [9]. The World Health Organization has developed the BMI maps for children and adolescents aged 2–19 to analyze the calculation results [10]. In addition, the weight to height ratio could be assessed using the regression scores, centile charts, and sigma deviations [10].

Obesity is an excess development of the visceral and subcutaneous adipose tissue rather than the total body fat mass [11–13]. Despite the positive correlation between the BMI and the child's anthropometric data, BMI does not reflect the actual body fat percentage, which is continuously changing in children during various age periods. The example of such period is the childhood intensive period of growth, when BMI may indicate the normal weight to height ratio, and the actual fat mass may be underestimated, which could result in the erroneous interpretation of the study results [8, 14]. In this regard, the use of the anthropometric method only as the diagnostic criterion of overweight and obesity could be questionable. Moreover, low comparability of the research results may be the consequence of the use of different anthropometric diagnostic parameters [3, 6, 9, 15].

In contrast, biophysical methods ensure higher accuracy of the results when measuring the body weight characteristics. Bioimpedance analysis (BIA) of body composition has become the most widely used method. BIA is based on the difference between the resistance (impedance) values of the fat mass and fat-free (lean) body mass, as well as on the total body water and body composition. The assessment results are used in clinical practice to analyze the nutritional status and nutrient intake, the risk of metabolic syndrome, obesity, disorders of cardiovascular system and other systems of the body; the results are also used as the diagnostic criteria for estimation of the therapy efficacy in patients with various diseases [16–19]. For its part, comparison of the results of bioimpedance measurement of the fat mass as a percentage of the body mass and BMI in healthy children shows that a broad range of the body fat percentage values corresponds to the same BMI values [20]. Thus, the use of data, obtained by BIA of body composition, in combination with the anthropometric data as the diagnostic criteria for the abnormal patterns of the children's physical development needs to be studied.

The study was aimed to assess the role of BIA of body composition in the diagnosis of the physical development disorders in children and adolescents.

METHODS

The cross-sectional cohort study of the prevalence of physical development disorders among the secondary school students of the general educational institutions in Samara based on the anthropometric and bioimpedance measurement data was carried out. The children were examined at their educational institutions from March to May 2021, with interruptions for spring vacation (March 22–28) and public holidays. A total of 431 children aged 12–16 (the median age was 13 years 8 months) were examined: 230 boys (53.4%) and 201 girls (46.6%) of grades 5–9 of the general education schools.

Inclusion criteria: age 12–16 years, permanent residence in the territory of Samara region; compliance with the health status group I or II based on medical documentation; informed consent to the study participation submitted by parents (legal representatives). Exclusion criteria: age at the time of examination less than 11 years 6 months and one day or over 16 years 6 months and one day; chronic disorders; taking medications; prominent limb swelling; permanent residence outside of Samara region; no informed consent to participation or refusal of participation provided by parents (legal representatives).

Anthropometric indicators were measured in the following way: body height was measured with the MSK-233 stadiometer (Medstalkonstruktsiya; Russia) to within 5 mm, and body weight was measured with the VEM-150-A1 medical scales (Massa-K; Russia) to within 50 g. Body composition was defined by BIA using the ABC-01 internal environment analyzer (Medass; Russia) with the current probe frequency of 50 kHz in accordance with the tetrapolar electrode scheme, involving electrode positioning on the wrist and ankle when the subject is in the supine position. Examination was not preceded by intense physical activity, eating or drinking. Room temperature was controlled in the rooms, where the examination was carried out.

The children's physical development was assessed based on the height to weight ratio in two different ways. The first method involved estimation of physical development with the use of the regional regression models, fitted with body weight as dependent variable and height, developed for Samara region [21]. The second method involved calculating the BMI for age Z-score (BAZ), and the resulting values were analyzed in accordance with the WHO standards [10] using the WHO AnthroPlus software (2009) (WHO; Switzerland) [22]. BMI was calculated as the child's weight (kg) divided by the square of height (m2). Nutritional status was further assessed based on the data obtained by BIA of body composition, the body fat percentage (%BF). The criteria for the estimation of the results are presented in Table 1.

The raw data were acquired and stored using the Microsoft Excel 2013 software (Microsoft; USA). Statistical processing

Table 1. Criteria for assessment of the children's physical development

Indicator	Assessment methods		
	BAZ, SDS [10]	Regression scores, σR [22]	BIA, %BF [23]
Underweight	< –2.0	< –1.0	< 15th percentile
Normal development	from –2.0 to +1.0	from +1.0 to +1.5	from 25th to 75th percentile
Overweight	from +1.0 to +2.0	≥ + 1.5	from 85th to 97th percentile
Obesity	≥ + 2.0	–	≥ 97th percentile

Table 2. Distribution of anthropometric indicators based on the BAZ indices in the studied sample of school students

Studied group	Z-score				
	< –2.0	from –2.0 to –1.0	from –1.0 to +1.0	from +1.0 to +2.0	≥ + 2.0
Boys, abs. (%)	4 (1.7)	16 (7)	131 (56.9)	59 (25.7)	20 (8.7)
Girls, abs. (%)	3 (1.5)	32 (15.9)	124 (61.7)	23 (11.5)	19 (9.4)
All examined children, abs. (%)	7 (1.6)	48 (11.1)	255 (59.1)	82 (19.1)	39 (9.1)

Note: normal values are highlighted

of the results was performed by the analysis of variance with the Statistica 13.1 software package (StatSoft Inc.; USA). Statistical significance of the differences was analyzed using the Pearson's χ^2 test. The differences were considered significant when $p < 0.05$.

RESULTS

Analysis of anthropometric traits in the studied group of children showed that the gradual increase in the height was observed both in boys and girls aged 12–16. In view of the fact that body weight is a dynamic parameter, depending primarily on the actual nutrition and the levels of physical activity, the analysis of dynamic changes in this trait has revealed no gradual increase with age and has reflected the correlation of the mean values with the percentage of children with the physical development disorders in the specified age group (Fig. 1).

Thus, when assessing physical development using the regional regression scores, it was found that more than 2/3 of the examined school students were constituted by children with the normal pattern of physical development, while the percentage of children, who's body weight deviated from the reference values, was 30.44% in boys, and 38.36% in girls. However, the percentage of overweight children in boys and girls was the same (22.61% and 23.43%), and the proportion of underweight children was higher in the group of girls (14.93%), than in the group of boys (7.83%, $p < 0.01$).

Estimation of physical development based on the BAZ indices showed that in the studied group, children with normal body weight (70.2%) prevailed among both boys (147/230, 63.9%), and girls (157/201, 77.6%). Low body weight was found in seven children (1.6%) in the studied sample: four boys, and three girls. Excess body weight and obesity were revealed in less than one third of the surveyed children (in 19.1%, and 9.1%, respectively). Furthermore, there were no significant differences in the percentage of obese children among boys and girls ($p = 0.207$), while the proportion of overweight children was significantly higher in boys, than in girls ($p < 0.01$). Severe obesity (BAZ > +3.0) was found in three boys, and two girls (Table 2).

Comparison of the results, obtained by assessing physical development in accordance with the regional scores and the WHO standards (BAZ, Z-score), showed that Z-score revealed a significantly larger number of overweight and obese children among boys ($p < 0.01$). Regression scores revealed the insignificantly higher proportion of underweight boys ($p = 0.285$) and the significantly higher proportion of underweight girls ($p < 0.01$) (Fig. 2).

Based on the BIA data, a half of children in the studied sample had the excessive fat content. Furthermore, excess body weight was found in 42.2% of boys and 40.8% of girls, and obesity was found in 6.5% and 7.5%, respectively. Based on the %BF, 6.1% of boys and 3.5% were underweight. Thus, BIA of body composition in children revealed a normal body fat percentage, appropriate for age, gender, and anthropometric data, only in a half of the surveyed children, which made up 45.2% in the group of boys, and 48.3% in the group of girls (Fig. 3).

When assessing body fat percentage in children with various levels of physical development based on the regression scores, the following was found: in the group with normal physical development, the proportion of children with normal body fat percentage was 40%, while 44.7% of the surveyed individuals had excess fat content, and about 16.8% had low fat content. In the group of overweight children, high fat content values were found only in 72.7% of cases, which was indicative of the excess in other body weight characteristics (skeletal muscle mass, total body water, etc.) in 27.3% of children in this subgroup. The surveyed underweight children had a low body fat percentage in a half of cases (Fig. 4).

Studying the nutritional status in children with the relevant BAZ characteristics revealed 39.7% of surveyed individuals with normal body fat percentage; 21.9% of children had the low body fat percentage, and 38.2% of children had the excess body fat content. Among the surveyed children with BAZ between +1.0 and +2.0 Z-score (overweight), excess body fat percentage was revealed only in 56.1% of cases, 36.6% had a normal body fat content, and 7.3% had a low fat content. Obesity, defined based on BAZ, was confirmed by the %BF values in 16.7% of cases, and low body weight was confirmed in 71.4% of cases of the appropriate subgroup of the sample (Fig . 4).

Thus, body weight aberrations, diagnosed based on the regional scores, were confirmed by the data of BIA in the

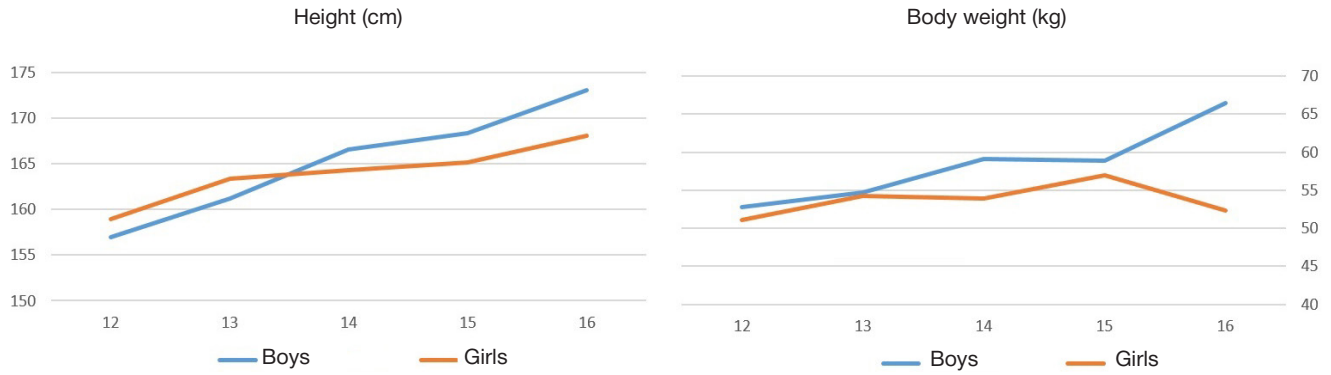

Fig. 1. Age-dependent changes of anthropometric indicators of physical development in the studied sample of children

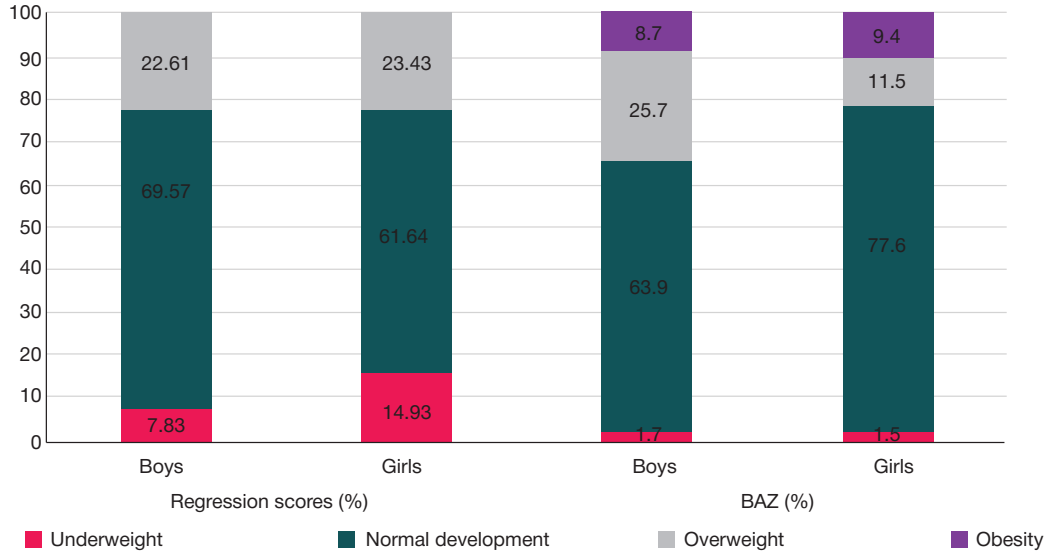

Fig. 2. Comparison of the results of the physical development assessment with the use of regression scores and BAZ indices in the groups of boys and girls, constituting the studied sample

significantly larger number of cases compared to the results of the assessment based on the BAZ indices (82/431, 19.7% and 61/431, 14.15%, $p < 0.05$).

DISCUSSION

Our research, focused on studying the anthropometric indicators, involving the assessment of the school students aged 12–16 based on the regression scores, as well as on the calculated BAZ indices and %BF values, revealed numerous overweight and obese children. When using the anthropometric diagnosis methods, the most pronounced fluctuations of body weight, including the upward (excess weight) and downward (underweight) bias, were identified by assessment, involving the use of regression scores. It is interesting to note that when using the body fat percentage values obtained by BIA as a criterion of excess body weight instead of the results of estimation based on the regional standards and BMI, the proportion of children, who could be diagnosed with overweight and obesity, changed significantly. No significant differences in the number of children with the normal pattern of physical development and children with body weight fluctuations between boys and girls were revealed based on the %BF values. Furthermore, BIA made it possible to reveal a large proportion of overweight and obese children among the individuals with the normal pattern of physical development (based on the regression scores and BAZ indices).

The period of development between 12–16 years of age is a critical period, when the risk of obesity increases by several times [7, 24]. Moreover, 60% of children with excess body weight in adolescence would be obese in adulthood, with the more severe course of obesity, prominent body weight increase and high prevalence of comorbidities, in contrast to the adult-onset obesity [7, 25]. That is why the early detection of premorbid conditions, aimed at adjusting the child's diet and daily routine, is a crucial step in preventive medicine in terms of obesity prevention. According to our study, the results of which are in line with the results, obtained by other researchers [5, 6, 9], the anthropometric trait assessment results could be considered the most important criteria to be used in the routine check-ups, allowing one to refer the child to endocrinologist and nutritionist, and if necessary, for further treatment.

However, the findings showed that only 2/3 of the school students, diagnosed with overweight with the use of anthropometric techniques, had the excess body fat content. Nevertheless, body fat percentage was normal in one third of children in the surveyed sample, and no therapeutic interventions were required. Therefore the method of BIA, allowing one to detect changes not only in the body fat mass, but also in all the fat-free (lean) body mass components, could be considered the diagnostic method, allowing the specialists to start treatment, such as diet therapy, and to dynamically monitor the efficiency of the interventions.

Close practical links between the BIA of body composition and the anthropometric assessment of young patients were frequently discussed in scientific literature [19, 26, 27] with the emphasis on the high level of accountability of the biophysical method. Unfortunately, the diagnostic significance and the

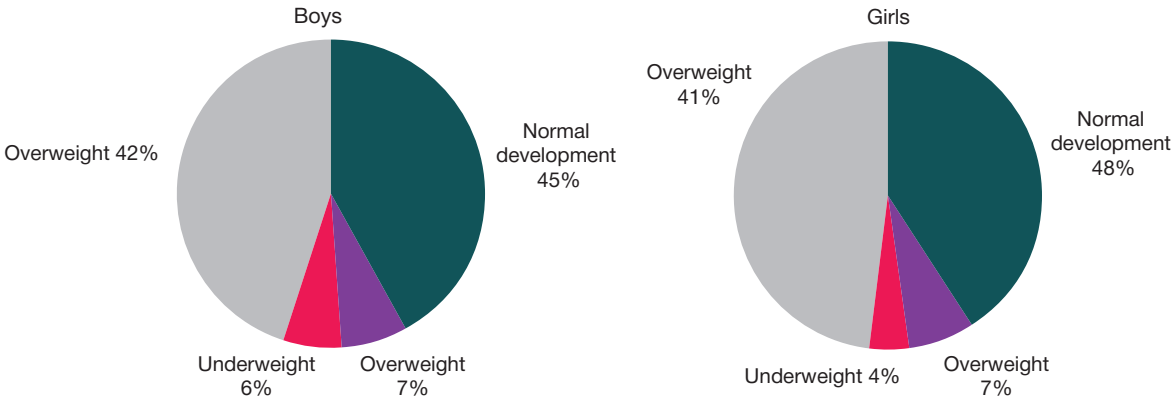

Fig. 3. Distribution of %BF in the groups of boys and girls, constituting the studied sample

Fig. 4. Comparison of %BF distributions depending on the levels of physical development when using regression scores and BAZ indices in the studied sample

criteria for the BIA results interpretation in combination with the anthropometric data have not been reflected in the federal guidelines on the diagnosis and treatment of obesity, which hampers the practical application of the method.

CONCLUSIONS

The study of anthropometric traits in the Samara school students aged 12–16 has revealed a significant proportion of children, having problems with physical development. The highest proportion of children with body weight fluctuations has been revealed by the assessment with the use of the regional age-based and gender-based regression scores, fitted with body weight as dependent variable and height. The analysis of body fat content in children with different levels of physical development has made it possible to identify the excess body fat percentage in children with the normal pattern of physical development (harmonious physical development). Thus, bioimpedance analysis of body composition in combination with the anthropometric data could be used as a reliable method for the diagnosis of the nutritional status disorders in children and adolescents.

References

1. Chernykh AM, Kremleva AS, Belova AI. 20-year monitoring of physical developmental characteristics in school-age children and adolescents living in Kursk. Russian Bulletin of Hygiene. 2021; (1): 42–6. DOI: 10.24075/rbh.2021.008.
2. Milushkina OYu, Skoblina NA, Markelova SV, Tatarinchik AA, Melikhova EP, Libina II, et al. The impact of electronic devices on the physical growth and development of modern youth and recommendations on their safe use. Bulletin of RSMU. 2019; (4): 83–9. DOI: 10.24075/brsmu.2019.046.
3. Novikova II, Gavrish SM, Romanenko SP, Sorokina AV, Serenko VV, Kreimer MA. Comparative assessment of the informativity of indication methodsexcess body weight. Sanitary doctor. 2021; (4) 67–8. DOI: 10.33920/med-08-2104-07. Russian.
4. Shestera AA, Khmelnitskaya EA, Kiku PF, Perelomova OV, Kaerova EV, Sabirova KM. Physical development and functional possibilities of youth of Vladivostok. Public Health and Life Environment. 2019; (11): 61–5. DOI: https://doi.org/10.35627/2219-5238/2019-320-11-61-65. Russian.
5. Latyshevskaya NI, Yatsyshen VV, Davidenko LA, Yatsyshen TL. Dynamics of anthropometric indices of children and adolescents in the city of Volgograd (1976–2016). Hygiene and Sanitation. 2018; 97(9): 844–7. DOI: http://dx.doi.org/10.18821/0016-9900-2018-97-9-844-847. Russian.
6. Tsukareva EA, Avchinnikov AV, Alimova IL. Assessment of physical development and diet of primary school children in Smolensk. Voprosy pitaniia. 2019; 88 (4): 34–40. DOI: 10.24411/0042-8833-2019-10039. Russian.
7. Gavryushin MYu, Sazonova OV, Milushkina OYu, Skoblina NA, Borodina LM, Gorbachev DO. Actual problems of assessment and correction of the nutritional status of modern children. In: Gerasimenko NF, Glybochko PV, Esaulenko IE, Popov VI, Starodubov VI, Tutelyan VA, editors. Youth health: new challenges and prospects: a monograph in 5 vols. Vol. 3: Technologies for reducing health risks. Prevention and medical examination. Healthy eating. Moscow; 2019. p. 250–70. Russian.
8. Girsh YaV, Gerasimchik OA. The role and place of bioimpedance analysis assessment of body composition of children and adolescents with different body mass. Bulletin of Siberian Medicine. 2018; 17 (2): 121–32. DOI: https://doi.org/10.20538/1682-0363-2018-2-121-132. Russian.
9. Namazova-Baranova LS, Yeletskaya KA, Kaytukova EV, Makarova SG. Evaluation of the physical development of children of secondary school age: an analysis of the results of a cross-sectional study. Pediatric pharmacology. 2018; 15 (4): 333–42. DOI: https://doi.org/10.15690/pf.v15i4.1948. Russian.
10. De Onis M, Onyango AW, Borghi E, et al. Development of a WHO growth reference for school-aged children and adolescents. Bulletin of the World Health Organization. 2007; (85): 660–7. DOI: 10.2471/blt.07.043497.
11. Borodkina DA, Gruzdeva OV, Kvitkova LV, Barbarash OL. Body fat distribution: the answer to the apparent paradox of obesity

in cardiology? Obesity and metabolism. 2017; 14 (2): 3–8. DOI: 10.14341/omet201723-8. Russian.
12. Demyanenko IA, Tkach AV. Functional morphology of adipose tissue and its role in the formation of metabolic syndrome. Crimea Journal of Experimental and Clinical Medicine. 2021; 11 (1): 51–60. DOI: 10.37279/2224-6444-2021-11-1-51-60. Russian.
13. Galimov OV, Khanov VO, Ziangirov RA, Galimova ES, Minigalin DM, Galimov DO. Stomach wall changes after gastroplication in patients with morbid obesity. Bulletin of RSMU. 2020; (4): 67–71. DOI: 10.24075/brsmu.2020.041.
14. Grossman DC, Bibbins-Domingo K, Curry SJ, et al. Screening for obesity in children and adolescents us preventive services task force recommendation statement. Journal of the American Medical Association. 2017; 317 (23): 2417–26. DOI: 10.1001/jama.2017.6803.
15. Gritsinskaya VL. Evaluation of physical development of school-age boys in Saint Petersburg with the use of the anthropometric calculator of WHO. Public Health and Life Environment. 2018; (2): 16–19. Russian.
16. Almeida Y, Costa Maia C, Barros N, Moreno L, Carioca A, Loureiro A. Is bioelectrical impedance vector analysis a good indicator of nutritional status in children and adolescents? Public Health Nutrition. 2021; 24 (14): 4408–16. DOI:10.1017/S1368980021002226.
17. Karanikas I, Karayiannis D, Karachaliou A, Papanikolaou A, Chourdakis M, Kakavas S. Body composition parameters and functional status test in predicting future acute exacerbation risk among hospitalized patients with chronic obstructive pulmonary disease. Clinical Nutrition. 2021; 40 (11): 5605–14. DOI: 10.1016/j.clnu.2021.09.035.
18. Canfell OJ, Littlewood R, Wright ORL,Walker JL. Clinical relevance and validity of tools to predict infant, childhood and adulthood obesity: A systematic review. Public Health Nutrition. 2018; 21 (17): 3135–47. DOI: 10.1017/S1368980018001684.
19. Perevoshchikova NK, Seliverstov IA, Drakina SA, Chernykh NS. Bioelectrical impedance analysis in clinical practice. Mother and Baby in Kuzbass. 2021; 3 (86): 11–20. DOI: 10.24412/2686-7338-2021-3-11-20. Russian.
20. Smirnova GA, Andriyanov AI, Kravchenko EV, Konovalova IA. The selection of optimal methods for determining the perfect body weight for the assessment of the nutritional status. Problems of Nutrition. 2019; 88 (5): 39–44. DOI: 10.24411/0042-8833-2019-10052. Russian.
21. Vdovenko SA, Sazonova OV, Ponomarev VA, Mazur LI, Gavryushin MYu, Borodina LM. Ocenochnye tablicy fizicheskogo razvitiya detej i podrostkov shkol'nogo voz-rasta Samarskoj oblasti. Metodicheskie rekomendacii. Samara, 2018; 46 p. Russian.
22. Growth reference 5–19 years. Application tools. WHO AnthroPlus software [Internet]. [cited 2021 Aug 12]. Available from: https://www.who.int/toolkits/growth-reference-data-for-5to19-years/application-tools.
23. Rudnev SG, Soboleva NP, Sterlikov SA, Nikolaev DV, Starunova OA, Chernyh SP et al. Bioimpedansnoe issledovanie sostava tela naselenija Rossii. M.: RIO CNIIOIZ MZ RF, 2014; 493 p. Russian.
24. Vasyukova OV. Obesity in children and adolescents: diagnosis criteria. Obesity and metabolism. 2019; 16 (1): 70–3. DOI: https://doi.org/10.14341/omet10170. Russian.
25. Dadaeva VA, Aleksandrov AA, Drapkina OM. Prevention of obesity in children and adolescents. Profilakticheskaya Meditsina. 2020; 23 (1): 142–7. DOI: https://doi.org/10.17116/profmed202023011142. Russian.
26. Lir DN, Perevalov AYa. The effectiveness of the improvement of health in the schoolchildren staying in a country summer camp. Voprosy kurortologii, fizioterapii, i lechebnoi fizicheskoi kultury. 2017; 94 (4): 48–53. DOI: https://doi.org/10.17116/kurort201794448-53. Russian.
27. Gavryushin MYu, Markelova SV, Skoblina NA, Milushkina OYu, Sazonova OV. Evaluation of the effectiveness of children's health improvement in camps: actual problems and its solutions. Problems of balneology, physiotherapy, and exercise therapy. 2021; 98 (4): 32–41. DOI: https://doi.org/10.17116/kurort20219804132. Russian.

Литература

1. Черных А. М., Кремлева А. С., Белова А. И. Мониторинг физического развития школьников города Курска в динамике двадцати лет наблюдения. Российский вестник гигиены. 2021; (1): 42–6. DOI: 10.24075/rbh.2021.008.
2. Милушкина О. Ю., Скоблина Н. А., Маркелова С. В., Татаринчик А. А., Мелихова Е. П., Либина И. И. и др. Влияние электронных устройств на физическое развитие современной молодежи и рекомендации по регламенту их использования. Вестник РГМУ. 2019; (4): 87–94. DOI: 10.24075/vrgmu.2019.046.
3. Новикова И. И., Гавриш С. М., Романенко С. П., Сорокина А. В., Серенко В. В., Креймер М. А. Сравнительная оценка информативности методов индикации избыточной массы тела. Санитарный врач. 2021; (4) 67–8.
4. Шестёра А. А., Хмельницкая Е А., Кику П. Ф., Переломова О. В., Каерова Е. В., Сабирова К. М. Физическое развитие и функциональные возможности молодежи города Владивостока. Здоровье населения и среда обитания. 2019; 11 (320): 61–5. DOI: http://doi.org/10.35627/2219-5238/2019-320-11-61-65.
5. Латышевская Н. И., Яцышен В. В., Давыденко Л. А., Яцышена Т. Л. Динамика физического развития детей и подростков города Волгограда в 1976–2016 гг. Гигиена и санитария. 2018; 9 7(9): 844–7. DOI: http://dx.doi.org/10.18821/0016-9900-2018-97-9-844-847.
6. Цукарева Е. А., Авчинников А. В., Алимова И. Л. Оценка физического развития и режима питания детей младшего школьного возраста, проживающих в Смоленске. Вопросы питания. 2019; 88 (4): 34–40. DOI: 10.24411/0042-8833-2019-10039.
7. Гаврюшин М. Ю., Сазонова О. В., Милушкина О. Ю., Скоблина Н. А., Бородина Л. М., Горбачев Д. О. Актуальные проблемы оценки и коррекции пищевого статуса современных детей. В книге: Герасименко Н. Ф., Глыбочко П. В., Есауленко И. Э., Попов В. И., Стародубов В. И., Тутельян В. А., редакторы. Здоровье молодежи: новые вызовы и перспективы: монография в 5 т. Т. 3: Технологии снижения рисков здоровью. Профилактика и диспансеризация. Здоровое питание. М., 2019; с. 250–70.
8. Гирш Я. В., Герасимчик О. А. Роль и место биоимпедансного анализа в оценке состава тела детей и подростков с различной массой тела. Бюллетень сибирской медицины. 2018; 17 (2): 121–32. DOI: 10.20538/1682-0363-2018-2-121-132.
9. Намазова-Баранова Л. С., Елецкая К. А., Кайтукова Е. В., Макарова С. Г. Оценка физического развития детей среднего и старшего школьного возраста: анализ результатов одномоментного исследования. Педиатрическая фармакология. 2018; 15 (4): 333–42. DOI: 10.15690/pf.v15i4.1948.
10. De Onis M, Onyango AW, Borghi E, et al. Development of a WHO growth reference for school-aged children and adolescents. Bulletin of the World Health Organization. 2007; (85): 660–7. DOI: 10.2471/blt.07.043497.
11. Бородкина Д. А., Груздева О. В., Квиткова Л. В., Барбараш О. Л. Распределение жировых отложений: разгадка кажущегося парадокса ожирения в кардиологии? Ожирение и метаболизм. 2017; 14 (2): 3–8. DOI: 10.14341/omet201723-8.
12. Демьяненко И. А., Ткач А. В. Функциональная морфология жировой ткани и ее роль в формировании метаболического синдрома. Крымский журнал экспериментальной и клинической медицины. 2021; 11 (1): 51–60. DOI: 10.37279/2224-6444-2021-11-1-51-60.
13. Галимов О. В., Ханов В. О., Зиангиров Р. А., Галимова Е. С., Минигалин Д. М., Галимов Д. О. Изменения в стенке желудка после гастропликации у пациентов с морбидным ожирением. Вестник РГМУ. 2020; (4): 70–5. DOI: 10.24075/vrgmu.2020.041.
14. Grossman DC, Bibbins-Domingo K, Curry SJ, et al. Screening

for obesity in children and adolescents us preventive services task force recommendation statement. Journal of the American Medical Association. 2017; 317 (23): 2417–26. DOI: 10.1001/jama.2017.6803.
15. Грицинская В. Л. Оценка физического развития мальчиков школьного возраста г. Санкт-Петербурга с использованием антропометрического калькулятора ВОЗ. Здоровье населения и среда обитания. 2018; (2): 16–19.
16. Almeida Y, Costa Maia C, Barros N, Moreno L, Carioca A, Loureiro A. Is bioelectrical impedance vector analysis a good indicator of nutritional status in children and adolescents? Public Health Nutrition. 2021; 24 (14): 4408–16. DOI:10.1017/S1368980021002226.
17. Karanikas I, Karayiannis D, Karachaliou A, Papanikolaou A, Chourdakis M, Kakavas S. Body composition parameters and functional status test in predicting future acute exacerbation risk among hospitalized patients with chronic obstructive pulmonary disease. Clinical Nutrition. 2021; 40 (11): 5605–14. DOI: 10.1016/j.clnu.2021.09.035.
18. Canfell OJ, Littlewood R, Wright ORL,Walker JL. Clinical relevance and validity of tools to predict infant, childhood and adulthood obesity: A systematic review. Public Health Nutrition. 2018; 21 (17): 3135–47. DOI: 10.1017/S1368980018001684.
19. Перевощикова Н. К., Селиверстов И. А., Дракина С. А., Черных Н. С. Биоимпедансный анализ в клинической практике. Мать и Дитя в Кузбассе. 2021; 3 (86): 11–20. DOI: 10.24412/2686-7338-2021-3-11-20.
20. Смирнова Г. А., Андриянов А. И., Кравченко Е. В., Коновалова И. А. Выбор оптимальных методик определения идеальной массы тела для оценки состояния питания. Вопросы питания. 2019; 88 (5): 39–44. DOI: 10.24411/0042-8833-2019-10052.
21. Вдовенко С. А., Сазонова О. В., Пономарев В. А., Мазур Л. И., Гаврюшин М. Ю., Бородина Л. М. Оценочные таблицы физического развития детей и подростков школьного возраста Самарской области. Методические рекомендации. Самара, 2018; 46 с.
22. Growth reference 5–19 years. Application tools. WHO AnthroPlus software [Internet]. [cited 2021 Aug 12]. Available from: https://www.who.int/toolkits/growth-reference-data-for-5to19-years/application-tools.
23. Руднев С. Г., Соболева Н. П., Стерликов С. А., Николаев Д. В., Старунова О. А., Черных С. П. и др. Биоимпедансное исследование состава тела населения России. М.: РИО ЦНИИОИЗ МЗ РФ, 2014; 493 с.
24. Васюкова О. В. Ожирение у детей и подростков: критерии диагноза. Ожирение и метаболизм. 2019; 16 (1): 70–3. DOI: https://doi.org/10.14341/omet10170.
25. Дадаева В. А., Александров А. А., Драпкина О. М. Профилактика ожирения у детей и подростков. Профилактическая медицина. 2020; 23 (1): 142–7. DOI: https://doi.org/10.17116/profmed202023011142.
26. Лир Д. Н., Перевалов А. Я. Эффективность оздоровления школьников за время пребывания в летнем загородном учреждении отдыха. Вопросы курортологии, физиотерапии и лечебной физической культуры. 2017; 94 (4): 48–53. DOI: https://doi.org/10.17116/kurort201794448-53.
27. Гаврюшин М. Ю., Маркелова С. В., Скоблина Н. А., Милушкина О. Ю., Сазонова О. В. Оценка эффективности оздоровления детей в лагерях: современные проблемы и пути решения. Вопросы курортологии, физиотерапии и лечебной физической культуры. 2021; 98 (4): 32–41. DOI: https://doi.org/10.17116/kurort20219804132.

CONSOLIDATION AND RECONSOLIDATION OF VISUAL AND SEMANTIC MEMORY IN PARKINSON'S DISEASE

Nikishina VB[1], Petrash EA[1] ✉, Kuznetsova AA[2], Shuteeva TV[2], Zakharova IA[1]

[1] Pirogov Russian National Research Medical University, Moscow, Russia

[2] Kursk State Medical University, Kursk, Russia

Cognitive and mnestic impairments have a significant negative impact on the quality of parkinsonian patients' life. Memory impairment causes changes in the mechanisms of information processing. The aim of this study was to investigate the characteristics of transformations undergone by memorized visual and semantic content during memory consolidation and reconsolidation in patients with Parkinson's disease. The study was conducted on 32 male patients with PD (ICD code: G20). Among the patients, 9 had rigidity/bradykinesia-dominant PD, 11 had tremor-dominant PD, and 12 suffered from a mixed type of PD. Short-term memory span was assessed using the 10 words and the visual memory tests proposed by Luria. As stimulus materials we used a symbolic representation of the old Greek letter resembling an owl and a translated excerpt from a Canadian aboriginal epic. Regardless of the PD form, the quality of the memorized information was either altered or completely lost. The mechanisms underlying such transformations differed quantitively depending on the PD form. Transformation of the memorized information occurred in the conditions of both incidental and deliberate memorization and was represented by distortions (substitution of the original content with confabulations) and simplifications of the structural and semantic organization. We consolidated significantly lesser amount of auditory verbal (p = 0.018) and visual (p = 0.029) information. This trend was consistent with the pronounced distortion of content during its retrieval.

Keywords: visual memory, semantic memory, deliberate memorization, incidental memorization, consolidation, reconsolidations, Parkinson's disease

Author contributions: Nikishina VB — study concept; interpretation and summarization of the obtained empirical data; Petrash EA– study concept; processing, interpretation and summarization of the obtained empirical data; Kuznetsova AA — interpretation and summarization of the obtained empirical data; Shuteeva TV — implementation of the experiment, collection of primary empirical data; Zakharova IA — implementation of the experiment, collection of primary empirical data.

Compliance with ethical standards: the study complied with the legislation on public health protection; informed consent was obtained from all study participants (Protocol of the Ethics Committee No. 207 dated April 19, 2021).

✉ **Correspondence should be addressed:** Ekaterina A. Petrash
Ostrovityanova, 1, Moscow, 117997, Russia; petrash@mail.ru

Received: 02.12.2021 **Accepted:** 20.12.2021 **Published online:** 31.12.2021

DOI: 10.24075/brsmu.2021.069

КОНСОЛИДАЦИЯ–РЕКОНСОЛИДАЦИЯ ЗРИТЕЛЬНО-ОБРАЗНОЙ И СЕМАНТИЧЕСКОЙ ПАМЯТИ ПРИ БОЛЕЗНИ ПАРКИНСОНА

В. Б. Никишина[1], Е. А. Петраш[1] ✉, А. А. Кузнецова[2], Т. В. Шутеева[2], И. А. Захарова[1]

[1] Российский национальный исследовательский медицинский университет имени Н. И. Пирогова, Москва, Россия

[2] Курский государственный медицинский университет, Курск, Россия

Когнитивные и мнестические нарушения играют существенную роль в снижении качества жизни пациентов с болезнью Паркинсона (БП). Нарушения памяти приводят к изменению (трансформации) механизмов переработки информации. Целью работы было изучить особенности трансформации зрительно-образного и семантического содержания, подлежащего запоминанию, в процессах консолидации и реконсолидации у пациентов с БП. Объем выборки составил 32 пациента мужского пола с диагнозом G20 «болезнь Паркинсона»: 12 пациентов со смешанной (акинетико-ригидно-дрожательной) формой, 9 пациентов с акинетико-ригидной формой и 11 пациентов с дрожательной формой болезни Паркинсона. Объем кратковременной памяти оценивали с помощью методик «10 слов» и «Зрительная память» А. Р. Лурия. Стимульный материал для экспериментального этапа исследования представлял собой символическое изображение буквы древнегреческого алфавита, напоминающего сову, а также текст из эпоса индейцев Канады на русском языке. Установлено, что вне зависимости от формы заболевания при БП фиксируется изменение качества запоминаемой информации либо ее полная потеря. Механизмы потери информации имеют качественные различия при разных формах заболевания. Трансформация сохраняемой информации при целенаправленном и при нецеленаправленном запоминании происходит либо в форме искажения (подмены исходного содержания конфабуляторным), либо в форме сокращения (упрощения структурно-семантической организации). Консолидируется значимо меньший объем информации как слухоречевой (p = 0,018), так и зрительно-образной (p = 0,029). Данная тенденция соотносится с выраженным искажением в процессе извлечения информации.

Ключевые слова: зрительно-образная память, семантическая память, целенаправленное запоминание, нецеленаправленное запоминание, консолидация, реконсолидация, болезнь Паркинсона

Вклад авторов: В. Б. Никишина — формирование концепции исследования, интерпретация и обобщение полученного эмпирического материала; Е. А. Петраш — формирование концепции исследования, обработка, интерпретация и обобщение полученного эмпирического материала; А. А. Кузнецова — интерпретация и обобщение полученного эмпирического материала; Т. В. Шутеева — проведение исследования, сбор первичного эмпирического материала; И. А. Захарова — проведение исследования, сбор первичного эмпирического материала.

Соблюдение этических стандартов: исследование одобрено этическим комитетом РНИМУ им. Пирогова (протокол № 207 от 19 апреля 2021 г.), проведено в соответствии с требованиями Основ законодательства «Об охране здоровья граждан»; все участники подписали информированное согласие на обследование.

✉ **Для корреспонденции:** Екатерина Анатольевна Петраш
ул. Островитянова, д. 1, г. Москва, 117997, Россия; petrash@mail.ru

Поступила: 02.12.2021 **Статья принята к печати:** 20.12.2021 **Опубликована онлайн:** 31.12.2021

DOI: 10.24075/vrgmu.2021.069

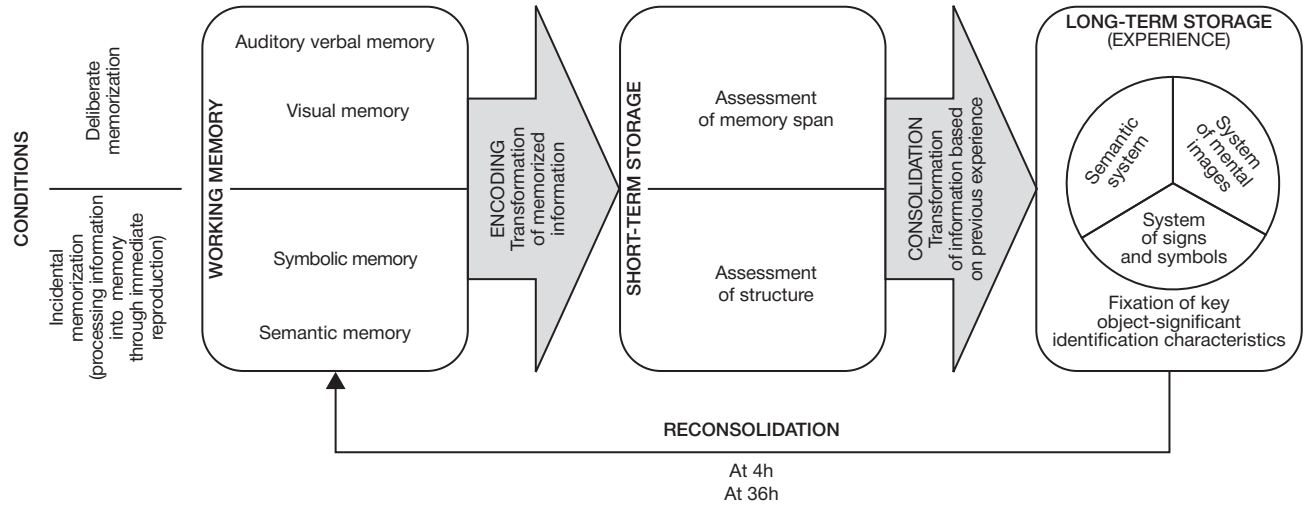

Fig. 1. Schematic representation of consolidation and reconsolidation of visual and semantic information

Parkinson's disease (PD) is an age-related progressive neurodegenerative disorder characterized by high rates of disability and poor prognosis. Being the second most common neurodegenerative disorder, PD poses a serious challenge to healthcare and society.

The diversity of clinical manifestations of PD is linked to the death of dopaminergic neurons in the striopallidar system. In addition to motor symptoms, which are highly common in parkinsonian patients, PD has varied non-motor manifestations, including autonomic and sensory dysfunction, pain, affective disorders, and cognitive impairment. The diversity of symptoms and the high rate of cognitive impairment diminish the quality of life of parkinsonian patients and their families and are the focus of clinical attention.

In all its diversity of forms and processes, memory has adaptive potential that maintains the quality of life in parkinsonian patients.

Studies of cognitive and, more specifically, mnestic functions in PD patients have been implemented by Russian [1] and foreign [2–21] researchers.

Parkinsonian patients are reported to suffer a significantly declining quality of life [2]. No association has been found between the cognitive status of PD patients on the MMSE scale and attention/memory deficit experienced by the patients.

PD is characterized by a long preclinical stage lasting up to 20–30 years. The clinical manifestations of the disease appear when degeneration of substantia nigra neurons and striatal axons reaches 50–60% and 70–80%, respectively [11]. In addition to dopaminergic neurons in the striata nigra, dopaminergic neurons in other brain regions, including the tuberoinfundibular system, are affected. Disruption of the dopaminergic pathway in the striatum critically affects the continuous process of working memory updating [7]. Neurodegeneration begins in the dorsal vagal and the anterior olfactory nuclei and then spreads sequentially to the locus coeruleus, substantia nigra and basal regions of the anterior brain; it is only in the advanced stages of the disease that neurodegeneration hits the neocortex, especially the limbic and the multimodal association cortices of the frontal and temporal lobes [18].

The underlying mechanism of PD involves intraneuronal aggregation of pathological alfa-synuclein, the primary component of Lewy bodies. In neurodegenerative disorders, chronic activation of the microglia and astrocytes results in reactive microgliosis and astrogliosis. In PD, oligodendrocytes are also involved, which suggests that PD affects signal transmission in the brain. Gliosis caused by neurodegeneration blocks transmission of nerve impulses and impedes formation of new neuronal connections, which form the morphological and functional basis of memory consolidation and reconsolidation. Impairment of temporal processing is associated with neuronal apoptosis, which hampers information transfer from short-term to long-term memory and back [6]. In addition to the overall visuospatial dysfunction, patients with PD have verbal memory impairment. A direct association has been established between the duration of the disease and visuospatial short-term memory impairment [13].

The methodology of our research into consolidation and reconsolidation of visual and semantic memory in parkinsonian patients is premised on the concept of working memory developed by Velichkovsky BB (2015). Working memory (WM) is a system of cognitive processes that enable temporary information storage and processing. Being structurally heterogenous, WM consists of multiple components for temporary information storage and processing that have various functional characteristics; WM also includes a system of functional mechanisms. [20, 21]. WM is not stimulus-specific, and its content is determined by the type of memory involved in input processing. Based on the functional outcome, memory can be classified into nonverbal (visual, symbolic and auditory) and semantic. Based on the type of regulation, memorization can be classified into deliberate (intentional) and incidental (unintended).

Regardless of whether memorization is deliberate or incidental, incoming information is simplified (compressed) at the encoding stage. During processing, information is converted into a primary mnestic image or primary semantic content. In WM, storage is implemented by means of short-term and long-term storage mechanisms. Short-term storage mechanisms are used for temporary storage of information essential for solving a current cognitive task [1, 2].

Fig. 1 shows schematic representation of consolidation and reconsolidation of visual and semantic information.

During memory consolidation, short-term memories are converted into long-term memories, and the retained information, be it visual or semantic, undergoes further transformations in accordance with the previous experience. Freshly learned experiences are compared to "old" information stored in the long-term memory. Long-term memory harbors information that can be re-activated to solve a current

task. Consolidated memories are retrieved (i.e. undergo reconsolidation) from long-term memory, which comprises a system of images, symbols, signs, and a semantic system organized into a coherent experience. Both visual and semantic information learned in the previous experience undergoes reconsolidation and is transformed in accordance with fixed object-significant identification characteristics.

Any WM impairment reduces human capacity to process information or make an optimal decision and lessens the overall adaptive potential [1, 2].

The aim of this study was to investigate the characteristics of visual and semantic content transformation during memory consolidation and reconsolidation in patients with PD. We hypothesize that information acquired through either deliberate or incidental memorization by such patients is distorted or completely lost in the absence of pronounced cognitive dysfunction and regardless of the PD form (rigidity/bradykinesia-dominant, tremor-dominant or mixed).

METHODS

A total of 32 male patients diagnosed with Parkinson's disease (ICD disease code: G20) were enrolled in the study. Clinical manifestations assessed on the Hoehn and Yahr scale were consistent with stage 2 of the disease at the time of this study. The participants were stratified into 3 groups by the form of the disease: group 1 (n = 12) included patients with mixed PD, group 2 (n = 9) comprised patients with rigidity/bradykinesia-dominant PD, and group 3 consisted of patients with tremor-dominant PD (n = 11). Inclusion criteria: age of 60–65 years (mean age: 62.4 ± 2.1 years), duration of PD no more than 3 years (mean duration: 2.2 ± 0.57 years), absence of cognitive disorders (MMSE score: at least 24 points). All patients were receiving levodopa therapy at baseline (average dose: 594.2 ± 236.2 mg a day).

Exclusion criteria: severe chronic disorders, TB, viral hepatitis, HIV, and other recurrent infections.

The study was conducted in 3 stages. In the first stage, the patients underwent a physical and neurological examination.

In the second stage, the storage capacity of explicit (intentional) short-term visual and auditory verbal memory was assessed. The span of auditory verbal memory was assessed using a Luria memory words test. Briefly, the patient was read a list of 10 semantically unrelated monosemantic one- and two-syllable words denoting concrete objects and was asked to recall the words immediately after presentation. The procedure was repeated 5 times. The following parameters were recorded: the number of correctly recalled words, the number of repeated words during each recall round, and the number of words that were not on the list. Short-term visual memory span was assessed using a Luria visual memory method. Briefly, the patient was shown a table of 16 cells; each cell contained an outline drawing of an object (a geometric shape or an item). The patient was given 2 min to look at the images. Then, the patient was asked to name the objects they were able to memorize. The procedure was repeated 5 times. The following parameters were recorded: the number of correctly reproduced visual stimuli, the number of repeated objects during each recall round, and the number of new words that were not present in the original table.

In the third stage, we empirically studied consolidation and reconsolidation of explicit and implicit visual and semantic memory types in patients with PD. The methodology for this stage was adopted from Bartlett's experiment on memory

Fig. 2. A stimulus drawing selected for the study of implicit memory

reconstruction during its active retrieval. Each patient was instructed about the experiment individually.

During the experiment, the patient was presented with a visual stimulus — a symbolic drawing shown in Fig.2. This particular stimulus was reliably unfamiliar to the patients, hence its choice. The drawing was a letter from the old Greek alphabet that resembled an owl. The symbolic drawing (symbol) had 4 parts: a head, a body, a wing and a leg. Each of these parts consisted of smaller elements, e.g. the head consisted of 2 elements: the head itself and a tick, etc.

The stimulus material for the study of semantic memory was a Russian translation of an excerpt from a Canadian aboriginal epic. The excerpt contained 79 units of meaning (33 sentences, 295 words, a total of 1,427 characters). The units of meaning were defined as grammatical forms charged with semantic content and implemented in different combinations of nouns (the central lexical units of the language) with other forms (adjectives, verbs, pronouns). Semantic memory was assessed using the following parameters: the number of correctly reproduced sentences, the number of correctly reproduced semantic units, the number of incorrectly reproduced sentences, the number of semantic errors, the number of errors in the order of sentences, the number of errors in the order of semantic units. The data were collected into a specially designed semantic card.

For immediate reproduction of the presented stimulus material, the patients were instructed to draw a copy of the original visual stimulus. Next, the patients were asked to retell the Indian story immediately after hearing it. Reproduction ensured that information was retained. Then, the patients were asked to draw the presented visual stimulus from memory and to retell the text 40 min, 4 h and 36 h after the initial presentation.

Statistical analysis was conducted using descriptive (means and standard deviations) and comparative (the nonparametric Mann–Whitney U and Wilcoxon sign-ranked tests) statistics. Absolute values were analyzed.

RESULTS

The experiment revealed that the span of short-term visual and auditory verbal memory was reduced in parkinsonian patients regardless of the PD form. The graphic representation of the results in Fig. 3 reflects the number of reliably correct responses following presentation of the verbal stimuli.

The comparative analysis of short-term auditory verbal and visual memory aided by the non-parametric paired Mann–

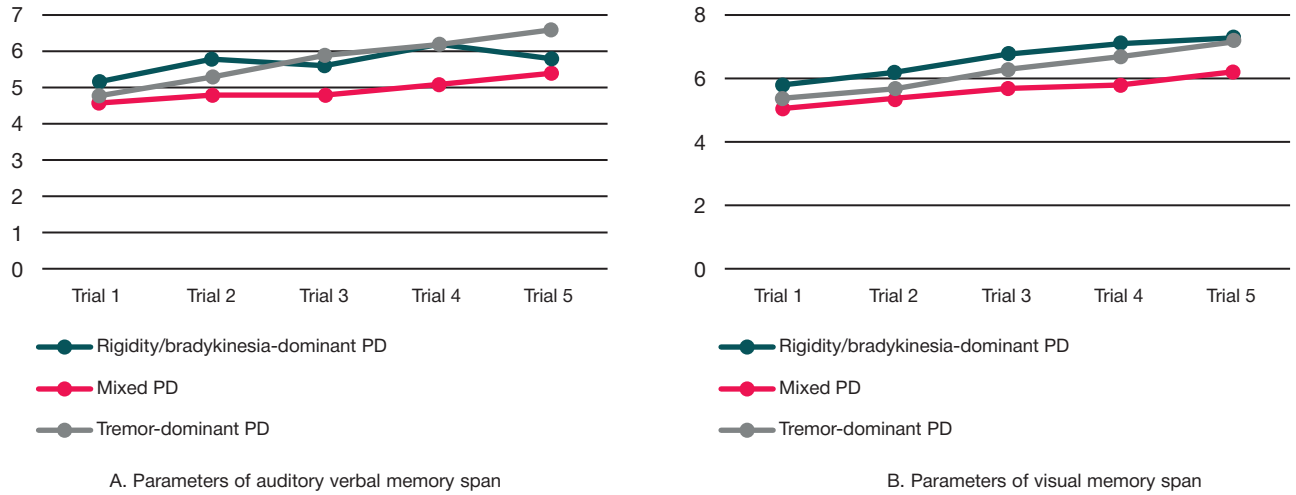

A. Parameters of auditory verbal memory span

B. Parameters of visual memory span

Fig. 3. Auditory verbal and visual memory curves for patients with different forms of PD

Whitney U test detected no significant differences ($p \leq 0.0$) in the span of the studied short-term memory types between the patients with different forms of PD. However, there were some qualitative differences.

Errors made by the patients with bradykinesia-dominant PD were mostly perseverative reproduction of the actual visual and auditory verbal stimuli without confabulation (addition of new information, false memories). The patients with the mixed form of PD made a lot of confabulation errors, i.e. repeatedly reported words and objects that were absent in the initial presentations. The proportion of such additions was as high as 51.18 ± 6.34%. About half of the reported visual and verbal stimuli were additions semantically unrelated to the presented stimulus material. The proportion of confabulation errors made by the patients with tremor-dominant PD was also significant (34.44 ± 5.12%). However, unlike patients with mixed PD, the additions made by this group of patients when reporting the auditory verbal stimuli were mostly verbs semantically related to the presented verbal stimuli. Responses to the presented visual stimuli were word combinations of two types: noun + adjective and noun + verb. The patients with tremor-dominant PD demonstrated these response types when reproducing the presented and false stimuli.

These findings suggest that, regardless of the PD type, both visual and auditory verbal information underwent a transformation (was altered) at the stage of deliberate memorization during the presentation of the stimuli. With every subsequent presentation and reproduction of the stimuli, the patients did not correct the errors, but instead persisted in reproducing false memories, or confabulations. This suggests consolidation of false memories by means of their transfer to the long-term memory storage.

In the next stage, incidental memorization was studied by studying consolidation and reconsolidation of visual and semantic memory. We discovered that the semantic content of verbal information was completely lost during incidental memorization by patients with PD. The semantic information was altered at the stage of its encoding during immediate reproduction of the heard text. In total, 23–28% of the semantic content was missing. During story retelling, a significant proportion of semantic units was lost. The proportion of the omitted semantic units increased to 50–53% after a 40-minute delay. Four hours after the initial presentation, the patients with any form of PD were able to reproduce only 1/4 of the story's semantic content (21–23%). The loss of the original semantic content was accompanied by the simplification of linguistic and semantic structures: the patients used syntactically simple sentences and named only objects and actions. Some sentences were merely object descriptions; structurally, they were a combination of a noun and an adjective. Story retelling was reduced to the description of objects and their actions; causal relationships were totally missing. Regardless of the PD form, a complete loss of the semantic content was demonstrated by all the patients after a 36-hour delay. Substitutions were the most prevalent type of error: the patients named the objects, described their characteristics and actions but did not make causal connections. And even with substitutions, there was a 3-fold reduction in the qualitative and quantitative structure of the text: the retold story contained 81 words and 23 semantic units vs 295 words and 79 semantic units in the original text. This reduction occurred regardless of the PD form. The retold story was lexically and syntactically simplistic and was unrelated to the original text. These findings suggest inhibition of verbal information in patients with PD.

While retelling the story immediately after its presentation, patients with rigidity/bradykinesia-dominant PD cut down the original story considerably but preserved its gist. There were almost no alterations during immediate recall. The participants with tremor-dominant PD reproduced the original semantic content overall correctly but still abridged it and made some insertions. This group of patients created causal links between the newly introduced and the initially present objects. The participants with tremor-dominant PD uttered short simple sentences consisting of 4 words at best, with preserved semantic content. The patients with mixed PD incorrectly reproduced a few semantic units during immediate recall (24 correct semantic units vs 79 units in the original text) but preserved the main idea. Similar to the patients with tremor-dominant PD, the patients with mixed PD simplified language structures while retelling the story, using unexpanded sentences, which obfuscated its understanding.

Story retelling 40 minutes after its initial presentation revealed further loss of the semantic content regardless of the PD form. In the stories retold by the patients with mixed PD, only 6 sentences were consistent with the initial text in terms of semantic content. Other semantic units, which were mostly descriptions of objects and actions, were altered or substituted. The patients with rigidity/bradykinesia-

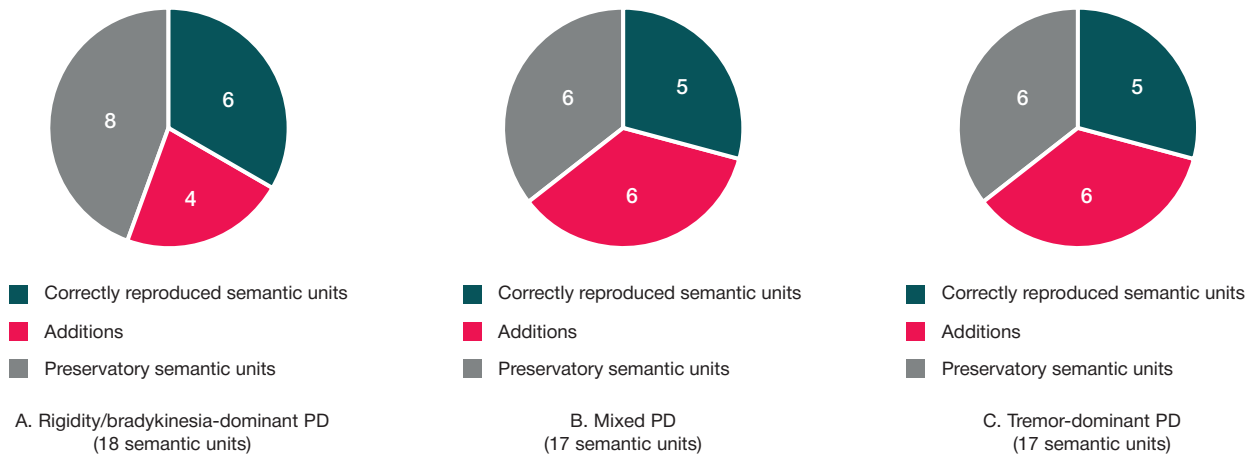

Fig. 4. Characteristics of the reproduced semantic units in patients with different forms of PD

dominant PD preserved the original semantic content in 11–13 sentences. In this group of patients, perseverative (2–3 times) repetition of sentences was observed. The patients with tremor-dominant PD retold the story using 8 sentences. The retold stories were dominated by descriptions of objects but there was a dearth of actions and their descriptions. Causal links were present in 1–2 sentences. The semantic content was altered or substituted.

After a 4-hour delay, the patients with any form of PD were able to reproduce 22–25% of the original semantic content. Their stories were dominated by object and action naming. The objects mentioned in the initial text were substituted. The story was retold in short kernel sentences (subject + predicate). The sentences were ungrammatical and lacked agreement. A tendency to perseveration was observed in the patients with mixed and rigidity/bradykinesia-dominant PD: sentences were repeated up to 4 times. The causal relationships were totally missing.

After a 36-hour delay, the total loss of the original semantic content was demonstrated by all the patients regardless of the PD form. The number of causal relationships ranged from 1 to 4. The number of insertions (new objects) varied from 5 to 7, which was comparable with the number of objects in the presentation (Fig. 4).

After a 36-hour delay, the patients with rigidity/bradykinesia-dominant PD were able to reproduce 18 semantic units, of them 6 were consistent with the initial semantic content of the presented text, 4 units were confabulations (the patients introduced new objects, object characteristics or causal relationships). The overwhelming majority of semantic units in the retold story were perseverative, i.e. repeated multiple times in different parts of the retold text. Perseverative confabulations (falsely reproduced semantic units absent in the initial text) were the most prevalent errors made by the patients with mixed PD. The patients with tremor-dominant PD correctly reproduced only 5 of 79 semantic units contained in the original text. Confabulations (semantic units containing information about objects and their actions from the initial text) were used by the patients in other semantic fields. For example, the initial text contained a sentence about seal hunting: *One night two young men from Egulac went down to the river to hunt seals.* The retold story did not contain information about seal hinting. The sentence reproduced by the patient was as follows: *Men liked seals, big and beautiful animals. They were resting on the shore, basking in the sun*. This example demonstrates that the semantic content of the reproduced statement deviated from the original sentence; information about seals was semantically misrepresented.

The following patterns were detected while studying visual memory consolidation and reconsolidation (Fig. 5).

Regardless of the PD form (tremor-dominant, rigidity/bradykinesia-dominant, mixed), the patients transformed the presented symbolic drawing into a non-abstract image at the stage of visual information retrieval. When the patients were drawing a copy of the presented symbolic picture (i.e. the stage of encoding, or, in other words, reproduction of the symbol from the template), they tended to transform the symbol into a non-abstract image (bird, owl). This tendency intensified with every subsequent reproduction. The original content was altered, simplified or totally lost. The number of major elements present in the original drawing and the accuracy of their reproduction (number of smaller elements, their arrangement in the picture, including relative to each other, the shape and size of elements) decreased; new elements absent in the original drawing were introduced to the composition.

At the stage of incidental memorization of the presented drawing, the latter underwent transformation from being symbolic to becoming descriptive. This resulted in memorizing the altered image.

All the patients with rigidity/bradykinesia-dominant PD altered the presented visual stimulus only slightly during copying. The number of details, their shapes and inter-element arrangement were reproduced correctly. The patients with tremor-dominant PD omitted some elements of the original drawing and altered their size but preserved the general layout. The patients with mixed PD reproduced a very altered silhouette; the details were also very different from the original drawing.

After a 40-minute delay, further alteration of the memorized, now non-abstract image of a bird (an owl) was observed, mostly in the number of the details. Regardless of the PD form, the drawing looked simplified: its parts were distorted and the elements were few. There were new additions positioned predominantly in the bottom of the drawing. Introduction of new elements to the drawing was accompanied by the omission of the original elements. The patients with rigidity/bradykinesia-dominant PD added partially or completely overlapping lines. The patients with tremor-dominated PD simplified the elements and their initial arrangement. Because some lines in the drawing partially overlapped, this created a variety of new elements initially

Fig. 5. Drawings made by the patients with different PD forms in the immediate recall test and after a 40-minute, 4-hour and 36-hour delay

absent in the presented stimulus. The patients with mixed PD added new elements to the drawing by retrieving them from the non-abstract image of the bird they memorized. The following elements could be clearly identified in the reproduced drawing: a head, ears, a beak, eyes, a wing, legs, and fine details like toes.

After a 4-hour delay, we observed a transformation of the memory image (its reconstruction, in Bartlett's terms) characterized by the loss of the initial elements: several elements were fused into one (tremor-dominant PD) and new elements were introduced (rigidity/bradykinesia-dominant and mixed PD). Regardless of the PD form, the patients tended to simplify the image by reducing the number of parts initially present in the drawing and adding new lines that significantly enhanced the contours of the elements. Superimposition of new elements not found in the original drawing was typical for the patients with mixed PD.

After a 36-h delay, the shape of the initial symbol was completely distorted: the number of parts was reduced to one (the contour of the figure in the drawing) or 2.

Pairwise comparison revealed no significant differences between the groups of patients with different PD forms in the number of correctly reproduced semantic units during the text recall task and the number of correctly reproduced details of the symbolic drawing after a 36-hour delay following incidental memorization (Fig. 6).

The statistical analysis of significance of differences uncovered the following trends. Regardless of the PD form, the patients demonstrated a complete loss of the visual and semantic content in the absence of cognitive impairment. This indicates impairment of consolidation and reconsolidation of memory traces in PD. The trend may be explained by the fact that at the stage of encoding (copying the symbol from the presented visual template and then during immediate recall

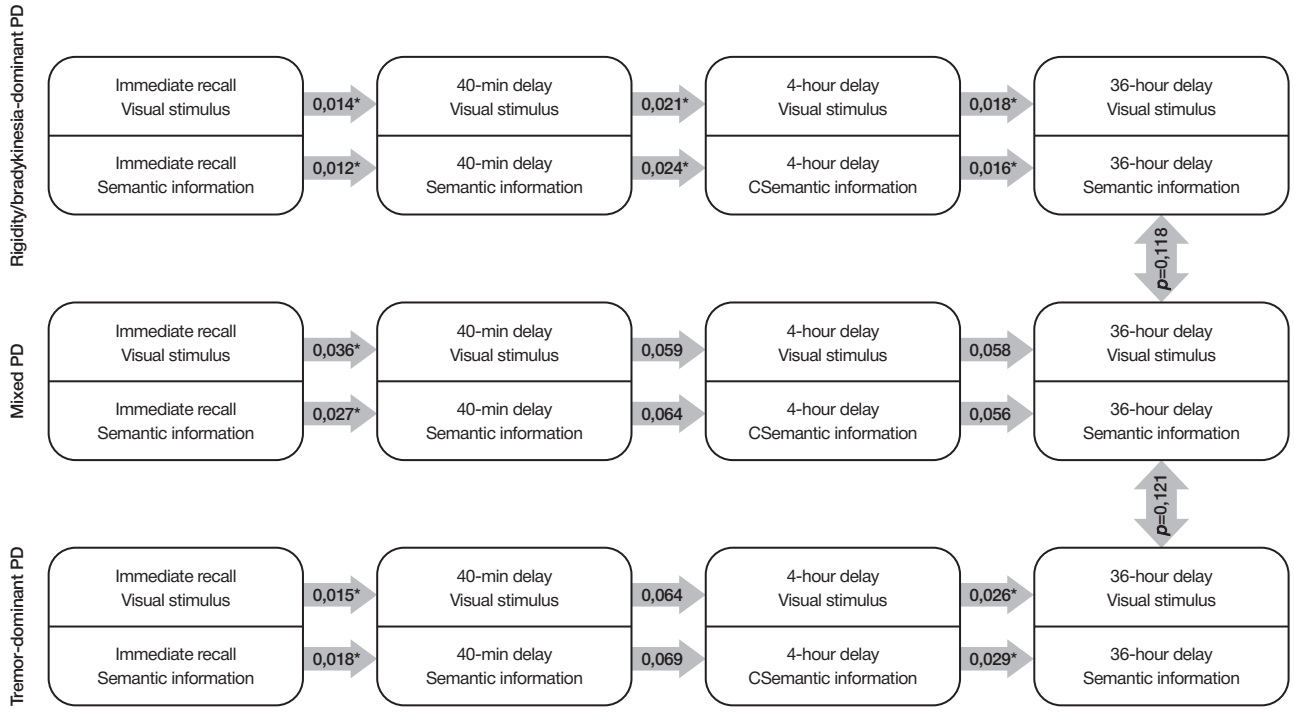

Fig. 6. Schematic representation of the significance of differences in the number of reproduced semantic units by patients with PD grouped by the form of the disease

of textual semantic content) information undergoes a certain transformation: the symbol becomes distorted and more concrete, the linguosemantic structure of the initial texts gets simplified, the sentences become shorter, less expanded and are often substituted by a combination of words.

The quality of retrieved information (its amount and accuracy) undergoes significant changes or can even be completely lost. Regardless of the PD form (tremor-dominant, rigidity/bradykinesia-dominant, mixed), a significantly smaller amount of information, both auditory verbal and visual, is consolidated. This is consistent with the distortion of information during its retrieval.

Differences observed between the groups during immediate recall and after 40-minute, 4-hour and 36-hour delays suggest that each form of PD is characterized by a specific type of information transformation. A significant amount of information, be it visual or semantic, is lost in rigidity/bradykinesia-dominant PD. Information is simplified and the resultant gaps are filled with perseverative simplified structures. Patients with mixed PD alter the content by introducing confabulations and also by perseveration. Similar to patients with mixed PD, patients with tremor-dominant PD distort information at the stage of encoding by introducing confabulations semantically close to the presented stimulus. This trend detected during the study of consolidation and reconsolidation of visual and semantic memory is corroborated by the results of research into the span of short-term visual and auditory verbal memory types. Regardless of the PD form, short-term memory span was reduced in all the patients. The errors made by the patients depended on the form of the disease.

DISCUSSION

Short-term visual and auditory verbal memory span was reduced in the patients with any PD form. This finding was consistent with the reports of other researchers describing short-term memory impairments, attention deficit, and poor memory for routine activities in patients with PD [5]. Memory tests demonstrate that patients with PD have recall rather than recognition difficulty [5]. An attempt to identify PD-specific memory problems was made in an earlier study [16]. The study reported spontaneous organization of memorized information, which is also consistent with the results of our study of deliberate and incidental memorization and recall.

CONCLUSIONS

Mnestic changes due to the pathological processes associated with PD affect the qualitative and quantitative characteristics of memory consolidation and reconsolidation, including accuracy and memory span, regardless of the disease form (rigidity/bradykinesia-dominant, tremor-dominant or mixed) or result in the lack of presentation of the reconsolidated content during recall. Alterations depend on the type of the disease: elements fusion is typical for tremor-dominant PD, addition of new elements is observed in tremor-dominant and rigidity/bradykinesia-dominant PD, whereas the superimposition of new elements absent in the presented visual stimulus occurs in mixed PD. Transformations of consolidated and reconsolidated information during incidental and deliberate memorization were represented by substitution (confabulation) of the original content and reduction (simplification of the structural and semantic structure of content organization). The patients were able to consolidate only a smaller amount of visual and auditory verbal information. With every recall, memory is reconstructed and its content is recategorized. Reconsolidation always follows recategorization. This trend is consistent with pronounced distortion of information during reconsolidation.

Considering the need for improving the quality of life of parkinsonian patients, mnemotechnics should be included in the programs of social adaptation. Mnemotechnics will facilitate consolidation and reconsolidation of visual and semantic information regardless of PD type and, therefore, involvement of cortical and subcortical brain structures into the process at the morphofunctional level through creation of new neuronal connections. Optimization of mnestic processes of consolidation and reconsolidation will in turn increase the compensatory and adaptive potential, as well as the quality of life of patients with PD.

References

1. Nikishina VB, Shuteeva TV, Zapesotskaya IV, Petrash EA. Sub"ektivnaja ocenka boli v strukture nemotornyh projavlenij bolezni Parkinsona. Kurskij nauchno-prakticheskij vestnik «Chelovek i ego zdorov'e». 2017; 4: 67–76. Russia.
2. Barone P, Antonini A, Colosimo C, et al. A multicenter assessment of nonmotor symptoms and their impact on quality of life in Parkinson's disease. Movemant Disorders. 2009; 24 (11): 1641–9. DOI: 10.1002/mds.22643.
3. Berganzo K, Tijero B, González-Eizaguirre A, Somme J, Lezcano E, Gabilondo I, et al. Motor and nonmotor symptoms of Parkinson's disease and their impact on quality of life and on different clinical subgroups. Neurologia. 2016; 31 (9): 585–591. DOI: 10.1016/j.nrleng.2014.10.016.
4. Brefel-Courbon C, Ory-Magne F, Thalamas C, Payoux P, Rascol O. Nociceptive brain activation in patients with neuropathic pain related to Parkinson's disease. Parkinsonism and Related Disorders. 2013; 19 (5): 548–52. DOI: 10.1016/j.parkreldis.2013.02.003.
5. Brown RG, Marsden CD. Cognitive function in Parkinson's disease: from description to theory. Psychology, Medicine. Trends in Neurosciences. 1990; 13 (1): 21–29. DOI: 10.1016/0166–2236(90)90058-I.
6. D'Iorio A, Maggi G, Vitale C, Amboni M, Di Meglio D, Trojano L, et al. Prospective memory in Parkinson's disease: the role of the motor subtypes. J Neurol. 2019; 266 (10): 2505–11. DOI: 10.1007/s00415–019–09448–0.
7. Fellman D, Salmi J, Ritakallio L, Ellfolk U, Rinne JO, Laine M. Training working memory updating in Parkinson's disease: A randomised controlled trial. Neuropsychol Rehabil. 2020; 30 (4): 673–708. DOI: 10.1080/09602011.2018.1489860.
8. Flowers KA, Pearce I, Pearce JM. Recognition memory in Parkinson's disease. Neurology, Neurosurgery and Psychiatry. 1984; 47: 1174–81. DOI: 10.1136/jnnp.47.11.1174.
9. Gabrieli JDE, Singh J, Stebbins GT, Goetz CG. Reduced working memory span in Parkinson's disease: Evidence for the role of a frontostriatal system in working and strategic memory. Neuropsychology. 1996; 10 (3): 322–32. DOI: 10.1037/0894–4105.10.3.321.
10. Hou J-GG, Lai EC. Non-motor symptoms of Parkinson's disease. International Journal of Gerontology. 2007; 1 (7): 53–64. DOI: 10.1016/S1873–9598(08)70024–3.
11. Jeon BS, Jackson-Lewis V, Burke RE. 6-Hydroxydopamine lesion of the rat substantia nigra: time course and morphology of cell death. Neurodegeneration. 1995; 4: 131–7.
12. Pourzinal D, Yang JHJ, Bakker A, McMahon KL, Byrne GJ, Pontone GM, et al. Hippocampal correlates of episodic memory in Parkinson's disease: A systematic review of magnetic resonance imaging studies. Journal of Neuroscience Research. 2021; 99 (9): 2097–116. DOI: 10.1002/jnr.24863.
13. Ramos AA, Machado L. A Comprehensive meta-analysis on short-term and working memory dysfunction in Parkinson's disease. Neuropsychol Rev. 2021; 31 (2): 288–311. DOI: 10.1007/s11065–021–09480-w.
14. Siciliano M, Trojano L, Micco RD, Sant'Elia V, Giordano A, Russo A, et al. Correlates of the discrepancy between objective and subjective cognitive functioning in non demented patients with Parkinson's disease. Journal of Neurology. 2021; 268: 3444–55.
15. Schmidt N, Tödt I, Berg D, Schlenstedt C, Folkerts A-K, Ophey A, et al. Memory enhancement by multidomain group cognitive training in patients with Parkinson's disease and mild cognitive impairment: long term effects of a multicenter randomized controlled trial. Journal of neurology. 2021; 268: 4655–66.
16. Taylor AE, Saint-Cyr JA, Lang AE. Memory and learning in early Parkinson's disease: Evidence for a "Frontal Lobe Syndrome". Brain and cognition. 1990; 13 (2): 21–32. DOI: 10.1016/0278–2626(90)90051-O.
17. Tweedy J, Langer K, McDowell F. The effect of semantic relations on the memory deficit associated with Parkinson's disease. Journal of Clinical Neuropsychology.1982; 4 (3): 235–47. DOI: 10.1080/01688638208401132.
18. Volterra A, Meldolesi J. Astrocytes, from brain glue to communication elements: the revolution continues. Nat Rev Neurosci. 2005; 6: 626–40.
19. Weingartner H, Burns S, Diebel R, Le Witt P. A. Cognitive impairments in Parkinson's disease: Distinguishing between effort-demanding and automatic cognitive processes. Psychiatry Research. 1984; 11 (3): 223–35. DOI: 10.1016/0165–1781(84)90071–4.
20. Velichkovsky BB. Rabochaja pamjat' cheloveka: ctruktura i mehanizmy. M.: Kogito-centr, 2015; 247 s. Russia.
21. Velichkovsky BB. Testirovanie rabochej pamjati: ot prostogo k slozhnomu i snova k prostomu. Teoreticheskaja i jeksperimental'naja psihologija. 2014; 7 (2): 133–42.

Литература

1. Никишина В. Б., Шутеева Т. В., Запесоцкая И. В., Петраш Е. А. Субъективная оценка боли в структуре немоторных проявлений болезни Паркинсона. Курский научно-практический вестник «Человек и его здоровье». 2017; 4: 67–76.
2. Barone P, Antonini A, Colosimo C, et al. A multicenter assessment of nonmotor symptoms and their impact on quality of life in Parkinson's disease. Movemant Disorders. 2009; 24 (11): 1641–9. DOI: 10.1002/mds.22643.
3. Berganzo K, Tijero B, González-Eizaguirre A, Somme J, Lezcano E, Gabilondo I, et al. Motor and nonmotor symptoms of Parkinson's disease and their impact on quality of life and on different clinical subgroups. Neurologia. 2016; 31 (9): 585–591. DOI: 10.1016/j.nrleng.2014.10.016.
4. Brefel-Courbon C, Ory-Magne F, Thalamas C, Payoux P, Rascol O. Nociceptive brain activation in patients with neuropathic pain related to Parkinson's disease. Parkinsonism and Related Disorders. 2013; 19 (5): 548–52. DOI: 10.1016/j.parkreldis.2013.02.003.
5. Brown RG, Marsden CD. Cognitive function in Parkinson's disease: from description to theory. Psychology, Medicine. Trends in Neurosciences. 1990; 13 (1): 21–29. DOI: 10.1016/0166–2236(90)90058-I.
6. D'Iorio A, Maggi G, Vitale C, Amboni M, Di Meglio D, Trojano L, et al. Prospective memory in Parkinson's disease: the role of the motor subtypes. J Neurol. 2019; 266 (10): 2505–11. DOI: 10.1007/s00415–019–09448–0.
7. Fellman D, Salmi J, Ritakallio L, Ellfolk U, Rinne JO, Laine M. Training working memory updating in Parkinson's disease: A randomised controlled trial. Neuropsychol Rehabil. 2020; 30 (4): 673–708. DOI: 10.1080/09602011.2018.1489860.
8. Flowers KA, Pearce I, Pearce JM. Recognition memory in Parkinson's disease. Neurology, Neurosurgery and Psychiatry. 1984; 47: 1174–81. DOI: 10.1136/jnnp.47.11.1174.
9. Gabrieli JDE, Singh J, Stebbins GT, Goetz CG. Reduced working memory span in Parkinson's disease: Evidence for the role of a frontostriatal system in working and strategic memory. Neuropsychology. 1996; 10 (3): 322–32. DOI: 10.1037/0894–4105.10.3.321.
10. Hou J-GG, Lai EC. Non-motor symptoms of Parkinson's disease. International Journal of Gerontology. 2007; 1 (7): 53–64. DOI: 10.1016/S1873–9598(08)70024–3.
11. Jeon BS, Jackson-Lewis V, Burke RE. 6-Hydroxydopamine lesion of the rat substantia nigra: time course and morphology of cell death. Neurodegeneration. 1995; 4: 131–7.
12. Pourzinal D, Yang JHJ, Bakker A, McMahon KL, Byrne GJ, Pontone GM, et al. Hippocampal correlates of episodic memory in Parkinson's disease: A systematic review of magnetic resonance imaging studies. Journal of Neuroscience Research. 2021; 99 (9): 2097–116. DOI: 10.1002/jnr.24863.

13. Ramos AA, Machado L. A Comprehensive meta-analysis on short-term and working memory dysfunction in Parkinson's disease. Neuropsychol Rev. 2021; 31 (2): 288–311. DOI: 10.1007/s11065–021–09480-w.
14. Siciliano M, Trojano L, Micco RD, Sant'Elia V, Giordano A, Russo A, et al. Correlates of the discrepancy between objective and subjective cognitive functioning in non-demented patients with Parkinson's disease. Journal of Neurology. 2021; 268: 3444–55.
15. Schmidt N, Tödt I, Berg D, Schlenstedt C, Folkerts A-K, Ophey A, et al. Memory enhancement by multidomain group cognitive training in patients with Parkinson's disease and mild cognitive impairment: long-term effects of a multicenter randomized controlled trial. Journal of neurology. 2021; 268: 4655–66.
16. Taylor AE, Saint-Cyr JA, Lang AE. Memory and learning in early Parkinson's disease: Evidence for a "Frontal Lobe Syndrome". Brain and cognition. 1990; 13 (2): 21–32. DOI: 10.1016/0278–2626(90)90051-O.
17. Tweedy J, Langer K, McDowell F. The effect of semantic relations on the memory deficit associated with Parkinson's disease. Journal of Clinical Neuropsychology.1982; 4 (3): 235–47. DOI: 10.1080/01688638208401132.
18. Volterra A, Meldolesi J. Astrocytes, from brain glue to communication elements: the revolution continues. Nat Rev Neurosci. 2005; 6: 626–40.
19. Weingartner H, Burns S, Diebel R, Le Witt P. A. Cognitive impairments in Parkinson's disease: Distinguishing between effort-demanding and automatic cognitive processes. Psychiatry Research. 1984; 11 (3): 223–35. DOI: 10.1016/0165–1781(84)90071–4.
20. Величковский Б. Б. Рабочая память человека: структура и механизмы. М.: Когито-центр, 2015; 247 с.
21. Величковский Б. Б. Тестирование рабочей памяти: от простого к сложному и снова к простому. Теоретическая и экспериментальная психология. 2014; 7 (2): 133–42.

FACTORS ASSOCIATED WITH INCREASE IN ALCOHOL CONSUMPTION DURING FIRST MONTHS OF COVID-19 PANDEMIC AMONG ONLINE SOCIAL MEDIA USERS IN RUSSIA

Gil AU ✉, Demin AK

Sechenov First Moscow State Medical University (Sechenov University), Moscow, Russia

The significant proportion of the Russian population are active online social media users. Changes in alcohol consumption in this target group during the COVID-19 pandemic remain understudied. The aim of this survey was to investigate changes in alcohol consumption and factors associated with the increase in alcohol use among online social media users in Russia during the first months of the COVID-19 pandemic. An online survey was conducted among 1,518 users of online social networking services popular in Russia from June to September 2020. The survey revealed that 35.4% of men and 25.6% of women started drinking more frequently during the first months of the pandemic; 24.9% of men and 17.7% of women increased their usual consumption (volume) of alcohol on a typical drinking occasion, whereas 28.5% of men and 27.9% of women increased the frequency of heavy episodic drinking. Adjusted binary logistic regression analysis revealed a positive association between the increase in the frequency of alcohol consumption and the following factors: age from 18 to 29 years (OR: 1.710; 95% CI: 1.002–2.917), severe restrictions in everyday private life (OR: 3.127; 95% CI: 1.011–9.675) and severe negative professional or financial consequences due to the spread of SARS-CoV-2 (OR: 2.247; 95% CI: 1.131–4.465). The odds of an increase in the frequency of heavy episodic drinking were more than twice higher (OR: 2.329; 95% CI: 1.001–5.428) among those who had experienced severe negative consequences of the pandemic to their professional and financial situation. Higher typical frequency and usual consumption (volume) of alcohol on a typical drinking occasion and higher typical frequency of heavy episodic drinking before the pandemic were positively significantly associated with the increase in these parameters of alcohol consumption during the first months of the pandemic. In times of large-scale epidemics and public health crises, it is advisable to consider the possibility of implementing screening and brief interventions, including via online social media, to prevent problems associated with alcohol use.

Keywords: alcohol, COVID-19, coronavirus, pandemic, social media, Facebook, VKontakte, Odnoklassniki, Twitter, Russia

Author contributions: Gil AU planned the study, designed the electronic questionnaire form, collected date, performed statistical analysis, interpreted the results and wrote the manuscript; Demin AK interpreted the results and wrote the manuscript.

Acknowledgements: the authors thank Uri and Raisa Gil for their help in disseminating information about the survey in online social media, for their critical comments on the interpretation and discussion of the results.

✉ **Correspondence should be addressed:** Artyom U. Gil
Trubetskaya, 8, str. 2, Moscow, 119991, Russia; gil.artyom@gmail.com

Received: 21.11.2021 **Accepted:** 19.12.2021 **Published online:** 30.12.2021

DOI: 10.24075/brsmu.2021.064

ФАКТОРЫ, ВЗАИМОСВЯЗАННЫЕ С РОСТОМ ПОТРЕБЛЕНИЯ АЛКОГОЛЯ В ПЕРВЫЕ МЕСЯЦЫ ПАНДЕМИИ COVID-19 СРЕДИ ПОЛЬЗОВАТЕЛЕЙ СОЦИАЛЬНЫХ ОНЛАЙН-СЕТЕЙ В РОССИИ

А. Ю. Гиль ✉, А. К. Дёмин

Первый Московский государственный медицинский университет имени И. М. Сеченова (Сеченовский Университет), Москва, Россия

Значительная часть населения активно пользуется социальными онлайн-сетями, однако изменения потребления алкоголя в этой целевой группе в период пандемии COVID-19 малоизучены. Целью исследования было оценить изменения потребления алкоголя и факторов, связанных с ростом его потребления, в первые месяцы пандемии COVID-19 среди пользователей социальных онлайн-сетей в России. В период с июня по сентябрь 2020 г. 1518 пользователей наиболее популярных в России социальных онлайн-сетей прошли опрос в отношении изменений потребления алкоголя в первые месяцы пандемии COVID-19. Выявлено, что в первые месяцы пандемии 35,4% мужчин и 25,6% женщин увеличили частоту употребления алкоголя; 24,9% мужчин и 17,7% женщин увеличили разовый объем потребления алкоголя, и 28,5% мужчин и 27,9% женщин увеличили частоту случаев эпизодического употребления алкоголя в больших разовых количествах. На многофакторном уровне возраст 18–29 лет (ОШ = 1,710; 95% ДИ = 1,002–2,917), очень сильные ограничения в повседневной жизни (3,127; 1,011–9,675) и очень сильные негативные последствия в отношении профессиональной или финансовой ситуации в связи с распространением SARS-CoV-2 (2,247; 1,131–4,465) были положительно взаимосвязаны с ростом частоты потребления алкоголя. Шансы увеличения частоты эпизодического употребления алкоголя в больших разовых количествах были более чем в два раза выше (2,329; 1,001–5,428) среди лиц, испытавших очень сильные негативные последствия в отношении профессиональной или финансовой ситуации. Более высокие привычные частота употребления алкоголя, разовый объем употребляемого алкоголя и частота эпизодического употребления алкоголя в больших разовых количествах до пандемии были положительно статистически значимо связаны с ростом этих параметров потребления алкоголя в первые месяцы пандемии.

Ключевые слова: алкоголь, COVID-19, коронавирус, пандемия, социальные сети, Facebook, ВКонтакте, Одноклассники, Twitter, Россия

Вклад авторов: А. Ю. Гиль — планирование исследования, разработка электронной формы сбора данных; сбор, обработка и статистический анализ данных; интерпретация результатов, написание статьи; А. К. Дёмин — интерпретация результатов исследования, написание статьи.

Благодарности: авторы благодарят Ю. Я. Гиль и Р. Г. Гиль за помощь в распространении информации об опросе в социальных сетях, за ценные критические замечания в отношении интерпретации и обсуждения результатов исследования.

✉ **Для корреспонденции:** Артем Юрьевич Гиль
ул. Трубецкая, д. 8, стр. 2, г. Москва, 119991; gil.artyom@gmail.com

Поступила: 21.11.2021 **Статья принята к печати:** 19.12.2021 **Опубликована онлайн:** 30.12.2021

DOI: 10.24075/vrgmu.2021.064

Decisive action taken to counter COVID-19 in Russia and worldwide during the first months of the pandemic slowed the spread of SARS-CoV-2 infection, but it also had a significant impact on many other aspects of life. During the nationwide Russian lockdown, implemented in the second quarter of 2020, the official unemployment rate grew by 2.1%, reaching 6.4%, and the real disposable income of the population fell by 8.4% in comparison with the same period in 2019 [1]. Income reduction and complete loss of income were reported by 61% and 13.5% of the population, respectively; 9.8% of the Russian population lost their jobs [2]. According to recent studies investigating the impact of COVID-19 restrictions across countries, the rates of depression, anxiety and stress among some population groups, especially among women, young adults and people with chronic diseases, have increased [3, 4]. In times of crisis, some turn to alcohol to cope with psychoemotional stress; this can heighten the risk of adverse short-term and long-term health effects and negative social consequences [5, 6]. Increased substance use following large-scale disasters is often the sign of people adopting a self-medicating strategy to deal with emotional distress [7–9]. Research warns that the COVID-19 pandemic may lead to a medium- and long-term increase in alcohol consumption, especially among men [10]. Early studies into the effects of the pandemic have discovered an association between poor overall mental health and increased alcohol use [11]. According to a study conducted in Canada, stress was the third most common (44%) cause of drinking during the pandemic. In the USA, psychological distress caused by the pandemic was associated with increased frequency of alcohol use in both men and women [12]. Research demonstrates that while some proportion of the adult population are increasing their alcohol consumption during the pandemic, an equal proportion are cutting down on alcohol, and 50–70% of the population are not changing their level of alcohol consumption [11, 13]. Because changes in alcohol consumption during the current pandemic may have serious long-term social and economic implications for individuals, groups of people and society as a whole [14, 15], there is a need to monitor these changes and analyze the contributing factors that come forward during a large-scale crisis.

In Russia, online social networking services are actively used by the significant proportion of the population. This opens up a possibility to rapidly assess alcohol consumption among Russian residents and remotely (i.e., via the Internet) implement brief interventions aimed at preventing health problems and other adverse outcomes associated with alcohol use. The aim of this study was to assess changes in alcohol consumption and the factors associated with the increase in alcohol use in the first months of the COVID-19 pandemic among online social media users in Russia in order to explore the possibility of delivering screening and preventive interventions, including those implemented via the Internet, aimed at identifying and preventing alcohol-related problems during large-scale epidemics and public health crises.

METHODS

An anonymous online survey was conducted from June 18 to September 30, 2020 among users of online social media popular in Russia (Odnoklassniki, VKontakte, Facebook and Twitter). The following inclusion criteria were applied: age ≥ 18 years, being an Internet user with or without a user account in the online social media mentioned above, informed consent to participate in the anonymous confidential online survey. Non-inclusion criteria: permanent residence of the respondent outside Russia. Exclusion criteria: refusal to participate or have one's personal data processed at any stage of the study, inconsistent contradictory answers to the questions included in the survey. Any participant could refuse to participate at any stage of the study. The link to the survey was posted in the online social media in various groups, on popular pages and in the news feed. The survey was adapted from the pan-European study of alcohol use during the COVID-19 pandemic [10] and modified to assess alcohol consumption behaviors in the 3 months preceding the survey. A few original questions were added to the questionnaire to assess consumption of unrecorded alcohol, such as the homemade alcohol (*samogon*, homemade wine, *braga*), alcohol brought from abroad, falsified and counterfeit alcoholic beverages, alcohol-containing liquids not intended for drinking, and other types of unrecorded alcohol. Changes in alcohol use during the first months of the pandemic were assessed from changes in the amount and frequency of alcohol consumption and the frequency of heavy episodic drinking defined as 6 or more drinks or 60g of pure ethanol on a single occasion. Statistical analysis included calculation of descriptive statistics and estimation of the proportion of respondents stratified by sociodemographic or other characteristics who had reduced or increased the frequency of drinking or the amount of alcohol consumed. We also assessed associations between the increase in drinking frequency / amount of consumed alcohol during the first months of the pandemic (dependent variables) and the sociodemographic factors, typical frequency of drinking, the typical amount of consumed alcohol, and the typical frequency of heavy episodic drinking in the past 12 months preceding the pandemic, the perceived strength of COVID-19-associated restrictions in public and everyday private life, stress, negative impact of the pandemic on professional and financial situation, and other adverse consequences of the pandemic (independent variables). The presence, direction, strength and statistical significance of the associations were assessed using unadjusted and adjusted binary logistic regression analysis. Odds ratios (OR) and 95% confidence intervals (95% CI) were calculated as measures of association. Data processing and statistical analysis were conducted in SPSS v.22 (Chicago, IL; USA).

RESULTS

Of 1,518 respondents, 57.9% were women and 42.1% were men. The majority of the respondents (87.1%) had had an alcoholic drink at least once in 12 months preceding the study (Table 1). Over half of the respondents (55.9%) were 30–49 years old and almost two-thirds had attended and/or completed higher education (63.8%). More men than women lived in larger settlements ($p = 0.010$) and higher-income households ($p < 0.001$). During the first months of the pandemic, their income had changed or fallen less often than that of women ($p = 0.014$). The usual frequency of drinking, the number of standard drinks consumed on a typical occasion, the frequency of heavy episodic drinking, and the proportion of persons consuming unrecorded alcohol were higher among men than among women ($p < 0.001$). Overall, the male respondents reported they had encountered restrictions in public ($p = 0.007$) and everyday private ($p = 0.003$) life less often than women. However, almost a quarter of men (23.2%) and a third of women (30.8%) said they had encountered severe restrictions in public life, whereas one-fifth of men (19.9%) and a quarter of women (25.4%) reported having faced severe restrictions in their everyday private life during the first months of the pandemic. Men had experienced the negative effects of the pandemic on their professional or financial situation significantly less frequently than women ($p = 0.005$). Only 30.4% of men and 23.5% of women reported they had experienced no negative effects on their professional or financial situation. The pandemic

was a source of stress for 50.4% of men and 69.5% of women ($p < 0.001$). A history of confirmed SARS-CoV-2 infection in a respondent, their family or close friends was reported by 21.9% of the participants, with no significant differences by sex (Table 1). In the first months of the pandemic, 35.4% of men and 25.6% of women had used alcohol more frequently than before the pandemic; 24.9% of men and 17.7% of women had increased usual consumption (volume) of alcohol on a typical drinking occasion; the frequency of heavy episodic drinking had increased in 28.5% of men and 27.9% of women.

Results of unadjusted and adjusted logistic regression analysis are shown in Tables 2–4.

Factors associated with the increase in the frequency of alcohol consumption during the first months of the pandemic

After adjustment for confounders, positive statistically significant associations between the increase in the frequency of alcohol consumption during the first months of the pandemic and the following factors were identified: age of 18–29 years (OR: 1.710; 95% CI: 1.002–2.917), higher typical frequency of alcohol use before the pandemic (from OR: 3.190, 95% CI: 1.887–5.392 for consumption 2–4 times a months, to OR: 18.727, 95% CI: 9.639–36.383 for consumption more than 2–3 times a month), higher usual consumption (volume) of alcohol on a typical drinking occasion before the pandemic (from OR: 1.941, 95% CI: 1.244–3.029 to OR: 2.234, 95%CI: 1.180–4.233), heavy episodic drinking with a frequency of once a month (OR: 2/061; 95% CI: 1.157–3.671) and once a week before the pandemic (OR: 2.012; 95% CI: 1.081–3.746), severe restrictions in everyday private life due to SARS-CoV-2 containment measures (OR: 3.127; 95% CI: 1.011–9.675) and severe negative consequences of the pandemic to the professional or financial situation (OR: 2.247; 95% CI: 1.131–4.465, Table 2).

Factors associated with the increase of the usual consumption (volume) of alcohol on a typical drinking occasion during the first months of the pandemic

Positive statistically significant associations were identified between the increase of the usual consumption (volume) of

Table 1. Sociodemographic characteristics of the respondents and characteristics related to typical alcohol use and the SARS-CoV-2 pandemic, by sex (%)

Characteristic	Men	Women	Both sexes	p^*
	n (%)	*n* (%)	*n* (%)	
Age (years)				
18–29	150 (23.5)	172 (19.6)	322 (21.2)	0.159
30–49	351 (54.9)	497 (56.5)	848 (55.9)	
≥ 50	138 (21.6)	210 (23.9)	348 (22.9)	
Education				
Secondary or below	143 (22.4)	161 (18.3)	304 (20.0)	0.108
Primary /vocational school or college	95 (14.9)	151 (17.2)	246 (16.2)	
Higher (complete or incomplete)	401 (62.8)	567 (64.5)	968 (63.8)	
Settlement size				
≤ 50,000 population	111 (17.4)	196 (22.3)	307 (20.2)	0.010
50,000 to 1 million	251 (39.3)	362 (41.2)	613 (40.4)	
Over 1 million	277 (43.3)	321 (36.5)	598 (39.4)	
Income per household member (rubles)				
≤ 9,999	130 (20.3)	221 (25.1)	351 (23.1)	< 0.001
10,000–19,999	157 (24.6)	225 (25.6)	382 (25.2)	
20,000–39,999	136 (21.3)	226 (25.7)	362 (23.8)	
40,000–59,999	116 (18.2)	128 (14.6)	244 (16.1)	
≥ 60,000	100 (15.6)	79 (9.0)	179 (11.8)	
Changes in the average monthly household income since the beginning of the SARS-CoV-2 pandemic				
Did not change or increased	341 (53.4)	402 (45.7)	743 (48.9)	0.014
Slightly fell	124 (19.4)	187 (21.3)	311 (20.5)	
Moderately fell	79 (12.4)	149 (17.0)	228 (15.0)	
Dropped significantly	95 (14.9)	141 (16.0)	236 (15.5)	
Typical frequency of alcohol use in the past 12 months before pandemic				
Never	84 (13.4)	108 (12.6)	192 (12.9)	< 0.001
Once a month or less frequently	121 (19.3)	314 (36.5)	435 (29.3)	
2–4 times a month	183 (29.2)	227 (26.4)	410 (27.6)	
2–3 times a week	118 (18.8)	116 (13.5)	234 (15.7)	
More often than 2–3 times a week	121 (19.3)	95 (11.0)	216 (14.5)	
Number of standard alcoholic drinks consumed on a typical drinking occasion in the past 12 months before pandemic**				
1–2	136 (26.0)	424 (57.1)	560 (44.2)	< 0.001
3–6	256 (48.9)	256 (34.5)	512 (40.4)	
7+	131 (25.0)	63 (8.5)	194 (15.3)	

Table 1 cont.

Characteristic	Men	Women	Both sexes	*p**
	n (%)	*n* (%)	*n* (%)	
Typical frequency of heavy episodic drinking (6 or more standard drinks on a single occasion) in the past 12 months before pandemic				
Never	191 (31.3)	446 (52.3)	637 (43.6)	<0.001
Less than once a month	124 (20.3)	176 (20.7)	300 (20.5)	
Once a month	96 (15.7)	102 (12.0)	198 (13.5)	
Once a week	136 (22.3)	96 (11.3)	232 (15.9)	
Every day or almost every day	63 (10.3)	32 (3.8)	95 (6.5)	
Reported consumption of unrecorded alcohol				
Yes	320 (51.3)	359 (41.9)	679 (45.8)	< 0.001
No	304 (48.7)	498 (58.1)	802 (54.2)	
Reported encountering COVID-19-related restrictions in public life in the past 3 months				
No restrictions	61 (9.7)	65 (7.5)	126 (8.4)	0.007
Slight restrictions	222 (35.3)	267 (30.8)	489 (32.7)	
Moderate restrictions	200 (31.8)	267 (30.8)	467 (31.2)	
Severe restrictions	146 (23.2)	267 (30.8)	413 (27.6)	
Reported encountering COVID-19-related restrictions in their everyday private life in the past 3 months				
No restrictions	81 (12.8)	72 (8.3)	153 (10.2)	0.003
Slight restrictions	255 (40.3)	317 (36.6)	572 (38.2)	
Moderate restrictions	171 (27.0)	257 (29.7)	428 (28.6)	
Severe restrictions	126 (19.9)	220 (25.4)	346 (23.1)	
Reported negative consequences of the pandemic to their professional or financial situation in the past 3 months				
No negative consequences	189 (30.4)	203 (23.5)	392 (26.4)	0.005
Slight negative consequences	235 (37.8)	336 (38.9)	571 (38.5)	
Moderate negative consequences	114 (18.4)	163 (18.9)	277 (18.7)	
Severe negative consequences	83 (13.4)	161 (18.7)	244 (16.4)	
Reported confirmed SARS-CoV-2 infection in themselves, their family or close friends in the past 3 months				
Yes	137 (22.1)	186 (21.8)	323 (21.9)	0.949
No	484 (77.9)	667 (78.2)	1151 (78.1)	
Reported stress due to the spread of SARS-CoV-2 in the past 3 months				
Yes	292 (50.4)	574 (69.5)	866 (61.6)	< 0.001
No	287 (49.6)	252 (30.5)	539 (38.4)	

Note: * — significance of differences between the groups was assessed using χ^2-test for heterogeneity; ** — among alcohol drinkers (those who consumed alcohol at least once in the past 12 months).

Table 2. Associations of sociodemographic factors, typical frequency and volume of alcohol use, unrecorded alcohol consumption, negative consequences of the COVID-19 pandemic with the increase in the frequency of alcohol consumption in the first months of the COVID-19 pandemic, 2020, (OR, 95% CI)

Variables	Respondents who increased frequency of alcohol consumption		Unadjusted	Adjusted
	n / N	%	OR (95% CI)	OR (95% CI)
Sex				
Male	191/539	35.4	1.511 (1.188–1.921)	0.946 (0.664–1.348)
Female	198/743	26.6	1.0	1.0
Age (years)				
18–29	91/267	34.1	1.559 (1.076–2.257)	1.710 (1.002–2.917)
30–49	228/734	31.1	1.358 (0.994–1.856)	1.082 (0.690–1.698)
≥ 50	70/281	24.9	1.0	1.0
Education				
Secondary or below	69/236	29.2	1.610 (1.027–2.525)	1.514 (0.807–2.839)
Primary /vocational school or college	39/191	20.4	1.0	1.0
Higher (complete or incomplete)	281/855	32.9	1.908 (1.305–2.789)	1.644 (0.952–2.842)
Settlement size				
≤ 50,000 population	54/240	22.5	0.506 (0.356–0.718)	0.952 (0.576–1.574)

Table 2 cont.

Variables	Respondents who increased frequency of alcohol consumption		Unadjusted	Adjusted
	n / N	%	OR (95% CI)	OR (95% CI)
50,000 to 1 million	141/510	27.6	0.666 (0.512–0.865)	1.272 (0.871–1.858)
Over 1 million	194/532	36.5	1.0	1.0
Income per household member (rubles)				
≤ 9,999	73/276	26.4	0.622 (0.409–0.944)	1.048 (0.561–1.957)
10,000–19,999	83/305	27.2	0.646 (0.430–0.972)	1.009 (0.569–1.791)
20,000–39,999	101/321	31.5	0.794 (0.533–1.181)	1.222 (0.705–2.117)
40,000–59,999	73/219	33.3	0.864 (0.564–0.324)	0.934 (0.528–1.650)
≥ 60,000	59/161	36.6	1.0	1.0
Changes in the average monthly household income since the beginning of the SARS-CoV-2 pandemic				
Did not change or increased	166/628	26.4	1.0	1.0
Slightly fell	84/258	32.6	1.344 (0.980–1.841)	1.074 (0.687–1.680)
Moderately fell	58/194	29.9	1.187 (0.832–1.693)	0.822 (0.485–1.393)
Dropped significantly	81/202	40.1	1.863 (1.336–2.598)	1.432 (0.803–2.552)
Typical frequency of alcohol use in the past 12 months before pandemic				
Once a month or less frequently	32/430	7.4	1.0	1.0
2–4 times a month	110/404	27.2	4.653 (3.053–7.093)	3.190 (1.887–5.392)
2–3 times a week	115/233	49.4	12.121 (7.788–18.865)	7.017 (3.898–12.632)
More often than 2–3 times a week	132/215	61.4	19.780 (12.576–31.110)	18.727 (9.639–36.383)
Number of standard alcoholic drinks consumed on a typical drinking occasion in the past 12 months before pandemic				
1–2	84/517	16.2	1.0	1.0
3–6	198/505	39.2	3.325 (2.477–4.461)	1.941 (1.244–3.029)
7+	91/186	48.9	4.938 (3.409–7.152)	2.234 (1.180–4.233)
Typical frequency of heavy episodic drinking (6 or more standard drinks on a single occasion) in the past 12 months before pandemic				
Never	61/441	13.8	1.0	1.0
Less than once a month	69/289	23.9	1.954 (1.333–2.864)	1.184 (0.712–1.969)
Once a month	77/192	40.1	4.171 (2.809–6.194)	2.061 (1.157–3.671)
Once a week	119/229	52.0	6.739 (4.634–9.801)	2.012 (1.081–3.746)
Every day or almost every day	51/92	55.4	7.749 (4.738–12.674)	1.094 (0.444–2.695)
Reported consumption of unrecorded alcohol				
Yes	221/642	34.4	1.498 (1.174–1.912)	1.246 (0.897–1.730)
No	158/609	25.9	1.0	1.0
Reported encountering COVID-19-related restrictions in public life in the past 3 months				
No restrictions	17/87	19.5	1.0	1.0
Slight restrictions	84/407	20.6	1.071 (0.598–1.916)	0.703 (0.250–1.977)
Moderate restrictions	133/413	32.2	1.956 (1.108–3.454)	1.068 (0.349–3.270)
Severe restrictions	151/363	41.6	2.933 (1.659–5.184)	1.020 (0.315–3.299)
Reported encountering COVID-19-related restrictions in their everyday private life in the past 3 months				
No restrictions	18/111	16.2	1.0	1.0
Slight restrictions	101/470	21.5	1.414 (0.815–2.453)	1.636 (0.622–4.304)
Moderate restrictions	133/385	34.5	2.727 (1.579–4.711)	2.594 (0.890–7.564)
Severe restrictions	134/304	44.1	4.073 (2.342–7.081)	3.127 (1.011–9.675)
Reported negative consequences of the pandemic to their professional or financial situation in the past 3 months				
No negative consequences	65/318	20.4	1.0	1.0
Slight negative consequences	142/492	28.9	1.579 (1.129–2.208)	1.240 (0.772–1.990)
Moderate negative consequences	87/239	36.4	2.228 (1.525–3.255)	1.524 (0.848–2.739)
Severe negative consequences	89/211	42.2	2.839 (1.930–4.177)	2.247 (1.131–4.465)
Reported confirmed SARS-CoV-2 infection in themselves, their family or close friends in the past 3 months				
Yes	82/278	29.5	0.956 (0.714–1.280)	0.846 (0.575–1.245)
No	295/969	30.4	1.0	1.0
Reported stress due to the spread of SARS-CoV-2				
Yes	254/746	34.0	1.587 (1.218–2.068)	1.306 (0.892–1.911)
No	108/440	24.5	1.0	1.0

alcohol on a typical drinking occasion during the pandemic and the following factors: drinking alcohol 2 times a week and more often before the pandemic (from OR: 2.587; 95% CI: 1.360–4.918 to OR: 12.021; 95% CI: 5.712–25.300), consuming 3 or more alcoholic drinks on a typical drinking occasion before the pandemic (for 3–6 drinks OR: 2.145; 95% CI: 1.270–3.623; for 7 or more drinks OR: 2.922; 95% CI: 1.448–5.894) and increased frequency (once a week) of heavy episodic drinking (OR: 2.380; 95% CI: 1.180–4.800) (Table 3).

Table 3. Associations of sociodemographic factors, typical frequency and volume of alcohol use, consumption of unrecorded alcohol, negative consequences of the COVID-19 pandemic with the increase in the usual consumption (volume) of alcohol on a typical drinking occasion in the first months of the COVID-19 pandemic, 2020, (OR, 95% CI)

Variables	Respondents who increased the usual consumption (volume) of alcohol on a typical drinking occasion		Unadjusted	Adjusted
	n / N	%	OR (95% CI)	OR (95% CI)
Sex				
Male	129/519	24.9	1.537 (1.166–2.026)	0.875 (0.592–1.295)
Female	127/717	17.7	1.0	1.0
Age (years)				
18–29	55/261	21.1	1.353 (0.872–2.100)	1.609 (0.875–2.961)
30–49	157/708	22.2	1.444 (0.999–2.088)	1.396 (0.838–2.325)
≥ 50	44/267	16.5	1.0	1.0
Education				
Secondary or below	49/244	21.9	1.680 (0.990–2.851)	1.810 (0.884–3.703)
Primary /vocational school or college	25/175	14.3	1.0	1.0
Higher (complete or incomplete)	182/837	21.7	1.667 (1.059–2.625)	1.797 (0.950–3.398)
Settlement size				
≤ 50,000 population	39/232	16.8	0.614 (0.412–0.915)	0.986 (0.568–1.709)
50,000 to 1 million	90/491	18.3	0.682 (0.503–0.925)	1.017 (0.664–1.558)
Over 1 million	127/513	24.8	1.0	1.0
Income per household member (rubles)				
≤ 9,999	54/259	20.8	0.926 (0.573–1.497)	1.300 (0.647–2.609)
10,000–19,999	60/295	20.3	0.897 (0.561–1.436)	1.434 (0.755–2.723)
20,000–39,999	66/310	21.3	0.951 (0.598–1.511)	1.473 (0.794–2.734)
40,000–59,999	41/214	19.2	0.833 (0.502–1.383)	0.887 (0.460–1.710)
≥ 60,000	35/158	22.2	1.0	1.0
Changes in the average monthly household income since the beginning of the SARS-CoV-2 pandemic				
Did not change or increased	102/603	16.9	1.0	1.0
Slightly fell	50/255	19.6	0.417 (0.288–0.603)	0.917 (0.550–1.528)
Moderately fell	41/186	22.0	0.499 (0.324–0.769)	0.990 (0.559–1.753)
Dropped significantly	63/192	32.8	0.579 (0.366–0.916)	1.686 (0.915–3.104)
Typical frequency of alcohol use in the past 12 months before pandemic				
Once a month or less frequently	21/421	5.0	1.0	1.0
2–4 times a month	66/386	17.1	3.929 (2.353–6.559)	2.587 (1.360–4.918)
2–3 times a week	70/225	31.1	8.602 (5.105–14.494)	4.617 (2.309–9.233)
More often than 2–3 times a week	99/204	48.5	17.959 (10.703–30.136)	12.021 (5.712–25.300)
Number of standard alcoholic drinks consumed on a typical drinking occasion in the past 12 months before pandemic				
1–2	44/509	8.6	1.0	1.0
3–6	132/492	26.8	3.875 (2.682–5.598)	2.145 (1.270–3.623)
7+	76/186	40.9	7.302 (4.771–11.174)	2.922 (1.448–5.894)
Typical frequency of heavy episodic drinking (6 or more drinks on a single occasion) in the past 12 months before pandemic				
Never	32/440	7.3	1.0	1.0
Less than once a month	45/284	15.8	2.401 (1.485–3.882)	1.434 (0.781–2.632)
Once a month	43/192	22.4	3.680 (2.244–6.034)	1.876 (0.956–3.681)
Once a week	90/228	39.5	8.315 (5.317–13.004)	2.380 (1.180–4.800)
Every day or almost every day	46/92	50.0	12.750 (7.397–21.978)	2.376 (0.905–6.240)
Reported consumption of unrecorded alcohol				
Yes	145/620	23.4	1.385 (1.046–1.834)	0.906 (0.628–1.308)
No	106/587	18.1	1.0	1.0

Table 3 cont.

Variables	Respondents who increased the usual consumption (volume) of alcohol on a typical drinking occasion		Unadjusted	Adjusted
	n / N	%	OR (95% CI)	OR (95% CI)
Reported encountering COVID-19-related restrictions in public life in the past 3 months				
No restrictions	13/84	15.5	1.0	1.0
Slight restrictions	49/378	13.0	0.813 (0.419–1.579)	1.092 (0.341–3.497)
Moderate restrictions	88/408	21.6	1.502 (0.795–2.839)	1.472 (0.409–5.298)
Severe restrictions	104/357	29.1	2.245 (1.191–4.231)	1.539 (0.407–5.820)
Reported encountering COVID-19-related restrictions in their everyday private life in the past 3 months				
No restrictions	16/108	14.8	1.0	1.0
Slight restrictions	55/449	12.2	0.803 (0.440–1.464)	0.809 (0.282–2.318)
Moderate restrictions	93/374	24.9	1.903 (1.065–3.400)	1.767 (0.550–5.681)
Severe restrictions	91/296	30.7	2.552 (1.421–4.584)	1.737 (0.509–5.931)
Reported negative consequences of the pandemic to their professional or financial situation in the past 3 months				
No negative consequences	42/308	13.6	1.0	1.0
Slight negative consequences	83/472	17.6	1.351 (0.903–2.021)	0.976 (0.566–1.683)
Moderate negative consequences	60/232	25.9	2.209 (1.425–3.425)	1.453 (0.761–2.776)
Severe negative consequences	67/205	32.7	3.075 (1.986–4.761)	2.072 (0.983–4.369)
Reported confirmed SARS-CoV-2 infection in themselves, their family or close friends in the past 3 months				
Yes	47/270	17.4	0.772 (0.544–1.098)	0.686 (0.442–1.064)
No	200/933	21.4	1.0	1.0
Reported stress due to the spread of SARS-CoV-2				
Yes	168/726	23.1	1.523 (1.116–2.077)	1.265 (0.819–1.952)
No	69/418	16.5	1.0	1.0

Table 4. Associations of sociodemographic factors, typical frequency and volume of alcohol use, consumption of unrecorded alcohol, negative consequences of the COVID-19 pandemic with the increase in the frequency of heavy episodic drinking in the first months of the COVID-19 pandemic, 2020, (OR, 95% CI)*

Variable	Respondents who increased the frequency of heavy episodic drinking		Unadjusted	Adjusted
	n / N	OR (95% CI)	OR (95% CI)	OR (95% CI)
Sex				
Male	117/411	28.5	1.028 (0.755–1.400)	0.759 (0.497–1.159)
Female	108/387	27.9	1.0	1.0
Age (years)				
18–29	50/173	28.9	1.370 (0.831–2.260)	1.732 (0.867–3.462)
30–49	140/472	29.7	1.422 (0.929–2.176)	1.363 (0.762–2.437)
≥ 50	35/153	22.9	1.0	1.0
Education				
Secondary or below	47/171	27.5	1.401 (0.792–2.477)	1.487 (0.700–3.157)
Primary /vocational school or college	23/108	21.3	1.0	1.0
Higher (complete or incomplete)	155/519	29.9	1.574 (0.957–2.588)	1.476 (0.753–2.894)
Settlement size				
≤ 50,000 population	36/153	23.5	0.698 (0.451–1.080)	1.043 (0.567–1.918)
50,000 to 1 million	81/292	27.7	0.871 (0.619–1.226)	1.534 (0.944–2.493)
Over 1 million	108/353	30.6	1.0	1.0
Income per household member (rubles)				
≤ 9,999	53/177	29.9	1.187 (0.688–2.047)	1.458 (0.680–3.130)
10,000–19,999	48/184	26.1	0.980 (0.566–1.698)	1.210 (0.589–2.488)
20,000–39,999	57/195	29.2	1.147 (0.670–1.964)	1.299 (0.650–2.596)
40,000–59,999	40/140	28.6	1.111 (0.627–1.970)	1.218 (0.593–2.501)
≥ 60,000	27/102	26.5	1.0	1.0

Table 4 cont.

Changes in the average monthly household income since the beginning of the SARS-CoV-2 pandemic				
Did not change or increased	90/380	23.7	1.0	1.0
Slightly fell	43/167	25.7	1.117 (0.734–1.700)	1.087 (0.618–1.914)
Moderately fell	41/130	31.5	1.484 (0.957–2.303)	1.246 (0.664–2.337)
Dropped significantly	51/121	42.1	2.348 (1.525–3.614)	1.624 (0.812–3.246)
Typical frequency of alcohol use in the past 12 months before pandemic				
Once a month or less frequently	13/142	9.2	1.0	1.0
2–4 times a month	56/277	20.2	2.514 (1.324–4.775)	1.315 (0.566–3.056)
2–3 times a week	64/192	33.3	4.962 (2.605–9.451)	2.756 (1.137–6.679)
More often than 2–3 times a week	92/187	49.2	9.610 (5.076–18.194)	6.581 (2.585–16.749)
Number of standard alcoholic drinks consumed on a typical drinking occasion in the past 12 months before pandemic				
1–2	21/171	12.3	1.0	1.0
3–6	122/403	30.3	3.101 (1.874–5.132)	1.583 (0.836–2.999)
7+	78/184	42.4	5.256 (3.056–9.040)	2.202 (1.014–4.779)
Typical frequency of heavy episodic drinking (6 or more drinks on a single occasion) in the past 12 months before pandemic				
Never	38/288	13.2	1.0	1.0
Less than once a month	46/190	24.2	2.102 (1.306–3.383)	2.561 (1.341–4.893)
Once a month	94/228	41.2	4.615 (2.998–7.104)	3.411 (1.746–6.665)
Once a week	47/92	51.1	6.871 (4.034–11.703)	2.647 (1.030–6.803)
Reported consumption of unrecorded alcohol				
Yes	127/430	29.5	1.166 (0.851–1.599)	0.897 (0.596–1.349)
No			1.0	1.0
Reported encountering COVID-19-related restrictions in public life in the past 3 months				
No restrictions	12/62	19.4	1.0	1.0
Slight restrictions	48/266	18.0	0.917 (0.454–1.854)	0.943 (0.263–3.379)
Moderate restrictions	79/239	33.1	2.057 (1.037–4.082)	1.553 (0.381–6.329)
Severe restrictions	81/224	36.2	2.360 (1.188–4.689)	0.820 (0.187–3.599)
Reported encountering COVID-19-related restrictions in their everyday private life in the past 3 months				
No restrictions	12/83	14.5	1.0	1.0
Slight restrictions	57/295	19.3	1.417 (0.720–2.787)	1.513 (0.467–4.899)
Moderate restrictions	78/222	35.1	3.205 (1.638–6.269)	2.690 (0.720–10.055)
Severe restrictions	75/191	39.3	3.825 (1.944–7.530)	3.889 (0.969–15.608)
Reported negative consequences of the pandemic to their professional or financial situation in the past 3 months				
No negative consequences	40/195	20.5	1.0	1.0
Slight negative consequences	72/306	23.5	1.192 (0.771–1.845)	0.699 (0.383–1.275)
Moderate negative consequences	54/153	35.3	2.114 (1.307–3.417)	1.280 (0.625–2.621)
Severe negative consequences	57/132	43.2	2.945 (1.805–4.804)	2.329 (1.001–5.428)
Reported confirmed SARS-CoV-2 infection in themselves, their family or friends in the past 3 months)				
Yes	48/171	28.1	0.986 (0.676–1.438)	0.893 (0.554–1.439)
No	171/603	28.4	1.0	1.0
Reported stress due to the spread of SARS-CoV-2				
Yes	140/423	33.1	1.749 (1.251–2.466)	1.004 (0.628–1.606)
No	69/313	22.0	1.0	1.0

Note: * — respondents who had never drunk 6 or more alcoholic drinks on a single occasion in the past 12 months were excluded from the analysis.

Factors associated with the increase in the frequency of heavy episodic drinking during the first months of the pandemic

Positive statistically significant associations were identified between the increase in the frequency of heavy episodic drinking during the pandemic and the following factors: drinking alcohol 2–3 times a week (OR: 2.756; 95% CI: 1.137–6.679) or more often before the pandemic (OR: 6.581; 95% CI: 2.585–16.749), having 7 or more drinks on a typical drinking occasion before the pandemic (OR: 2.202; 95% CI: 1.014–4.779) and heavy episodic drinking once a month or more often before the pandemic (from OR: 2.561; 95% CI: 1.341–4.893 to OR: 2.647; 95% CI: 1.030–6.803) (Table 4). The odds of increase in the frequency of heavy episodic drinking were significantly more than two times higher among persons who reported severe negative consequences of the pandemic to their financial or professional situation (OR: 2.329; 95% CI: 1.001–5.428).

DISCUSSION

The associations revealed in our study are corroborated by other research works conducted in various countries during the first months of the pandemic. Specifically, in an Israeli study male sex was associated with increased consumption of beer and strong liquors [16], whereas in another study conducted in Canada male sex, stress, the feelings of isolation and hopelessness were associated with increased frequency of alcohol use in the first months of the pandemic [17]. In a UK study, stress caused by the pandemic was associated with the rise in hazardous drinking [18]. High levels of anxiety and stress caused by the pandemic led to the increase in alcohol use in Australia, France and Canada [17, 19, 20].

A few studies investigated changes in alcohol consumption in the general population unstratified by pandemic-related factors. Thus, a French publication reported an increase in total alcohol consumption during the lockdown [20]; by contrast, alcohol use in Greece and Spain during the lockdown was declining [21, 22]. However, in Greece and Spain the decline was less pronounced among stressed individuals and those with low or middle income. Compared to the prepandemic level, alcohol was purchased in larger quantities during the lockdown by Russian [23, 24] and UK households [25]. During the first months of the pandemic, retail alcohol sales were on the rise in the US [26]. A global study investigating changes in the availability and use of psychoactive drugs and alcohol during the pandemic reported a 71% increase in alcohol consumption across the world [27]. However, according to another large-scale study, alcohol consumption in the general population decreased in most European countries, including Russia, during the first months of the pandemic, mostly due to the reduction in the frequency of heavy episodic drinking [22].

Our study discovered a significant increase in 3 key parameters of alcohol consumption during the first months of the pandemic among those individuals who initially had consumed alcohol in larger quantities and more frequently. These key parameters include the frequency of drinking, the usual consumption (volume) of alcohol on a typical drinking occasion and the frequency of heavy episodic drinking. These findings suggest polarization of alcohol use, i.e. a situation when alcohol consumption grows among those who drink more at baseline and declines among those who typically drink less. This is consistent with the results of another online survey conducted in the general adult population of Russia [28]. The associations established in our study between the increase in the frequency of alcohol use/heavy episodic drinking and such COVID-19-related factors as severe restrictions of everyday private life and the negative consequences of the pandemic to professional or financial situation uncover a new aspect or mechanism associated with stress which drives changes in drinking behaviors during the pandemic. Our findings go in line with the stress-associated patterns reported by the studies mentioned above and are consistent with previously reported changes in drinking behavior among Russians determined by certain sociodemographic characteristics, environmental factors and stress in times of socioeconomic and public health crises [29].

A potential limitation of this study might be the insufficient representativeness of the surveyed sample of online social media users in Russia. However, the size of this selection bias is likely small, because the survey was conducted among the users of social networking services highly popular in Russia and because the sociodemographic characteristics of the respondents were generally the same as those of the vast majority of online social media users in Russia. Besides, the consistency of the established patterns and associations with the results of other studies suggests that the probability of our results not being the consequence of selection bias is high. Another limitation of this study is that changes in alcohol consumption were assessed without differentiating between recorded and unrecorded alcohol. Therefore, additional analysis is needed to investigate changes in the consumption of unrecorded alcohol [30], considering its fairly high availability in Russia during the COVID-19 pandemic [31].

CONCLUSIONS

During the first months of the COVID-19 pandemic, over one-third of male and quarter of female online social media users in Russia increased the frequency of drinking. One in four men and one in five women increased their usual consumption (volume) of alcohol on a typical drinking occasion, and about one-third of men and women engaged in heavy episodic drinking more frequently than before the pandemic. Increased alcohol consumption during the first months of the pandemic was associated with male sex, younger age, severe restrictions imposed on everyday private life and severe negative consequences of the pandemic to the professional or financial situation. Further research is needed to investigate the possibility of implementing screening and brief interventions via online social media to prevent problems associated with alcohol use during large-scale epidemics and public health crises.

References

1. RosStat (Federal'naja sluzhba gosudarstvennoj statistiki). [procitirovano 18.10.2021]. Official Statistics. Dostupno po ssylke: https://eng.gks.ru/folder/11335.
2. Artamonov RE, Lavrentev NV. Opros obshhestvennogo mnenija naselenija RF. Izmenenija, vyzvannye jepidemiej koronavirusa i rezhimom samoizoljacii. Analiticheskij bjulleten' NIU VShJe. 2020; (3): 4–24. Available from: https://www.hse.ru/mirror/pubs/share/368507661.pdf.
3. McPhee MD, Keough MT, Rundle S, Heath LM, Wardell JD, Hendershot CS. Depression, Environmental Reward, Coping Motives and Alcohol Consumption During the COVID-19 Pandemic. Front Psychiatry. 2020; 11: 574676. PMID: 33192708; PMCID: PMC7661794. Available from: https://doi.org/10.3389/fpsyt.2020.574676.
4. Hamza CA, Ewing L, Heath NL, Goldstein AL. When social isolation is nothing new: a longitudinal study on psychological distress during COVID-19 among university students with and without preexisting mental health concerns. Can Psychol. 2021; 62 (1): 20–30. Available from: https://doi.org/10.1037/cap0000255.
5. Kuntsche E, Gabhainn SN, Roberts C, Windlin B, Vieno A, Bendtsen P, et al. Drinking motives and links to alcohol use in 13 European countries. J Stud Alcohol Drugs. 2014; 75 (3): 428–37. PMID: 24766755. Available from: https://10.15288/jsad.2014.75.428.
6. Cooper ML, Kuntshce E, Levitt A, Barber LL, Wolf S. Motivational models of substance use: a review of theory and research on motives for using alcohol, marijuana, and tobacco. In: Sher KJ, editor. The Oxford handbook of substance use and substance use disorders. 1st edition. Oxford (UK): Oxford University Press, 2016; p. 375–421.
7. Brooks SK, Webster RK, Smith LE, Woodland L, Wessely S, Greenberg N, et al. The psychological impact of quarantine and how to reduce it: rapid review of the evidence. Lancet. 2020; 395 (10227): 912–20. PMID: 32112714; PMCID: PMC7158942. Available from: https://10.1016/S0140–6736(20)30460–8.

8. de Goeij MC, Suhrcke M, Toffolutti V, van de Mheen D, Schoenmakers TM, Kunst AE. How economic crises affect alcohol consumption and alcohol-related health problems: a realist systematic review. Soc Sci Med. 2015; 131: 131–46. PMID: 25771482. Available from: https://10.1016/j.socscimed.2015.02.025.
9. Alexander AC, Ward KD. Understanding Postdisaster Substance Use and Psychological Distress Using Concepts from the Self-Medication Hypothesis and Social Cognitive Theory. J Psychoactive Drugs. 2018; 50 (2): 177–186. PMID: 29125424; PMCID: PMC6101235. Available from: https://10.1080/02791072.2017.1397304.
10. Rehm J, Kilian C, Ferreira-Borges C, Jernigan D, Monteiro M, Parry CDH, et al. Alcohol use in times of the COVID 19: Implications for monitoring and policy. Drug Alcohol Rev. 2020; 39 (4): 301–4. PMID: 32358884; PMCID: PMC7267161. Available from: https://10.1111/dar.13074.
11. Jacob L, Smith L, Armstrong NC, Yakkundi A, Barnett Y, Butler L, et al. Alcohol use and mental health during COVID-19 lockdown: A cross-sectional study in a sample of UK adults. Drug Alcohol Depend. 2021; 219: 108488. PMID: 33383352; PMCID: PMC7768217. Available from: https://10.1016/j.drugalcdep.2020.108488.
12. Rodriguez LM, Litt DM, Stewart SH. Drinking to cope with the pandemic: The unique associations of COVID-19-related perceived threat and psychological distress to drinking behaviors in American men and women. Addict Behav. 2020; 110: 106532. PMID: 32652385; PMCID: PMC7320671. Available from: https://doi.org/10.1016/j.addbeh.2020.106532.
13. Rotermann M. Canadians who report lower self-perceived mental health during the COVID-19 pandemic more likely to report increased use of cannabis, alcohol and tobacco. Ottawa (ON): Statistics Canada; 2020 [Statistics Canada, Catalogue No.: 45280001]. [cited 19.10.2021]. Available from: https://www150.statcan.gc.ca/n1/en/pub/45–28–0001/2020001/article/00008-eng.pdf?st=B5oO34OM.
14. Bambra C, Riordan R, Ford J, Matthews F. The COVID-19 pandemic and health inequalities. J Epidemiol Community Health. 2020; 74 (11): 964–8. Available from: https://doi.org/10.1136/jech-2020–214401.
15. Vigo D, Patten S, Pajer K, Krausz M, Taylor S, Rush B, et al. Mental health of communities during the COVID-19 pandemic. Can J Psychiatry. 2020; 65 (10): 681–7. Available from: https://doi.org/10.1177/0706743720926676.
16. Levy I, Cohen-Louck K, Bonny-Noach H. Gender, employment, and continuous pandemic as predictors of alcohol and drug consumption during the COVID-19. Drug Alcohol Depend. 2021; 228: 109029. PMID: 34500243; PMCID: PMC8411591. Available from: https://10.1016/j.drugalcdep.2021.109029.
17. Thompson K, Dutton DJ, MacNabb K, Liu T, Blades S, Asbridge M. Changes in alcohol consumption during the COVID-19 pandemic: exploring gender differences and the role of emotional distress. Health Promot Chronic Dis Prev Can. 2021; 41 (9): 254–263. English, French. PMID: 34164972. Available from: https://10.24095/hpcdp.41.9.02.
18. Clay JM, Stafford LD, Parker MO. Associations Between Self-reported Inhibitory Control, Stress, and Alcohol (Mis)use During the First Wave of the COVID-19 Pandemic in the UK: a National Cross-sectional Study Utilising Data From Four Birth Cohorts. Int J Ment Health Addict. 2021: 1–22. PMID: 34366730; PMCID: PMC8330475. Available from: https://10.1007/s11469–021–00599–8.
19. Rolland B, Haesebaert F, Zante E, Benyamina A, Haesebaert J, Franck N. Global Changes and Factors of Increase in Caloric/Salty Food Intake, Screen Use, and Substance Use During the Early COVID-19 Containment Phase in the General Population in France: Survey Study. JMIR Public Health Surveill. 2020; 6 (3): e19630. Available from: https://doi.org/10.2196/19630. Erratum in: JMIR Public Health Surveill. 2021; 7 (7): e31906. PMID: 32589149; PMCID: PMC7505683.
20. Stanton R, To QG, Khalesi S, Williams SL, Alley SJ, Thwaite TL, et al. Depression, Anxiety and Stress during COVID-19: Associations with Changes in Physical Activity, Sleep, Tobacco and Alcohol Use in Australian Adults. Int J Environ Res Public Health. 2020; 17 (11): 4065. PMID: 32517294; PMCID: PMC7312903. Available from: https://10.3390/ijerph17114065.
21. Panagiotidis P, Rantis K, Holeva V, Parlapani E, Diakogiannis I. Changes in Alcohol Use Habits in the General Population, during the COVID-19 Lockdown in Greece. Alcohol Alcohol. 2020; 55 (6): 702–4. PMID: 32959877; PMCID: PMC7543262. Available from: https://doi.org/10.1093/alcalc/agaa092.
22. Kilian C, Rehm J, Allebeck P, Braddick F, Gual A, Barták M, et al. Alcohol consumption during the COVID-19 pandemic in Europe: a large-scale cross-sectional study in 21 countries. Addiction. 2021. PMID: 34109685. Available from: https://10.1111/add.15530.
23. Issledovanija na osnove dannyh Sberbanka. 2020. [procitirovano 15.10.2021]. Dostupno po ssylke: https://www.sberbank.ru/ru/about/issledovaniya
24. Nemcov AV, Gridin RR. Kosvennye pokazateli potreblenija alkogolja vo vremja jepidemii koronavirusa v Rossii. Voprosy narkologii. 2020; (10): 16–33. Available from: https://10.47877/0234–0623_2020_10_16.
25. Anderson P, Llopis EJ, O'Donnell A, Kaner E. Impact of COVID-19 Confinement on Alcohol Purchases in Great Britain: Controlled Interrupted Time-Series Analysis During the First Half of 2020 Compared With 2015–2018. Alcohol Alcohol. 2021; 56 (3): 307–16. PMID: 33211796; PMCID: PMC7717153. Available from: https://doi.org/10.1093/alcalc/agaa128.
26. Castaldelli-Maia JM, Segura LE, Martins SS. The concerning increasing trend of alcohol beverage sales in the U.S. during the COVID-19 pandemic. Alcohol. 2021; 96: 37–42. PMID: 34245809; PMCID: PMC8421038. Available from: https://10.1016/j.alcohol.2021.06.004.
27. Farhoudian A, Radfar SR, Mohaddes Ardabili H, Rafei P, Ebrahimi M, et al. A Global Survey on Changes in the Supply, Price, and Use of Illicit Drugs and Alcohol, and Related Complications During the 2020 COVID-19 Pandemic. Front Psychiatry. 2021; 12: 646206. PMID: 34421664; PMCID: PMC8377291. Available from: https://10.3389/fpsyt.2021.646206.
28. Gil AYu, Vyshinskiy KV, Fadeeva EV, Khalfin R. A. Izmenenija osobennostej potreblenija alkogolja v Rossijskoj Federacii v pervye mesjacy pandemii COVID-19. Problemy standartizacii v zdravoohranenii. 2021; 5–6: 63–73. Available from: https://doi.org/10.26347/1607–2502202105–06063–073.
29. Nemtsov AV. A Contemporary History of Alcohol in Russia. Södertörn: Södertörn University, 2011; 348 r.
30. Gil A, Khalfin R, Krinitsky S, Nikoforov S, Ilchenko I, Kosagovskaya I, i dr. Upotreblenie surrogatnogo alkogolja licami s rasstrojstvami, svjazannymi so zloupotrebleniem alkogolem (na primere sub"ekta Rossijskoj Federacii). Problemy social'noj gigieny, zdravoohranenija i istorii mediciny. 2021; 29 (3): 486–91. Available from: https://doi.org/10.32687/0869–866X-2021–29–3–486–491.
31. Gil A. COVID-19: A need for stricter control over unrecorded alcohol in Russia. Adicciones. 2021; 33 (3): 281–4. Available from: https://doi.org/10.20882/adicciones.1634.

Литература

1. РосСтат (Федеральная служба государственной статистики). [процитировано 18.10.2021]. Official Statistics. Доступно по ссылке: https://eng.gks.ru/folder/11335.
2. Артамонов Р. Е., Лаврентьев Н. В. Опрос общественного мнения населения РФ. Изменения, вызванные эпидемией коронавируса и режимом самоизоляции. Аналитический бюллетень НИУ ВШЭ. 2020; (3): 4–24. Доступно по ссылке: https://www.hse.ru/mirror/pubs/share/368507661.pdf.
3. McPhee MD, Keough MT, Rundle S, Heath LM, Wardell JD, Hendershot CS. Depression, Environmental Reward, Coping Motives and Alcohol Consumption During the COVID-19 Pandemic. Front Psychiatry. 2020; 11: 574676. PMID: 33192708; PMCID: PMC7661794. Available from: https://doi.org/10.3389/fpsyt.2020.574676.
4. Hamza CA, Ewing L, Heath NL, Goldstein AL. When social isolation is nothing new: a longitudinal study on psychological distress during COVID-19 among university students with and without preexisting mental health concerns. Can Psychol. 2021; 62 (1): 20–30. Available from: https://doi.org/10.1037/cap0000255.

5. Kuntsche E, Gabhainn SN, Roberts C, Windlin B, Vieno A, Bendtsen P, et al. Drinking motives and links to alcohol use in 13 European countries. J Stud Alcohol Drugs. 2014; 75 (3): 428–37. PMID: 24766755. Available from: https://10.15288/jsad.2014.75.428.
6. Cooper ML, Kuntshce E, Levitt A, Barber LL, Wolf S. Motivational models of substance use: a review of theory and research on motives for using alcohol, marijuana, and tobacco. In: Sher KJ, editor. The Oxford handbook of substance use and substance use disorders. 1st edition. Oxford (UK): Oxford University Press, 2016; p. 375–421.
7. Brooks SK, Webster RK, Smith LE, Woodland L, Wessely S, Greenberg N, et al. The psychological impact of quarantine and how to reduce it: rapid review of the evidence. Lancet. 2020; 395 (10227): 912–20. PMID: 32112714; PMCID: PMC7158942. Available from: https://10.1016/S0140–6736(20)30460–8.
8. de Goeij MC, Suhrcke M, Toffolutti V, van de Mheen D, Schoenmakers TM, Kunst AE. How economic crises affect alcohol consumption and alcohol-related health problems: a realist systematic review. Soc Sci Med. 2015; 131: 131–46. PMID: 25771482. Available from: https://10.1016/j.socscimed.2015.02.025.
9. Alexander AC, Ward KD. Understanding Postdisaster Substance Use and Psychological Distress Using Concepts from the Self-Medication Hypothesis and Social Cognitive Theory. J Psychoactive Drugs. 2018; 50 (2): 177–186. PMID: 29125424; PMCID: PMC6101235. Available from: https://10.1080/02791072.2017.1397304.
10. Rehm J, Kilian C, Ferreira-Borges C, Jernigan D, Monteiro M, Parry CDH, et al. Alcohol use in times of the COVID 19: Implications for monitoring and policy. Drug Alcohol Rev. 2020; 39 (4): 301–4. PMID: 32358884; PMCID: PMC7267161. Available from: https://10.1111/dar.13074.
11. Jacob L, Smith L, Armstrong NC, Yakkundi A, Barnett Y, Butler L, et al. Alcohol use and mental health during COVID-19 lockdown: A cross-sectional study in a sample of UK adults. Drug Alcohol Depend. 2021; 219: 108488. PMID: 33383352; PMCID: PMC7768217. Available from: https://10.1016/j.drugalcdep.2020.108488.
12. Rodriguez LM, Litt DM, Stewart SH. Drinking to cope with the pandemic: The unique associations of COVID-19-related perceived threat and psychological distress to drinking behaviors in American men and women. Addict Behav. 2020; 110: 106532. PMID: 32652385; PMCID: PMC7320671. Available from: https://doi.org/10.1016/j.addbeh.2020.106532.
13. Rotermann M. Canadians who report lower self-perceived mental health during the COVID-19 pandemic more likely to report increased use of cannabis, alcohol and tobacco. Ottawa (ON): Statistics Canada; 2020 [Statistics Canada, Catalogue No.: 45280001]. [cited 19.10.2021]. Available from: https://www150.statcan.gc.ca/n1/en/pub/45–28–0001/2020001/article/00008-eng.pdf?st=B5oO34OM.
14. Bambra C, Riordan R, Ford J, Matthews F. The COVID-19 pandemic and health inequalities. J Epidemiol Community Health. 2020; 74 (11): 964–8. Available from: https://doi.org/10.1136/jech-2020–214401.
15. Vigo D, Patten S, Pajer K, Krausz M, Taylor S, Rush B, et al. Mental health of communities during the COVID-19 pandemic. Can J Psychiatry. 2020; 65 (10): 681–7. https://doi.org/10.1177/0706743720926676.
16. Levy I, Cohen-Louck K, Bonny-Noach H. Gender, employment, and continuous pandemic as predictors of alcohol and drug consumption during the COVID-19. Drug Alcohol Depend. 2021; 228: 109029. PMID: 34500243; PMCID: PMC8411591. Available from: https://10.1016/j.drugalcdep.2021.109029.
17. Thompson K, Dutton DJ, MacNabb K, Liu T, Blades S, Asbridge M. Changes in alcohol consumption during the COVID-19 pandemic: exploring gender differences and the role of emotional distress. Health Promot Chronic Dis Prev Can. 2021; 41 (9): 254–263. English, French. PMID: 34164972. Available from: https://10.24095/hpcdp.41.9.02.
18. Clay JM, Stafford LD, Parker MO. Associations Between Self-reported Inhibitory Control, Stress, and Alcohol (Mis)use During the First Wave of the COVID-19 Pandemic in the UK: a National Cross-sectional Study Utilising Data From Four Birth Cohorts. Int J Ment Health Addict. 2021: 1–22. PMID: 34366730; PMCID: PMC8330475. Available from: https://10.1007/s11469–021–00599–8.
19. Rolland B, Haesebaert F, Zante E, Benyamina A, Haesebaert J, Franck N. Global Changes and Factors of Increase in Caloric/Salty Food Intake, Screen Use, and Substance Use During the Early COVID-19 Containment Phase in the General Population in France: Survey Study. JMIR Public Health Surveill. 2020; 6 (3): e19630. Available from: https://doi.org/10.2196/19630. Erratum in: JMIR Public Health Surveill. 2021; 7 (7): e31906. PMID: 32589149; PMCID: PMC7505683.
20. Stanton R, To QG, Khalesi S, Williams SL, Alley SJ, Thwaite TL, et al. Depression, Anxiety and Stress during COVID-19: Associations with Changes in Physical Activity, Sleep, Tobacco and Alcohol Use in Australian Adults. Int J Environ Res Public Health. 2020; 17 (11): 4065. PMID: 32517294; PMCID: PMC7312903. Available from: https://10.3390/ijerph17114065.
21. Panagiotidis P, Rantis K, Holeva V, Parlapani E, Diakogiannis I. Changes in Alcohol Use Habits in the General Population, during the COVID-19 Lockdown in Greece. Alcohol Alcohol. 2020; 55 (6): 702–4. PMID: 32959877; PMCID: PMC7543262. Available from: https://doi.org/10.1093/alcalc/agaa092.
22. Kilian C, Rehm J, Allebeck P, Braddick F, Gual A, Barták M, et al. Alcohol consumption during the COVID-19 pandemic in Europe: a large-scale cross-sectional study in 21 countries. Addiction. 2021. PMID: 34109685. Available from: https://10.1111/add.15530.
23. Исследования на основе данных Сбербанка. 2020. [процитировано 15.10.2021]. Доступно по ссылке: https://www.sberbank.ru/ru/about/issledovaniya
24. Немцов А. В., Гридин Р. Р. Косвенные показатели потребления алкоголя во время эпидемии коронавируса в России. Вопросы наркологии. 2020; (10): 16–33. Доступно по ссылке: https://10.47877/0234–0623_2020_10_16.
25. Anderson P, Llopis EJ, O'Donnell A, Kaner E. Impact of COVID-19 Confinement on Alcohol Purchases in Great Britain: Controlled Interrupted Time-Series Analysis During the First Half of 2020 Compared With 2015–2018. Alcohol Alcohol. 2021; 56 (3): 307–16. PMID: 33211796; PMCID: PMC7717153. Available from: https://doi.org/10.1093/alcalc/agaa128.
26. Castaldelli-Maia JM, Segura LE, Martins SS. The concerning increasing trend of alcohol beverage sales in the U.S. during the COVID-19 pandemic. Alcohol. 2021; 96: 37–42. PMID: 34245809; PMCID: PMC8421038. Available from: https://10.1016/j.alcohol.2021.06.004.
27. Farhoudian A, Radfar SR, Mohaddes Ardabili H, Rafei P, Ebrahimi M, et al. A Global Survey on Changes in the Supply, Price, and Use of Illicit Drugs and Alcohol, and Related Complications During the 2020 COVID-19 Pandemic. Front Psychiatry. 2021; 12: 646206. PMID: 34421664; PMCID: PMC8377291. Available from: https://10.3389/fpsyt.2021.646206.
28. Гиль А. Ю., Вышинский К. В., Фадеева Е. В., Хальфин Р. А. Изменения особенностей потребления алкоголя в Российской Федерации в первые месяцы пандемии COVID-19. Проблемы стандартизации в здравоохранении. 2021; 5–6: 63–73. Доступно по ссылке: https://doi.org/10.26347/1607–2502202105–06063–073.
29. Nemtsov AV. A Contemporary History of Alcohol in Russia. Södertörn: Södertörn University, 2011; 348 p.
30. Гиль А. Ю., Хальфин Р. А., Криницкий С. М., Никифоров С. А., Ильченко И. Н., Косаговская И. И., и др. Употребление суррогатного алкоголя лицами с расстройствами, связанными со злоупотреблением алкоголем (на примере субъекта Российской Федерации). Проблемы социальной гигиены, здравоохранения и истории медицины. 2021; 29 (3): 486–91. Доступно по ссылке: https://doi.org/10.32687/0869–866X-2021–29–3–486–491.
31. Gil A. COVID-19: A need for stricter control over unrecorded alcohol in Russia. Adicciones. 2021; 33 (3): 281–4. Available from: https://doi.org/10.20882/adicciones.1634.